MODELING SAND TRANSPORT UNDER BREAKING WAVES

Bram Schnitzler

UNIVERSITY OF TWENTE.

UNIVERSITY OF TWENTE.

MODELING SAND TRANSPORT UNDER BREAKING WAVES

JULY 1, 2015

Master Thesis at
Research group Water Engineering and Management
Faculty of Engineering Technology
University of Twente

Author	Bram Schnitzler
E-mail Utwente	b.schnitzler@student.utwente.nl
E-mail private	bramschnitzler@gmail.com

Exam Committee

Graduation supervisor	dr. ir. J.S. Ribberink
Daily supervisors	dr.ir. J.J. van der Werf
	J. van der Zanden MSc.

PREFACE

You are currently reading my Master Thesis, the final project of the Master Civil Engineering and Management with as specialization Water Engineering and Management. I enjoyed working for five months on this Master thesis with the subject: 'Modeling of wave breaking effects on sediment transport in the SANTOSS model within Delft3D'. During the master thesis I learned a lot of the hydrodynamics and morphodynamics in the coastal zone. I also learned a lot of the reproduction of these hydrodynamics and morphodynamics with Delft3D and with the SANTOSS model. Despite some problems with compiling Delft3D at the start of this Master Thesis, the thesis went quite smooth, for which I am grateful.

I am especially thankful for my supervisors. Joep van der Zanden was always available to answer my questions. Joep sometimes was available for small questions; we also had multiple discussions of at least an hour on results and on how to proceed. Joep has a positive and critical attitude towards my project, which definitely improved this Master Thesis. Secondly, I want to thank Jebbe van der Werf for his knowledge on Delft3D and on his interest in the results. Jebbe helped me especially in the beginning of this Master Thesis on setting up the Delft3D model. He brought me in contact with Adri Mourits from Deltares, who also helped setting up and improving the model. Jebbe is always interested in the obtained results and the physics behind the results; this made the discussion on the results interesting. At last, I want to thank the graduation supervisor, Jan Ribberink. I especially want to thank Jan for his knowledge on the processes going on nearshore. Also a lot of thank for helping me starting the project. Jan was especially helpful during the preparation of the Master Thesis. Next to my supervisors I want to thank my fellow graduate students from room Horst Z-128. They caused distraction during lunch-, coffee- and other breaks.

I enjoyed working on my Master thesis including writing this report. I hope you will enjoy reading it.

Bram Schnitzler
Enschede, July 2015

ABSTRACT

Morphological models are often used to predict the effect of interventions on coasts. A sediment transport formula within such morphological models developed by among others the University of Twente is the SANTOSS model (van der A et al., 2013). The SANTOSS model calculates the near-bed sediment transport for regular non-breaking waves. These morphological models are simplifications of the reality and require constant improvement. To improve the predictive capability of existing sediment transport formulations for breaking-wave conditions, the University of Twente recently conducted measurements in the CIEM wave flume in Barcelona (van der Zanden et al., 2015).

The objective of this master thesis is to improve the prediction of sediment transport under breaking waves with the SANTOSS formula within the 3D hydrodynamic and morphodynamic software package Delft3D by adding wave breaking effects to the SANTOSS formula. This required firstly a calibration of a Delft3D model based on the measured hydrodynamics during the CIEM wave flume experiment. Secondly, wave breaking effects were included to the model in order to improve modeled sediment transport rates for this experiment. Finally, the improved model with breaking effects was applied within Delft3D and validated using a separate data set (LIP Experiments, Reniers & Roelvink, 1995).

During the calibration of the Delft3D model it seemed that Delft3D had troubles modeling regular waves. Delft3D uses a parameterization for the dissipation due to wave breaking which is developed for irregular breaking waves. This parameterization has been adapted to a parameterization which is suitable to model the dissipation of regular breaking waves. Therefore Delft3D was well suitable to reproduce the measured wave heights. The measured set-up/down was also modeled quite well with the Delft3D model. However, Delft3D was not able to reproduce the measured net currents properly. The measured net currents (undertow) were underestimated at the offshore side of the breaker bar and overestimated at the top of the breaker bar. These errors are most likely due to poor representation of the modeled the Stokes mass flux due to waves or due to rollers. To model sediment transport using the SANTOSS model, intra-wave velocities are required. Since Delft3D is a wave-averaged model the parameterization from Ruessink, Ramaekers, & Van Rijn (2012) is used to predict the intra-wave velocities. This model seemed not very suitable for this test-case. The parameterization method of Ruessink et al. (2012) is developed for field conditions, this is probably the reason of the underestimation of especially the peak orbital velocities and the acceleration skewness.

After finishing the calibration of the Delf3D model the different measured and modeled sediment transports components (wave- and current related bed-load and suspended transport) have been assessed. For both suspended and bed-load sediment transport discrepancies between model outcomes and measurements appear. In the breaking region, modeled reference concentrations and mixing coefficients are lower than values extracted from the measurements. This leads to an underestimation of suspended sediment concentrations, and in combination with the undertow current which magnitude was also underestimated, leads to a substantial underestimation of offshore-directed suspended sediment transport. Pre- and post-breaking, modeled concentrations are higher than measured and suspended transport is overestimated by the model. In terms of near-bed transport modeled with the SANTOSS formula, the transport in the post-breaking region is predicted quite accurately. However, the onshore directed sediment transport in the shoaling/breaking region is underestimated. The underpredictions of both offshore-directed suspended load and onshore-directed bed-load cancel each other out to some extent. This causes a proper prediction of the direction of total sediment transport, although the magnitude of the total sediment transport is underestimated. The SANTOSS near-bed transport formula performs approximately similar as the default transport formula within Delft3D (van Rijn, 2007a).

Since Delft3D seems not able to accurately reproduce the hydrodynamics and morphodynamics of this test-case, the SANTOSS model was run stand-alone with measured and Delft3D-modeled hydrodynamic input to check the effect of errors in the modeled hydrodynamics on the sediment transport. It seemed that small errors in the modeled hydrodynamics cause various errors in the SANTOSS model (crest/trough periods, phase lag, Shields parameter, etc.) which add substantial errors in the net transport rates. When looking at the modeled sediment transport it is better predicted for some locations using the modeled hydrodynamics. This is mainly due to an overestimation of the crest periods, due to an underestimation of the net currents. The near-bed sediment transport is therefore predicted better using the modeled hydrodynamics for some locations since there is more onshore directed sediment transport due to an overestimation of the crest period. Slope effects have been added to the SANTOSS model and the near-bed velocity reference height has been changed to see if the slope effect or changing the near-bed velocity reference height has remarkable effects. Adding slope effects improved the predicted sediment transport a little bit. Changing the near-bed velocity reference height to the height of the maximum overshoot velocity worsened the prediction of the sediment transport; since the peak orbital velocities at the maximum overshoot velocity height is larger than at the standard height of the lowest velocity measurement device (11 cm above the bed). The errors on the modeled hydrodynamics have a substantial effect on the predicted sediment transport rates; therefore wave breaking effects on near-bed sediment transport were mainly tested in the stand-alone SANTOSS model.

Three wave breaking effects have been tested during this study. The formulation for the wave Reynolds stress has been adapted to a formulation that also accounts for energy dissipation of rollers. The other wave breaking effects are adding turbulence to the root mean square orbital velocity (Reniers, Roelvink, & Thornton, 2004) and adding turbulence to the Shields parameter (Reniers et al., 2013) It seems that adding turbulence to the Shields parameter during the crest period (Ting & Kirby, 1995) with a calibration factor for the importance of the turbulence (Ribas, de Swart, Calvete, & Falqués, 2011; Van Thiel De Vries, 2009) seems to work well for this test case, this is also a physically representative formulation.

Computations with morphological updating have been done to check whether Delft3D predicts the locations of the breaker bar at the right location. Due to an underestimation of the offshore directed sediment transport and due to an underestimation of the onshore directed bed-load transport in front of the breaker bar Delft3D has trouble with predicting dimensions of the breaker bar. The breaker bar is higher and shorter (steeper slopes) compared to the breaker bar developed during the experiment.

The wave breaking effect added to the SANTOSS model has been tested on another experimental campaign in the CIEM wave flume in Barcelona with a nearly flat bottom (Ribberink et al., 2014) and on the LIP1B and LIP1C case (Reniers & Roelvink, 1995). The breaker bar developed during modeling of the first measurement campaign occurs more onshore than measured due to an underestimated of the offshore directed current-related suspension transport. The sediment transport predictions for the LIP cases are improved using the SANTOSS formula including wave breaking effects. The prediction of the sediment transport is especially improved at the locations where most (irregular) waves break. In the start of the flume of the LIP cases, the prediction of the sediment transport became worse. This is due to presence of modeled roller energy in the start of the flume due to irregular breaking waves.

TABLE OF CONTENTS

1 INTRODUCTION

1.1 Research Occasion

Protection of coastal areas against erosion and sedimentation is important and it is continuously required for the safety behind dunes. Protection against erosion and sedimentation is also important for social economical reasons since the coastal area is often used for recreational purposes. Protection of the coastal areas can be done by doing lots of kind of interventions like dredging, nourishments or hard structures. The consequences of these interventions are often predicted by morphological models. These morphological models are also used as management tools for policy makers. These morphological models are simplifications of the reality; therefore there are a lot of uncertainties in the morphological models.

A model that predicts the sand transport within morphodynamic models is the SANTOSS model developed by among others the University of Twente (van der A et al., 2013). The SANTOSS model is developed to model the near-bed sediment transport under regular non-breaking waves. SANTOSS formula and other sediment transport formulae commonly perform worse in the breaker region compared to deeper water (Van Rijn, Ribberink, Van Der Werf, & Walstra, 2013).

To keep improving the understanding of the physics in the coastal area and to keep improving the prediction of sediment transport the University of Twente did new experiments on sediment transport under breaking waves (van der Zanden et al., 2015) in the CIEM wave flume in Barcelona. In this wave flume a regular breaking wave was created which breaks on a breaker bar. These measurements have been done because the processes under breaking waves are not well understood. The measurements are very detailed at the breaker bar, so that a lot of data is available on the hydrodynamics and morphodynamics under breaking waves. The experiments will be used to test improvements on sediment transport predictions under regular breaking waves with the SANTOSS model in the 3D hydrodynamic and morphodynamic software package Delft3D. The SANTOSS model already has been implemented in Delft3D (Veen, 2014). The improvements for wave breaking effects are based on literature. An option to add wave breaking effects is to add local turbulence to either the bed shear stress (Reniers et al., 2013) or to the root mean square orbital velocity (Reniers et al., 2004).

1.2 Research Background

Waves approach the shore deform due to among other shoaling and wave breaking (See Figure 1-1). The deformation of the waves is not only visible on the wave height. The wave shapes also deform as wave approach the shore. Wave become velocity skewed and acceleration skewed as they approach the shore (See Figure 1-2).

Wave breaking can be classified in four categories; in this case there are plunging breaking waves. For this category the value wave similarity parameter β is between 0.5 and 3. The wave similarity parameter can be calculated with the wave steepness $\tan\beta$, the wave height H and the wave length L_0 (Battjes, 1974):

$$\xi = \frac{\tan\beta}{\sqrt{H/L_0}} \qquad \text{EQ. 1-1}$$

For plunging breakers, transport of turbulent energy is directed onshore (Ting & Kirby, 1995, 1996).

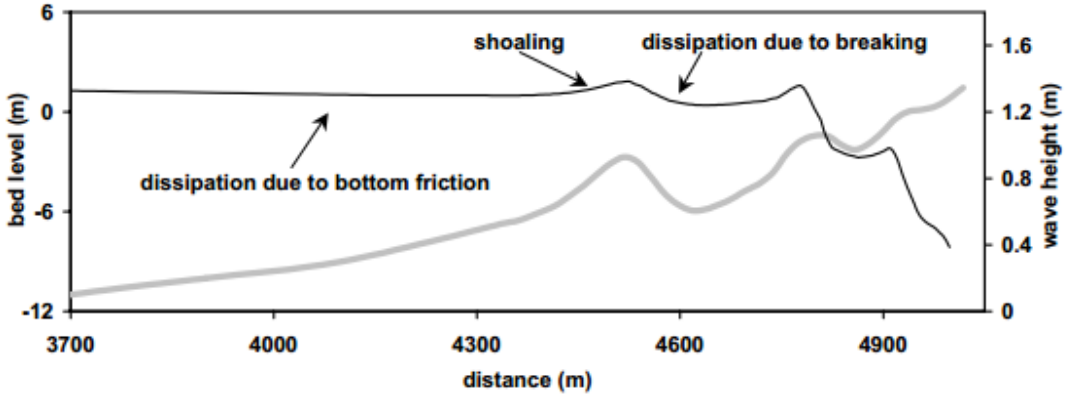

FIGURE 1-1: WAVE DEFORMATION (GRASMEIJER, 2002)

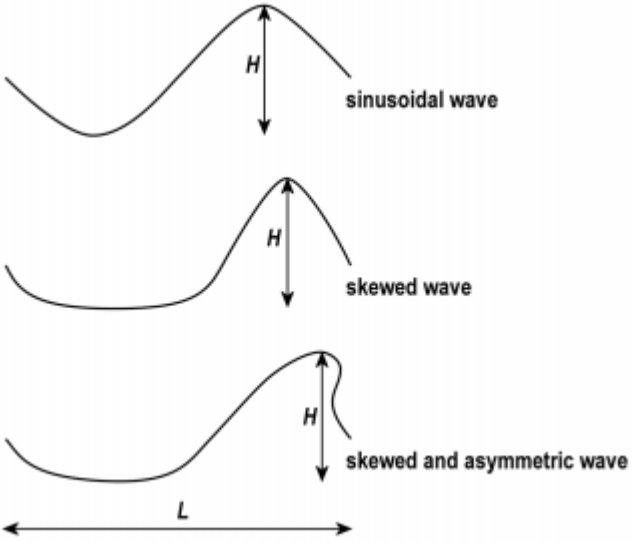

FIGURE 1-2: WAVE SKEWNESS AND ASYMMETRY (GRASMEIJER, 2002).

Sediment transport is the movement of particles in the water column. The driving parameter for sediment transport is bed shear stress. Bed shear stress is defined as the bottom friction by water per area. The bottom friction causes lower flow velocities near the bed and it also causes turbulence near the bed responsible for the picking up of sediment (see Figure 1-3).

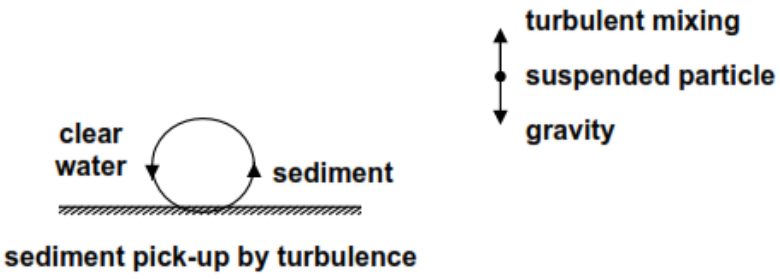

FIGURE 1-3: SEDIMENT PICK UP AND DEPOSITION

The bed shear stress is determined by the following formula:

$$\tau_b = \rho u_*^2 = \frac{1}{2}\rho f |\bar{U}|\bar{U} \quad \text{EQ. 1-2}$$

In which $\bar{U}$ is the depth averaged velocity, ρ is the density of water and f is a friction coefficient. The initiation of motion is determined by exceedance of the Shields parameter over the critical Shields parameter:

$$\theta = \frac{\tau_b}{(\rho_s - \rho)gD} > \theta_c \approx 0.03 - 0.05 \quad \text{EQ. 1-3}$$

The Shields parameter is commonly defined as a dimensionless bed shear stress.

1.3 Research objective

The objective of the research is to improve the sediment transport prediction by Delft3D for breaking wave conditions using the SANTOSS formula. The SANTOSS model is not developed to predict the near bed sediment transport under breaking waves (van der A et al., 2013), since it is developed for non-breaking waves. There are currently some suggestions on how to adjust the SANTOSS model for wave-breaking effects. These effects will be tested in Delft3D with the new highly detailed measurement of wave breaking in a flume (van der Zanden et al., 2015). It should be kept in mind that also suspended sediment might be modeled poorly. In that case it would be wiser to improve the suspended sediment predictions.

This introduces a mean to reach this objective; the current SANTOSS model will be validated for the highly detailed measurement on wave breaking in a flume and the results of the SANTOSS model will also be compared with the results of the commonly used net sediment transport model of van Rijn. This is required to complete the objective. In a previous study it seemed that the SANTOSS model within Delft3D predicts the net sediment transport reasonably well (Van der Werf, Veen, Ribberink, & van der Zanden, 2015; Veen, 2014).

1.4 Research questions

Five research questions have been formulated to help achieve the objective mentioned in the previous section. Each research question will be answered in a separate section starting with the first research question in the third section.

1. *How do the overall hydrodynamics below breaking waves look in the new Barcelona measurements and how well can Delft3D reproduce these hydrodynamics?*

2. *What are, according to measurements and Delft3D, the contributions of different transport components (bed-load, suspended load, current- and wave- related components) to the total sediment transport in the breaker zone and how well can Delft3D reproduce these transport components with the SANTOSS and the van Rijn (2007ab)(Bed load and suspended load/concentration) model?*

3. *How can the differences between Delft3D and the measured transport components be explained?*
   - 3.1. *Can wrong sediment transport predictions be explained by errors in the modeled overall hydrodynamics (wave height, set-up, undertow and orbital flow skewness/asymmetry)?*
   - 3.2. *Can sediment transport predictions be improved by changing the near-bed velocity reference height or by adding bed slope effects in the stand-alone model?*
   - 3.3. *Can wrong sediment transport predictions be explained by specific effects of wave breaking?*
   - 3.4. *Is it necessary to further improve the present Delft3D models for near-bed transport (SANTOSS) and /or suspended sediment transport?*

4. *How is it possible to account for wave-breaking effects in the SANTOSS transport model (stand-alone Matlab-model and/or Delft3D)?*
   4.1. Which model concepts are available?
   4.2. How well do they compare with the data and with the current models?
   4.3. What is the best (calibrated) concept?

5. *How does the SANTOSS model (in Delft3D or Matlab) with improvements for wave-breaking effects perform for other test cases?*

1.5 Research approach and reading guideline

1.5.1 *General research approach*

The SANTOSS model is a model that is currently under construction and the SINBAD project aims at improving the current SANTOSS model with wave-breaking and wave irregularity effects. During this project improvements for breaking wave effects on the SANTOSS model have been tested in a stand-alone Matlab version of the SANTOSS model and within the Delft3D environment. Possible improvements of the SANTOSS model have been tested stand-alone, because possible improvements are easier to implement in Matlab. The Delft3D environment is used as it is a more often used software package to model hydrodynamics and morphodynamics. Another reason for using Delft3D is that it calculates much more than the near-bed sediment transport only, also hydrodynamics and suspended sediment will be calculated.

During this research project measurements from the CIEM wave flume in Barcelona have been compared with model results and differences will be explained. Differences between model results and measurements have al lot of sources. Some of these sources are errors in the measurements, processes that are not well modeled, poor parameter settings or there might be numerical solving problems. This research project aims at approaching of the model results to the measurements of the experiments in the CIEM wave flume in Barcelona. This is done by firstly changing the parameter settings during a calibration and after that by changing the processes in a stand-alone SANTOSS model and in the Delft3D environment.

During this Master Thesis some formulations used in Delft3D and in the SANTOSS model have been adapted. To distinguish adapted formulations from standard formulations, the adapted formulations have been marked with an asterisk.

1.5.2 *Research question 1*

The first research question is answered in section 3 by first looking at the measured hydrodynamics. The hydrodynamics are explored and different hydrodynamics like wave height; set-up, net currents, orbital velocities, velocity skewness and acceleration skewness have been examined. Secondly the breaking waves in the wave flume have been reproduced in a Delft3D model. The hydrodynamics have been reproduced as well as possible by doing a calibration. The results of this calibration are compared to the measured hydrodynamics. After that, it is determined if the hydrodynamics are reproduced well enough so that it will not influence the sediment transport negatively. It is also examined why difference between the measured hydrodynamics and the modeled hydrodynamics occur.

1.5.3 *Research question 2*

A clear distinction between the different transport components is required to see where sediment transport predictions possibly go wrong. The different transport components, wave related bed-load transport, current related bed-load transport, wave related suspended load transport and current related suspended load transport, can be modeled separately in Delft3D. In Delft3D the SANTOSS model will be used for the near bed sediment transport. Also the van Rijn (2007ab) sediment transport formulas will be used. This is a transport formula for the current related

suspended sediment and a combined formula for wave related bed- and suspended load and current related bed-load. Since Delft3D requires a current related suspended sediment formula if SANTOSS is used the sediment transport formula of van Rijn (2007b) is used. This gives some overlap since the SANTOSS formula is not tuned to the van Rijn (2007b) suspended sediment transport formula; this is taken into account. Both models have a different distinction between bed-load and suspended load. Therefore, it is important to make a clear distinction between the different sediment transport components. Also, modeled suspended sediment concentrations are compared with the measured sediment concentration, including reference concentrations and sediment diffusivities. This helps assign possibly poorly modeled current related sediment transport to poorly modeled hydrodynamics or sediment concentrations. The second research question, from which the research approach is just discussed, will be answered in section 4.

1.5.4 *Research question 3*

The third research question, answered in section 5, aims at examining the differences between Delft3D and the measured transport. It is examined whether possible differences are caused by errors in the modeled overall hydrodynamics, if possible difference occur from missing bed slope effects or from the choice for the near-bed velocity reference height and/or if possible differences are caused by specific missing effects of wave breaking. Differences caused by errors in the hydrodynamics will be examined with a stand-alone Matlab version of SANTOSS. Hydrodynamic parameters are not included in the Matlab code because it is a stand-alone model. The hydrodynamics have been inserted manually. The measured hydrodynamics and the Delft3D modeled hydrodynamics have been inserted in this stand-alone Matlab model. The measured bed-load transport is available, this makes including suspended sediment transport unnecessary. The results of the stand-alone SANTOSS models can then be compared to the measurements, in this way it is assessed if errors in the modeled sediment transports are caused by errors in the modeled hydrodynamics. The effect of the bed slopes and the near-bed velocity reference height will also be examined in this section. In this way it is examined if possible differences between sand transport predictions and measurements are due to specific effects of wave breaking. The last part of this research question determines whether it is necessary to improve the current Delft3D models for near-bed transport and/or suspended sediment transport.

1.5.5 *Research question 4*

The fourth research question answers how it is possible to account for wave-breaking effects in the SANTOSS model. Therefore it is examined which model concepts on breaking wave effects are available. Three of these ideas that are tested are changing the formulations of the wave Reynolds stress, adding turbulence to the orbital velocities and adding turbulence to the Shields parameter (van der Zanden, 2014). The results of the models with improvements for breaking wave effects have been compared with the measurements and with the current models. The stand-alone Matlab model is used since it requires less time to test improvement for wave breaking effects. It is examined which model concept for breaking wave effects works best. This is done by comparing the results of the stand-alone Matlab model with different improvements for wave breaking effects with each other and with the measurements. At last, the best calibrated concept is tested in Delft3D. The near-bed sediment transport modeled with Delft3D including wave breaking effects within the SANTOSS model has been compared to the measurements. Also some morphological computations were done to examine how well DELFT3D predicts the breaker bar. The fourth research question is answered in section 6.

1.5.6 *Research question 5*

The last research question, answered in section 7, answers how the new improvements for wave-breaking effects perform for other experiments in Delft3D. Improvements have been tested on the LIP experiments (Reniers & Roelvink, 1995) and on another test case with a flat bed in the wave flume in Barcelona (Ribberink et al., 2014).

2 METHODOLOGY

The methodology will firstly give a brief introduction on Delft3D and secondly on the suspension- and bed-load transport. Thirdly the SANTOSS model, on which improvements will be tested, will be introduced. Fourthly the model set-up used in this project will be discussed and at last the CIEM wave flume experiments will be introduced.

2.1 Delft3D

The sand transport will be predicted with a stand-alone Matlab model and within the Delft3D environment. Delft3D is a 3 dimensional software package, which calculates flows, waves, sediment transport and morphological change. It consists of integrated modules which allow the simulation of hydrodynamic flow, computation of the transport of water-borne constituents, short waves generation and propagation, sediment transport and morphological changes, and the modeling of ecological processes and water quality parameters (Lesser, Roelvink, van Kester, & Stelling, 2004). Delft3D solves the unsteady shallow water equations. Delft3D uses a curvilinear grid in which the shallow water equations are solved. It is possible to calculate the sediment transport in Delft3D with a selection of sediment transport formula. A commonly used transport within Delft3D is the van Rijn (2007ab) model, discussed in section 2.1.3 and 2.1.4.

This Master Thesis involves the modeling of waves in Delft3D, it is therefore important to mention that Delft3D does not model individual waves. Delft3D models the forcing of waves through the wave propagation theory (See section 2.1.2).

2.1.1 *System of Equations*

To solve the numerical model the software packages uses a staggered grid, meaning that the water level points are located at the center of the grid cells and the velocity points are located at the faces of the grid cells (see Figure A-1).

The equations below are valid for a Cartesian rectangular grid (Lesser et al., 2004). The horizontal grid can be separated into σ-layers or z-layers, the difference is shown in Figure A-2. The thicknesses of these layers are user-defined. Thin layers are mostly used near the bottom and the water surface in the presence of wave while thicker layers are mostly used in the middle of the water column and near the water surface when waves are not present.

The systems of equations that Delft3D handles are the horizontal momentum equations, the continuity equation, the transport equation and a turbulence closure model. The equations are shown in Appendix A.2, first the continuity equations, then the two horizontal momentum equations, the transport equation and some discussion on the turbulence closure model are shown.

2.1.2 *Waves*

Delft3D is also able to account for wave effects (Deltares, 2014); short waves can be modeled in Deft3D through the wave propagation method calculated using the wave energy. Effects of wave breaking can be included using the roller model. For more extended waves modeling the separate Delft3D-Wave module needs to be applied (Deltares, 2014), this is not relevant for this study. So, only the wave propagation and the Roller model will be discussed here.

Wave propagation

Delft3D does not model the individual waves, but it models the forcing caused by short waves through wave propagation. The forcing of these short waves is calculated by using the group

velocity of the waves. This is equal to the velocity of short waves for shallow areas. Basis of the wave propagation theory is the wave energy balance:

$$\frac{\partial E}{\partial t} + \frac{\partial}{\partial x}\left(EC_g \cos(\alpha)\right) + \frac{\partial}{\partial y}\left(EC_g \sin(\alpha)\right) = -D_w - D_f \qquad \text{EQ. 2-1}$$

In this formula, E is the wave energy, C_g is the group velocity, α the wave direction with respect to the coast, D_w is the wave dissipation due to wave breaking and D_f is the wave dissipation due to bottom friction. The wave dissipation is calculated through the method of Roelvink (1993). The wave energy dissipation due to wave breaking is given by the formulation of Baldock, Holmes, Bunker, & Van Weert (1998).

Roller model
When waves break wave energy will be reduced rapidly and the energy will be transformed into roller energy throughout the roller model in Delft3D. The effect of wave breaking is not well understood, but ignoring the effect is as shown by recent studies not an option (Deltares, 2014). The energy balance for the roller model is shown below:

$$\frac{\partial E_r}{\partial t} + \frac{\partial}{\partial x}\left(2E_r C \cos(\alpha)\right) + \frac{\partial}{\partial y}\left(2E_r C \sin(\alpha)\right) = D_w - D_r \qquad \text{EQ. 2-2}$$

In this formula C is the wave celerity and D_r is the roller energy dissipation. The energy dissipation due to wave breaking is input for the roller model. The roller energy dissipation has influence on the surface stress.

2.1.3 *Suspended sediment model*

Suspended sediment transport is of large influence on the total amount of sediment transport. Especially near coasts with fine sediment. Suspended sediment is also important near wave breaking locations where a lot of turbulent mixing occurs.

Suspended sediment concentrations in Delft3D are calculated with the three-dimensional advection diffusion equation for suspended sediment (Deltares, 2014):

$$\frac{\partial c}{\partial t} + \frac{\partial uc}{\partial x} + \frac{\partial vc}{\partial y} + \frac{\partial c}{\partial z} - \frac{\partial}{\partial x}\left(\epsilon_{s,x}\frac{\partial c}{\partial x}\right) - \frac{\partial}{\partial y}\left(\epsilon_{s,y}\frac{\partial c}{\partial y}\right) - \frac{\partial}{\partial z}\left(\epsilon_{s,z}\frac{\partial c}{\partial z}\right) = 0 \qquad \text{EQ. 2-3}$$

In this equation the first term is the change of sediment concentration over time, the second and the third term are the change of sediment advection in the x and the y direction. The fourth term is the change of sediment concentration over depth. The last three terms are the sediment diffusivity in the x, y and z direction.

The bottom boundary conditions for EQ. 2-3 is calculated with the van Rijn(2007b) formula during this research. In this formula it is assumed that the sediment concentrations in the water column depends on a reference concentration on a reference height near the bed (see Figure 2-1).

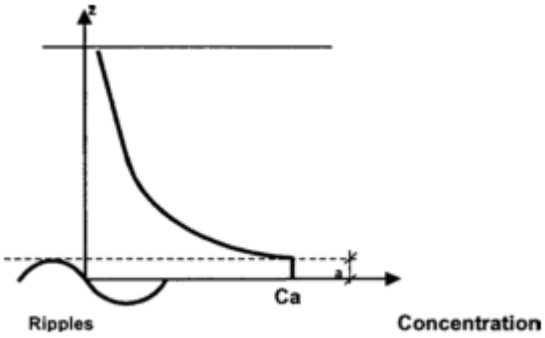

FIGURE 2-1: SUSPENDED SEDIMENT CONCENTRATION PROFILE OF THE VAN RIJN (2007B) METHOD. CA IS THE REFERENCE CONCENTRATION AND THE REFERENCE HEIGHT A.

The reference concentration c_a is calculated with the following formula:

$$c_a = 0.015(1 - P_{clay}) f_{silt} \frac{d_{50}}{a} \frac{T^{1.5}}{D_*^{0.3}} \quad \text{EQ. 2-4}$$

In this formula, $f_{silt} = 1$ for sand, $D_* = d_{50}\left[(s-1)\frac{g}{\nu^2}\right]^{1/3}$ is the dimensionless particle parameter, d_{50} is the median particle size of bed material, T is the dimensionless bed-shear stress parameter given by:

$$T = \frac{\tau'_{b,cw} - \tau_{b,cr}}{\tau_{b,cr}} \quad \text{EQ. 2-5}$$

With $\tau_{b,cr}$ is the time averaged critical bed shear stress and $\tau'_{b,cw}$ is the time averaged effective bed shear stress due to waves and currents. The reference level a from EQ. 2-4 is given by:

$$a = \max(0{,}5k_{s,c,s}, 0{,}5k_{s,w,s}) \quad \text{EQ. 2-6}$$

In this formula $k_{s,c,s}$ is current-related nikuradse roughness height and $k_{s,w,s}$ is the wave-related nikuradse roughness height. The total sediment transport per unit width is given by the integration of the net current u and the sediment concentration c between the reference level a and the still water level h:

$$q_{s,c} = \int_a^h u(z)c(z)dz \quad \text{EQ. 2-7}$$

2.1.4 *Bed load sediment*

The bed load sediment transport calculated by van Rijn (2007a) and the SANTOSS transport formula (van der A et al., 2013) will be compared with measurements during this research. Improving the SANTOSS formula is the objective of this research, the SANTOSS formula will be discussed separately in the next section. The van Rijn (2007a) model will be discussed in this section.

The van Rijn (2007a) model is a slightly diffent model then the the approximation method proposed by Van Rijn (1984a). This is done to better deal with steady flow including waves. The van Rijn (2007a) model reads:

$$q_b = \gamma \rho_s f_{silt} d_{50} D_*^{-0.3} \left(\frac{\tau'_{b,cw}}{\rho} \right)^{0.5} \left(\frac{\tau'_{b,cw} - \tau_{b,cr}}{\tau_{b,cr}} \right)^{\eta}$$ EQ. 2-8

γ And η are herein coefficients with respectively the values 0.5 and 1. ρ_s Is the sediment density. $\tau_{b,cr}$ Is the critical bed shear stress according to Shields. $\tau'_{b,cw}$ Is the grain-related bed-shear stress due to both currents and waves given by:

$$\tau'_{b,cw} = 0.5 \rho_w f'_{cw} \left(U_{\delta,cw} \right)^2$$ EQ. 2-9

With $U_{\delta,cw}$ is the velocity due to currents and waves at the edge of the wave boundary layer. f'_{cw} Is the grain friction coefficient due to currents and waves at this is given by the following formulation:

$$f'_{cw} = \alpha \beta f'_c + (1 - \alpha) f'_w$$ EQ. 2-10

In this formula α is a coefficient related to relative strength of wave and currents given by $\alpha = \frac{u_c}{(u_c + U_w)}$. β Is a coefficient related to the vertical structure of the velocity profile. f'_c And f'_w are the current and wave related grain friction based on the grain related roughness $k_{s,grain}$

$$f'_c = \left[18 \log \left(\frac{12h}{k_{s,grain}} \right) \right]^2$$
$$f'_w = \exp \left[-6 + 5.2 \left(\frac{A_w}{k_{s,grain}} \right)^{-0.19} \right]$$ EQ. 2-11

With h is the water depth and A_w is the peak orbital diameter near the bed.

In the bed-load transport vector an estimation for suspended sediment caused by wave asymmetry (See Figure 1-2) effects is also present:

$$q_{s,w} = f_{SUSW} \gamma V_{asym} \int_a^{\delta} c dz$$
$$V_{asym} = \frac{\left[(U_{on})^4 - \left(U_{off} \right)^4 \right]}{\left[(U_{on})^3 + \left(U_{off} \right)^3 \right]}$$ EQ. 2-12

With $q_{s,w}$ is the wave related suspended transport, f_{SUSW} is a user defined tuning parameter, γ is the phase factor with a value of 0.1 and V_{asym} is the velocity asymmetry factor. V_{asym} is calculated with the offshore (U_{off}) and onshore (U_{on}) peak orbital velocity. The concentration between van Rijn's (2007b) reference height a and the thickness of the suspension layer near the bed δ is taken into account to calculate the wave related suspended load. The suspension layer near the bed is given by $\delta = 3\delta_s$, with δ_s is the near bed sediment thickness layer.

2.2 SANTOSS model

2.2.1 *General*

The SANTOSS model is a newly developed practical sand transport formula that predicts the near bed net sand transport under non-breaking regular waves (van der A et al., 2013).

This new transport formula distinguishes itself from other formulas because it is a so-called semi-unsteady model taking phase lag effects into account (see section 2.2.2). This differs from quasi-steady sand transport formula because those formulas assume that sand transport immediately

reacts to flow conditions (da Silva, Temperville, & Seabra Santos, 2006). Semi unsteady formulas can also take effect from previous flow conditions on sand transport into account. The SANTOSS model is very useful for cross-shore sand transport under wave dominated conditions. The transport formula is based on the half wave-cycle concept from Dibajnia & Watanabe (1992), which describes the total net transport as the difference between the transported during the positive “crest” half cycle and the negative “trough” half-cycle. Using the sediment transported in the current half-cycle and which is entrained in the previous half cycle phase lag effects can be applied.

The net transport rate is given by the following formula (van der A et al., 2013):

$$\vec{\phi} = \frac{\vec{q}_s}{\sqrt{(s-1)gd_{50}^3}} = \frac{\sqrt{|\theta_c|}T_c\left(\Omega_{cc} + \frac{T_c}{2T_{cu}}\Omega_{tc}\right)\frac{\vec{\theta}_c}{|\theta_c|} + \sqrt{|\theta_t|}T_t\left(\Omega_{tt} + \frac{T_t}{2T_{tu}}\Omega_{ct}\right)\frac{\vec{\theta}_t}{|\theta_t|}}{T} \quad \text{EQ. 2-13}$$

The formula uses non-dimensional bed shear stress as the main forcing parameter. T_i and T_{iu} are the periods and the acceleration period of the crest and the trough (See Figure 2-2). The sand load entrained during each half wave Ω_i is given by the following formula:

$$\Omega_i = \begin{cases} 0 & if|\theta_i| \le \theta_{cr} \\ m(|\theta_i| - \theta_{cr})^n & if|\theta_i| > \theta_{cr} \end{cases} \quad \text{EQ. 2-14}$$

With $\theta_{cr}$is the critical Shields number, which is in the SANTOSS formula calculated according to Soulsby (1997). The Shields parameter vector $\vec{\theta_i}$ is calculated as follows (van der A et al., 2013).

$$\vec{\theta}_i = \left\{\frac{\frac{1}{2}f_{w\delta i}|u_{i,r}|u_{i,rx} + \tau_{wRe}}{(s-1)gd_{50}}, \frac{\frac{1}{2}f_{w\delta i}|u_{i,r}|u_{i,ry}}{(s-1)gd_{50}}\right\} \quad \text{EQ. 2-15}$$

In which the wave current friction factor $f_{w\delta}$ is calculated as the linear combination of the wave friction factor and the current friction factor (Ribberink, 1998). The wave Reynolds stress τ_{wRe} is a stress contribution due to progressive surface waves (Fredsoe & Deigaard, 1992; Nielsen, 2006). $u_{i,r}$ Is the root mean square velocity of a sinusoidal flow and $u_{i,rx}$ and $u_{i,ry}$ are the combined wave-current velocity vectors in the x and the y direction. The velocities are a combination of the orbital velocity of the waves and the current related velocity. The orbital velocity caused by wave will vary over time and over orientation. The orientation of the whole model is in the same direction as the orientation of the waves.

2.2.2 *Phase lag*

In the SANTOSS formula there are four contributions to the net sand transport (van der A et al., 2013). These are the sediment entrained and transported during the crest (Ω_{cc}) and the trough (Ω_{tt}) period and the sediment entrained in the crest and trough period transported respectively in the trough (Ω_{ct}) and the crest period (Ω_{tc}) (see Figure 2-2). Phase lag effects can especially be expected with a rippled bed during oscillatory flow conditions (van der Werf, Ribberink, O’Donoghue, & Doucette, 2006).

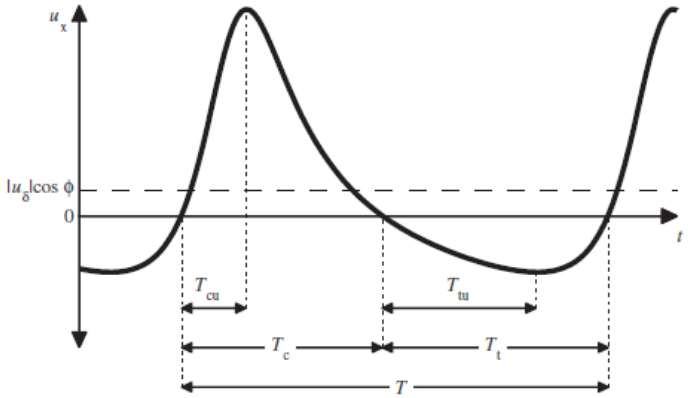

FIGURE 2-2: CREST AND TROUGH PERIODS OF OSCILLATORY FLOWS

Phase lag effects are implemented by dividing the sand entrained in the crest (Ω_c) and trough period (Ω_t) over transport in the current half wave cycle and the next half wave cycle. This is done by a phase lag parameter P_i. The phase lag parameters are calculated with the following formula:

$$P_c = \begin{cases} \alpha\left[\frac{1-\xi\hat{u}_c}{c_w}\right]\frac{\eta}{2(T_c-T_{cu})W_{sc}} & if\ \eta > 0\ (ripple\ regime) \\ \alpha\left[\frac{1-\xi\hat{u}_c}{c_w}\right]\frac{\delta_{si}}{2(T_c-T_{cu})W_{sc}} & if\ \eta = 0\ (sheet\ flow\ regime) \end{cases} \quad \text{EQ. 2-16}$$

$$P_t = \begin{cases} \alpha\left[\frac{1+\xi\hat{u}_t}{c_w}\right]\frac{\eta}{2(T_t-T_{tu})W_{st}} & if\ \eta > 0\ (ripple\ regime) \\ \alpha\left[\frac{1+\xi t}{c_w}\right]\frac{\delta_{si}}{2(T_t-T_{tu})W_{st}} & if\ \eta = 0\ (sheet\ flow\ regime) \end{cases} \quad \text{EQ. 2-17}$$

In which α is a calibration factor, η the ripple height calculated according to O'Donoghue, Doucette, van der Werf, & Ribberink (2006), δ_{si} the sheet flow layer thickness according to Dohmen-Janssen (1999) and W_{si} is the sediment settling velocity within the half cycle. The term with ripple height or the sheet flow layer thickness represents a ratio of the representative stirring height and the sediment settling distance in one half wave cycle.

The terms between the square brackets in EQ. 2-16 and EQ. 2-17 present an effect of progressive waves on the phase lag behavior. The effect is horizontal sediment advection caused by horizontal non-uniformity in the wave field. Kranenburg, Ribberink, Schretlen, & Uittenbogaard (2013) show that this effect leads to a compression of sand during the wave crest and dilution of sand during the wave trough. This causes a net transport in the direction of the wave propagation.

If the phase lag parameter P_i is lower than or equal to 1 there is no phase lag. If P_i exceeds 1 there is a phase lag. The fraction of the sand entrained that will be transported with a phase lag is than $1-\frac{1}{P_i}$. The fraction that is transported in the same half wave period it was entrained is then $\frac{1}{P_i}$ (van der A et al., 2013).

2.2.3 *Flow Regime*

EQ. 2-16 and EQ. 2-17 show that there are different calculations for different regimes to calculate the phase lag parameter. The determination of the flow regime depends on the presence of ripples. If the ripple height is zero ($\eta = 0$) then there is sheet flow. The ripple height and the ripple length are given by (O'Donoghue et al., 2006):

$$\frac{\eta}{\hat{a}} = m_\eta n_\eta \left(0.275 - 0.022\hat{\psi}^{0.42}\right)$$
$$\frac{\lambda}{\hat{a}} = m_\eta n_\eta \left(1.97 - 0.44\hat{\psi}^{0.21}\right)$$
EQ. 2-18

With η is the ripple height, λ is the ripple length, m_η and n_η are parameters depending on respectively the median grain size d_{50}, and the mobility number $\hat{\psi}$ and $\hat{a}$ is the orbital excursion amplitude. The mobility number depends on the flow properties:

$$\hat{\psi} = \frac{\max(\widehat{u_c}, \widehat{u_t})^2}{(s-1)g d_{50}}$$
EQ. 2-19

With $\widehat{u_c}$ is the peak orbital crest velocity, $\widehat{u_t}$ is the peak orbital trough velocity and s is the relative density of the sediment particles. The flow regime is quite important for the direction of the predicted sediment transport. When ripples are present it is most likely that phase lag occurs and the sediment transport will probably be offshore directed. For sheet-flow the sediment transport will probably be onshore directed.

2.2.4 *Implementation in Delft3D*

The Santoss model has been implemented in Delft3D by Veen (2014). During this implementation it seemed that some conceptual expansion of the SANTOSS model was required. SANTOSS requires intra wave velocities. Intra-wave velocities are not calculated in Delft3D since Delf3D just calculates the forcing by waves. Therefore, Veen (2014) implemented the approximation method of Abreu, Silva, Sancho, & Temperville (2010) by Ruessink, Ramaekers, & Van Rijn (2012) for the intra wave velocities in Delft3D. In this method the orbital flow characteristics are calculated. The velocity skewness and acceleration skewness required for SANTOSS are calculated from these orbital flow characteristics.

Another conceptual expansion is that the calculation for the crest and trough periods and the duration of the acceleration period of the crest and trough (See Figure 3-11) are based on the intra wave velocities. Previously the crest and trough periods were calculated with an approximation method using the peak orbital crest and trough velocity and the acceleration skewness.

2.3 Model set-up

In this section the grid used during the calibration will be shown. Also some initial and boundary conditions will be discussed. At last, some model settings will be discussed in this section.

2.3.1 *Grid*

The model grid consists of 263 cross-shore grid locations, one grid cell in the alongshore direction and 24 vertical layers. The grid is finest near the location of the breaker bar (~0.2 meter length for one grid cell). Near the boundaries the grid is much coarser (~0.9 meter length of one grid cell). This is a very fine grid, but this is desirable due to detailed measurements and energetic conditions (regular breaking waves, steep breaker bar and sheet flow conditions) The water depth near the open boundary (left side of the grid) is 2.55 meter. The grid is shown in Figure 2-3. The time-step used in the model is 0.06 seconds. This is required to deal with the drying and flooding conditions and corresponding Courant numbers near and at the shore.

A vertical layer dependency analysis has been done in Appendix B; the amount of layers does not have much effect on the hydrodynamics. When using six layers the distribution on the undertow seems a little bit rough. Twelve Layers is suitable to predict the hydrodynamics. For the suspended sediment concentration some more layers are required. The model results for the suspended sediment concentration converge with an increasing number of layers (See Figure

B-2). The model results using 24 and 36 layers are almost equal. Therefore 24 vertical layers will be used for further calculations. The layers thickness is defined as a percentage of the water depth and is as follows: 1%, 1.3%, 1.6%, 2%, 2.4%, 3.1%, 3.8%, 4.8%, 5.8%, 7%, 8.2 %, 9%, 9%, 8.2%, 7%, 5.8%, 4.8%, 3.8%, 3.1%, 2.4%, 2%, 1.6%, 1.3% and 1%.

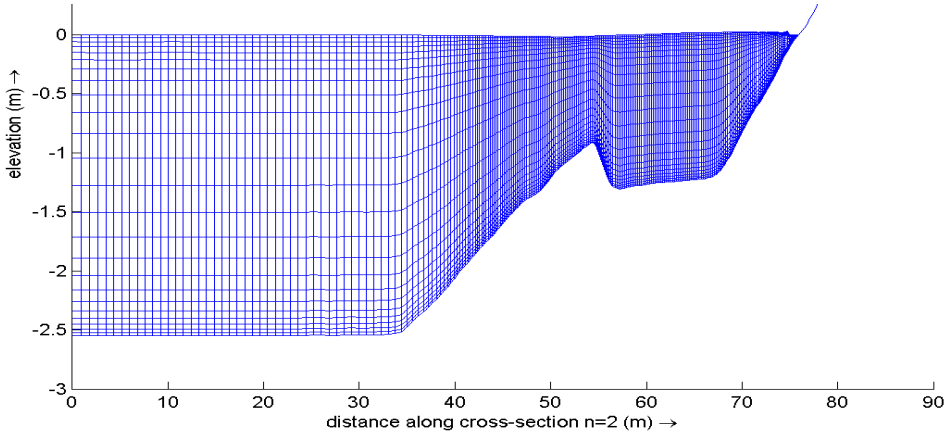

FIGURE 2-3: GRID DIMENSIONS.

2.3.2 *Initial and boundary conditions*

Initial conditions and boundary conditions are required to be able to run the model. The initial conditions are conditions that are specified at the start of the model run (t = 0 s). One of these initial conditions is the water level. The initial water level is set uniform to 0 meter. The other initial condition is the sediment concentration in the water column; this is set to 0 kg/m^3. During the measurements the water level in the wave flume was at rest. The sediment had the time to settle down; therefore the sediment concentration in the model has to be set to zero as well.

There is an open boundary in the model at location x = 0 m (see Figure 2-3). Waves are generated at the open boundary. The wave period is specified at four seconds and the waves are directed from the open boundary (x = 0) towards the beach. During the measurements the wave height was set by a wave paddle at 0.85 m. During the measurements it seemed that the wave height was not equal to 0.85 m. During the calibration there is accounted for the difference between the target wave height and measured wave height.

2.3.3 *Model settings*

The grain sizes used in the model are equal to the measured grain sizes. The median grain size (D50) is 246 µm. The 10 percentile grain size (D10) and the 90 percentile grain size (D90) are respectively 154 and 372 µm. The specific density, the density of the sediment with respect to the density of water is equal to 1.65.

The bottom roughness is of minor importance for waves. Even though, a bottom roughness is required. During the measurements the bottom roughness was not uniform. At the start of the wave flume (from x = 0 to x ~ 38 m) there was a smooth concrete bottom. For this part a Chezy roughness with a Chezy coefficient of 85 m$^{1/2}$/s has been used. In the middle part (From x ~ 38 to x ~ 68 m) there was a sandy bottom, for this part the bottom roughness caused by bed-forms has been used as bottom roughness. At the end of the flume (from x ~ 68 m) the sandy bottom was covered with plastic, iron and concrete tiles. The bottom was much rougher at this part than at the beginning of the flume. A Chezy roughness with a Chezy value of 45 m$^{1/2}$/s is used at the end of the flume. The bottom roughness in the middle part of the flume caused by bed forms is computed by a quadratic combination of roughness from ripples and mega ripples using the method of van Rijn (2007a). From the measurement it seemed that rippled bed forms are

especially important behind the breaker bar and the roughness caused by the breaker bar can be modeled as a roughness caused by megaripples.

Morphodynamic updating has been switched off during the calibration. The bottom used during modeling in Delft3D is fixed to exclude morphodynamic effect. Morphodynamics are an additional complexity during modeling and are not necessarily required to improve the modeling of sediment transport in Delft3D with the SANTOSS model for breaking wave effects. To minimize the effect of bottom development on the measurement only the measurements of the first measurement run on each day has been used (van der Zanden et al., 2015).

2.4 Description of the dataset

The processes under breaking waves are not well understood and therefore new large scale experiments on breaking waves in the CIEM wave flume in Barcelona have been done (van der Zanden et al., 2015). The wave flume is 100 m long and 3 m wide. At one side of the flume a wave paddle is located and at the other side of the wave flume a beach is constructed. With this wave paddle regular breaking waves were generated.

2.4.1 *Set-up*

The set-up of the experiment is shown in Figure 2-4. The wave paddle is shown on the left and the beach is shown on the right. The waves are breaking at the top of the breaker bar. Measurements are done with a mobile-frame trolley and a profiling trolley. Measurements with the mobile-frame trolley are done every run of 15 minutes. In total six runs of 15 minutes have been done. After every two runs of 15 minutes the whole bed profile has been measured with the profiling trolley. After one day of measurements the mobile-frame trolley is relocated and the bottom profile is restored to the initial bottom profile. The mobile-frame trolley is located at 12 different locations around the breaker bar (see Figure 2-5). In this way very detailed measurements around the breaker bar are available.

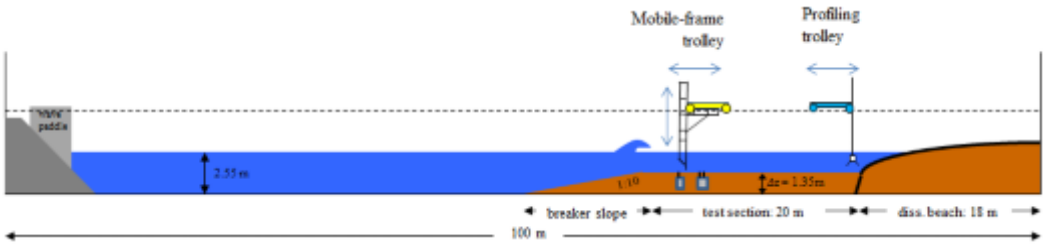

FIGURE 2-4: SET-UP OF THE CIEM WAVE FLUME EXPERIENTS (VAN DER ZANDEN ET AL., 2015)

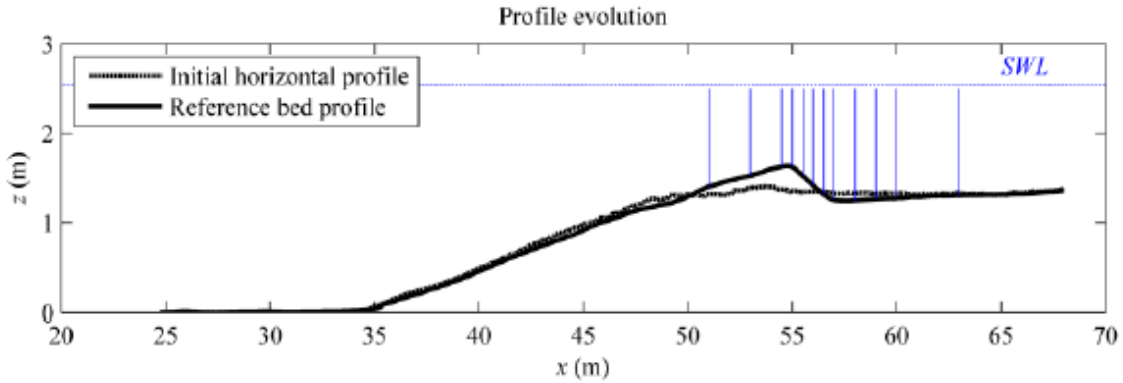

FIGURE 2-5: MEASUREMENTS LOCATIONS

2.4.2 *Regular breaking waves*

During the experiment regular waves which break at the top of the breaker bar were generated. The waves had a period of four seconds and the target wave height at the wave paddle was 0.85 meter. The water level near the wave paddle was 2.55 meter. The bottom slope was 1:10 which creates a plunging wave. The results of the measurements for the velocity, the net sediment transport and the suspended sediment transport will be discussed in the next sections.

Aim of this experiment was to simulate energetic field conditions, the wave height is relative large compared to the water depth. This caused sheet flow in front of the breaker bar. Sheet flow conditions occur when the flow has a high mobility number. A simplification during the measurements compared to field conditions were the generating of regular breaking waves. Wave regularity causes wave breaking at a steady location. This causes a breaker bar with very steep slope. This is visible in Figure 2-6.

2.4.2.1 Net Sand transport

The net sediment transports are calculated from the bed profile changes measured with the profiling trolley. The difference in bed profile between two successive runs can be used to calculate the net sediment transport with the following formula.

$$\frac{\partial q_s}{\partial x} = (1-\epsilon)\frac{\partial z_b}{\partial t} \qquad \text{EQ. 2-20}$$

Since the sediment transport at the wave paddle is known and equal to zero the sediment transport at every location in the flume can be calculated. The porosity ϵ is assumed to be 0.4.

The changes in bed profile are shown in Figure 2-6. It is clearly visible that the breaker bar evolves throughout the experiment. In 365 minutes the breaker bar increases with approximately 50 centimeter. The bed levels in front and behind the breaker bar decreases. This would imply that net sediment transports are onshore in front of the breaker bar and offshore behind the breaker bar. This is confirmed in Figure 2-6, which represent the net sediment transport.

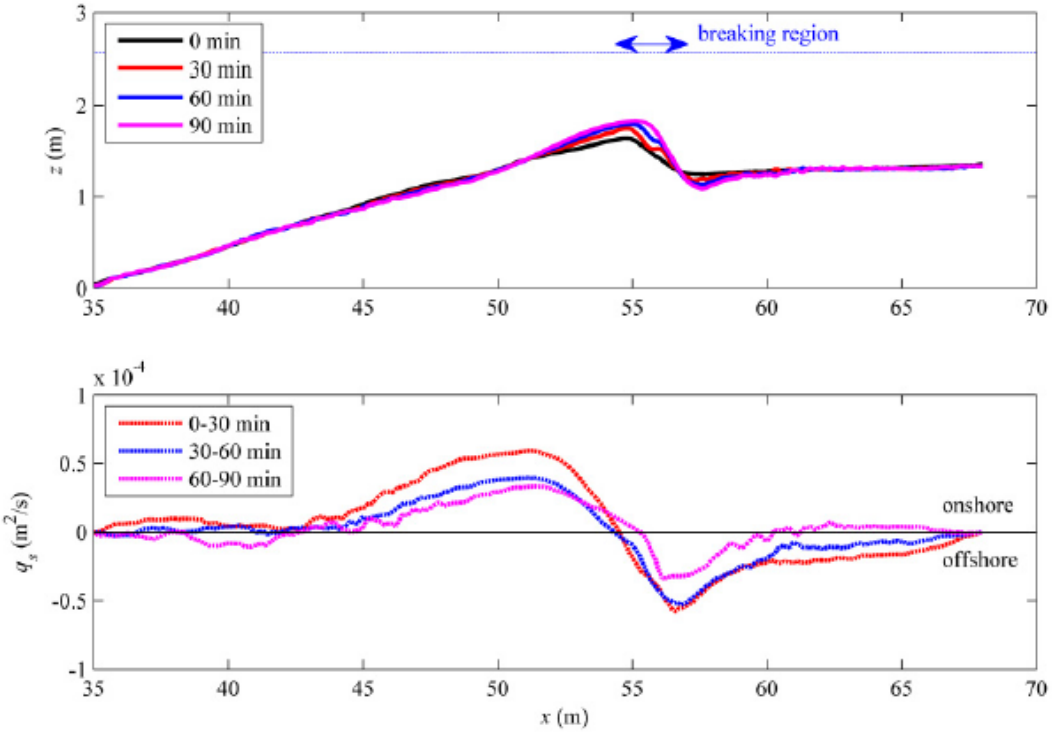

FIGURE 2-6: BED EVOLUTION AND NET SEDIMENT TRANSPORT DURING THE CIEM WAVE FLUME EXPERIMENTS (VAN DER ZANDEN ET AL., 2015)

2.4.2.2 Velocities

The velocities are measured with the mobile-frame trolley. Velocities are measured in three dimensions and at three locations at the mobile-frame trolley. The most important location is approximately 11 centimeter above the bed. At every measurement location along the flume the distance between the bed and the lowest velocity measuring device (ADV) was set at 11 centimeter. The measurements results in maximum and minimum orbital velocity. The minimum velocity for the trough and the maximum velocity for the crest are shown in Figure 2-7. The velocities have also been measured with an Acoustic Concentration and Velocity Profiler (ACVP), this device measures the velocity profile from the bed to 15 centimeter above the bed.

Next to the oscillatory flow an undertow was observed. Figure 2-7 shows the undertow as an offshore directed superimposed current. Net offshore currents where mainly observed near the bottom, that is why the current is called an undertow. The undertow was highest at the lee side of the breaker bar.

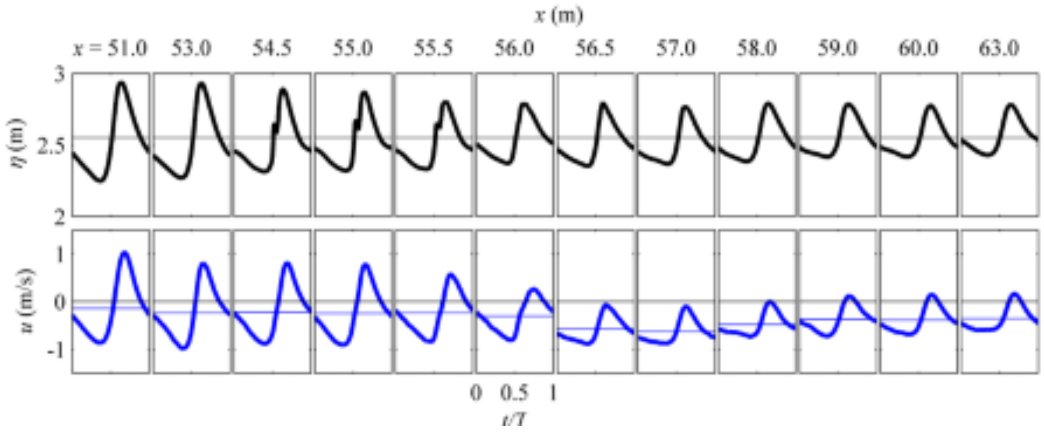

FIGURE 2-7: PHASE-AVERAGED WATER SURFACE ELEVATION AND PHASE AVERAGED HORIZONTAL VELOCITIES FROM T=0 TO T = 15 MINUTES. THE HORIZONTAL BLUE LINE INDICATES THE MEAN CURRENT

2.4.2.3 Suspended sediment

At the mobile-frame trolley there are also some measurement devices that measure the average suspended sediment concentration (TSS device). Together with the undertow this concentration can help calculating the current related suspended sediment transport. In Figure 2-8 the time-averaged suspended sediment concentrations are shown.

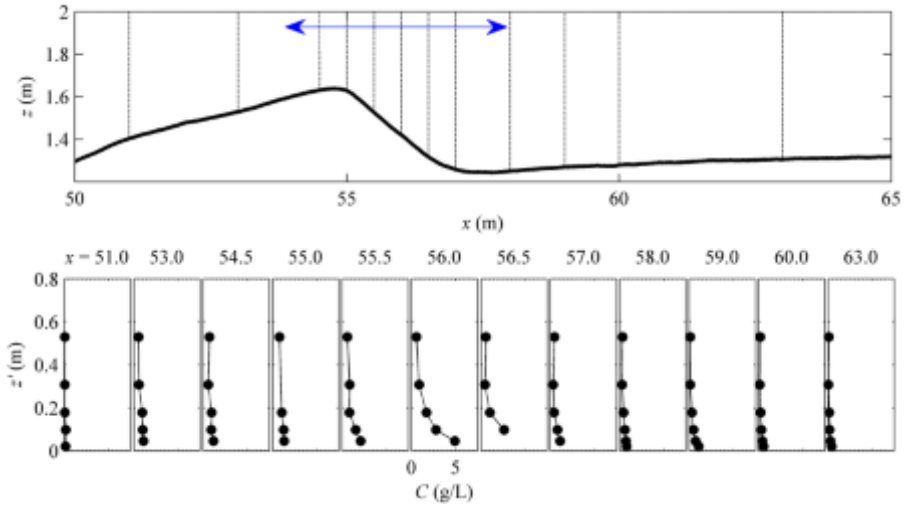

FIGURE 2-8: TIME AVERAGED SUSPENDED SEDIMENT CONCENTRATION DURING THE CIEM WAVE FLUME EXPERIMENTS. THE FIRST FIGURE SHOWS THE LOCATION OF THE MEASUREMENTS, THE SECOND FIGURES SHOWS THE SUSPENDED SEDIMENT CONCENTRATION.

It is visible that behind the breaker bar where the jet of the breaking wave would probably hit the bed the sediment concentration are clearly larger than at other locations.

3 MEASURED AND MODELED HYDRODYNAMICS

In this section it will be examined how well Delft3D (see section 2.1 for an introduction of Delft3D) can reproduce the hydrodynamics measured during the CIEM wave flume experiments. Firstly the measured hydrodynamics and the reproduction of those hydrodynamics by Delft3D will be examined. During the reproduction of these hydrodynamics, some improvements for regular breaking waves have been tested; these tests will be discussed as well. Secondly the measured wave skewness and wave asymmetry will be shown and the reproduction by the parameterization method used in Delft3D will be discussed. At last, some conclusions of this section will be drawn.

3.1 Hydrodynamics

The model set-up used during this project is discussed in section 2.3. Delft3D contains user defined calibration parameters and input settings. The goal of the calibration is to approach the results of the measurements with the model predictions by adapting the calibration parameters and the input settings. During the calibration the modeled results will be compared with the measurements. This comparison will be evaluated and as long as the modeled results are not satisfying enough the input calibration parameters and the input settings will be adjusted.

The paper of Giardino, Brière, & van der Werf (2011) and Veen (2014) have been used as a guideline during the calibration of the hydrodynamics. During the calibration of the hydrodynamics the modeled wave height, set-up and undertow are compared with the measurements. Delft3D has a number of calibration parameters that influence the hydrodynamic output. The hydrodynamic parameters in Table 3-1 are the parameters that are used for the hydrodynamic calibration. The physical meaning of the parameters and the formulations in which the parameters are used are discussed as well. The calibrated parameter value has been shown in this table as well.

Next to the calibration parameters there are user defined formulations which are discussed. The implementation of the formulas in the Delft3D model will be discussed firstly.

TABLE 3-1: OPTIMAL HYDRODYNAMIC PARAMETER SETTING

Parameter	Description	Symbol	Value
Hs	Wave height at wave paddle	H_s	0.80 m
Fwee	Bottom friction factor	f_w	0
Gamdis	Wave breaking index	γ	0.58
Alfaro	Roller dissipation coefficient	α_{rol}	6
F_lam	Breaker Delay	F_lam	0
Betaro	Rollers lope parameter	β_{rol}	0.2
Vicouv	Bankground horizontal eddy viscosity	υ_H^{back}	0 m^2/s
Vicoww	Background vertical eddy viscosity	υ_V^{back}	0 m^2/s
Alfa	Reflection parameter	α	0
Dryflc	Dyring and flooding criterion		0.2 m

Delft3D has a drying and flooding criterion which determines the minimum water depth required for computations. Due to a large number of vertical layers Delft3D cannot work with the hydrodynamics on such a small scale near area which successively drying and flooding. If the drying and flooding criterion is too low, water levels will vary due to computational errors near the drying and flooding area. The drying and flooding criterion is therefore set to 0.2 meter. When the

water depth at certain locations is lower than 0.2 m, then Delft3D will not perform computations for those locations.

3.1.1 *Formulations*

In the turbulent closure schemes there is accounted for increased roughness effects due to waves. The additional bed shear stress is added to the roughness height. In Delft3D there are different formulations which can calculate this additional bed shear stress. The wave stress formula of van Rijn, Walstra, & Ormondt (2004) have been used. This wave stress formula predicted the undertow best.

Delft3D has four different turbulence closure models which can be used. Turbulence and space varying viscosity is very important for predicting the strong undertow. The k-epsilon turbulence closure models predict the undertow best at most locations. Therefore this closure model has been used.

3.1.2 *Wave height*

The wave heights are measured with Resistance Wave Gauges (RWGs) and Pore Pressure Transducers (PPTs). There were two kinds of PPTs, those located at the wall at different location in the wave flume and the PPT located at the measurement frame. The wave heights were averaged over all measurement runs. Error bars have been included to indicate errors due to difference between runs.

The wave heights measured at the mobile frame were not as reliable as other measured wave heights and those wave heights have therefore been excluded from this research. The measured wave heights are shown in Figure 3-1.

The wave height in the roller model in Delft3D is determined by the linear wave theory. In the linear wave theory the wave height is calculated from the wave energy.

$$E = \frac{1}{8}\rho_w g H_{rms}^2 \qquad \text{EQ. 3-1}$$

In this formula E is the short wave energy, ρ_w is the specific density of water, g is the acceleration gravity and H_{rms} is the root mean square wave height. Since there are regular waves, the wave averaged wave heights do not change over time. So the short wave energy formulation changes to:

*
$$E = \frac{1}{8}\rho_w g H^2 \qquad \text{EQ. 3-2}$$

The wave energy balance in Delft3D is dependable on energy change over the 2 horizontal directions as shown in EQ. 2-1. During the measurements the wave energy only changes over one direction. In the Delft3D model this direction is the x direction. Also the angle of the wave ray with respect to the coast line was zero during the measurements. This reduces the energy balance to:

$$\frac{\partial}{\partial x}\left(E c_g\right) = -D_w - D_f \qquad \text{EQ. 3-3}$$

The wave energy dissipation is given by the parameterization of Baldock et al. (1998):

$$D_w = \frac{1}{4}\alpha_{rol}\rho_w g f_p \exp\left(-\frac{H_{max}^2}{H_{rms}^2}\right)\left(H_{max}^2 + H_{rms}^2\right) \qquad \text{EQ. 3-4}$$

With α_{rol} is the roller dissipation coefficient (Alfaro), ρ_w the water density, g the gravitational acceleration, f_p the peak frequency, H_{max} the maximum wave height and H_{rms} the root mean square wave height.

The parameterization of Baldock et al. (1998) is developed for irregular waves. During the calibration there are regular waves. Therefore the formula for energy dissipation due to breaking waves has been changed to a formula applicable for regular waves proposed by Van Rijn & Wijnberg (1996).

*
$$D_w = \frac{1}{4}\alpha_{rol}\rho_w g \frac{1}{T} H_{max}^2 Q_b \qquad \text{EQ. 3-5}$$

With Q_b is parameter indicating wave breaking, Q_b is 1 when waves break and Q_b is 0 when waves are not breaking. Waves break when the relative wave height is larger than the wave breaking index $\left(\frac{H_{rms}}{h} > \gamma\right)$.

Applying just the conditions mentioned above seemed not suitable (See Appendix C.1). Therefore another condition has been implemented based on the measured decreasing wave height. A criterion has been added to the source code, waves continue breaking as long as the wave height during the next step is higher than a relative depth (reldep parameter in Delft3D). This relative depth has been extracted from the measurements and is set to 0.35 meter. This results in the following wave breaking conditions:

*
$$\begin{aligned} &Q_b = 1 && if \quad \frac{H_{rms}}{h} > \gamma \\ &Q_b = 1 && if \quad Q_{b_{x-1}} = 1 \; and \; H_{rms_{x+1}} > reldep \\ &Q_b = 0 && otherwise \end{aligned} \qquad \text{EQ. 3-6}$$

This transition from breaking to non-breaking and the adaptation of the source code is explained in Appendix C.1. The reasoning behind the changes to the source code is explained as well. The effect of different energy dissipation due to wave breaking models on the wave height is shown in Figure C-1.

With the formulation for the energy dissipation due to wave breaking changed it is much easier to better predict the steep decrease of the wave height due to wave breaking. The steepness of the slope is determined by the roller dissipation coefficient (Alfaro). The default value for Alfaro is 1 and the advised range of Alfaro is between 0.5 and 2. An Alfaro of 6 was required to predict the energy dissipation due to wave breaking well (Figure D-1). A lower value for Alfaro reduces the wave energy dissipation due to wave breaking; the decrease in wave height would be underestimated using a lower value for Alfaro. So it seems that the wave breaking model used still underestimates the energy dissipation due to wave breaking.

The maximum wave height from EQ. 3-5 is given by:

$$H_{max} = \frac{0.88}{k}\tanh\left(\frac{\gamma}{0.88}kh_{ref}\right) \qquad \text{EQ. 3-7}$$

k Is the wave number in this formula and γ is the wave breaking index (Gamdis). The wave breaking index (Gamdis) is an important parameter to determine the wave breaking location (See Figure D-2). A wave breaking index of 0.58 is used which is in the advised range. A wave breaking index of 0.58 gives the proper location for wave breaking. A lower value causes waves that breaker to early and higher values then 0.58 cause's waves that break too late. The breaker delay accounts for the effect that it takes approximately an order of one wave length to start and

stop breaking (Roelvink, Meijer, Houwman, Bakker, & Spanhoff, 1995). A breaker delay is not required since the location of wave breaking has been calibrated with the wave breaking index.

The energy dissipation due to bottom friction is given by (Stive & Vriend, 1994; Svendsen, 1984):

$$D_f = f_w \frac{\rho_w}{\sqrt{\pi}} u_{orb}^3 \qquad \text{EQ. 3-8}$$

In this formula f_w is a bottom friction parameter and u_{orb} is the orbital velocity of the waves. The energy dissipation due to bottom friction has been excluded, even though the wave height is overestimated offshore of the breaker bar. If the bottom friction would have been included the peak wave height in front of the breaker location would be lower than the current peak wave height. The calibration, with the parameter values as mentioned above, results in the wave heights shown in Figure 3-1.

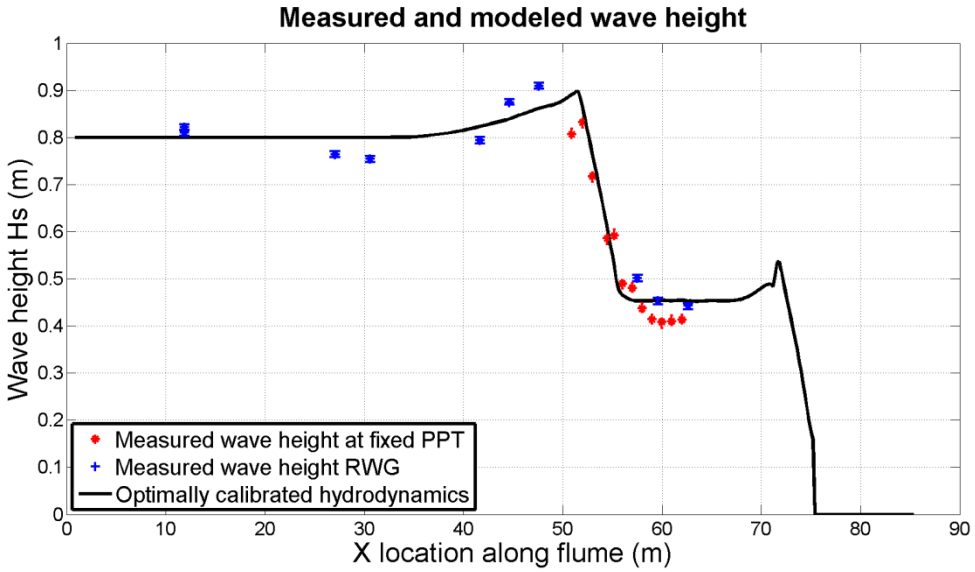

FIGURE 3-1: CALIBRATED WAVE HEIGHTS. THE LINE SHOWS THE CALIBRATED WAVE HEIGHTS, ASTERISK SHOW THE MEASURED WAVE HEIGHT WITH PPT'S AND THE PLUS SIGN SHOW THE MEASURED WAVE HEIGHT WITH THE RWG'S.

3.1.3 *Set-up*

The set-up is just as the wave height derived from the RWG and PPT water level measurements. The set-up measured with the PPT at the mobile frame has been excluded from the results because of the unreliability of these measurements (See section 3.1.2). The set-down at the beginning of the flume, where no set-down is to be expected, is larger than zero. This suggests that either the set-down is overestimated or that the water level was not exactly 2.55 meter. Around and behind the breaker bar from X = 50 m and onshore set-up occurs.

The set-up in Delft3D can be influenced by the energy dissipation of the roller model. Energy of the roller will be transferred to the water column in the energy balance of the roller model. The energy balance of the roller model is derived from EQ. 2-2 and is as follows:

$$\frac{\partial}{\partial x}\left(2E_r c_{ph}\right) = D_w - D_r \qquad \text{EQ. 3-9}$$

The roller energy dissipation given by:

$$D_r = 2\beta_{rol} g \frac{E_r}{c_{ph}} \qquad \text{EQ. 3-10}$$

The parameter β_{rol} (Betaro) in this formula is important for determining the set-up and the undertow. This parameter determines the wave energy transferred from the roller model to the underlying water, this parameter barely has effect on the wave height. This makes it possible to separately calibrate the wave height and the set-up.

The set down is underestimated for the largest part of the wave flume (see Figure 3-2). The set-down in front of the wave breaking seems impossible to obtain. Only by using uncommon values for the certain parameters the set-up in the breaker region was modeled quite well, but this caused fluctuation in the set-down in front of the wave breaking location and this also causes poor predictions of the undertow. The set-up as shown causes the best prediction of the undertow. To obtain this set-up the background vertical and horizontal eddy viscosity (Vicouv and Vicoww) have been set to zero. The roller slope parameter (Betaro) has been set to 0.2, this was especially important for the undertow. Also the set-up experiences effects from changing the roller slope parameter. A roller slope parameter value of 0.2 caused a quite good prediction of the set-up and it causes an as well as possible prediction of the undertow.

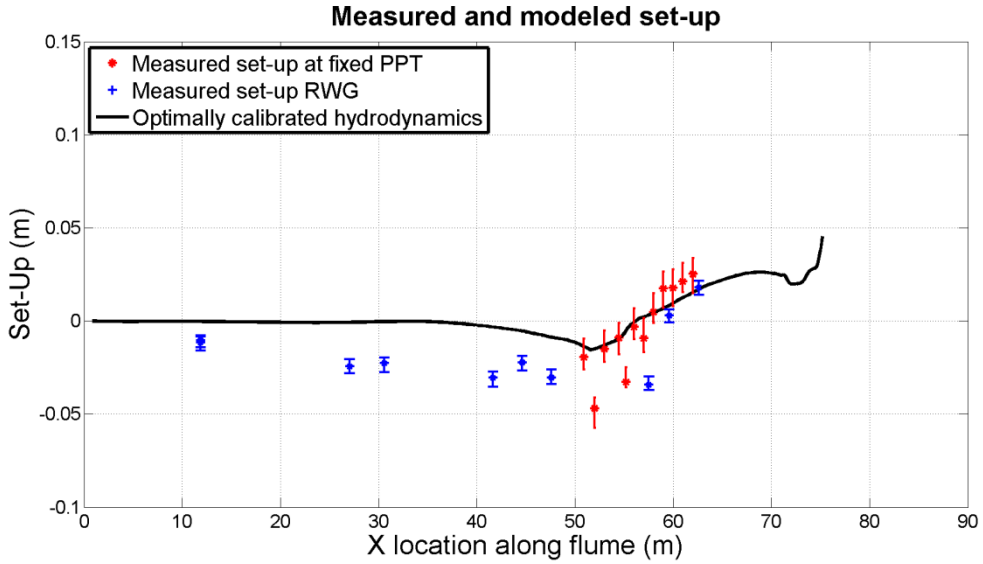

FIGURE 3-2: CALIBRATED SET-UP. THE LINE SHOWS THE CALIBRATED SET-UP, RED ASTERISK SHOW THE MEASURED SET-UP WITH PPT'S AND THE BLUE PLUS SIGN SHOW THE MEASURED SET-UP WITH THE RWG'S.

3.1.4 *Undertow*

The undertow compensates for the onshore directed mass transport under waves and under rollers called the Stokes drift due to respectively waves and rollers. The undertow is extracted from intra-wave velocity profiles measured with Acoustic Doppler Velocimeters (ADVs) and Acoustic Concentrations and Velocity Profilers (ACVPs). The ADVs measure the velocity at 11, 37 and 84 centimeter above the bed. The ACVPs measure the velocity profile from the bed to 15 centimeter above the bed with a vertical resolution of 0.15 centimeter. Both the ADVs and the ACVPs show quite reliable results. This is confirmed by the fact that the measurement obtained by the lowest ADV show almost equal results to the measurement obtained by the ACVP.

The undertow is equal to the average velocity. The average velocity near the bottom is directed offshore. Towards the still water level the net offshore current decreases and for some locations it becomes onshore directed. When the net current is integrated over the water depth the results will be equal to the onshore directed Stokes mass flux. The measured undertow is shown in

Figure 3-3. For some locations the ACVPs measure the undertow below the bed level. This has two reasons. The first reason is that during the measurement sometimes ripples appear and disappear, therefore the local bed level increases and decreases. The second reason is that the bed level is measured with a different measurement device; this causes differences in the measured bed level.

As mentioned in section 3.1.3 the undertow showed a strong relationship with the set-up. The parameter Betaro is important for the set-up and the undertow (See Figure D-3). The parameter settings to obtain the set-up shown above also predict the most optimal undertow. A lower value than 0.2 causes a better prediction on top of the breaker bar (x = 52.9 to x = 55.9 m), but this causes a worse prediction at the lee side of the breaker bar (x = 56.4 to x = 57.9 m). A higher value than 0.2 cause's inversed results compared to using a lower value for Betaro.

One parameter was changed to improve the undertow after improving the set-up. This is the reflection parameter; the reflection parameter alpha makes the open offshore water level boundary less reflective for disturbances that occur at the start of the computation. This reflection parameter damps small disturbances in the model out. It also damps out the undertow. Therefore the reflection parameter has been set to zero. To deal with the small disturbances, output has been averaged over the model time.

The best modeled undertow is shown in Figure 3-3. In front of the breaking location and behind the breaking location the undertow is predicted quite well. But it is very hard to predict the undertow near the breaker location well. The undertow is underestimated near the breaker locations (X locations 55.9 until 57.9 m). All parameters with possible effect on the prediction of the undertow have been varied. Improvements of the predicted undertow due to these variations where either not found or the predicted undertow improved for some locations and worsened for the other locations (See Appendix C for source code adaptations and Appendix D parameter adaptation).

Some adaptations to the source code have been done to test improvements for the prediction of the net current. Looking at the results it seems that the Stokes mass flux is underestimated behind the breaking location (x = 56.4 to x = 57.9 m). Therefore the Stokes drift due to rollers has been made depth dependable according to Uchiyama, McWilliams, & Shchepetkin (2010). After testing the depth dependable Stokes drift it seemed that for some location the undertow was predicted better (From x = 55.9 to x = 57.9 m) and for the other locations the predictions of the undertow got worse (See Figure C-3). The derivation of the depth dependable Stokes drift due to rollers and the results obtained after using this equation are shown in Appendix C.2. When using the depth dependable stokes drift due to rollers the undertow for most locations became worse, therefore this equation for the Stokes drift has not been used.

The best obtainable results are shown in Figure 3-3 including an indication with regard to the breaker which is shown in Figure 3-4. The diamond shown in these figures is the net current at the corresponding height used in the SANTOSS formula. This is equal to a representative height modeled in Delft3D at approximately 5 centimeter above the bed. For predicting the sand transport with the SANTOSS formula it is important that this net current is predicted well. This is not the case, especially for locations x = 55.9 to x = 57.9 m the undertow is underestimated. For the locations x = 54.4 to x = 55.4 m the undertow is over estimated.

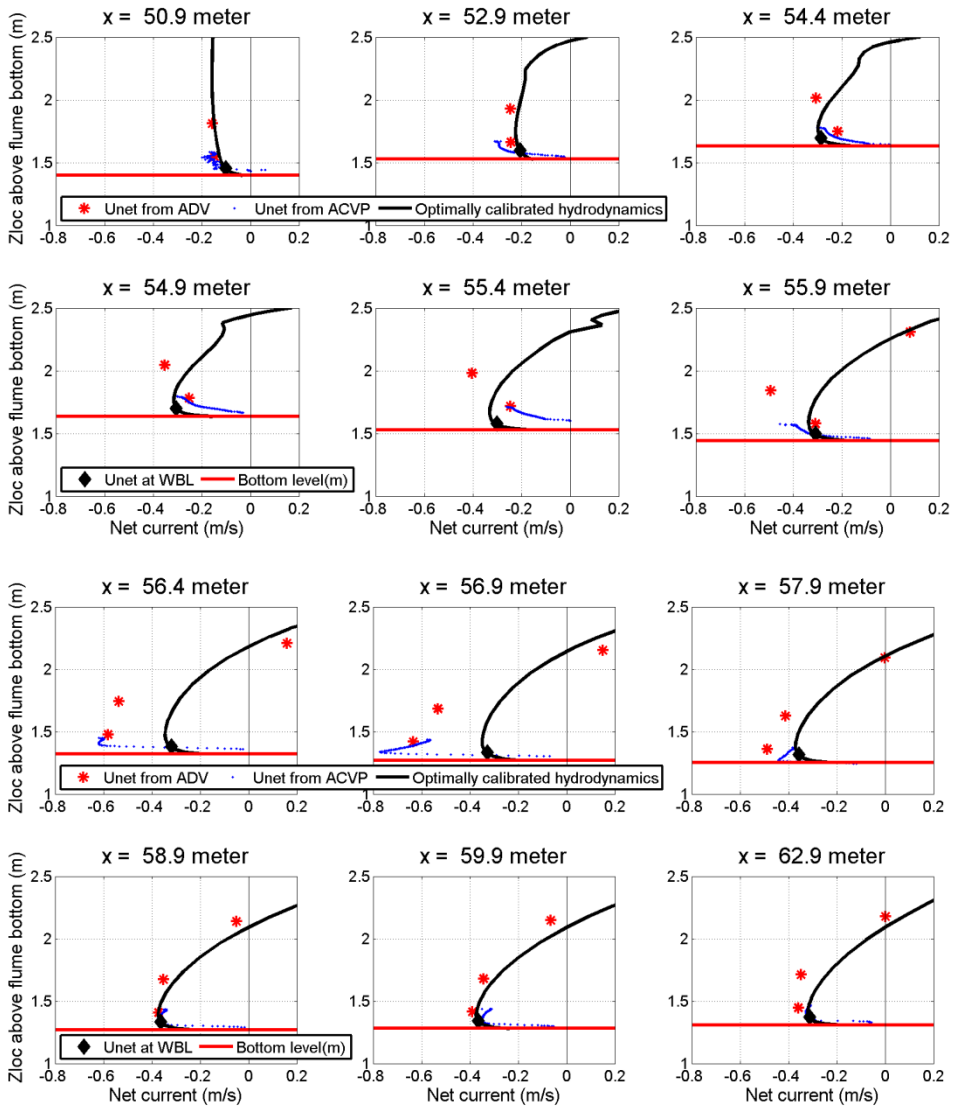

FIGURE 3-3: MEASURED AND MODELED UNDERTOW. THE UNDERTOW IS MEAUSRED WITH THE ADV AND THE AVCP DEVICES. THE NET CURRENT AT THE WAVE BOUNDARY LAYER (UNET AT WBL) IS SHOWN WHILE THE NET CURRENT AT THIS HEIGHT IS INPUT FOR THE SANTOSS MODEL.

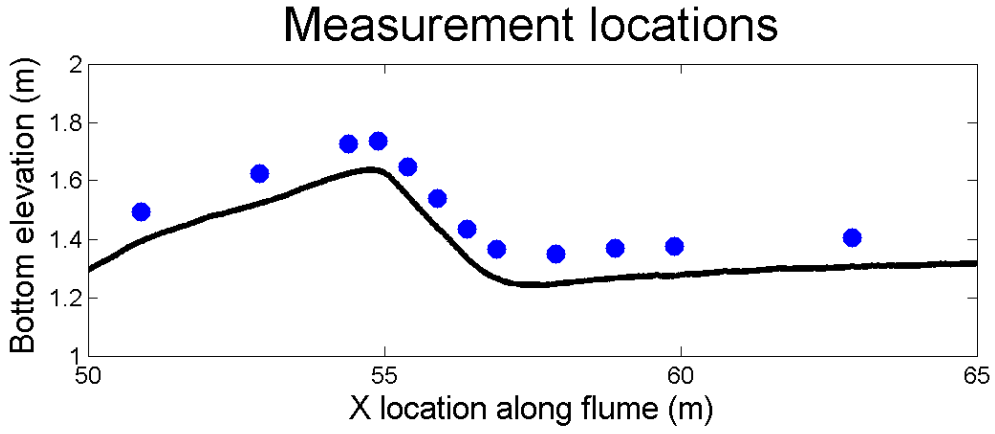

FIGURE 3-4: MEASUREMENT LOCATIONS

3.1.5 *Net Vertical currents*

The net vertical currents are important for the determinion of the suspension concentrations. Therefore the measured vertical currents have been compared to the modeled vertical currents in Figure 3-5. There are some uncertainties in the measured vertical currents. The vertical currents measured with the ACVPs do not match with the measured vertical current of the lowest ADV for some locations. The vertical currents seem to be downwards directed in front of and at the top of the breaker bar, while the direction suddenly changes to upward from x = 55.9 m and onshore.

The modeled vertical current are almost always upwards directed. Onshore of the breaker bar, for x is larger than 57.9 meter, the vertical currents almost decreased to zero. For some locations the vertical currents show a local decrease of the vertical current. This is due to the mass flux due to rollers which is applied in the top part of the water column.

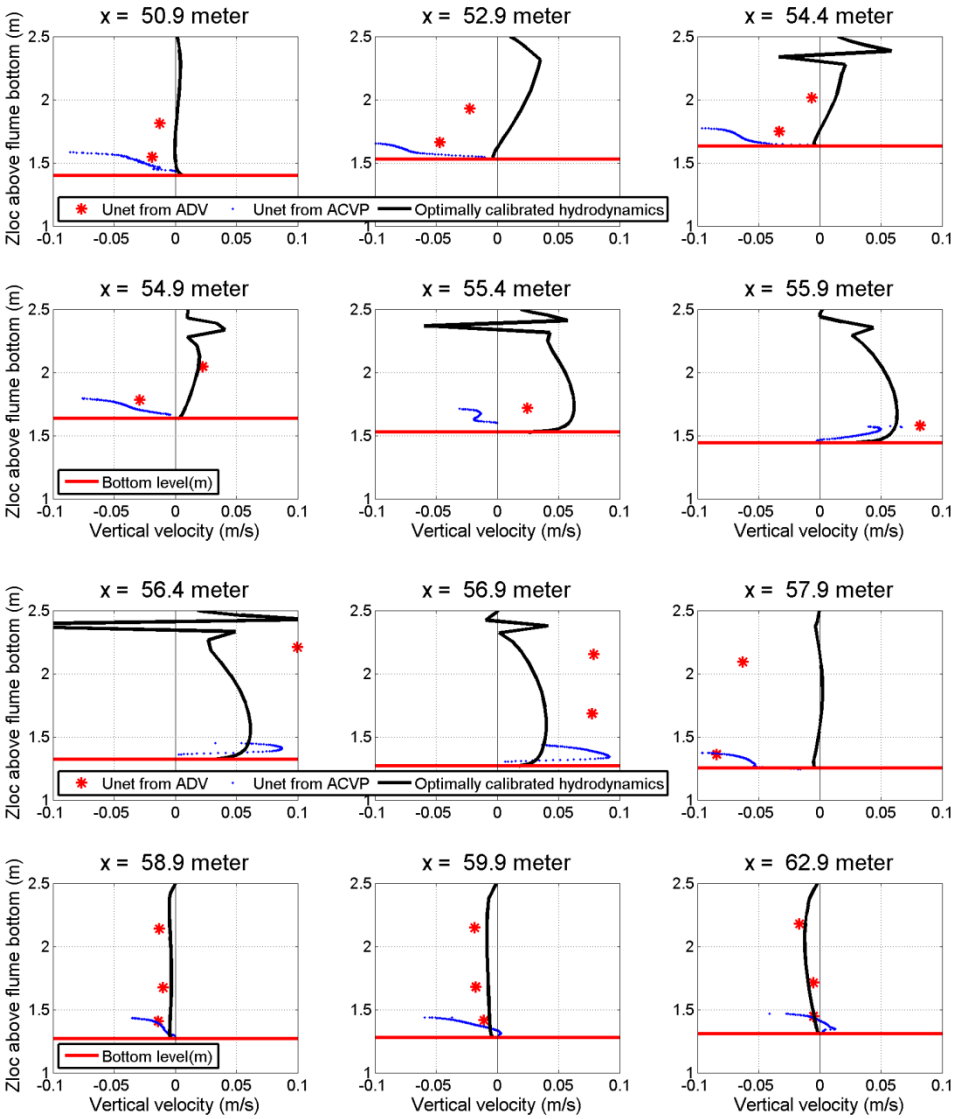

FIGURE 3-5: MEASURED AND MODELED VERTICAL VELOCITIES. THE VERTICAL VELOCITIES ARE MEAUSRED WITH THE ADV AND THE AVCP DEVICES.

3.2 Wave skewness and asymmetry

Veen (2014) implemented the approximation method of Abreu, Silva, Sancho, & Temperville (2010) by Ruessink, Ramaekers, & Van Rijn (2012) for the orbital flow velocity skewness and asymmetry in Delft3D. The results of this approximation method will be compared with the measured wave skewness and asymmetry. Firstly the approximation method will be discussed, then the measurements and the model results will be discussed and then the suitability of the approximation method of Ruessink et al. (2012) will be discussed.

3.2.1 *Approximation method*

With the wave number, calculated with the linear wave theory, the wave height and the water depth the Ursell number (Ursell, 1953) can be calculated.

$$Ur = \frac{3}{4}\frac{0.5 H_s k}{(kd)^3} \quad \text{EQ. 3-11}$$

According to Ruessink et al. (2012) a Boltzmann sigmoid function should be used to determine the relation between the Ursell number and the total measure of non-linearity B. Also the phase ψ can be determined from the Ursell number.

$$B = p1 + \frac{p2}{1 + \exp\left(\frac{p3 - \log U_r}{p4}\right)} \quad \text{EQ. 3-12}$$

$$\psi = -90° + 90° \tanh\left(\frac{p5}{U_r^{p6}}\right) \quad \text{EQ. 3-13}$$

p1 To p6 are calibration parameters with advised values of p1 = 0, p2 = 0.857, p3 = -0.471, p4 = 0.297, p5 = 0.815 and p6 = 0.672. The total measure of non-linearity can be used to calculate the parameter of skewness or nonlinearity r with the following formula (Malarkey & Davies, 2012):

$$B = \frac{3b}{\sqrt{2(1 - b^2)}} \; with \; b = \frac{r}{1 + \sqrt{1 - r^2}} \quad \text{EQ. 3-14}$$

Since there is not a single solvable relation between the total measure of linearity B and the parameter of skewness or nonlinearity r. Veen (2014) used basic fitting with a third order polygon to calculate r from a given B. The result of that basic fitting is given with the formula below. The basic fitting result in an R squared of 0.9998.

$$r = 0.0517B^3 - 0.4095B^2 + 1.0853B - 0.0099 \quad \text{EQ. 3-15}$$

The wave form parameter ϕ can be calculated from the phase with the following formula (Malarkey & Davies, 2012):

$$\phi = -\psi - \frac{\pi}{2} \quad \text{EQ. 3-16}$$

With the wave form parameter and the parameter of skewness or nonlinearity known, the Orbital velocities and the acceleration corresponding to those orbital velocities can be calculated (Abreu et al., 2010). For the orbital velocities and the accelerations corresponding to those orbital velocities the angular frequency ω and the wave period T_p are required as well:

$$U(t) = U_W * \sqrt{1-r^2} * \frac{\left[\sin(\omega t) + \frac{r sin(\phi)}{1+\sqrt{1-r^2}}\right]}{[1-\cos(\omega t+\phi)]} \quad \text{EQ. 3-17}$$

$$a(t) = U_w \omega \sqrt{1-r^2}\, \frac{\cos(\omega t) - r\cos(\phi) - \frac{r^2}{1+\sqrt{1-r^2}}\sin(\phi)\sin(\omega t+\phi)}{[1-r\cos(\omega t+\phi)]^2} \quad \text{EQ. 3-18}$$

The corresponding velocity skewness (R) and the acceleration skewness or velocity asymmetry (β) which is input for the SANTOSS model can respectively be described by:

$$R = \frac{U_{max}}{U_{max} - U_{min}} \quad \text{EQ. 3-19}$$

$$\beta = \frac{a_{max}}{a_{max} - a_{min}} \quad \text{EQ. 3-20}$$

The wave skewness and wave asymmetry are calculated with:

$$S_u = \frac{\overline{U_w}^3}{\sigma_{U_w}^3} \quad \text{EQ. 3-21}$$

$$A_u = \frac{H(\overline{U_w})^3}{\sigma_{U_w}^3} \quad \text{EQ. 3-22}$$

U_w Is the orbital velocity amplitude, σ_{U_w} is the standard deviation of the orbital velocity amplitude and $H(U_w)$ is a Hilbert transform of the orbital velocity amplitude.

3.2.2 *Measurements and modeling results*

The modeled results with the hydrodynamics calibrated in section 3.1 and the advised parameter settings for the Boltzmann Sigmoid function and the measurements are shown for respectively the peak orbital velocities, the flow velocity skewness and flow velocity asymmetry in Figure 3-6, Figure 3-7 and Figure 3-8.

The peak orbital velocities are predicted quite well (see Figure 3-6). Especially after wave breaking the orbital flow velocities are predicted well. At the breaker bar there is some underestimation of the orbital flow velocity. This underestimation might be quite important, because due to this underestimation rippled flow regime might be predicted instead of sheet flow regime. The flow regime is quite important for the direction of sediment transport (See section 2.2.3).

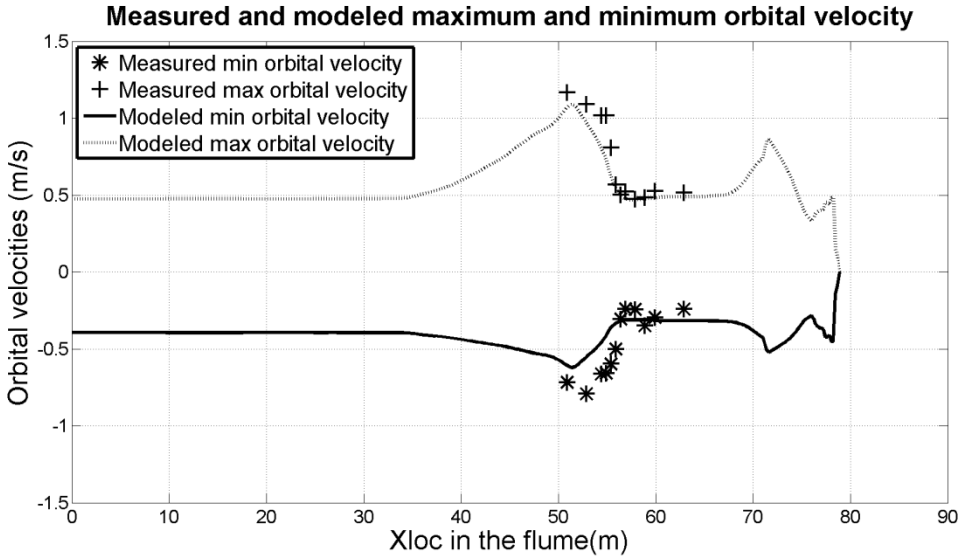

FIGURE 3-6: MEASURED AND MODELD PEAK MINIMAL AND MIAXIMUM ORBITAL VELOCITIES

The measured velocity skewness is determined with EQ. 3-19 and the acceleration skewness is determined with EQ. 3-20. The peak crest and trough velocities and accelerations are required. Figure 3-9 shows some examples of intra-wave velocities and acceleration to indicate how the velocity and acceleration skewness are determined. Velocities and accelerations are clearly higher in front of and at the top of the breaker bar compared to offshore of the breaker bar. This is also shown in Figure 3-6. There are some local variations in the accelerations, but this will barely have effect on the acceleration skewness.

The measured velocity skewness shows much more variation than the model results (see Figure 3-7). The measurement are very detailed around the breaker bar, a lot more processes are going on around the breaker bar than the processes used in the parameterization method, it is therefore assumable considering the measurement that the parameterization method is too simple for the energetic conditions during the measurements. The order of magnitude of the orbital flow velocity is predicted quite well by the parameterization method.

The scatter in the orbital flow skewness is also present in the orbital flow asymmetry (see Figure 3-8). This is quite logic because the orbital flow asymmetry depends a lot on the orbital flow skewness. While the order of magnitude of the orbital skewness was predicted quite well, the orbital flow asymmetry is underestimated.

The flow asymmetry is underestimated throughout the whole flume. Ruessink et al. (2012) mentioned that the relation between the Ursell number and B and ψ is empirical. So, the parameter settings used in these relations might not be optimal for this case. Ruessink et al. (2012) mention in their study that for laboratory experiment the fits used will underestimate the wave skewness because the energy transfer from the primary wave-frequency to the higher harmonics is mostly larger for wave flume experiments compared to field measurements. This applies especially for the wave skewness after wave breaking. What the underestimation of the wave skewness effect does to the wave asymmetry is not understood according to Ruessink et al. (2012).

Since there is in-consistency between the measurements it will be discussed if the parameterization method is suitable for this specific study in the next section.

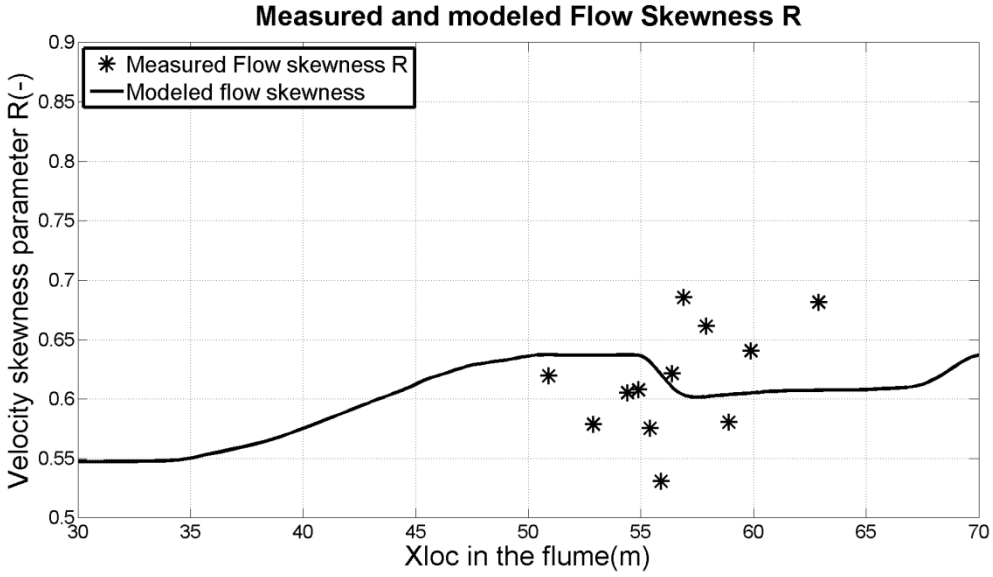

FIGURE 3-7: MEASURED AND MODELED FLOW VELOCITY SKEWNESS

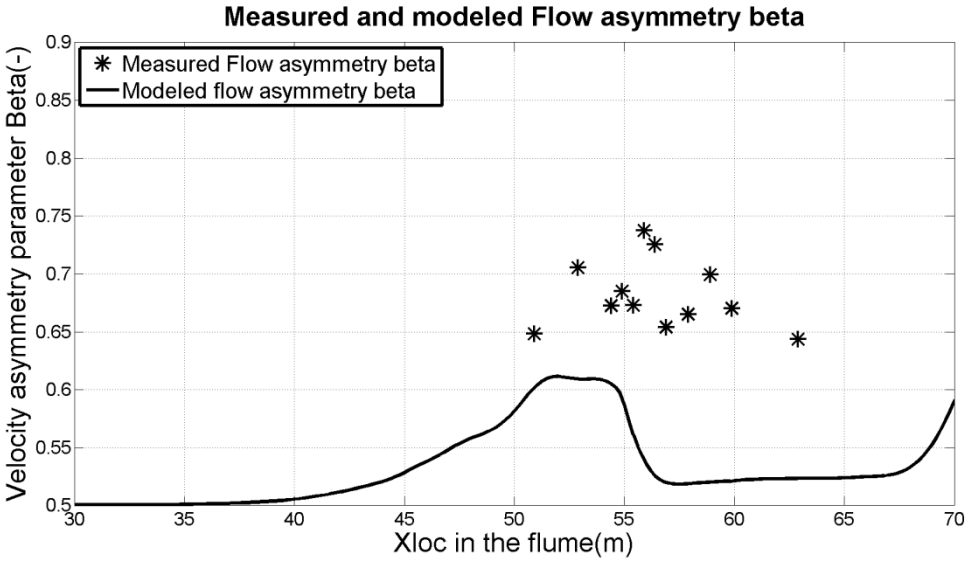

FIGURE 3-8: MEASURED AND MODELED FLOW VELOCITY ASSYMETRY

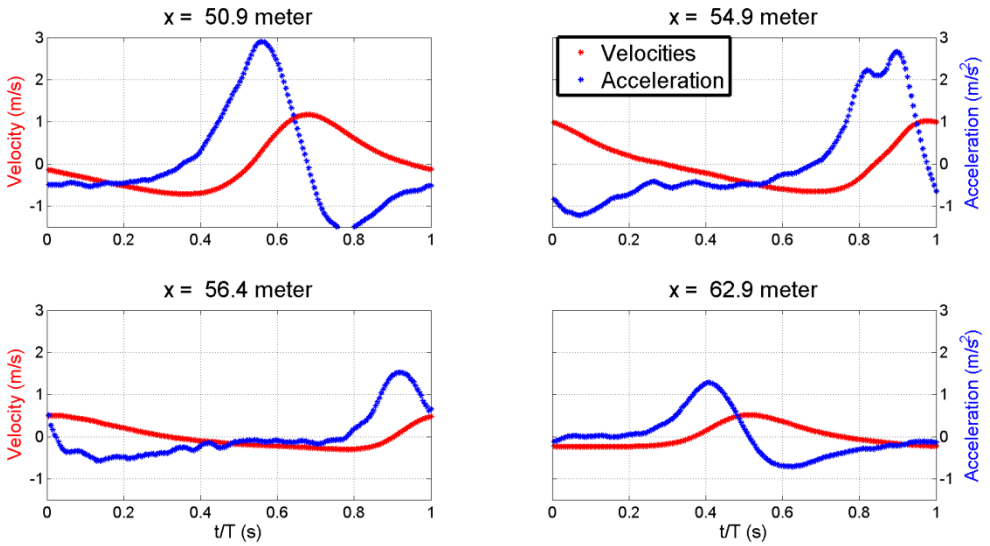

FIGURE 3-9: EXAMPLES OF INTRA-WAVE VELOCITIES AND ACCELERATION IN FRONT OF THE BREAKER BAR (X = 50.9 M), AT THE TOP OF THE BREAKER BAR (X = 54.9 M) AT THE LEE SIDE OF THE BREAKER (X = 56.4 M) BAR AND ONSHORE OF THE BREAKER BAR (X = 62.9 M).

3.2.3 *Suitability of the parameterization method*

The parameterization method used by Ruessink et al. (2012) is based on 33.962 individual estimates (the grey dots in Figure 3-10 and Figure 3-11). The advised parameter settings in the Boltzmann sigmoid function (EQ. 3-12) are based on this dataset. The measurements from the CIEM wave flume are therefore compared with the individual estimates. Ruessink et al. (2012) showed the relation between the wave skewness S_u (EQ. 3-21) and the Ursell number and the relation between wave asymmetry A_u (EQ. 3-22) and the Ursell number. The relation between the wave skewness and the Ursell number from Ruessink et al. (2012) and from the measurements are shown in Figure 3-10. The relation between the wave asymmetry and the Ursell number is shown in Figure 3-11. According to the measurements the Ursell number is height in front of and at the breaker bar (x < 55 meter). Behind the breaker bar the Ursell number is much lower. According the measurements there is al lot of variation in wave skewness and wave asymmetry for equal approximately Ursell numbers. The parameterization assumes equal wave skewness and asymmetry for equal Ursell number, therefore the parameterization method is not suitable.

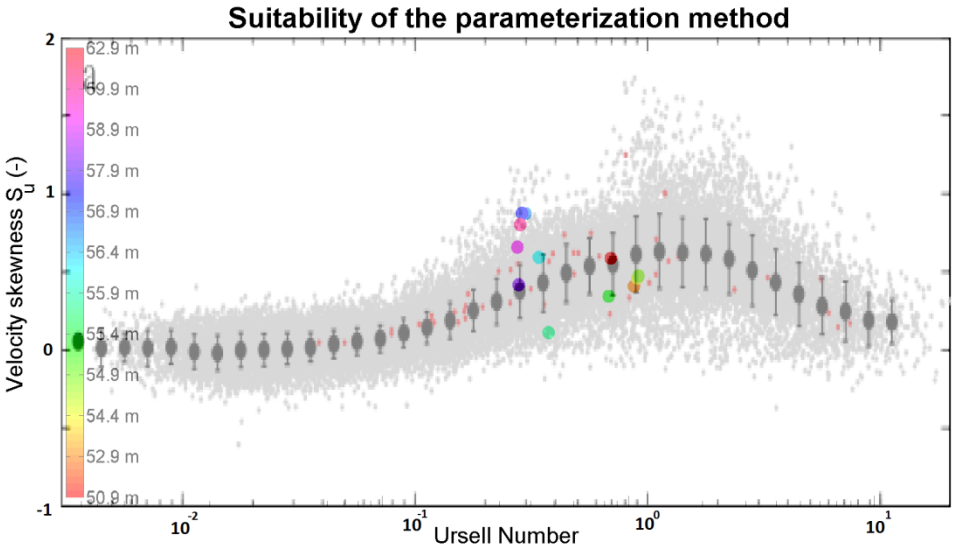

FIGURE 3-10: VELOCITY SKEWNESS AS A FUNCTION OF THE URSELL NUMBER

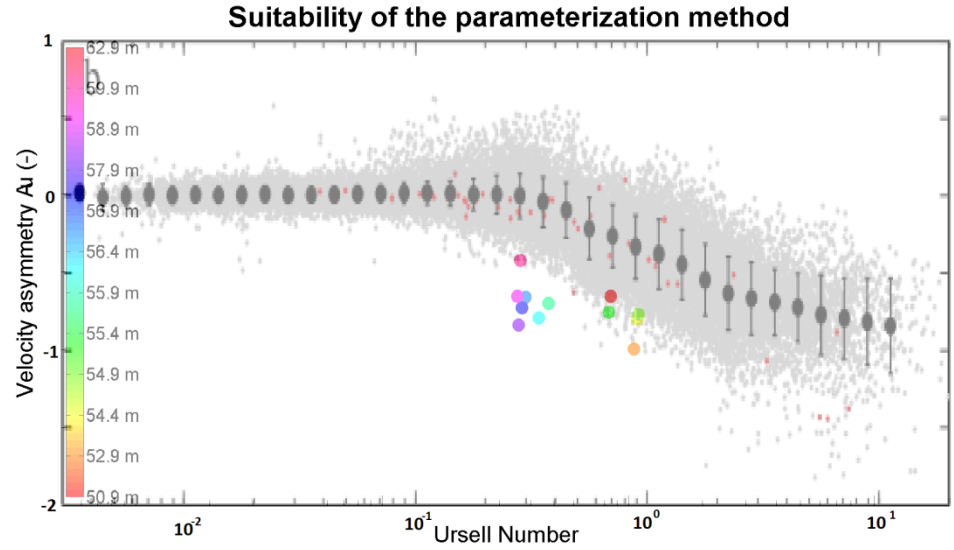

FIGURE 3-11: VELOCITY ASYMMETRY AS A FUNCTION OF THE URSELL NUMBER

The measured velocity skewness and asymmetry as a function of the x location in the flume showed quite varying results, but also the velocity skewness and asymmetry as a function of the Ursell number is quite varying. The varying of the velocity skewness and asymmetry cannot be predicted by the varying the parameter settings in the Boltzmann Sigmoid function (EQ. 3-12). The flow asymmetry is also outside the range of individual estimates used by Ruessink et al. (2012). This makes it quite hard for the parameterization method to predict the right wave skewness and wave asymmetry.

It seems that the Ursell number is not the only determining parameter for the wave skewness and asymmetry. The wave skewness seems to decrease when the water depth decreases. This is in contradiction with the Ursell number which increases with decreasing water depth. The locations behind the breaker bar all show a low Ursell number, with corresponding high wave skewness. This is also in contradiction with the parameterization method of Ruessink et al. (2012) where a decreasing Ursell number also causes a decreasing wave skewness. There is also a lot of local variation in the measurements. So it is possible that maybe local bed forms

have influence on the wave skewness and wave asymmetry. It is also possible that turbulence due to wave breaking has a lot of effect on the wave skewness and wave asymmetry. The strong undertow (See Figure 3-3) probably also has some effect on the measured wave skewness and wave asymmetry. Therefore it is quite hard to predict the measured wave skewness and wave asymmetry with just the Ursell number for this test case.

3.3 Conclusion

The wave height is predicted well with the adapted energy dissipation due to wave breaking model. The trend of the modeled set-up is equal to the trend of the measured set-up. The water level decreases offshore of the breaker bar while it increases around and behind the breaker bar. However the amount of set-down and set-up is underestimated by the Delft3D model. The undertow is underestimated at the onshore side of the breaker bar probably due to poor modeling of the Stokes mass flux due to waves or due to rollers.

The peak orbital crest and trough velocities are estimated quite well. There is some underestimation of the orbital velocities at the top of the breaker bar, but the trend in the model results is quite equal to the trend in the measurements. This underestimation is potentially important, since the measurements and the modeled peak orbital velocities are just in or out the sheet flow regime (see section 2.2.3). The flow regime is important for the direction of the sediment transport. The velocity skewness and velocity asymmetry are predicted very poorly. There seemed to be no clear trend in the measured wave skewness and wave asymmetry which is quite important if the wave skewness and wave asymmetry should be reproduced. The parameterization method used does seem unsuitable for the measurement used during this research.

During the calibration a good job was done on the wave height and the orbital velocities. Though, the overall conclusion is that some of the hydrodynamics are quite poorly modeled in Delft3D due to the fact that (i) Delft3D is developed using parameterizations suitable for irregular breaking waves, (ii) Delft3D cannot deal with the increasing water depth at offshore side of the breaker bar, (iii) Delft3D is a wave averaged model and (iv) Delft3D uses empirical formulations which are not suitable for the test case used during this project. The mismatch between the measured and the modeled hydrodynamics could have serious implications for the modeled sediment transport.

4 MEASURED AND MODELED SEDIMENT TRANSPORT

This section discusses the different sediment transport contributions. The measured suspended sediment concentrations will be compared with the modeled suspended sediment concentration. The different sand transport components modeled with the van Rijn (2007) and the SANTOSS model will be shown.

4.1 Sediment Concentrations

During the CIEM wave flume experiment the time averaged suspended sediment concentrations were measured with the TSS (Transverse Suction System) measurement devices. These TSS devices were location at the mobile measurement frame at six locations in the water column. These locations were (in centimeter above the bottom): 2, 4.5, 9.7, 17.8, 30.8 and 52.9. For some runs the lowest TSS device (2 centimeter above the bed) did not give a sediment concentration. This is due to clogging of TSS devices. The TSS gives probably an overestimation of the sediment concentrations behind the breaker bar. During the measurement ripples appeared. The height of the TSS compared to the bottom was then mostly smaller then the initial height. In this case higher sediment concentrations are given during further computations because the heights of the TSS devices are kept fixed at the values mentioned above.

The sediment concentrations are shown in Figure 4-1. The measured sediment concentrations are relatively low in front of the breaker bar (X= 50.9 meter). Behind the breaker bar the sediment concentration show a high value near the bottom with a decreasing value towards the water surface following a logarithmic profile. This corresponds to the way Delft3D calculates the suspended sediment concentrations.

Since there is no flow in the y direction and since there is after spin-up time no change over time due to wave averaged calculations EQ. 2-3 can be reduced to:

$$\frac{\partial uc}{\partial x} + \frac{\partial (w - w_s)c}{\partial z} - \frac{\partial}{\partial x}\left(\epsilon_{s,x}\frac{\partial c}{\partial x}\right) - \frac{\partial}{\partial z}\left(\epsilon_{s,z}\frac{\partial c}{\partial z}\right) = 0 \qquad \text{EQ. 4-1}$$

In this formulation, u and w are the flow components in the x and the z direction, w_s is the hindered sediment settling velocity, $\epsilon_{s,x}$ and $\epsilon_{s,z}$ are the eddy diffusivities of the sediment fraction and c is the mass concentration of sediment fraction.

Calibration on the sediment concentrations is hardly possible, since only changing the horizontal background eddy diffusivity has just influence on the sediment concentrations. There are also some multiplications factors which can reduce of increase the sediment transport of certain sediment transport components, but these multiplication factors are not physically responsibly. The default value for the horizontal background eddy diffusivity (Dicouv) is 0.01. Some calibration has been done on the horizontal background eddy diffusivity (See Appendix D.4.). It seems that changing the default Dicouv improves the predictions of the sediment concentration for one locations and it worsens the prediction of the sediment concentration for other locations (See Figure D-4). Therefore the Dicouv parameter is set to the default value 0.01. The vertical background eddy diffusivity has been set to the default value as well, since changing this parameter did not have any effect on the sediment transport. There are some other calibration parameters, these calibration parameters have all been set to the default value since these parameters are not physically responsibly. These parameters are just multiplication factors and

they are therefore set to the default value. An overview of the parameter settings is shown in Table 4-1.

TABLE 4-1: OPTIMAL MORPHODYNAMIC PARAMETER SETTING

Parameter	Description	Symbol	Value
Dicouv	Background horizontal eddy diffusivity	D_h^{back}	0.01m^2/s
Dicoww	Background vertical eddy diffusivity	D_v^{back}	10^-6 m^2/s
AlfaBs	Streamwise bed gradient factor for bed load transport	α_{bs}	1
AlfaBn	Transverse bed gradient factor for bed load transport	α_{bn}	1.5
Sus	Multiplication factor for suspended sediment reference concentration	f_{sus}	1
Bed	Multiplication factor for bed-load transport vector magnitude	f_{bed}	1
SusW	Wave-related suspended sed. transport factor	$f_{sus,w}$	1
BedW	Wave-related bed-load sed. transport factor	$f_{bed,w}$	1

The sediment concentrations in Delft3D are in equilibrium after approximately 1 minute. Therefore the first time-step has been excluded during the averaging of the modeled sediment concentrations. The result is shown in Figure 4-1.

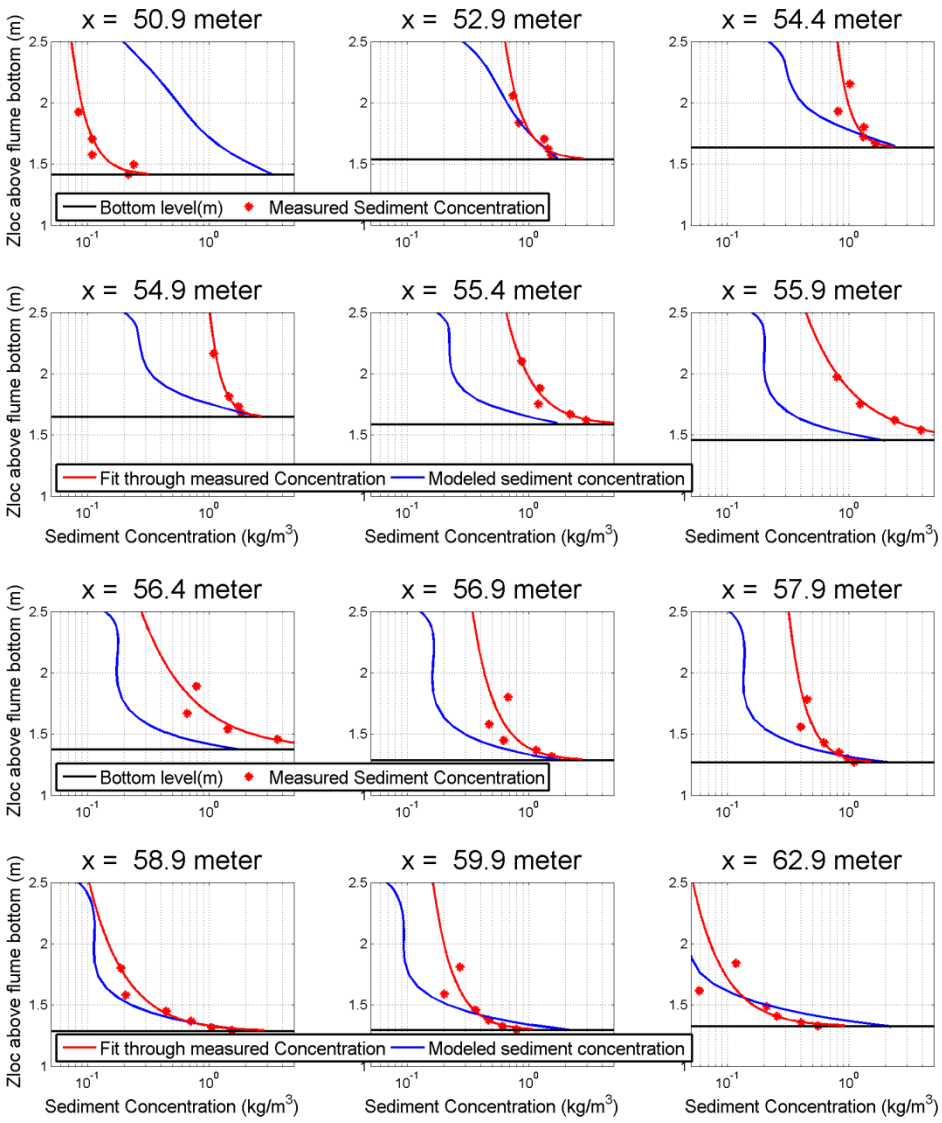

FIGURE 4-1: MEASURED SEDIMENT CONCENTRATIONS INCLUDING FIT TROUGH THE MEASUREMENTS AND MODELED SEDIMENT CONCENTRATIONS

There are large differences between the measured concentration and the modeled concentrations. At some locations, x = 58.9 to x = 62.9 m, the sediment concentrations are predicted quite well. At other locations the prediction of the sediment concentration is quite underestimated, except for x = 50.9 here the sediment concentrations are overestimated. This can either be due to wrong predictions of the reference concentration, it can be due to wrong prediction of the sediment mixing, or it can be due to errors in the vertical currents. To examine where the wrong predictions come from the reference concentrations and the sediment mixing from the measurements have been calculated. Therefore a power law fitting function has been used to plot a line trough the measured sediment concentrations, this is shown in Figure 4-1.

4.1.1 *Reference concentration*

The reference height, the height at which the reference concentration is modeled, is in the Delft3D model almost constant along the test section and approximately equal to 0.015 meter above the bed. Therefore the concentration from the fit between 1 and 2 centimeter has been used as reference concentration from the measurements. A comparison between the modeled reference concentration and the concentration obtained through the fit through the

measurements between 1 and 2 centimeter is shown in Figure 4-2. The reference concentrations obtained through the fits are not very accurate due to possible errors in the fits.

It seems that Delf3D overestimates the reference concentration in front of and behind the breaker bar. At the top of the breaker bar (x = 52.9 to x = 54.9 m) the reference concentrations are modeled quite well. At the onshore side of the breaker bar the reference concentration are underestimated a lot. The poor prediction of the reference concentration is definitely a reason for the poor prediction of the sediment concentration.

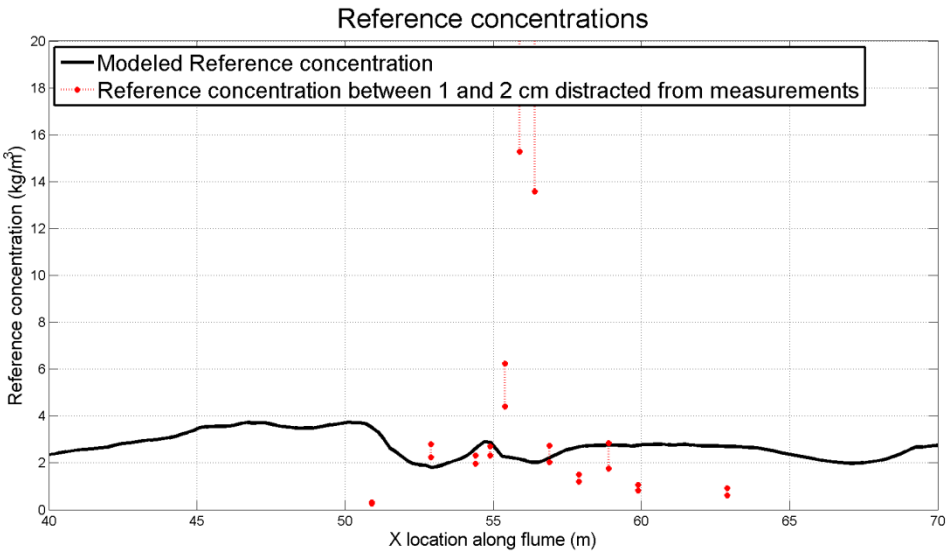

FIGURE 4-2: MEASURED AND MODELED REFERENCE CONCENTRATIONS

4.1.2 *Sediment mixing*

This section will compare the modeled sediment mixing with Delft3D and the sediment diffusion extracted from the measurements. The methods on how these sediment diffusions have been determined will be explained firstly.

4.1.2.1 Measurements

The sediment mixing has been extracted from the measured concentration profiles using the method proposed by Ribberink & Al-Salem (1994). They assume that the sediment diffusion is a linear distribution from zero at the bed (z = 0 m) to a maximum at the water surface (z = h).

$$\epsilon_s(z) = \epsilon_{s,max} \frac{z}{h} \qquad \text{EQ. 4-2}$$

The maximum sediment diffusion $\epsilon_{s,max}$ can be extracted from the concentration profile. Since it follows from EQ. 4-2 that the concentration profile follows a log-profile, the maximum sediment diffusion will also be extracted from a logarithmical function:

$$c(z) = c_a * \left(\frac{a}{z}\right)^{\frac{w_s h}{\epsilon_{s,max}}} \qquad \text{EQ. 4-3}$$

Implementing EQ. 4-2 in EQ. 4-3 and rewriting for the sediment diffusion ϵ_s gives:

$$\epsilon_s = \frac{w_s z \log\frac{a}{z}}{\log\frac{c(z)}{c_a}} \qquad \text{EQ. 4-4}$$

*

With z is the height above the bed, w_s is the settling velocity, $c(z)$ is the concentration at height z and c_a is the reference concentration at a = 1 centimeter above the bottom. The settling velocity has been extracted from Delft3D and assumed uniform with a value of $w_s = 0.032\, m/s$. The reference height for the reference concentration c_a is, according to Delft3D between 1 and 2 centimeter.

The resulting sediment diffusions are shown in Figure 4-4. The sediment diffusion has been calculated from the measurements concentration by the TSS devices. The reference heights used is 1 centimeter above the bed.

The measured sediment diffusivities are extracted from the measured sediment concentration assuming linearly increasing sediment diffusivity from the bottom towards the free water surface neglecting vertical velocities and assuming a uniform and steady settling velocity. Neglecting the vertical velocities, which are taken into account in Delft3D (see EQ. 4-1 and Figure 3-5), definitely causes errors in the measured sediment diffusivity, since vertical velocity affect the vertical sediment distribution. The other assumptions, linearly increasing sediment diffusivity and a uniform and steady settling velocity, are also simplifications which can cause errors in the measured sediment diffusivity. This makes it quite hard to judge how well the sediment diffusivities are modeled.

4.1.2.2 Delft3D

During this project the sediment mixing model of van Rijn (1993) has been used in Delft3D. This method overrules the sediment mixing due to the $K-\epsilon$ turbulence model. When waves are included in the model the eddy diffusivities of the sediment fraction is given by:

$$\epsilon_{s,z} = \sqrt{\epsilon_{s,c}^2 + \epsilon_{s,w}^2} \qquad \text{EQ. 4-5}$$

With $\epsilon_{s,c}$ is the current related mixing and $\epsilon_{s,w}$ is the wave related mixing. The current related mixing (See Figure 4-3) is given by:

$$\epsilon_{s,c} = \begin{cases} \kappa\beta u_{*,c} z\left(1-\frac{z}{h}\right), & when\ z < 0.5h \\ 0.25\kappa\beta u_{*,c} h, & when\ z \geq 0.5h \end{cases} \qquad \text{EQ. 4-6}$$

In this formula κ is the Von Karman constant (=0.41), β is the van Rijn's beta factor of the sediment fraction given by van Rijn (1984b):

$$\beta = 1 + 2\left(\frac{w_s}{u_{*,c}}\right)^2 \qquad \text{EQ. 4-7}$$

In this formula, w_s is the settling velocity of non-cohesive sediment and $u_{*,c}$ is the local bed shear stress due to currents. z Is the water level and h is the total water depth. The wave related mixing $\epsilon_{s,w}$ is calculated by using a smoothed step type distribution over the vertical, with a linear transition between the two hinge points (See Figure 4-3).

$$\epsilon_{s,w} = \begin{cases} \epsilon_{s,bed} = 0.018 f_d \beta \delta_s^{(l)} U_{\delta,r}, & when\ z \leq \delta_s \\ \epsilon_{s,bed} + \left(\epsilon_{s,max} - \epsilon_{s,bed}\right) * \left(\frac{z-\delta_s}{0.5h-\delta_s}\right), & when\ \delta_s < z < 0.5h \\ \epsilon_{s,max} = \frac{0.035\gamma_{br} h H_s}{T_p}, & when\ z \geq 0.5h \end{cases} \qquad \text{EQ. 4-8}$$

f_d Is a damping factor as a function of the Shields parameter $f_d = \sqrt{250/\theta}$ (see EQ. 1-3). δ_s Is the near bed sediment thickness layer given by:

$$\delta_s = \min(0.2, \max\{0.05, \gamma_{br}\delta_w\}) \quad \text{EQ. 4-9}$$

With γ_{br} is an empirical coefficient related to wave breaking and δ_w is the thickness of the wave boundary layer given by:

$$\delta_w = 0.36\hat{A}_\delta \left(\frac{\hat{A}_\delta}{k_{s,w}}\right)^{-0.25} \quad \text{EQ. 4-10}$$

$\hat{A}_\delta$ Is in this formula the near-bed peak orbital excursion given by $\hat{A}_\delta = \omega\hat{U}_\delta = \frac{H}{2\sin(kh)}$ and $k_{s,w}$ is the wave related bed roughness. $U_{\delta,r}$ is the representive peak orbital velocity near the bed according to the method of Isobe & Horikawa (1982):

$$U_{\delta,r} = \left(0.5\left(U_{\delta,for}\right)^3 + 0.5\left(U_{\delta,back}\right)^3\right)^{1/3} \quad \text{EQ. 4-11}$$

With $U_{\delta,for}$ and $U_{\delta,back}$ are respectively the peak orbital velocity in the forward and the backward direction. The empirical coefficient related to wave breaking γ_{br} is given by:

$$\gamma_{br} = \begin{cases} 1 + \left(\frac{H_s}{h} - 0.4\right)^{0.5}, & when \frac{H_s}{h} > 0.4 \\ 1, & when \frac{H_s}{h} \leq 0.4 \end{cases} \quad \text{EQ. 4-12}$$

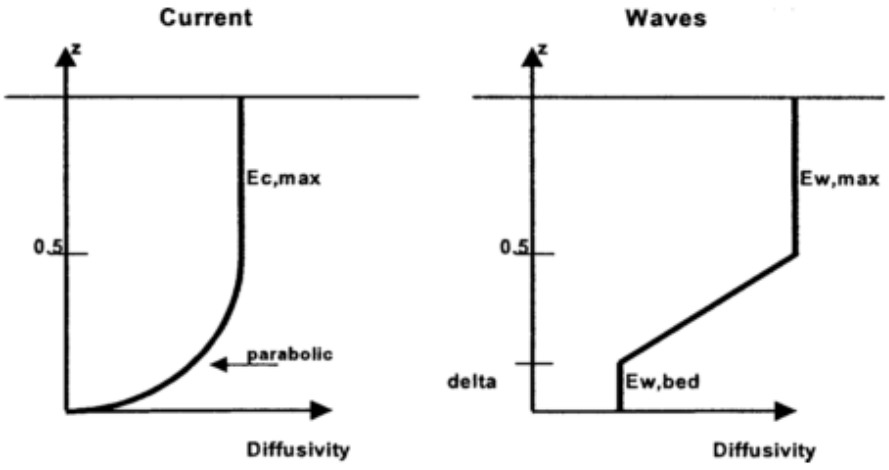

FIGURE 4-3: SEDIMENT MIXING COEFFICIENTS FOR CURRENTS AND WAVES ACCORDING TO VAN RIJN (2007B)

The resulting modeled diffusion is shown in Figure 4-4. The sediment diffusion in front of the breaker bar and at the breaker bar is mostly determined by sediment diffusion due to waves. Onshore of the breaker bar sediment diffusion due to waves reduces and the sediment diffusion due to currents becomes more important.

4.1.2.3 Comparison between the measurements and Delft3D

A comparison between the measured and modeled sediment diffusivity is visible in Figure 4-4. The sediment diffusion is generally underestimated; it is very likely that this is due to the exclusion of the vertical currents during the calculation of the measured sediment diffusivity. Since the vertical currents are mostly upwards directed (See Figure 3-5), the measured sediment diffusion is probably over estimated.

Near the bottom the order of magnitude of the sediment diffusion is quite good. Higher in the water column the sediment diffusion is underestimated a lot. The underestimation could also be due to the uncertainty in the sediment diffusion extracted from the measurements, since some assumptions have been done.

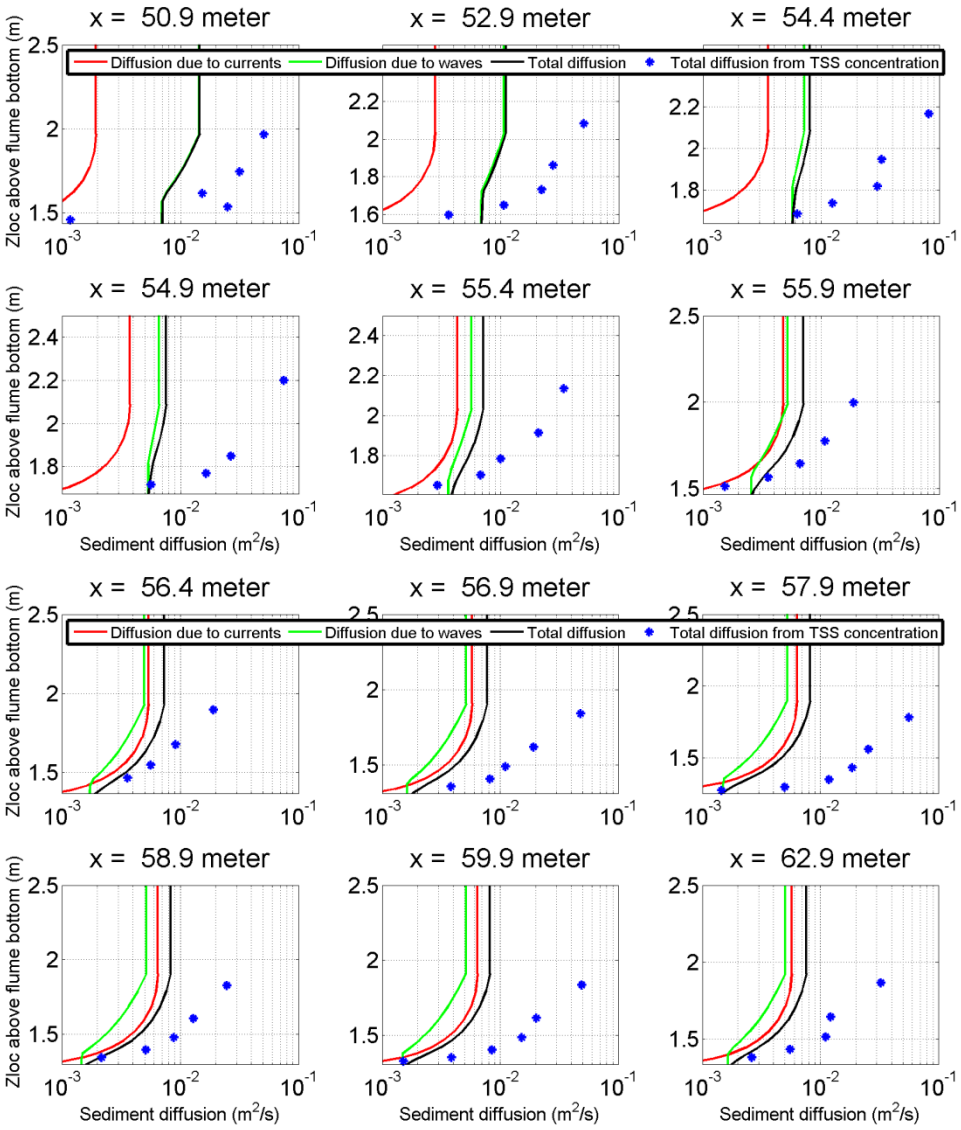

FIGURE 4-4: DIFFUSION MODELED WITH DELFT3D AND THE DIFFUSION EXTRACTED FROM THE MEASUREMENT

4.2 Sediment transport components

Suspended sediment in Delft3D is calculated according to EQ. 2-4 up to and including EQ. 2-7. Applying EQ. 2-7 with the undertow shown in Figure 3-3 and the sediment concentrations shown in Figure 4-1 results in the total suspended sediment transport.

In the van Rijn bed load transport model (van Rijn, 2007a) the total bed load is equal to the sum of the bed load due to currents, the bed load due to waves and the suspended load due to waves. The bed load due to currents ($q_{b,c}$) and waves ($q_{b,w}$) are given by:

$$q_{b,c} = \frac{U_{\delta,c}}{U_{\delta,c} + U_{\delta,w}} * q_b$$
$$q_{b,w} = \frac{U_{\delta,w}}{U_{\delta,c} + U_{\delta,w}} * q_b \qquad \text{EQ. 4-13}$$

With $U_{\delta,c}$ and $U_{\delta,w}$ are respectively the velocity due to currents and due to waves at the edge of the wave boundary layer and q_b is the total bed load transport calculated with EQ. 2-8. The suspended load due to waves is calculated with EQ. 2-12. Since bed load due to currents and wave is only distinguished by distinguishing orbital velocity due to currents and waves it is not very interesting. Therefore bed load transport due to currents and waves will be combined into bed load without suspended transport due to waves.

4.2.1 *Suspended transport due to currents*

EQ. 2-7 is used in Delft3D to calculate the suspended sediment transport due to currents; this equation can also be used to calculate the measured sediment transport. The measured net currents and suspended sediment concentration are only measured at a few locations in the water column. Therefore fits have been drawn through the measurement to be able to integrate the net current times the sediment concentration over the whole water column. These fits are shown in Appendix G.1. The measured suspended sediment transport due to currents seem quite accurate, though, there are still some uncertainties discussed in Appendix G.1.

In the comparison between the measured and modeled suspended transport due to currents it has to be taken into account that there are some errors in the measured suspended load due to an interpolations of the measured currents. The uncertainty in the measured concentrations and the measured velocities will also be present in the measured suspended load due to currents. Then there are some other uncertainties; a logarithmical line is fitted through the measured net currents and concentrations since data was not available at all locations in the water column. These fitted lines could have errors since there is no unlimited availability of data. The reference border for suspended sediment in the measurements is taken at 1 centimeter, which is approximately equal to the modeled reference height (~0.015 meter). The interpolation of the net currents and the sediment concentration also cause some more errors and uncertainties. The water level in the top of the water column is only averaged over a part of the wave period. Since the measurement device (ADV) was not always under the water level during the wave trough. During the interpolation only 3 points where taken into account. These three measurements locations were all required for the interpolations; therefore it was not possible to validate the interpolation with measurements. It is assumable that there are errors in the interpolations. The sudden change in net current for the x = 50.9 to x = 55.4 m between 0.5 and 1 meter above the bed is not very physically representative (See Figure G-1)

The integration of the sediment concentration times the net currents results in the measured transport shown in Figure 4-5. The modeled suspended transports due to currents are shown as well. Over- and underestimation of the suspended transport due to currents shows a relationship with the over- and underestimation of the net currents and the sediment concentration. At x = 50.9 m the sediment concentration are overestimated where the suspended sediment transport due to currents is not. The net currents at this location are not very strong, this compensates for

the overestimation of the suspended sediment concentration. At X = 60.9 m there is an overestimation of the suspended transport due to currents, this is due to an overestimation of the sediment concentration near the bed. At all other locations the suspended sediment transport due to currents is underestimated. This is due to either an underestimation of the sediment concentration, or due to an underestimation of the net current or both.

To indicate whether the errors in the suspended sediment transport due to currents are mainly caused by the errors in the concentrations or by the errors in the modeled net current, the modeled net current has been multiplied with the measured concentrations and the modeled concentration has been multiplied with the modeled net currents in Appendix F. It seems that the sediment concentration is the main reason for the errors in the sediment transport due to currents. Though, not much attention should be paid to this comparison, since the integration of the modeled net currents multiplied with the modeled concentration does not match up with the modeled suspended sediment transport due to currents (See Figure 4-5 and Figure F-2).

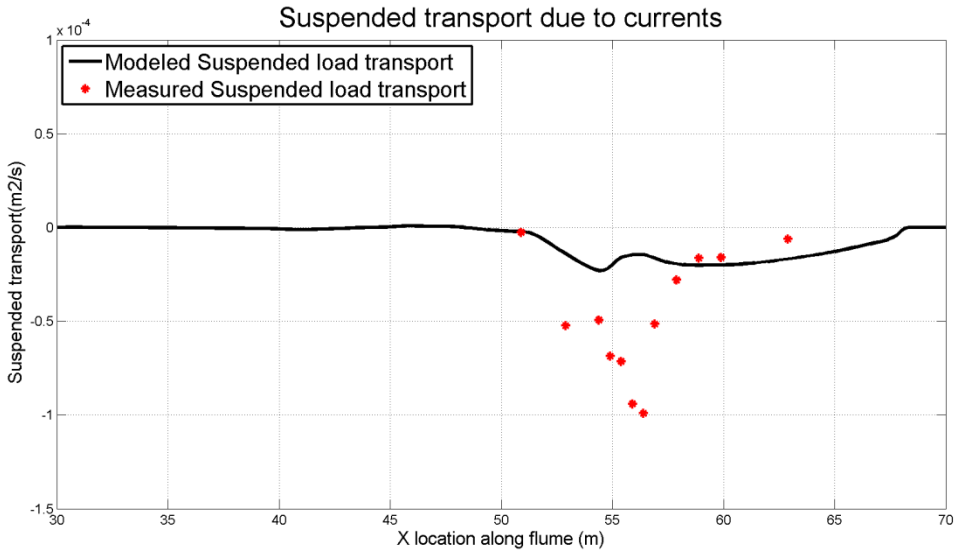

FIGURE 4-5: MEAUSURED AND MODELED SUSPENDED LOAD TRANSPORT DUE TO CURRENTS

4.2.2 *Suspended transport due to waves*

Instead of the net currents, the orbital flow has been used to integrate the concentration and the currents over the whole water column. To do this, the sediment transport is calculated during several stages of a wave (See Appendix G.2 and Appendix G.3). The total suspended load due to waves is then the averaged sediment transport over the several wave stages. This results in the measured suspended load due to waves shown in Figure 4-6, which also shows the modeled suspended transport due to waves. The measured suspended transport due to waves is not very accurate due to possible errors in the intra wave velocities and the intra wave sediment concentrations; this is discussed in Appendix G.2 and Appendix G.3 and it has been discussed for the net currents in section 4.2.1.

The modeled suspended transport due to waves is overestimated in front of the breaker bar (x = 50.9 m). This is due to an overestimation of the sediment concentration (See Figure 4-1). The suspended transport due to waves at the top of the breaker bar is underestimated. This is probably due to an underestimation of the sediment concentrations. It can also be due to an under estimation of the orbital velocities (See EQ. 2-12). Onshore of the breaker bar there is almost no suspended sediment transport due to waves, this is modeled well by the Delft3D model.

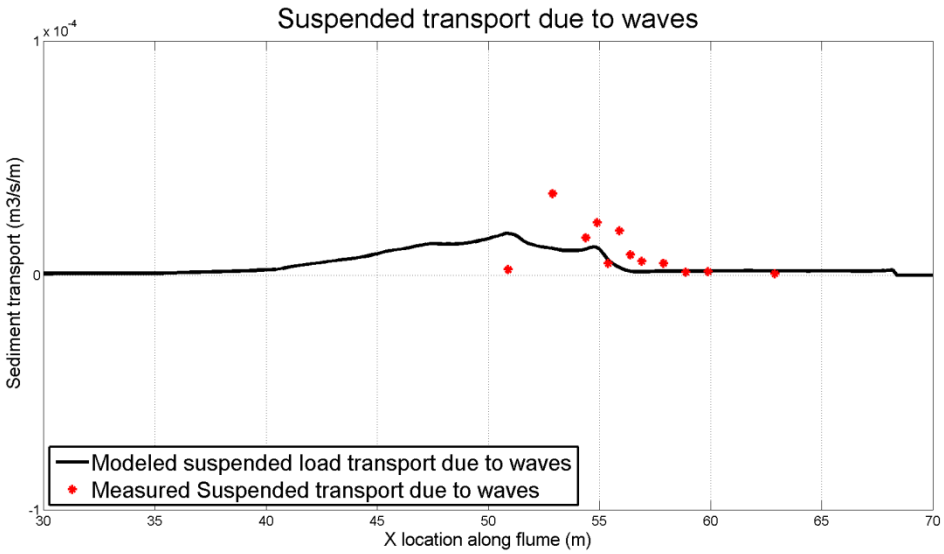

FIGURE 4-6: MEASURED AND MODELED SUSPENDED LOAD DUE TO WAVES

Both the SANTOSS formula and the van Rijn (2007a) assume that suspended transport due to waves only occurs in the lower part of the water column. The SANTOSS formula assumes that sediment transport due to wave only occurs in the wave boundary layer, with the wave boundary layer calculated differently than in van Rijn (2007b) (EQ. 4-10) formula and it is calculated as follows (Sleath, 1987):

$$\delta = 0.27 * k_{sw} * \left(\frac{\hat{A}_\delta}{k_{sw}}\right)^{0.67} \qquad \text{EQ. 4-14}$$

With δ is the wave boundary layer thickness, $\hat{A}_\delta$ is the horizontal excursion amplitude of the free-stream orbital flow and k_{sw} is the wave-related roughness given by:

$$k_{sw} = \max\{d_{50}, d_{50} * [\mu + 6(\langle|\theta|\rangle - 1)]\} + \frac{0.4\eta^2}{\lambda} \qquad \text{EQ. 4-15}$$

With d_{50} is the median grain size, μ is a parameter dependable on the median grain size, η and λ are respectively the ripple height and ripple length and $\langle|\theta|\rangle$ is the time averaged absolute Shields stress. The wave boundary layer thickness varies between 0.01 and 0.07 meter. Therefore a uniform wave boundary layer thickness of 5 centimeter is assumed, which is approximately the mean.

The van Rijn (2007a) assumes that suspended sediment transport due to waves only occurs in the suspension layer (See EQ. 2-12) equal to three times the thickness of the effective near-bed sediment mixing layer, given by EQ. 4-9. Therefore the thickness of the suspension layer varies between 0.15 and 0.6 meter. During the computations it seemed that for this case the suspension layer varied from 0.15 to 0.6 meter. A suspension layer thickness of 0.4 meter seems average and therefore this value will be used as a uniform value for the suspension layer.

The measured sediment transport can be integrated over the fluxes in the whole water column, just in the wave boundary layer or in the suspension layer using the intra-wave orbital velocity and concentrations (See respectively Figure G-2 and Figure G-3). The result is shown in Figure 4-7; it is clearly visible that suspended sediment transport due to waves does not just occur in the wave boundary layer. The suspended sediment transport due to waves integrated over the whole

water column is clearly higher than the suspended sediment transport due to waves integrated in the wave boundary layer.

Since there are uncertainties in the measured intra-wave orbital velocities and the intra-wave concentrations there is also uncertainties in the suspended sediment transport due to waves. Taking the errors into account it is still visible that the suspended sediment transport due to waves above the wave boundary layer cannot be neglected. There is also clear difference between the total measured suspended sediment transport due to waves and the suspended sediment transport due to waves in the suspension layer.

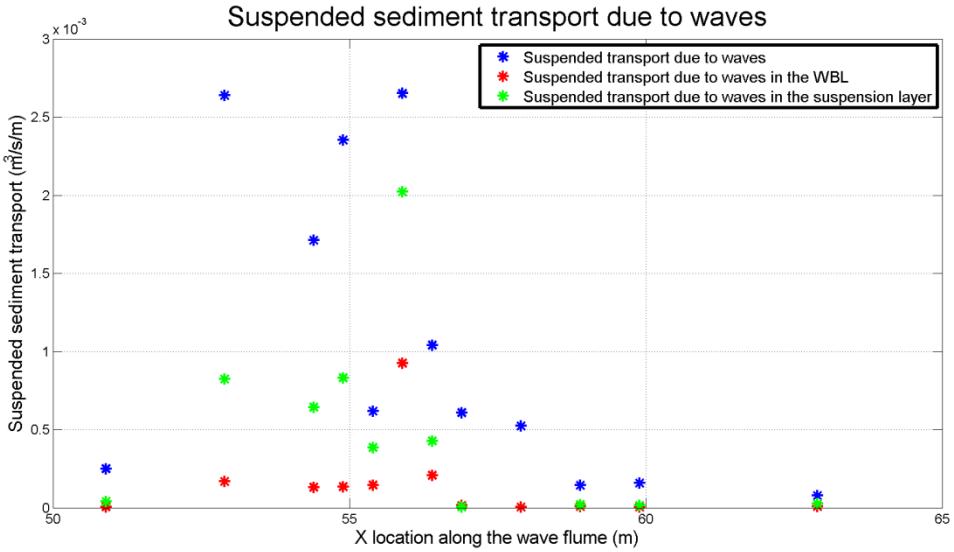

FIGURE 4-7: MEASURED SUSPENDED SEDIMENT TRANSPORT DUE TO WAVES IN THE WHOLE WATER COLUMN AND IN THE WAVE BOUNDARY LAYER

4.2.3 *Bed load transport*

The measured bed load transport is calculated by subtracting the suspended load due to currents and waves from the total sediment transport measured with the profiling trolley (See section 2.4.2.1). The errors made by calculating the measured suspended load due to currents and due to waves are also present in the measured total bed load transport. There is large onshore directed bed load at the breaker bar which is due to sheet flow during the measurements.

The bed load transport is shown in Figure 4-8. The bed load in front of the breaker bar is under estimated. This can either bed due to an under estimation of the velocity due to currents and waves at the edge of the wave boundary layer (see EQ. 2-9) or the van Rijn (2007a) model is not suitable for this test case. The bed load transport in the trough behind the breaker bar is also underestimated, further onshore the bed load transport is modeled quite well. There are some local differences compared with the measurements behind the breaker bar, but it is quite well possible that these differences are due to errors in the measurements.

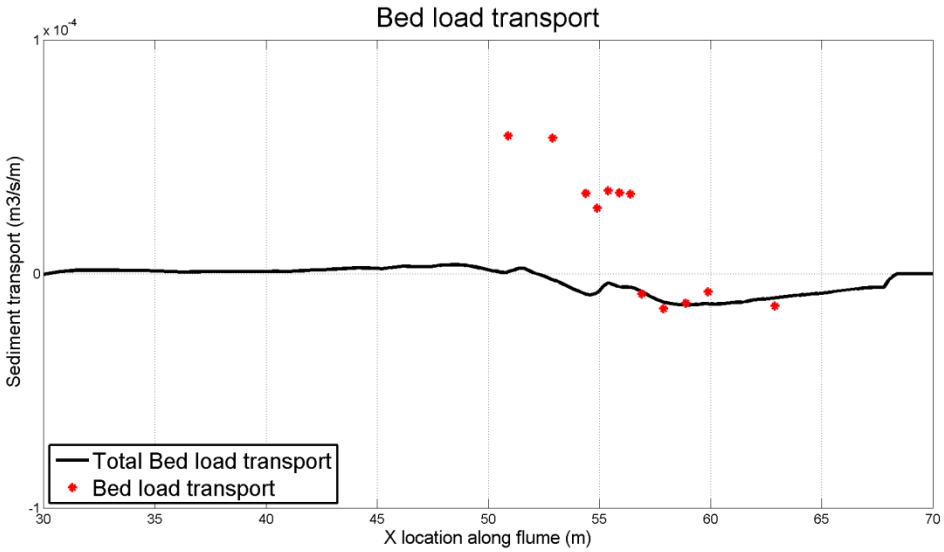

FIGURE 4-8: MODELED BED LOAD COMPENTS MODELED WITH VAN RIJN (2007A) AND THE MEASURED TOTAL BED LOAD TRANSPORT

4.2.4 *Comparison of the transport components*

Adding all these components to each other gives the total modeled sediment transport. The measured and modeled sediment transports including all the modeled sediment transport components are shown in Figure 4-9.

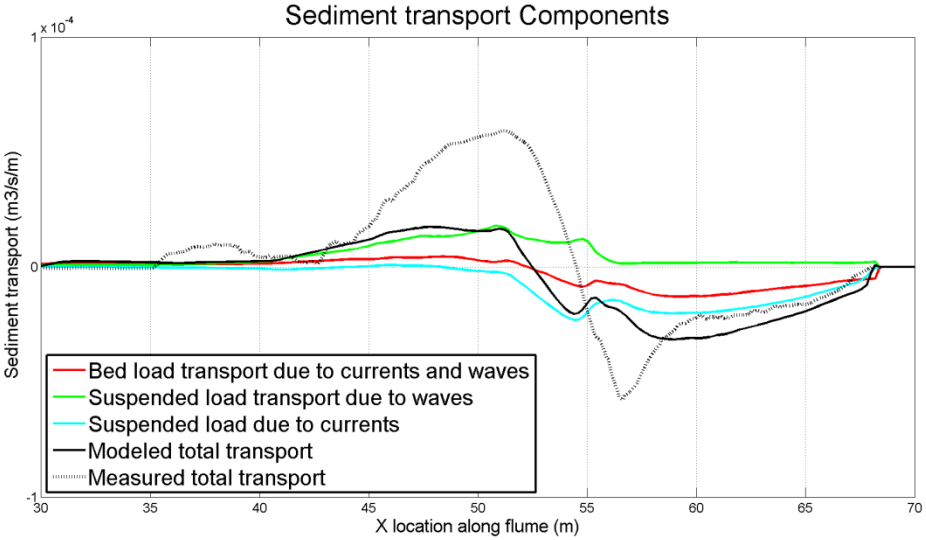

FIGURE 4-9: MEASURED TOTAL TRANSPORT AND MODEL TRANSPORT COMPONENTS INCLUDING TOTAL TRANSPORT

To indicate the importance of the different transport components during the measurements and the modeled per test section the magnitude of the sediment transport split up for the different transport components has been divided over four flume sections. These four sections are the stoss side of the breaker bar (x= 50.9 and 52.9 meter), the top of the breaker bar (x= 54.4, 54.9 and 55.4 meter), the lee side of the breaker bar (x = 55.9, 56.4 and 56.9 m) and the inner surf zone (x= 57.9, 58.9, 59.9 and 62.9 m). To indicate the importance of the measured and modeled transport components for different flume sections the absolute value of the sediment transport is used. The result is shown in Table 4-2.

According to the measurements all transport components are important. Were suspended transport due to currents seems to have the largest contribution to the total sediment transport.

The suspended transport due to waves is at the lee side of the breaker bar and in the inner surf zone less important. This is quite well in agreement with the modeled sediment transport. The suspended load due to waves is a lot more important at the stoss side off the breaker bar during modeling. Bed load at the stoss side of the breaker bar is less important during modeling compared to the measurements. Since the magnitude of all transport components is underestimated for most locations during the percentage of the total transports are also lower.

TABLE 4-2: MEASURED AND MODELED TRANSPORT COMPONENTS IN DIFFERENT FLUME SECTIONS IN 10^5 M^3/S/M

	Measured transport * 10^5 m^3/s/m				
		Stoss side	Top	Lee side	inner surf zone
Total		4.98	3.02	5.03	2.67
Bed load	amount	5.85	4.46	2.58	1.22
	percentage	118%	148%	51%	46%
Suspended load currents	amount	6.86	6.31	8.16	1.67
	percentage	138%	209%	162%	62%
Suspended load waves	amount	1.87	3.66	1.12	0.22
	percentage	38%	121%	22%	8%
	Modeled transport * 10^5 m^3/s/m				
		Stoss side	Top	Lee side	inner surf zone
Total		1.01	3.64	1.86	2.92
Bed load	amount	0.21	2.90	0.74	1.18
	percentage	21%	80%	40%	40%
Suspended load currents	amount	0.77	3.85	1.51	1.91
	percentage	77%	106%	81%	65%
Suspended load waves	amount	1.48	1.62	0.25	0.19
	percentage	146%	44%	13%	6%

The measured transports are based on the difference between the bottom profile at the start of the measurement and the bottom profile after 30 minutes of measurements. The measured sediment transport therefore also depends on the change of the bottom profile. To get insight in the effect of the bottom profile on the measured sediment transport a test with the bottom profile after 15 minutes of measurements has been performed in Appendix E. The effect on the sediment transport is very small; therefore bottom updating during the measurements will not be taken into account.

4.3 Comparison between van Rijn (2007a) and SANTOSS

Figure 4-10 compares the van Rijn (2007a) model and the SANTOSS formula (van der A et al., 2013). Both models are designed to predict the total bed load transport including the suspended transport due to waves. Therefore the modeled bed transport will be compared with the bed load transport including the suspended transport due to waves. The measured bed load transport has been added to Figure 4-10 as well.

During the comparison between SANTOSS and van Rijn it has to be mentioned that SANTOSS calculates the near bed sediment transport. Van Rijn calculates the bed load transport below the reference height. The near bed sediment transport is defined as the sediment transport below the wave boundary layer (See EQ. 4-14).

When the current related suspended transport modeled with van Rijn (2007b) is added to the near-bed sediment transport modeled with the SANTOSS formula, some overlap might occur.

The reference height above which suspension transport due to currents occurs according to van Rijn (2007b) is lower than the wave boundary layer calculated by SANTOSS (EQ. 4-14) below which near-bed sediment transport occurs. The sediment transport between the reference height and the wave boundary layer is according to the model concept then transported in the van Rijn (2007b) current related suspended transport model and in the SANTOSS near-bed transport model.

To prevent this overlap during a comparison between SANTOSS and the measurements, the measured suspended sediment transported in the wave boundary layer has been excluded from the total measured suspended sediment transport. The wave boundary layer is assumed to be uniform and equal to five centimeter. Excluding the suspended sediment transport in the wave boundary layer decreases the offshore directed measured suspended sediment. Since the bed load is equal to the suspended sediment distracted from the total sediment transport the onshore directed bed-load transport decreases as well.

The models show quite equal results. Especially at the breaker bar the results are quite equal. Both models underestimate the sediment transport at the breaker bar a lot. The SANTOSS model seems to overestimate the sediment transport in front of the breaker a little bit. The SANTOSS model shows some irregularities in the near-bed sediment transport. At x = 49 and x = 53 m there are some local decreases in the transport, the causes of the local decreases will be discussed in section 6.3.

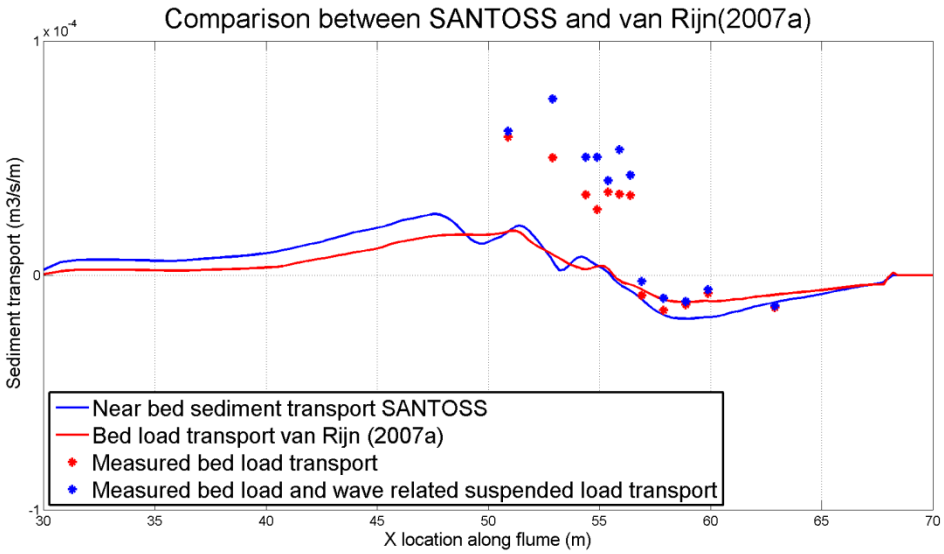

FIGURE 4-10: MEASURED BED LOAD TRANSPORTS AND MODELED BED LOAD TRANSPORT BY VAN RIJN (2007A) AND SANTOSS

By comparing SANTOSS and van Rijn (2007a) it has to be mentioned that both sand transport formulas use different orbital velocities as input. While SANTOSS use the method of Abreu et al. (2010) (EQ. 3-17) the orbital velocities in van Rijn are calculated with Isobe & Horikawa (1982). The differences are shown in Figure 4-11. Van Rijn uses higher orbital velocities in front of and behind the breaker bar. Compared to the measurements the method of Abreu et al. (2010) seem to predict the orbital flow velocities a little bit better. The higher prediction of the orbital velocities in front of and behind the breaker bar by Isobe & Horikawa (1982) does not lead to higher prediction sediment transport in the van Rijn (2007a) model.

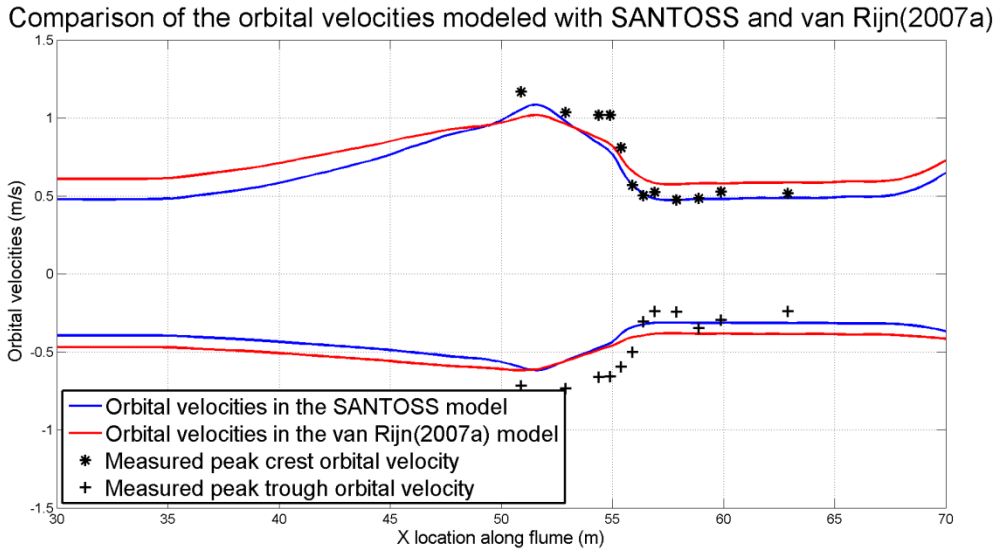

FIGURE 4-11: DIFFERENCES BETWEEN ORBITAL VELOCITIES USED IN VAN RIJN (2007A) AND SANTOSS

4.4 Conclusion

In section 4.1 it seems that the sediment concentrations are overestimated in front of the breaker bar and underestimated in the rest of the model. This is due to errors in the reference concentrations and errors in the sediment mixing. The underestimation of the sediment concentration also causes an underestimation of the offshore directed suspended sediment transport due to currents. The underestimation of the offshore directed suspended sediment transport due to currents can for some locations also be due to underestimations of the net currents.

The suspended transport due to waves is especially over estimated in front of the breaker bar. At the top of the breaker bar the suspended sediment transport due to waves is underestimated. The onshore directed bed load transport in front of the breaker bar modeled with van Rijn (2007a) is underestimated a lot.

The bed load transport onshore of the breaker bar is modeled well. Offshore and at the breaker bar the bed load transport is underestimated.

Since there is mostly underestimation of the magnitude of sediment transport in the different transport components the magnitude of the total sediment transport is also underestimated for most locations as well.

During the comparison between the SANTOSS near-bed transport model and the bed load model of van Rijn it seemed that both models perform approximately equal within Delft3D, even though both models use different formulations for the orbital velocities. Both models underestimate the wave related suspended transport since they assume that wave related suspended sediment transport only occurs near the bottom. During the measurements it seems that suspended sediment transport higher in the wave column cannot be neglected.

5 STAND-ALONE SANTOSS COMPUTATIONS

This section will investigate whether it is necessary to improve the current SANTOSS with wave breaking effects. At first, some adjustments to the stand-alone SANTOSS were made; these adjustments are discussed in Appendix H. The output of the stand-alone SANTOSS model will secondly be compared using measured hydrodynamics and modeled hydrodynamics in Delft3D. Errors in the modeled sediment transport will be assigned in this section to either errors in the modeled hydrodynamics, missing wave breaking effects or to other causes. Thirdly some bed slope effects have been added to the stand-alone SANTOSS model. van der A et al. (2013) advises to use the model of Apsley & Stansby (2008) which adds slope effects to the critical bed shear stress. Also a bed slope model used in Delft3D (Bagnold, 1966) will be tested in the stand-alone SANTOSS model. During the measurement it seems that the overshoot velocity was significantly higher compared to the velocity at the wave boundary layer height. This has been found in the literature as well (Bakker & Van Doorn, 1978). Therefore fourthly the near-bed velocity reference height has been varied in this section as well to see the effect of the near-bed velocity reference height on the modeled sediment transport. At last it will be discussed whether there are missing wave breaking effects and if the current models should be improved for wave breaking effects.

5.1 Errors in the Hydrodynamics

Errors in the modeled sediment transport in the Delft3D model can be due to errors in the modeled hydrodynamics. Therefore the stand-alone SANTOSS model will be used to assign errors in the modeled sediment transport to the modeled hydrodynamics. The modeled hydrodynamics is used as input for the stand-alone SANTOSS model. The height used to extract the input from the measurement is set equal to the height at which the hydrodynamics are modeled in Delft3D. This height is the so-called reference height in Delft3D and it is approximately equal to 5 centimeter above the bed. See Figure 5-9 for the near-bed velocity reference heights used in the comparison with the modeled hydrodynamics and the corresponding orbital velocities and net currents at those heights.

The input for the stand alone SANTOSS model has already been discussed in section 3. An overview of the input will be shown below and the errors will be shortly discussed.

There are some minor errors in the wave height (See Figure 5-1). In front of the breaker and offshore off the breaker bar there is some over estimation. In the other parts the measured wave heights fluctuate due to measurements errors. The wave height in this part is modeled quite well.

The orbital velocities are measured quite well onshore of the breaker bar (x > 56 meter) (See Figure 5-2). In front of the breaker bar there is some underestimation of the orbital velocities. The net currents are modeled poorly in Delft3D. The modeled net currents are almost constant throughout the wave flume. From the measurements it seemed that there are variations in the net currents. From locations x ~54 to x ~ 56 meter the net current is over estimated, while more onshore, x ~56 to x ~59 meter, the net currents are under estimated. Especially for x = 56.5 and x = 57.0 m there is a large underestimation of the net current. The velocity skewness and acceleration (See Figure 5-3) skewness are predicted by Delft3D as quite constant throughout the wave flume. The measured velocity skewness and acceleration skewness vary a lot. Therefore the modeled velocity skewness is under and over-estimated. The acceleration skewness is under estimated throughout the whole flume.

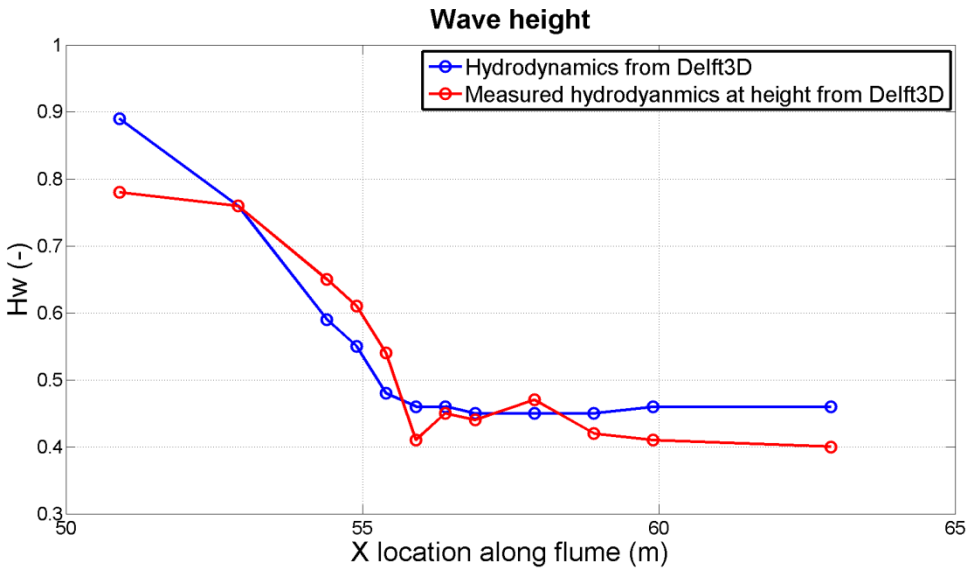

FIGURE 5-1: MEASURED AND MODELED (DELFT3D) WAVE HEIGHT

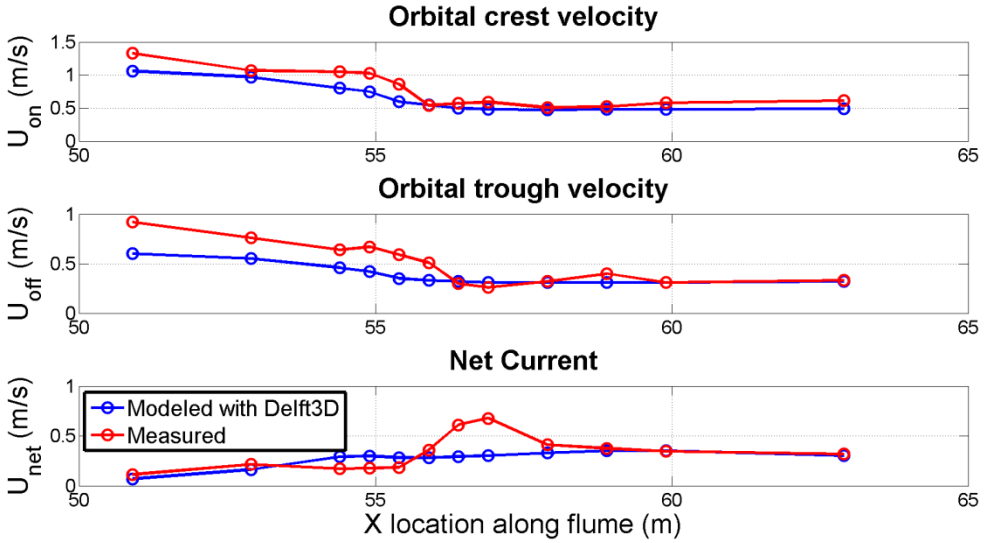

FIGURE 5-2: MEASURED AND MODELED (DELFT3D) ORBITAL CREST AND TROUGH VELOCITES AND NET CURRENT

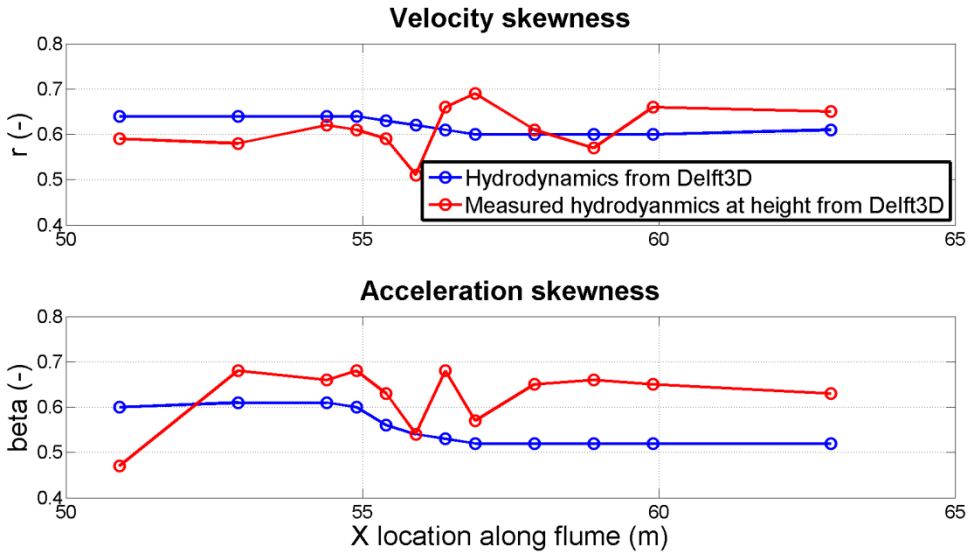

FIGURE 5-3: MEASURED AND MODELED (DELFT3D) VELOCITY AND ACCELERATION SKEWNESS

The result of the stand-alone computation is compared with the input extracted from the measurements and the results of the stand-alone computation with those measurements in Appendix I. From Appendix I it seems that especially the poorly modeled undertow in Delft3D has a lot of effect on the periods, roughness, bed shear stresses and ripples. All these errors affect the sediment load entrained (See Figure I-5) and the phase lags (See Figure I-6).

Appendix I shows all steps the SANTOSS models follows. This section continues with the sediment load entrained and transported during the crest and the trough (See EQ. I-15).

From Figure 5-4 it seems that there is no phase lag on the sand entrained during the crest period for the measured and the modeled hydrodynamics. All the sediment entrained during the crest period is also transported during the crest period. For the sand entrained during the trough period there are phase lag effects for x > 55 meter for the measured hydrodynamics a for x > 53 for the modeled hydrodynamics. The amount of sand entrained during the trough and transported during the trough is approximately equal to the amount of sand entrained during the through and transported during the crest onshore of the breaker bar.

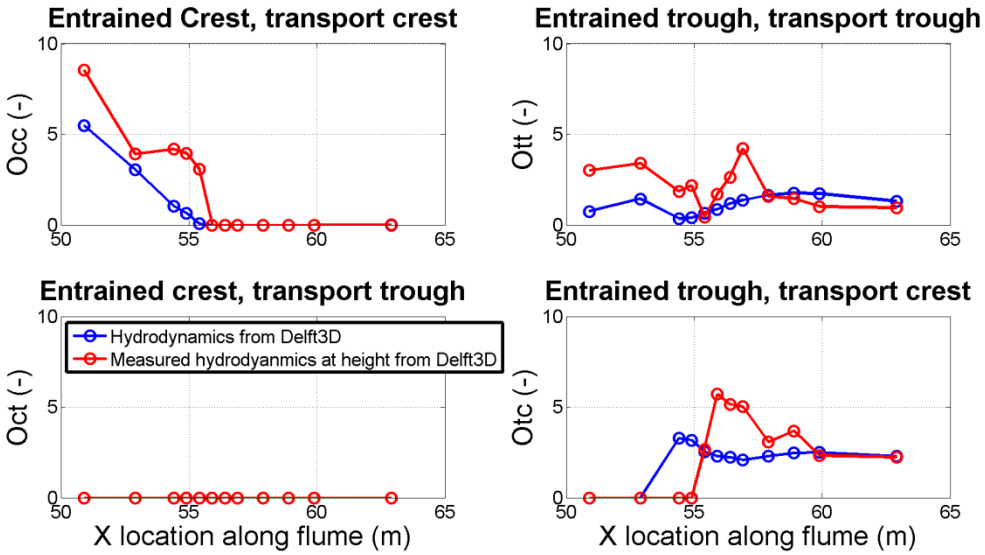

FIGURE 5-4: SAND LOAD ENTRAINED DURING THE CREST AND TROUGH AND TRANSPORTED DURIN THE CREST AND TROUGH MODELED WITH THE MEASURED AND THE MDOELED (DELFT3D) HYDRODYNAMICS

The total sediment transport is calculated with EQ. 2-13. The result is shown in Figure 5-5. Two things stand out, the negative transport at x = 53 m with the measured hydrodynamics and the strong overestimation of the offshore directed sediment transport at locations x = 56.5 and x= 57.0 m. The negative transport is due to a local decrease in the peak orbital crest velocity. The overestimation of the negative transport at locations x = 56.5 and x = 57.0 m is due to the absence of the crest period. The load entrained during the trough period and transport during the crest period cannot be transported because there is no crest period.

The difference between the modeled hydrodynamics and the measured hydrodynamics at the other locations are not very outstanding. There is some underestimation with the modeled hydrodynamics at x = 55.5 and x = 56.0 m due to an under estimation of the modeled net current. The pattern of the sediment transport is better modeled using the measured hydrodynamics. The modeled hydrodynamics shows less difference in the hydrodynamics with adjacent locations.

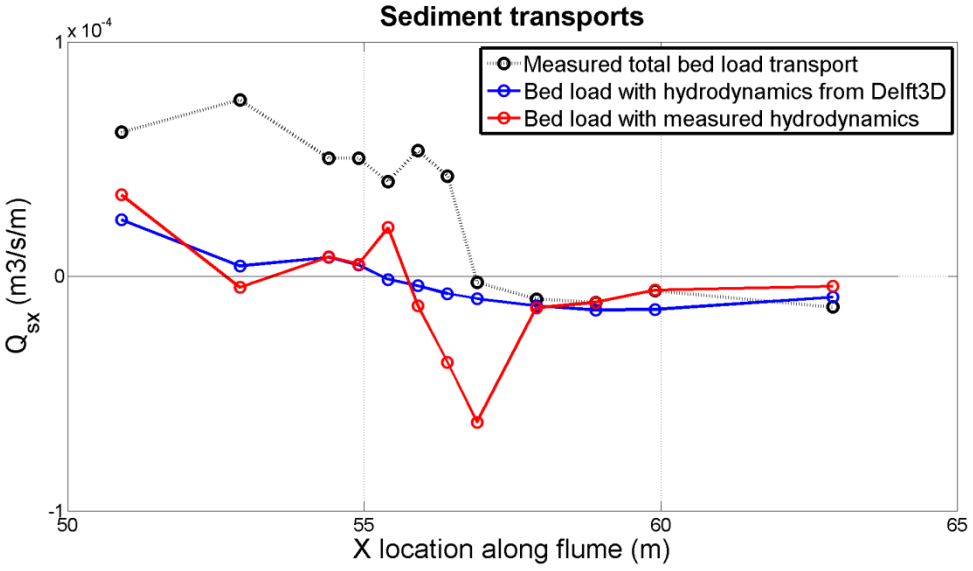

FIGURE 5-5: SEDIMENT TRANSPORT MODELED WITH THE MEASURED AND THE MODELED (DELFT3D) HYDRODYNAMICS

5.2 Bed slope effects

5.2.1 *Slope effect on the critical bed shear stress*

In the stand-alone SANTOSS model there are no bed slope effects included. The SANTOSS model is limited to horizontal bed conditions (van der A et al., 2013). The bed slope can have an effect on the critical shear stress due to a gravitational component and on sediment that is in motion.

Van der A et al. (2013) advise to use the bed slope effect by Apsley & Stansby (2008) on the critical shear stress. Veen (2014) implemented this effect only for the longitudinal critical shear stress since Nomden (2011) concluded that the general method of Apsley & Stansby (2008) causes problems in combination with the phase lag effect. Though this model is implemented and tested in the stand-alone SANTOSS formula, the model reads the following equations:

* $$\theta_{cr_{lo}} = \frac{\sin(\varphi_r + \beta)}{\sin(\varphi_r)} * \theta_{cr,0} \quad with\ \varphi_r = \tan^{-1}\left(\frac{30}{180} * \pi\right)$$ EQ. 5-1

With φ_r is the angle of repose on a natural talud and β is the angle (positive in the upslope direction and negative in the down slope direction) of the bed slope given by:

* $$\beta = \tan^{-1}\left(\frac{dz_b}{dx}\right)$$ EQ. 5-2

With $\frac{dz_b}{dx}$ is the local bed slope.

5.2.2 *Slope effects from Delft3D*

The default bed slope effect from Delft3D has been implemented and tested in the stand-alone model as well. In Delft3D the sediment transport is affected by the longitudinal bed slope (See Figure 5-7) through the model of Bagnold (1966). This model is applied after the transport rates have been calculated. Therefore this model with be applied after the calculation of the final transport rates as well. The sediment transport corrected for bed slope effect $\vec{q}_s'$ is calculated with the following formula:

* $$\vec{q}_s' = \alpha_s * \vec{q}_s$$ EQ. 5-3

With $\vec{q}_s$ is the net transport rate according to EQ. 2-13 and α_s is the correction factor for bed slope effects calculated by:

* $$\alpha_s = 1 + \alpha_{bs} * \left(\frac{\tan(\varphi_r)}{\cos\left(\tan^{-1}\left(\frac{dz}{ds}\right)\right)\left(\tan(\varphi_r) - \frac{dz}{ds}\right)} - 1\right)$$ EQ. 5-4

With $\frac{dz}{ds}$ is bed slope in the direction of bed load transport and α_{bs} is a tuning parameter with a default value of 1 in Delft3D and Therefore this default value has been used in the stand-alone Santoss formula as well.

5.2.3 *Results of the bed slope effects models*

The result of the models of Apsley & Stansby (2008), Bagnold (1966) and the models combined are shown in Figure 5-6. It seems that the model of Apsley & Stansby (2008) barely has effect on the net sediment transport. The model of Bagnold (1966) decreases the upslope transport and increases the down slope transport. This model performs as it could be expected from a model

that calculates the effect of bed slope on sediment transport. Up slope transport is decreased and down slope transport is increased. The importance of the calibration parameter α_{bs} is hard to determine, since it is not clear if onshore directed transport is missing due to an underestimation of the slope effect or if it is due to missing wave breaking effects.

The model of Apsley & Stansby (2008) has very little effect on the sediment transport. This model changes the critical bed shear stress. Since the actual bed shear stress is well above the critical bed shear stress. A small change of the critical bed shear stress barely has effect on the sediment transport. This is visible in Figure 5-6.

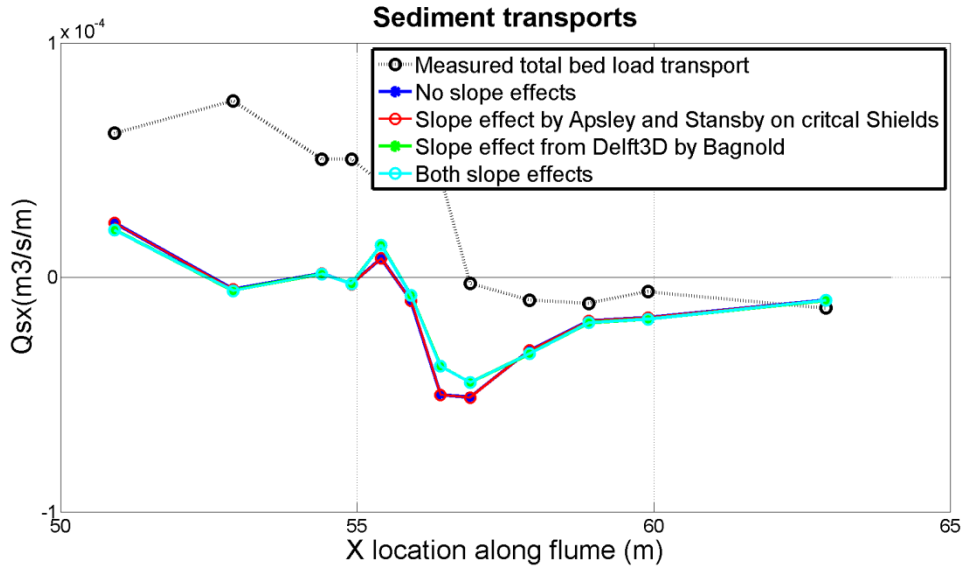

FIGURE 5-6: SEDIMENT TRANSPORT WITH THE SLOPE EFFECT BY APSLEY AND STANSBY (2008) AND BAGNOLD (1966) AND A COMBINATION OF BOTH MODELS

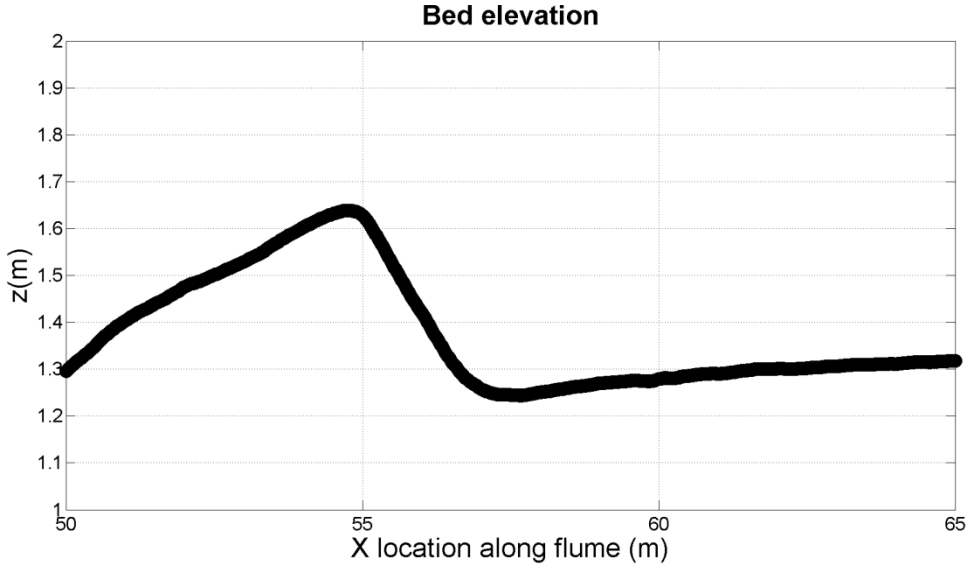

FIGURE 5-7: BED ELEVATION

5.2.4 *Bagnold (1966) during crest and trough*

Disadvantage of the bed slope model of Bagnold (1966) is that it cannot change the direction of the sediment transport, since the formula is designed for rivers with sediment transport in one direction. The sediment transport is changed dependable on the direction and the magnitude of

the sediment transport, but it can only change the magnitude of the sediment transport. During nearshore waves, the SANTOSS formula differs between onshore directed transport and offshore directed transport (EQ. 2-13). Therefore the Bagnold (1966) can also be applied differently during the crest and trough. EQ. 2-13 is therefore changed to:

$$\vec{\phi} = \frac{\vec{q}_s}{\sqrt{(s-1)g d_{50}^3}} = \frac{\alpha_{sc}\sqrt{|\theta_c|}T_c\left(\Omega_{cc} + \frac{T_c}{2T_{cu}}\Omega_{tc}\right)\frac{\vec{\theta}_c}{|\theta_c|} + \alpha_{st}\sqrt{|\theta_t|}T_t\left(\Omega_{tt} + \frac{T_t}{2T_{tu}}\Omega_{ct}\right)\frac{\vec{\theta}_t}{|\theta_t|}}{T} \quad \text{EQ. 5-5}$$

With α_{sc} and α_{st} are the correction factors for bed slope effects during the crest and the trough:

$$\alpha_{sc} = 1 + \alpha_{bs} * \left(\frac{\tan(\varphi_r)}{\cos\left(\tan^{-1}\left(-\frac{dz_b}{dx}\right)\right)\left(\tan(\varphi_r) + \frac{dz_b}{dx}\right)} - 1\right)$$

$$\alpha_{sc} = 1 + \alpha_{bs} * \left(\frac{\tan(\varphi_r)}{\cos\left(\tan^{-1}\left(\frac{dz_b}{dx}\right)\right)\left(\tan(\varphi_r) - \frac{dz_b}{dx}\right)} - 1\right) \quad \text{EQ. 5-6}$$

$\frac{dz_b}{dx}$ Is the bed slope. During the crest period, the sediment transport is onshore directed, therefore the direction of the bed slope is changed assuming that a down slope bed is negative and an upslope bed is positive. For an up slope bed the onshore directed sediment transport during the crest is now decreased while the offshore directed sediment transport during the trough is increased. This is vice versa for down slope beds. The result on the total sediment transport is visible in Figure 5-8. At location x= 54.4 meter where there is an upslope bed the total transport currently changes from onshore directed to offshore directed

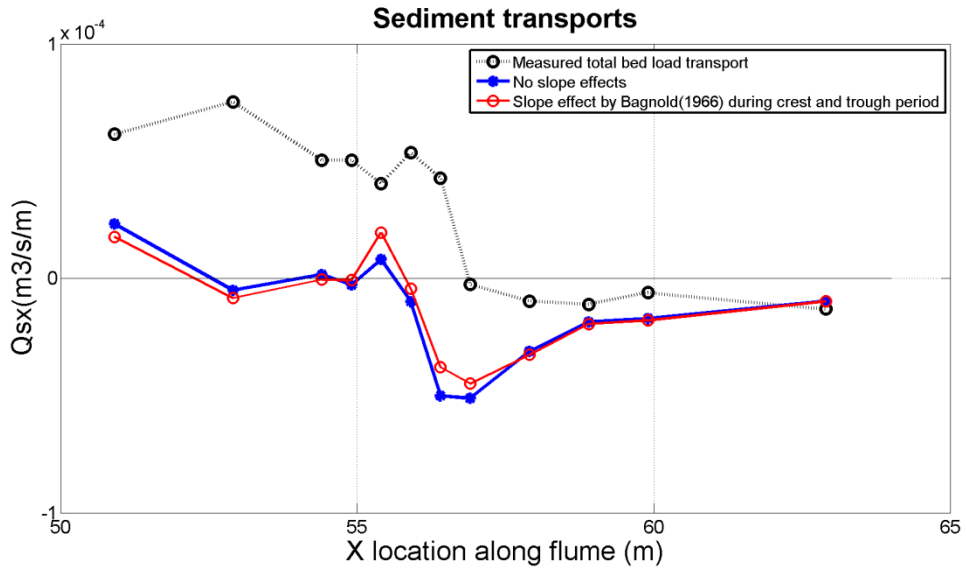

FIGURE 5-8: SEDIMENT TRANSPORT WITH THE SLOPE EFFECT AND BAGNOLD (1966) APPLIED DIFFERENTLY DURING THE CREST AND THE TROUGH PERIOD.

5.3 Near-bed velocity reference height

The orbital velocities and the net currents were measured at different heights during the CIEM wave flume experiments. The SANTOSS model is developed for predicting the net sand transport at the edge of the wave boundary layer. Van der A et al. (2013) indicate that the height

of the wave boundary layer is of minor importance for predicting the net sediment transport with the SANTOSS formula. Though, there are certainly differences between the near-bed orbital velocities and net currents according to Figure 5-9. It is therefore assumable that the height of the input does have effect on the sediment transport.

Four different heights have been tested in the stand-alone SANTOSS model. The standard height, which is the height of the lowest ADV (11 cm), the height which was output from Delft3D, the height of the maximum overshoot velocity and the averaged values of the ACVP measurements have been used. The heights used are shown in Figure 5-9. The orbital velocities and net current for the averaged height are not the orbital velocities and net current at that height, but for the averaged height the orbital velocities and the net current are also averaged.

The effect of choosing different heights on the orbital velocities is shown in Figure 5-10. The peak orbital velocities are largest for the overshoot velocity. For x = 57 m the net current is significantly higher using the overshoot velocity compared to other heights. The orbital velocities and the net currents at the other heights are quite well comparable to each other. There are some minor differences, but these do not stand out.

The result, using the different heights as inputs on the sediment load entrained and transported are shown in Figure 5-11. The standard height, the output height of Delft3D and the averaged height have quite equal results. The height obtained from Delft3D leads to a somewhat stronger phase lag effect for the trough, the sediment entrained during the trough and transported during the crest is a little bit higher.

Using the overshoot velocity causes a much larger sand load entrained during the crest in front of and at the breaker bar. This also increases the onshore directed sediment transport (See Figure 5-12). The higher measurement of the net current at x = 57 m using the maximum overshoot height has a large effect on the sand load entrained during the trough. The phase lag is also very high, but since there is no crest period sand entrained during the trough and transported during the crest period is not possible. Therefore there is only sand transport in the offshore direction.

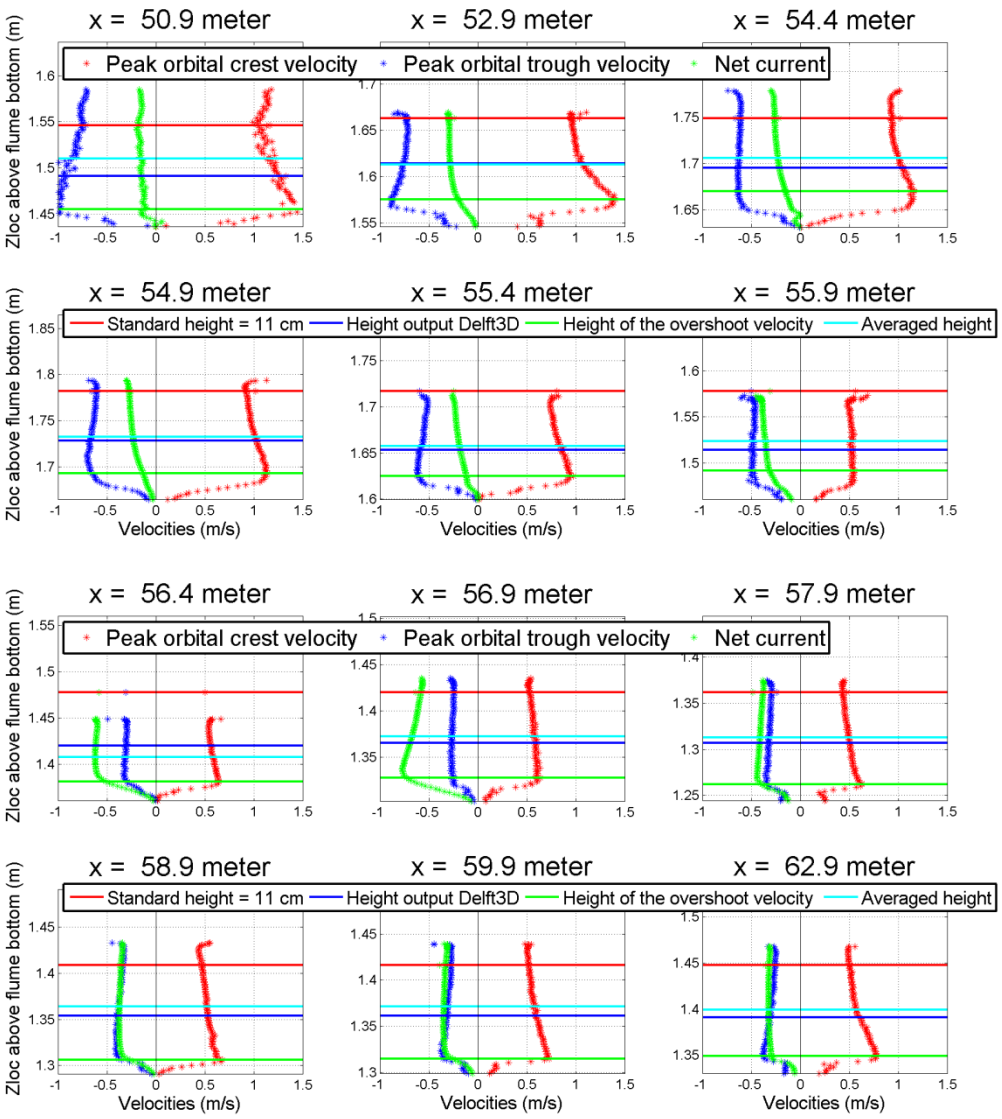

FIGURE 5-9: NEAR-BED ORBITAL VELOCITIES AND NET CURRENTS AND DIFFERENT NEAR-BED VELOCITY REFERENCE HEIGHTS.

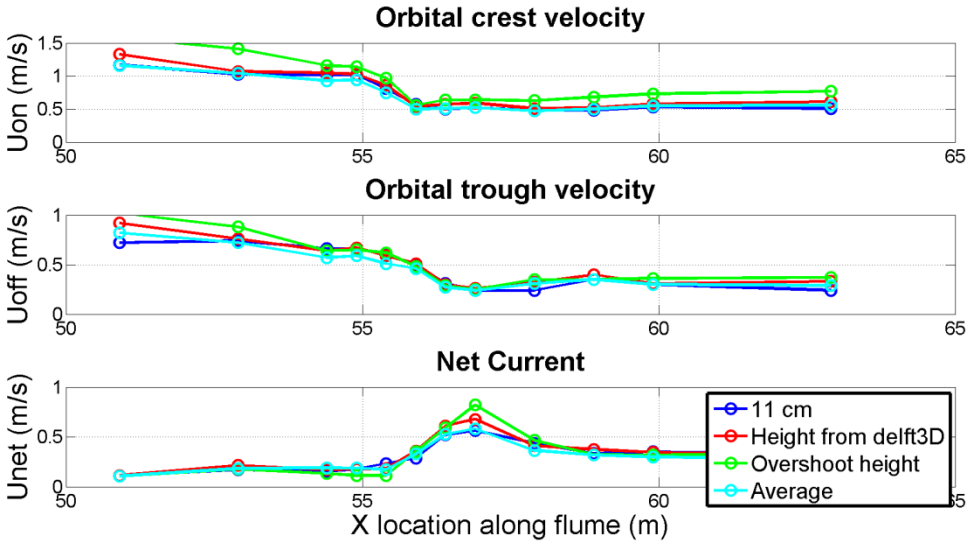

FIGURE 5-10: ORBITAL VELOCITIES AND NET CURRENTS AT DIFFERENT HEIGHTS

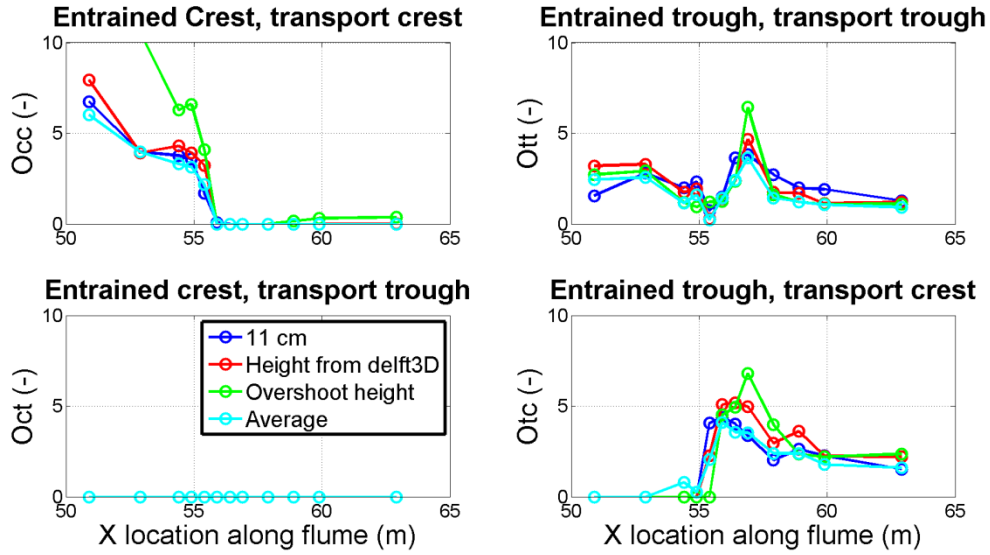

FIGURE 5-11: SAND LOAD ENTRAINED EN TRANSPORTED WITH DIFFERENT HEIGHTS AS INPUT.

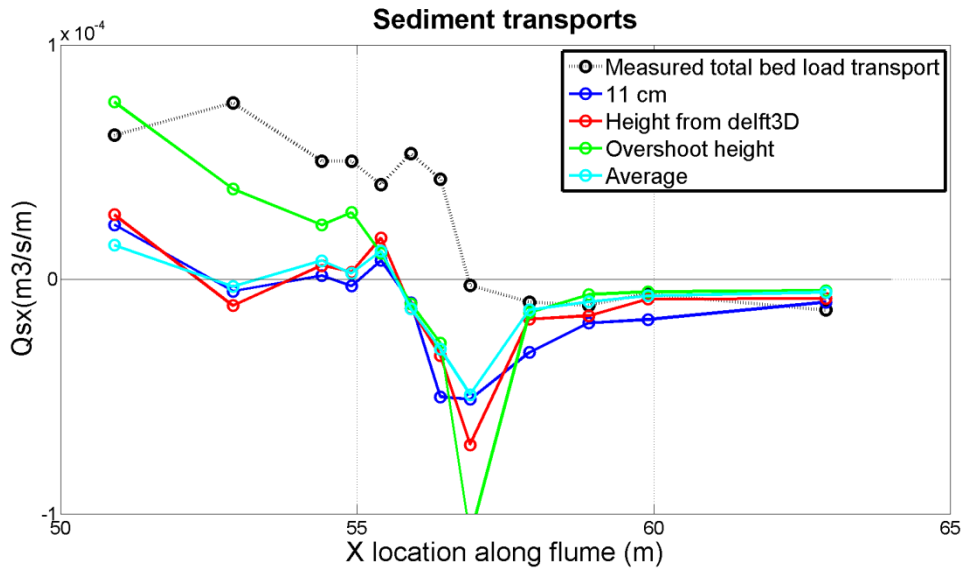

FIGURE 5-12: SEDIMENT TRANSPORTS WITH DIFFERENT HEIGHT AS INPUT.

5.4 Missing wave breaking effects

From x = 50.9 to x = 57.9 m onshore directed sediment transport is missing (See Figure 5-8 and Figure 5-12). This missing onshore directed sediment transport is due to the model concept of the SANTOSS formula. The missing onshore directed sediment transport can have multiple reasons:

- For locations x = 54.9 to x = 55.9 m there is no crest period, but there is still onshore directed sediment transport. The SANTOSS formula cannot predict onshore directed sediment transport without a crest period.
- The bed slope effects are underestimated. At the lee side of the breaker bar onshore directed sediment transport is missing, it is quite well possible that this is due to an under estimation of the bed slope effects.
- The onshore directed sediment transport is underestimated near the wave breaking location. It is assumable that wave breaking does have effect on the sediment transport. Since wave breaking effects are not taken into account into the current SANTOSS model it is quite well possible that the missing onshore directed sediment transport is underestimated due to missing wave breaking effects.

5.5 Conclusion

The difference between the measured and the modeled hydrodynamics as input to the SANTOSS formula significantly influences the predicted sediment transport. This is especially due to an under- and overestimation of the modeled net current. Errors in the predicted net current cause errors in the predicted half-cycle periods, phase lag, Shields and the sand load entrained. Due to these errors in the modeled net current the sediment transport is predicted better for some locations using the modeled hydrodynamics. Therefore errors in the modeled hydrodynamics cause a better prediction of the sediment transport for some locations.

The errors in the hydrodynamics are too large to properly judge improvements of wave breaking effects on the SANTOSS model within the Delft3D software package. Therefore improvements for wave breaking effects in the SANTOSS formula will mainly be tested in the stand-alone SANTOSS formula.

Changing the near-bed velocity reference height does not have a strong impact on the sediment transport. The slope effects improve the sediment transport, especially using the Bagnold (1966) formula differently during the crest and the trough period.

It seems that the onshore directed sediment transport is underestimated and for some locations it is even predicted in the wrong direction. This can due to missing wave breaking effects. The SANTOSS sediment transport formula should therefore be improved so that it can deal with wave breaking effects.

Improving the current models for suspended sediment is probably also necessary. Since Delft3D models too many errors in hydrodynamics and morphodynamics for this test case. Improvements will therefore only be compared in the stand-alone model were effects of error is the hydrodynamics and suspension transports are excluded.

6 POSSIBLE IMPROVEMENTS IN SANTOSS

In this section three possible improvements of the SANTOSS formula will be tested. These improvements are obtained from literature. The wave Reynolds stress is currently related to the wave energy(Nielsen, 2006). In the calculation of the wave Reynolds stress it is not account for the energy dissipation of rollers. It could be possible that the wave Reynolds stress is also dependable on the roller energy dissipation. Therefore the formulation of the wave Reynolds stress has been changed so that roller energy dissipation is taken into account as well. Turbulence seems important under breaking waves (Ting & Kirby, 1995, 1996). Therefore turbulence due to breaking waves have been implemented in the Shields parameter (Reniers et al., 2013) and in the orbital velocity amplitude (Reniers, Roelvink, & Thornton, 2004).

6.1 Performance of possible improvements

6.1.1 *Wave Reynolds stress due to wave energy dissipation and roller energy dissipation*

The Shields parameter is currently calculated according to EQ. I-8. The wave Reynolds stress is applied as a stress at the edge of the wave boundary layer that accounts for the vertical orbital water particle motions in and out of the wave boundary layer for progressive surface waves (Nielsen, 2006; van der A et al., 2013). The wave Reynolds stress in EQ. I-8 can be extended to an equation that accounts for wave breaking effect by adding the roller energy dissipation to the wave energy dissipation. This changes EQ. I-8 to:

* $$\theta_i = \frac{\frac{1}{2} f_{w\delta i} |u_{i,r}| u_{i,r}}{(s-1) g d_{50}} + \frac{\tau_{br}}{(s-1) g d_{50}} \qquad \text{EQ. 6-1}$$

With τ_{br} is the wave Reynolds stress due to wave energy dissipation and roller energy dissipation. Nielsen (2006) (See EQ. I-10) indicates that the shear stress depends on the energy dissipation of the waves. The shear stress can be calculated with (Dunn, 2003; Longuet-Higgins, 2005):

$$\rho \overline{\tau_{br}} = -\rho (\overline{\tilde{u}\tilde{w}})_{\infty} = \frac{D_e}{c} \qquad \text{EQ. 6-2}$$

With D_e consisting of the total energy dissipation consisting of the wave energy dissipation and the roller energy dissipation:

* $$-D_e = \frac{\partial}{\partial x}(Ec) + \frac{\partial}{\partial x}(E_r c) \qquad \text{EQ. 6-3}$$

Rewriting with EQ. 3-3 and EQ. 3-9 gives:

* $$\begin{aligned} -D_e &= -D_w - D_f + \left(\frac{D_w + D_r}{2}\right) \\ D_e &= \frac{1}{2}(D_w + D_r) + D_f \end{aligned} \qquad \text{EQ. 6-4}$$

Implementing EQ. 6-4 in EQ. 6-2 gives:

* $$\overline{\tau_{br}} = \frac{D_w + D_r + 2D_f}{2\rho c} \qquad \text{EQ. 6-5}$$

In this formula, D_w, D_f and D_r can be calculated the same way as in Delft3D. The equations used are EQ. 3-5, EQ. 3-8 and EQ. 3-10 for respectively the dissipation due to wave breaking, bottom friction and due to roller energy loss. The roller energy E_r depends on the roller mass balance. The roller mass balance cannot be solved for the stand alone SANTOSS model. Therefore an approximation method for the roller energy will be used according to Uchiyama et al. (2010):

$$E_r = 0.5 * \rho_w * g * H * hw * ar0 * Q_s \quad \text{EQ. 6-6}$$

In this formula $ar0$ is an empirical constant equal to 0.06 and Q_s is the fraction of broken waves. The fraction of broken waves is either one or zero because there are regular breaking waves. Therefore the conditions used to determine the fraction of breaking waves from Eq. 3-6 have been used to determine the fraction of broken waves Q_s. This causes probably an overestimation of the roller energy (See Figure 6-3). The roller energy is largest in front of the breaker bar (x = 50.9 m), during modeling in Delft3D it seemed that the roller was not fully developed at x = 50.9 m (See Figure 6-3 and Figure C-4). Therefore there is some overestimation of the roller energy in front of the breaker bar, which will also cause an overestimation of the wave Reynolds stress in front of the breaker bar. The increased Shields parameter is shown in Figure 6-1. The Shields parameter of the crest increases in front of and at the breaker bar where there is energy dissipation. Another option is to use the roller energy as input in the SANTOSS model (See Figure C-4). This decreases the roller energy a little. The roller energy in front of the breaker bar is then equal to zero.

The increase of the Shields parameter of the crest also causes and increases of the sand load entrained during the crest. The Shields parameter behind the breaker bar (x = 56 to x = 57.5 m) is now larger than the critical Shields parameter (See EQ. 2-14). Sand load will be entrained during the crest period while this was not the case without the additional bed shear stress due to breaking waves. For the locations in front of the breaker bar and on top of the breaker bar the amount of sand load entrained is increased due to an increase of the Shields parameter of the crest.

While there is no phase lag for the crest period, all sediment entrained during the crest will also be transported during the crest period (See EQ. I-15). This causes an increase of the onshore directed sediment transport. The onshore directed sediment transport is still under estimated in front of and at the breaker bar. For the locations x = 56.5 and 57 m there was an increase visible in the sand load entrained, but the shoreward directed sediment transport did not increase. This is due to the fact that there is no crest period at those locations. Without a crest period the SANTOSS model cannot predict onshore directed sediment transport (See EQ. 2-13).

There are almost no differences between the results with the modeled roller energy (Uchiyama et al., 2010) and the roller energy from Delft3D. This is due to the fact that the roller dissipation D_r is small compared to the dissipation due to wave breaking D_w (See Figure 6-3). Modeling the wave Reynolds stress due to wave energy dissipation and roller energy dissipation gives a little better prediction of the net sediment transport. To see if the extended wave Reynolds stress is realistic compared to the measurements the wave Reynolds stress has been extracted and compared to the modeled wave Reynolds stress in Appendix J. It seems that the wave Reynolds stresses are over estimated using the energy dissipation of the wave and the roller. Applying the wave Reynolds stress caused by energy dissipation due to waves and rollers is not very realistic and useful, since the actual wave Reynolds stress is overestimated and the prediction of the sediment transport does not improve.

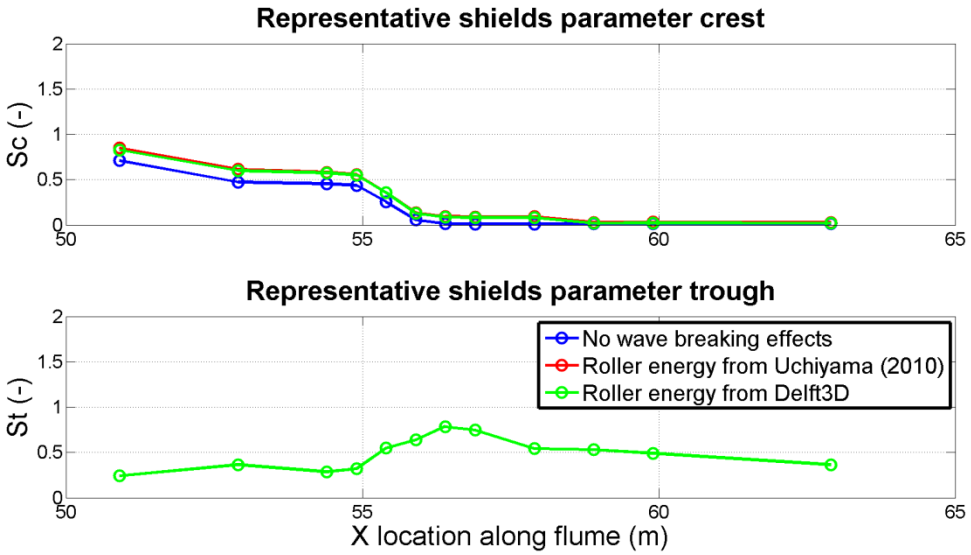

FIGURE 6-1: INCREASED SHIELDS PARAMETER CREST DUE TO ADDITIONAL BED SHEAR STRESS DUE TO BREAKING WAVES.

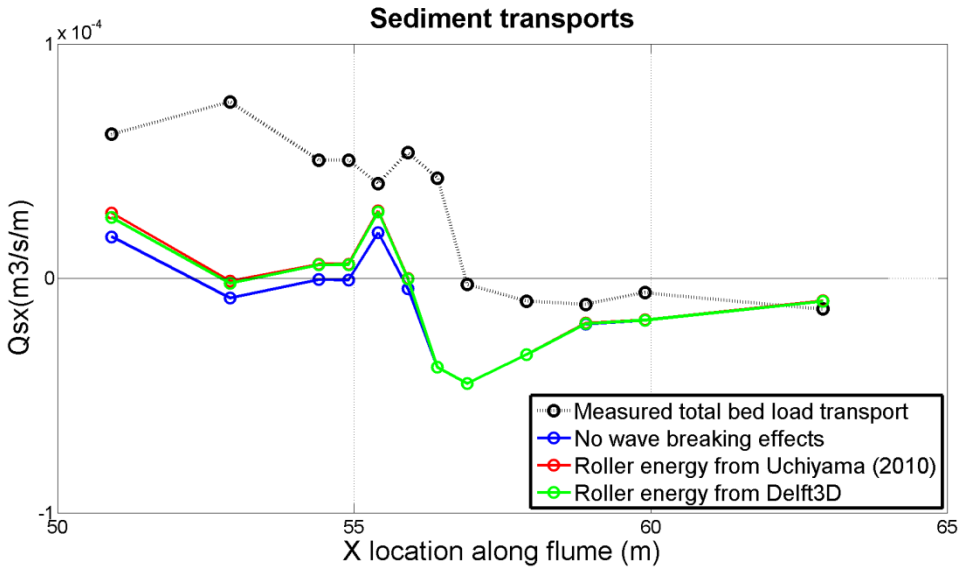

FIGURE 6-2: SEDIMENT TRANSPORT WITH AND WITHOUT ADDITIONAL BED SHEAR STRESS DUE TO BREAKING WAVES.

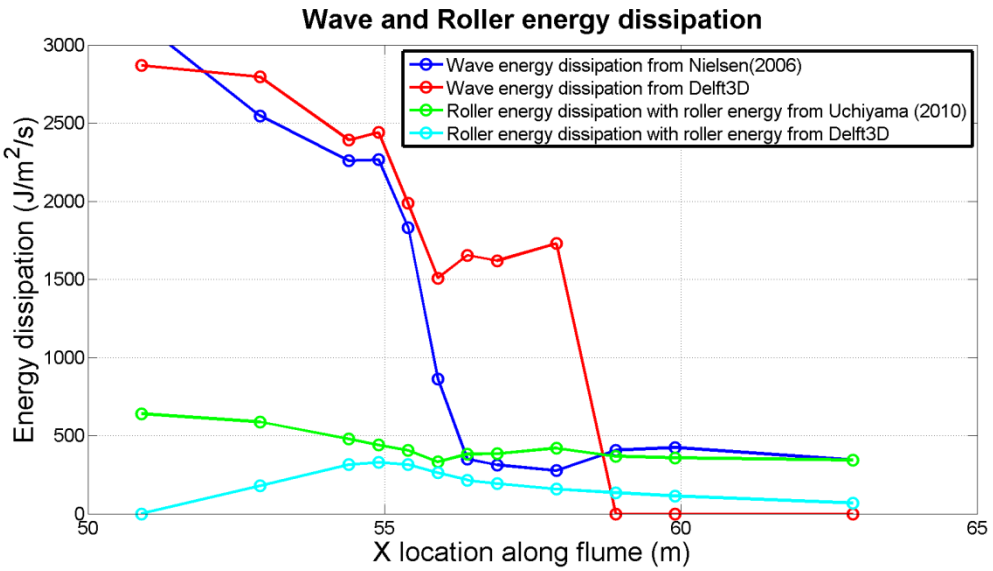

FIGURE 6-3: WAVE ENERGY DISSIPATION FROM NIELSEN (2006) AND FROM DELFT3D AND ROLLER ENERGY DISSIPATION WITH ROLLER ENERGY FROM UCHIYAMA (2010) AND FROM DELFT3D

6.1.2 *Adding turbulent values to the root mean square orbital velocity*

Reniers et al. (2004) assumes that sediment is stirred by a combined short-wave velocity and the wave-breaking induced turbulence motion, this combination is shown below:

*

$$u_{i,r} = \sqrt{u_{i,r}^2 + 0.5 * k_{bed}} \qquad \text{EQ. 6-7}$$

In which k_{bed} is the near-bed turbulence depending of the exponentially decreasing inverse relative wave height given by (Roelvink & Stive, 1989):

$$k_{bed} = \frac{\bar{k}}{\exp(h/H_{rms}) - 1} \qquad \text{EQ. 6-8}$$

Assuming that the length scale of vortices is equal to $l_v = 0.07h$, that the height over which dissipation takes place is equal to the water depth, neglecting advective and diffusive terms in the turbulence and assuming that turbulence is produced locally the near-bed turbulence can be calculated with (Reniers et al., 2004; Roelvink & Stive, 1989):

$$k_{bed} = \frac{(D_r/\rho)^{2/3}}{\exp(h/H_{rms}) - 1} \qquad \text{EQ. 6-9}$$

With D_r is the roller energy dissipation given by EQ. 3-10. The roller energy predicted by Uchiyama et al. (2010) (EQ. 6-6) is overestimated in front of the breaker bar and probably also throughout the rest of the wave flume (See Figure 6-3). Therefore the roller energy obtained from the Delft3D model has been used as input of the stand alone model (See section 6.1.1).

Van Thiel De Vries (2009) and Ribas, de Swart, Calvete, & Falqués (2011) replace the 0.5 from EQ. 6-7 with a calibration factor γ_{tur}:

*

$$u_{i,r} = \sqrt{u_{i,r}^2 + \gamma_{tur} k_{bed}} \qquad \text{EQ. 6-10}$$

Van Thiel De Vries (2009) uses a value of 12.4 for a wave-averaged turbulence model. Ribas et al. (2011) vary γ_{tur} in the range of 0 to 50. So, they found that the effect of turbulence is underestimated. The turbulence also affects the calculated half-cycle periods through the velocity modification in the SANTOSS model, therefore the earlier used measured periods cannot be used any further and the periods should calculated in the stand-alone SANTOSS model.

6.1.2.1 Crest/trough and crest with γ_{tur} is 0.5

Applying EQ. 6-7 for the crest and the trough and using 0.5 for γ_{tur} slightly increases the peak crest and trough orbital velocity as shown in Figure 6-4. The peak orbital velocities increase most before and at the breaker bar. The effect of the increased peak orbital velocities on the sediment loads is shown in Figure 6-5. The increased peak orbital velocities increases the sediment load entrained during the crest and trough period. The phase lag during the trough is also increased. This causes more transport during the crest of sediment that is entrained during the trough.

The results of increasing the peak orbital crest and trough velocity with turbulence with $\gamma_{tur} = 0.5$ on the sediment transport is shown in Figure 6-6. It seems that the effect of the increases peak trough velocity and the increases peak crest velocity cancel each other out. The total sediment transport has barely changed, while differences in the sediment entrained were clearly visible.

Ting & Kirby (1995) and Toomas (2001) found that turbulent transport is directed onshore for plunging waves and that turbulence has decreased to a wave averaged value during the wave trough. Therefore in this section the turbulent effect on the root mean squared velocity will also just be applied during the crest period.

Applying EQ. 6-7 just during the crest period results in an increased peak orbital crest velocity show in Figure 6-4. The resulting sediment entrained during the crest and trough and transport during the crest and trough are shown in Figure 6-6. The sediment load entrained during the crest is increased while the sediment load during the trough only decreased a little. This results in a slightly better prediction of the sediment transport. Therefore turbulence will only be applied during the crest period.

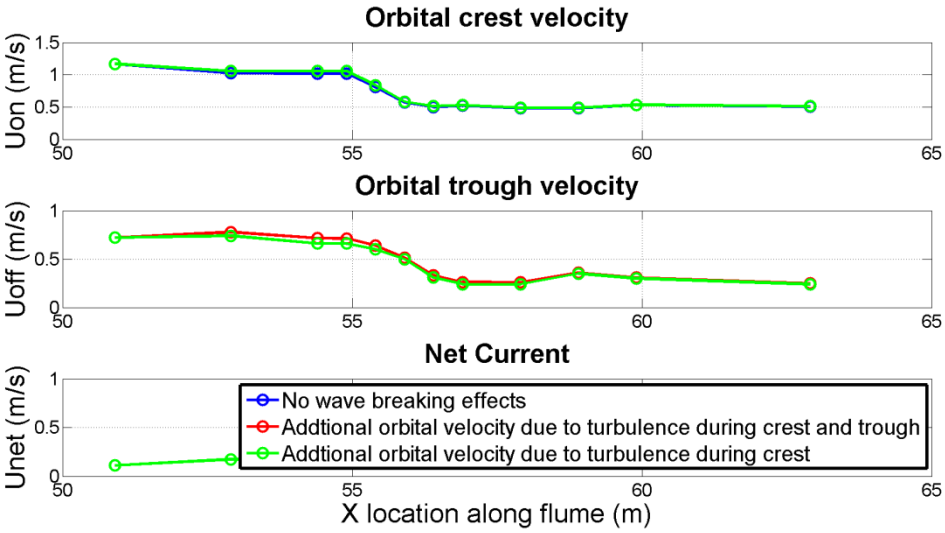

FIGURE 6-4: INCREASED PEAK ORBITAL CREST AND TROUGH VELOCITY WITH $\gamma_{tur} = 0.5$.

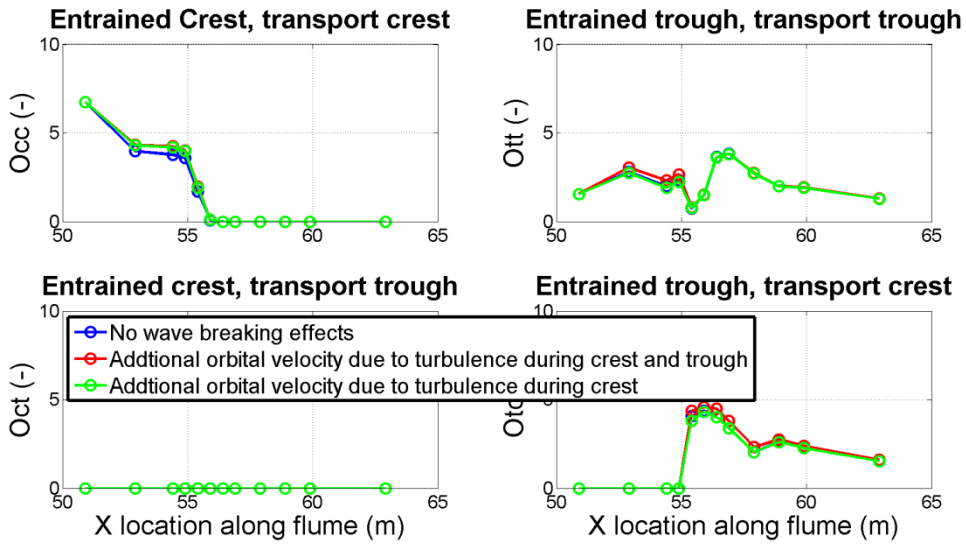

FIGURE 6-5: SEDIMENT TRANSPORT ENTRAINED AND TRANSPORTED DURING THE CREST AND TROUHG WITH AND INCREASED PEAK ORBITAL CREST AND TROUGH VELOCITY WITH $\gamma_{tur} = 0.5$.

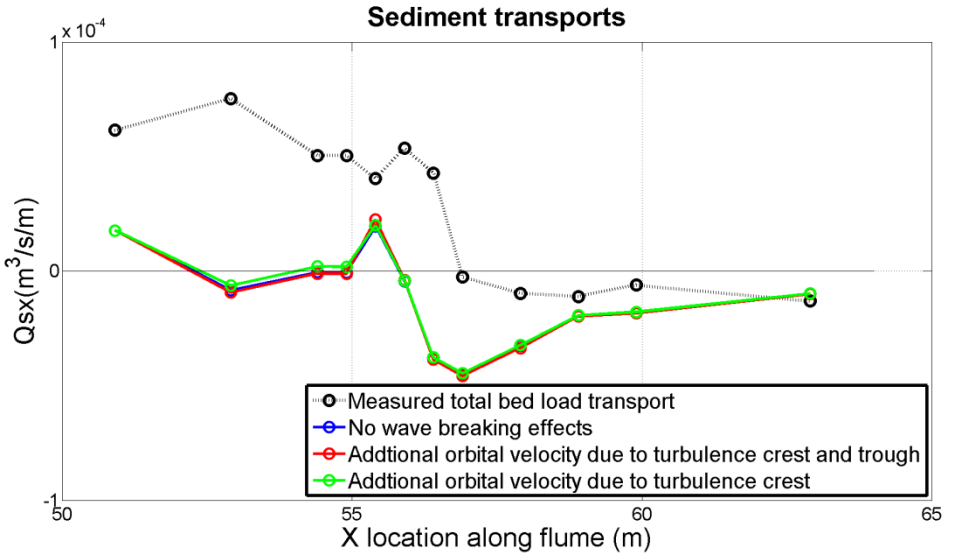

FIGURE 6-6: SEDIMENT TRANSPORT WITH AN INCREASED PEAK ORBITAL CREST AND TROUGH VELOCITY WITH $\gamma_{tur} = 0.5$.

6.1.2.2 Calibrated γ_{tur}

It seems from Figure 6-6 that the sediment transport is still under estimated. This might be due to the fact that the (effect of) turbulence is underestimated. Therefore the parameter γ_{tur} has been varied in the range of 1 to 10. The effect on the orbital crest velocity is visible in Figure 6-7. The increase of the orbital crest velocity due to turbulence causes an increase of the representative Shields parameter during the crest and a decrease of the representative Shields parameter during the trough. The sand load entrained during the crest therefore increases and the sand load entrained during the trough decreases (See Figure 6-8). The net sediment transport with varying γ_{tur} is shown in Figure 6-9. It seems that for a value of approximately 6 for γ_{tur} the sediment transport shows closest agreement with the measurements.

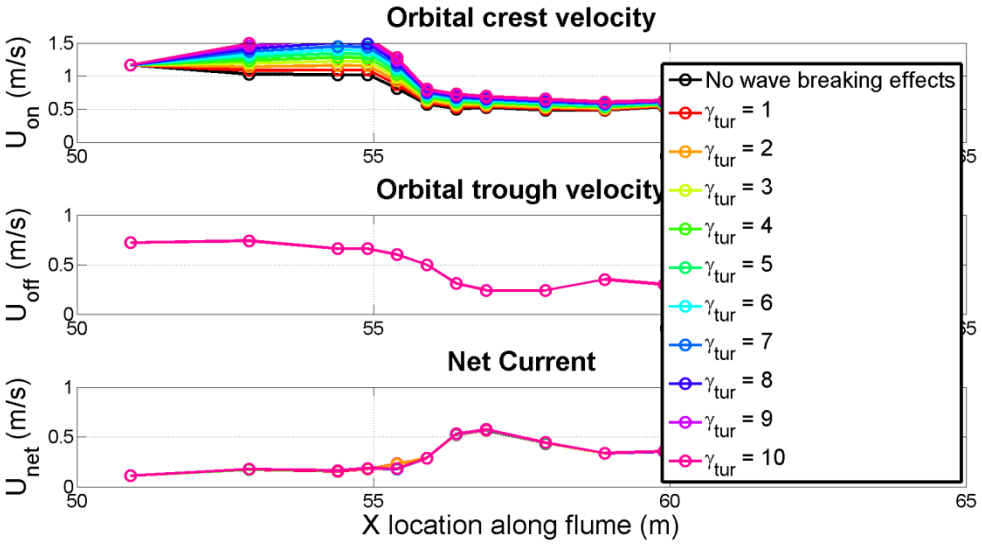

FIGURE 6-7: INCREASED PEAK ORBITAL CREST VELOCITY USING THE ROLLER ENERGY OBTAINED FROM DELFT3D AND A VARYING γ_{tur}.

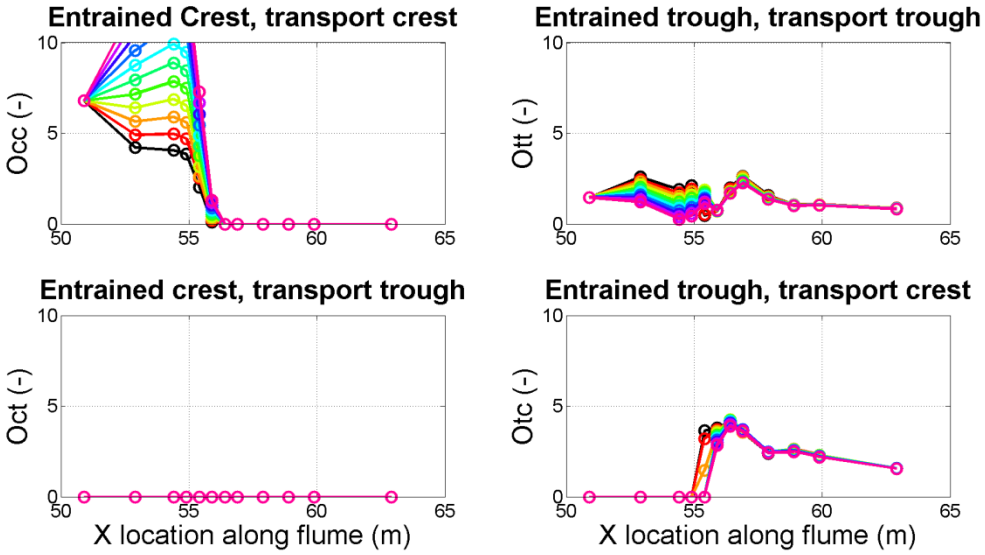

FIGURE 6-8: SAND LOAD ENTRAINED AND TRANSPORTED DURING THE CREST AND TROUGH WITH AN INCREASED PEAK ORBITAL CREST VELOCITY USING THE ROLLER ENERGY OBTAINED FROM DELFT3D AND A VARYING γ_{tur}.

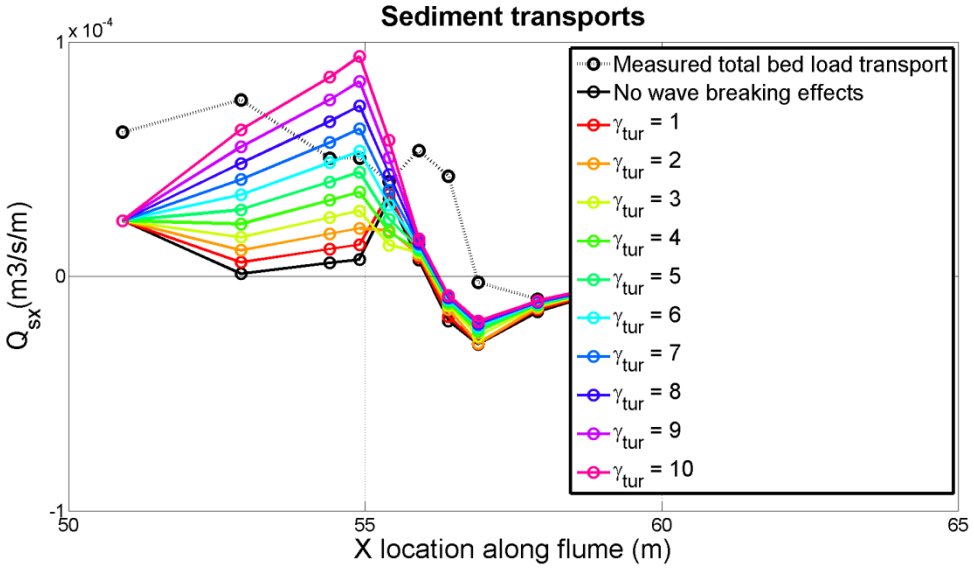

FIGURE 6-9: SEDIMENT TRANSPORT WITH AN INCREASED PEAK ORBITAL CREST VELOCITY USING THE ROLLER ENERGY OBTAINED FROM DELFT3D AND A VARYING γ_{tur}.

The modeled turbulence and the turbulence extracted from the measurements are shown in Appendix K. It seems that the turbulence is overestimated by approximately an order of magnitude using γ_{tur} equals six. The strength of the roller-induced turbulence k_{bed} seems to be higher than the representative orbital velocity. This was also found by Ribas et al. (2011) who found a value of 50 for γ_{tur} in an almost similar formulation calculation for the stirring velocity.

6.1.3 *Additional bed shear stress due to turbulence*

Reniers et al. (2013) add additional bed shear stress to the intra wave dependent Shields parameter.

$$\theta'(t) = \frac{0.5 f_{2.5}\left[u_{i,r}^2(t) + k_{bed}(t)\right]}{g\Delta D} \quad \text{EQ. 6-11}$$

Rewriting this for the bed shear stress due to turbulence gives:

$$\tau_{tur} = 0.5 f_{2.5} k_{bed}(t) \quad \text{EQ. 6-12}$$

With $f_{2.5}$ is the wave friction factor which is taken equal to the current and wave related friction factor from EQ. I-4. The turbulence is taken steady throughout the crest period of the wave and it is assume to be zero during the trough period of the wave since Ting & Kirby (1995) and Toomas (2001) found that turbulent transport is directed onshore for plunging waves. This changes EQ. 6-12 to

$$\tau_{tur} = 0.5 f_{w\delta c} k_{bed} \quad \text{EQ. 6-13}$$

In which k_{bed} is the near-bed turbulence depending given by EQ. 6-9. An option to increase the effect of turbulence on the Shields parameter is by adding a calibration parameter to EQ. 6-13. This gives the following formula:

$$\tau_{tur} = 0.5 f_{w\delta c} \gamma_{tur} k_{bed} \quad \text{EQ. 6-14}$$

Increasing the calibration factor also increases the representative Shields parameter during the crest. Especially at the top of the breaker bar the representative Shields parameter increase a

lot. At this location the roller energy is also high. The increase of the representative Shields parameter increase the sand load entrained during the crest as well. This increase the onshore directed bed-load transport (See Figure 6-10). A value for γ_{tur} of 4 seems optimal for the locations x = 53 to x = 55.5 m. For the locations x = 56 to x = 57.5 m there is no crest period. Onshore directed sediment transport can therefore not be predicted.

From Figure 6-10 it seems that the sediment load entrained during the crest and transported during the trough increases for location x = 56 to x = 57.5 m with an increasing value for γ_{tur}. This would imply that the offshore directed sediment transport would increase as well for these locations. Though, a criterion in the SANTOSS model has been added that if there is a very small crest period the sand load entrained in the crest period will not be transported. This also applies for the sand load entrained during the crest and transported during the trough.

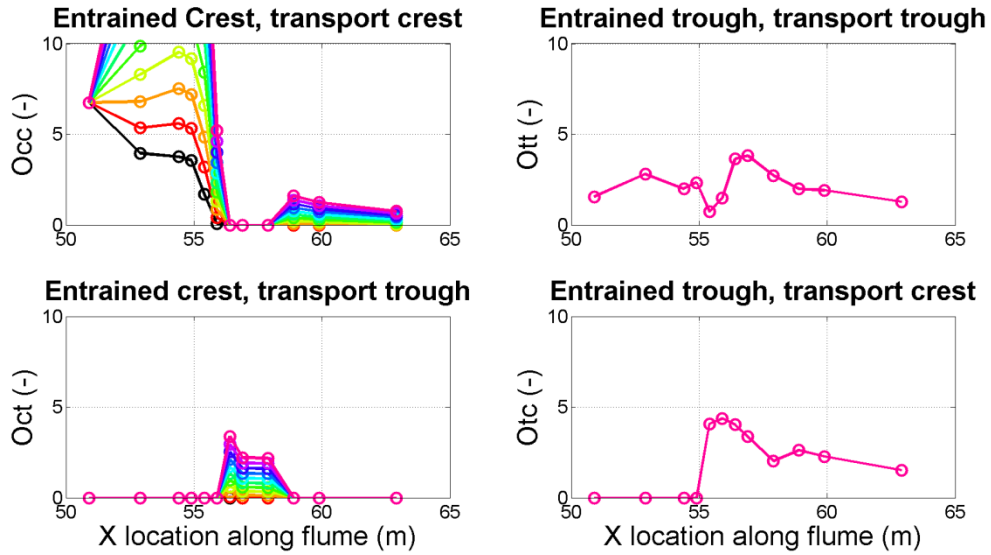

FIGURE 6-10: SAND LOAD ENTRAINED AND TRANSPORTED DURING THE CREST AND THE TROUGH PERIOD WITH AND WITHOUT ADDITIONAL BED SHEAR STRESS DUE TO THE MODELED TURBULENCE WITH A VARIED CALIBRATION PARAMETER γ_{tur}

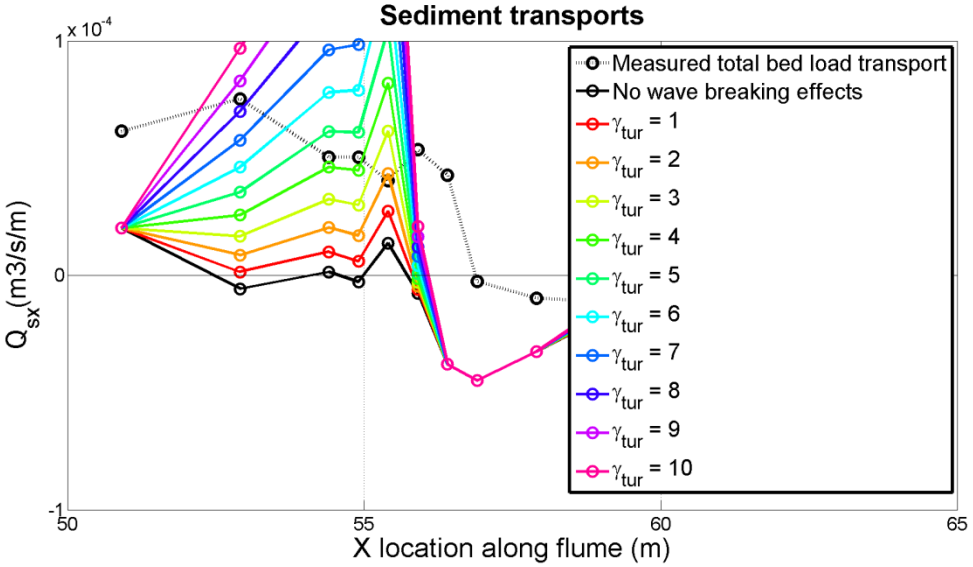

FIGURE 6-11: SEDIMENT TRANSPORT WITH AND WITHOUT ADDITIONAL BED SHEAR STRESS DUE TO THE MODELD TURBULENCE WITH A VARIED CALIBRATION PARAMETER γ_{tur}

6.2 Best model concept

Varying the calibration parameter for the near-bed turbulence clearly improves the prediction of the sediment transport as shown in section 6.1.2.2 and section 6.1.3. The effect of both models is approximately equal. There are two differences between both models. (1) When turbulence is added to the root mean squared onshore directed orbital velocity amplitude is that the orbital velocity amplitude increases as well, which has effect on the friction factor (see section I.2). This has a positive and a negative effect for the sediment transport. The representative Shields parameter during the crest is increased less, but the representative Shields parameter during the trough is decreased. This increases the sand transport during trough less compared with the turbulence added to the Shields parameter during the crest. But the sand transport during the trough is decreased; this is not the case when the turbulence is added to the Shields parameter. (2) When turbulence is added to the peak crest orbital velocity the calculated periods will change as well. While there is no crest period at some locations using turbulence in the bed shear stress models, there are crest periods at all locations if turbulence is added to peak crest orbital velocity. Physically it is not representative to increase the periods with the turbulence.

Another advantage of adding the turbulence to the root mean square crest orbital velocity amplitude is that it is found in literature that a calibration factor is required to increase the near-bed turbulence (Ribas et al., 2011; Van Thiel De Vries, 2009). Since they found that the importance of turbulence is underestimated, it is quite well possible that the importance of the turbulence is also underestimated when adding the turbulence to the Shields parameter.

Since it is physically not representative to increase the modeled periods by adding turbulence to the orbital velocities the best model concept to add breaking wave effects to the SANTOSS model for this test case is adding turbulent values to the Shields parameter during the crest with a calibration factor for the strength of the turbulence (See EQ. 6-14). Though, the modeled results for locations x = 55.9 to x = 57.9 m still show errors compared to the measurements. But, this cannot be improved by wave breaking effects. The poor modeling for locations x = 55.9 to x = 57.9 m is due to the model concept. The model concept requires significantly large crest periods to predict onshore directed sediment transport. Since there is a very small crest period onshore directed sediment transport is barely predicted.

6.3 Implementation in Delft3D

The model used in Reniers et al. (2013) with a calibration factor for the importance of the turbulence is implemented in Delft3D. The effect of using different values for γ_{tur} on the bed–load transport is shown in Figure 6-12. While a value of four for γ_{tur} seems to predict the near-bed sediment transport best using the stand-alone SANTOSS model, using a value of three for γ_{tur} in Delft3D overestimates the onshore directed bed-load transport on top of the breaker bar. This is due to errors in Delft3D discussed in section 3, 4 and 5. Especially the errors in the net-current seem to have effect on the sediment transport. An underestimation of the net current causes higher peak onshore velocity which increases the onshore directed sediment transport and therefore decreases the importance of turbulence. Looking at the total modeled sediment transport (see Figure 6-13) using $\gamma_{tur} = 1$ in the SANTOSS model seems to predict the total sediment transport best. The difference in the best value for γ_{tur} originates from the under prediction of the offshore directed suspended sediment transport (See Figure 4-5). It is not fair to compensate an under prediction of the suspended sediment transport with an increase of the bed-load transport. Therefore a value of two for γ_{tur} will be used in Delft3D. Using this value the total transport is overestimated, but the bed-load transport is modeled quite well (See Figure 6-12).

The transport modeled with the SANTOSS formula show some local decrease in bed load transport from x= 48 too x = 51 m and from x = 53 to x = 54 m. The local decrease in bed load transport from x = 48 to x = 51 m is due to transition from the ripple regime to the sheet flow regime. Since ripples are predicted (See EQ. 2-18) for x < 47 m a lot of sediment that is

entrained during the trough period will be transported during the crest period. Therefore the onshore directed sediment transport at x = 48 m is much larger that the onshore directed transport at x = 50 m, since ripples are absent at x = 50 m. The local decrease from x = 53 to x = 54 m is due to the transition from the sheet flow regime to the ripple regime. The transition from the ripple regime to the sheet flow regime (See EQ B.5 in van der A et al. (2013)) does not work very well for this test case, since these irregularities were not found in the measured sediment transport.

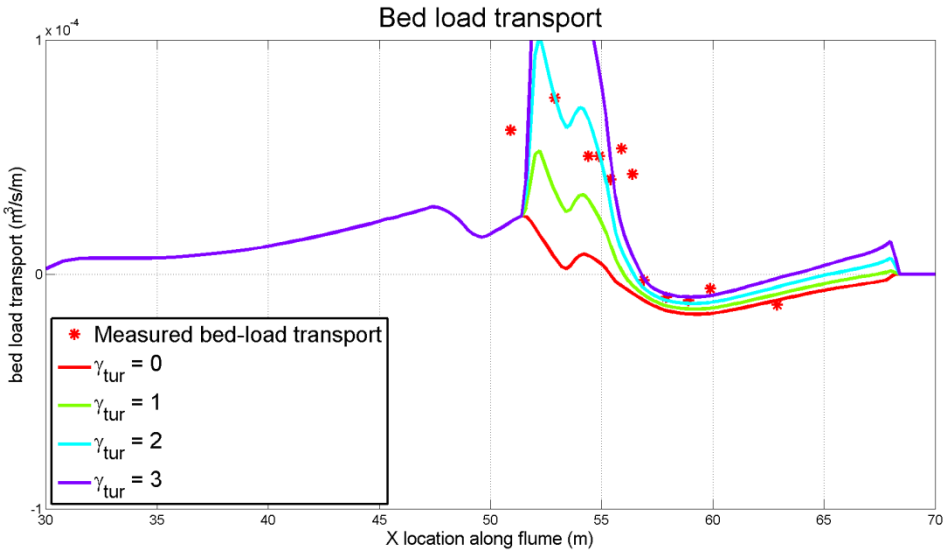

FIGURE 6-12: BED-LOAD TRANSPORT WITH IMPLEMENTED WAVE BREAKING EFFECT WITH A VARYING γ_{tur}

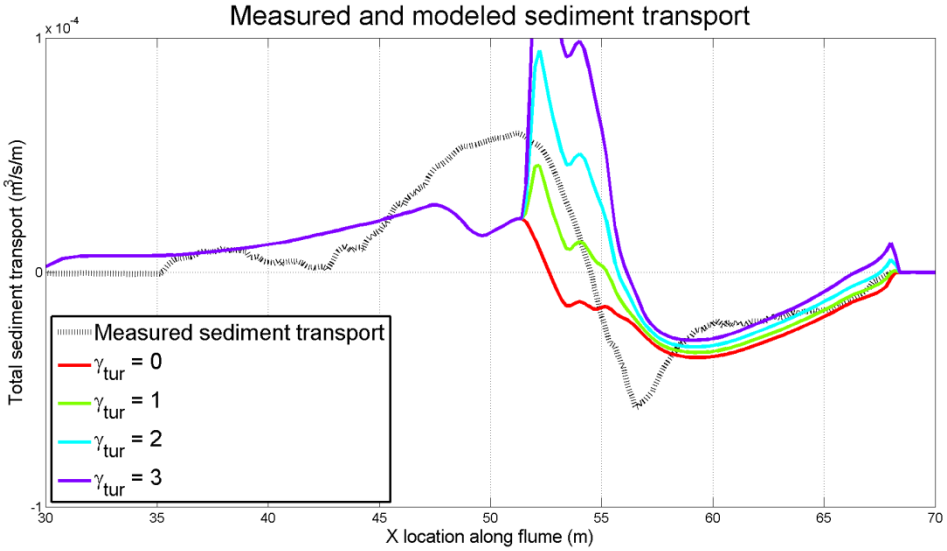

FIGURE 6-13: TOTAL TRANSPORT WITH IMPLEMENTED WAVE BREAKING EFFECT WITH A VARYING γ_{tur}

6.4 Morphological updating

Morphological updating can be calculated with EQ. 2-20. The change of the total transport over space determines the change of bed level over time. If the slope in the total transport is negative then the bed level will increase, if the slope is positive the bed level will decrease. The steepness of the slope of the sediment transport determines the speed of the morphological updating.

The morphology has been updated for 30 minutes without wave breaking effects and with wave breaking effects with $\gamma_{tur} = 2$.

6.4.1 *No wave breaking effect*

Figure 6-14 shows the morphological updating of the breaker bar using the SANTOSS model without wave breaking effects. There seems to be very little morphological change. There is only some bed level increase at x = 52 m. This is due to the slope in the sediment transport visible in Figure 6-13 ($\gamma_{tur} = 0$), due to the transition from the ripple regime to the sheet flow regime. Further, there are only some small morphological updates due to gentle slopes in the total sediment transport.

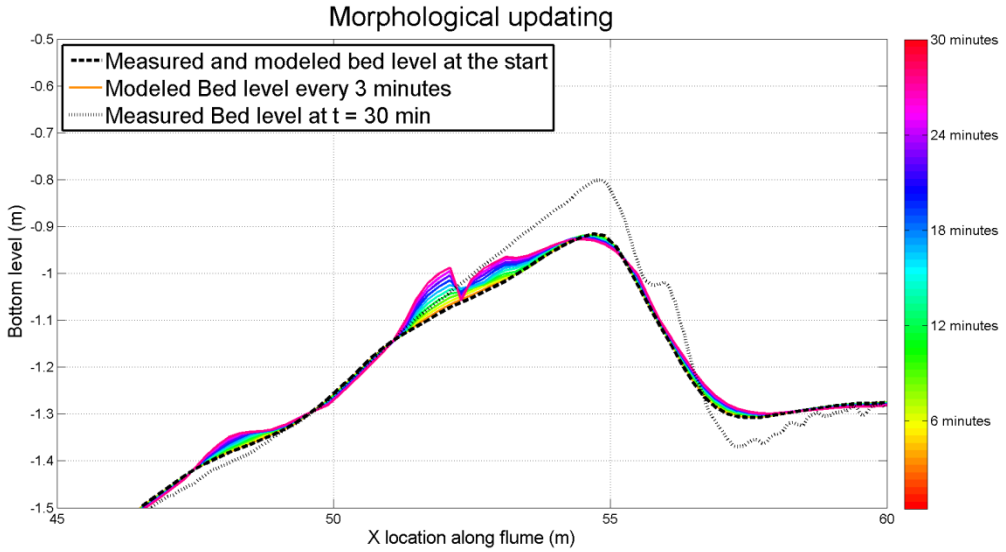

FIGURE 6-14: MORPHOLOGICAL UPDATING WITHOUT WAVE BREAKING EFFECTS

6.4.2 *Wave breaking with γ_{tur} equals 2*

When wave breaking effects are included the updating of the breaker bar is predicted at locations where the breaker bar is measured. The modeled breaker bar is smaller in and higher compared to the measured breaker bar, but the peak of the breaker bar is predicted at the right location. The final modeled decreasing slope in the bed load transport is predicted at same locations as it was measured and therefore the peak of the breaker bar is predicted at the right location. The over prediction of the height of the breaker bar is due to over prediction of the steepness of the slope in the total transport. This is especially due to the under prediction of the under prediction of the offshore directed suspended transport.

The decrease in bottom level for x = 51 to x= 53 m is due to the steep slope in the total transport for those locations (See Figure 6-16). This is due to the local effect wave breaking effect. The wave breaking effect only is applicable where there is roller energy. So, either the wave breaking effect should be applicable for other locations then where there is roller energy or the missing wave breaking effect is not the only reason for the under prediction of the onshore directed bed-load transport in front of the breaker bar.

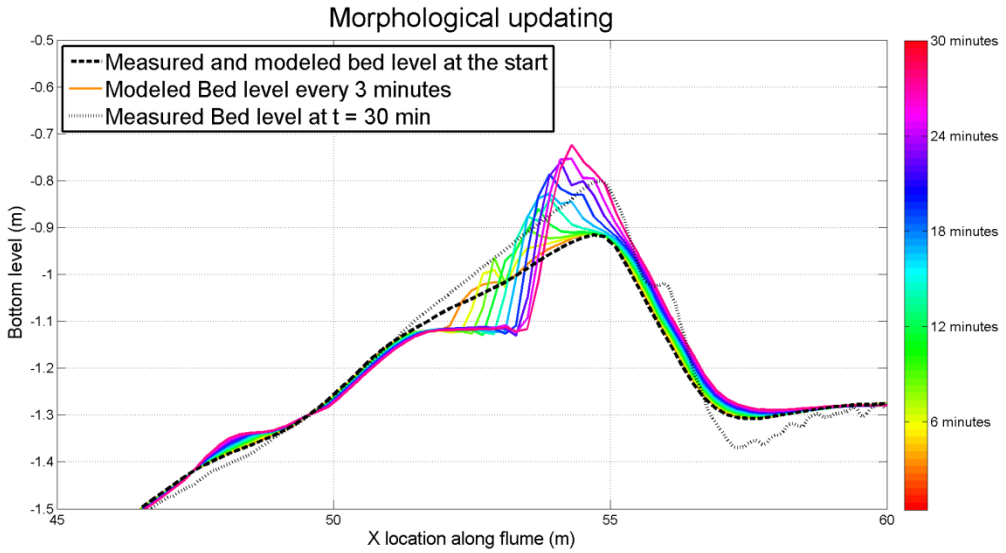

FIGURE 6-15: MORPHOLOGICAL UPDATING WITH WAVE BREAKING EFFECT WITH Γ_{TUR} EQUAL TO 2.

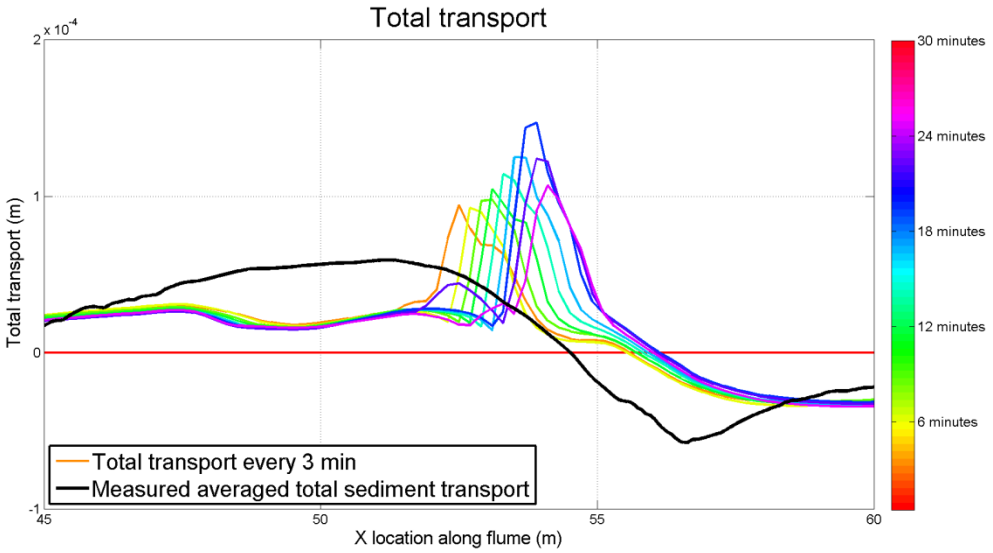

FIGURE 6-16: CHANGE OF TOTAL TRANSPORT DUE TO MORPHOLGICAL UPDATING WITH INCLUDED WAVE BREAKING EFFECT WITH Γ_{TUR} EQUAL TO 2.

6.5 Conclusion

The wave breaking effect applied in Reniers et al. (2013) with a calibration factor indicating the importance of the turbulence seems to be a good option to apply wave breaking effects in the SANTOSS model for this test case. The onshore directed near-bed sediment transport is increased at the wave breaking location where it was underestimated without wave breaking effects. Since the model adds turbulent values to Shields parameter and the turbulent is only large for during the crest plunging breaking waves (Ting & Kirby, 1995), the turbulence will only be applied to the onshore directed orbital velocity.

Using the stand-alone model with the measured hydrodynamics the advised value for the calibration parameter γ_{tur} is four. For the Delft3D model the advised value is two. This difference mainly occurs due to errors in the modeled hydrodynamics in Delft3D. Especially the underestimation of the net current in Delft3D causes less offshore directed near-bed sediment

transport; therefore less onshore directed near-bed sediment transport is required which seem to decrease the importance of turbulence during a calibration.

During the morphological computation two main things go wrong. The offshore directed suspended sediment transport behind the breaker bar is underestimated and the onshore directed bed load transport in front of the breaker bar is underestimated. This causes a smaller breaker bar in horizontal direction and a larger breaker bar in the vertical direction. The location of the peak of the breaker bar is modeled quite well, especially compared to the model which does not take the wave breaking effects in the SANTOSS model into account.

7 PERFORMANCE ON OTHER TEST CASES WITHIN DELFT3D

The performance of the wave breaking effects will be tested on three other cases within Delft3D. The CIEM wave flume experiments starting with a flat bottom is the first one (Ribberink et al., 2014). Then the erosive (LIP1B) and the accretive (LIP1C) LIP cases (Reniers & Roelvink, 1995) will be tested with the SANTOSS model including wave breaking effects.

7.1 Morphological run from flat bottom

The development of the breaker bar during the measurements shown in Figure 2-5 has been done starting from a flat bottom during an earlier experiment in the CIEM wave flume in Barcelona (Ribberink et al., 2014). In the current section the development of the breaker bar will be simulated. While waves only break for specific conditions ($\frac{H}{h} > \gamma = 0.58$, see Table 3-1) in Delft3D, a small initial breaker bar is required. The bottom profile after one hour of measurements has therefore been used as start bottom during the computation. The model has been run for 395 minutes. This amount arises from the measurements length (365 minutes (Ribberink et al., 2014)), excluding the first 60 minutes and including the measurements length of second campaign (90 minutes (van der Zanden et al., 2015)). This computation has been done with and without wave breaking effect.

7.1.1 *Without wave breaking effect*

Doing a morphological computation for 395 minutes without wave breaking effects simulates a breaker bar more offshore compared to the measured breaker bar (See Figure 7-1). Since the bed-load transport is underestimated, the breaker bar is predicted in front of the measured breaker bar. What does stand out is the steepness of the breaker bar. The modeled breaker bar has a much steeper slope compared to the measured breaker bar. In seems that bed-slope effects do not have a lot of effect on the modeled bed-load transport. This is also visible in the development of the total sediment transport (See Figure 7-2). While bed slopes increase, the total sediment transport does not decrease. The modeled sediment transports looks quite similar to the measured sediment transport. This is due to the fact that both the offshore directed suspended sediment transport and the onshore directed near/bed sediment transport are underestimated.

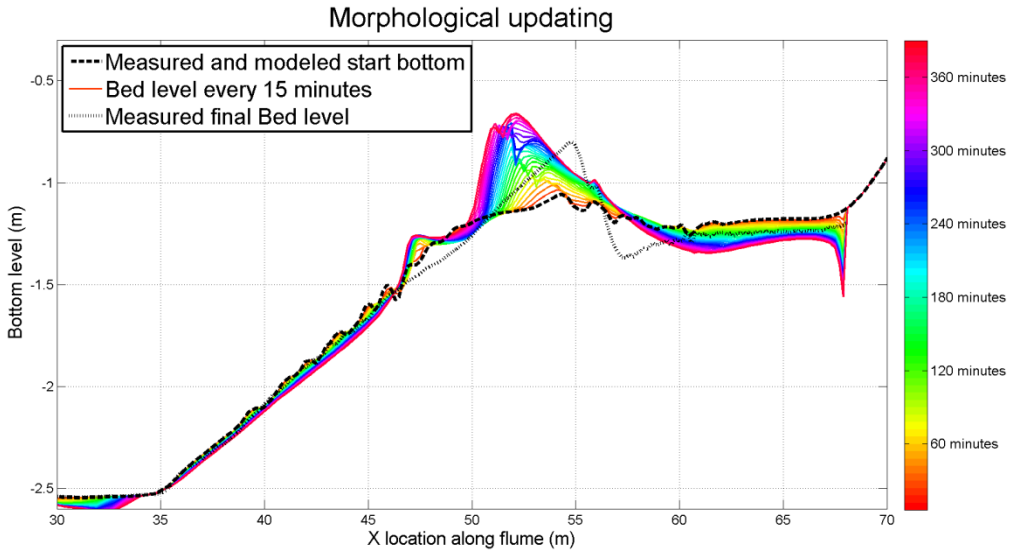

FIGURE 7-1: MORPHOLOGICAL UPDATING FOR 395 MINUTES WITHOUT WAVE BREAKING EFFECTS

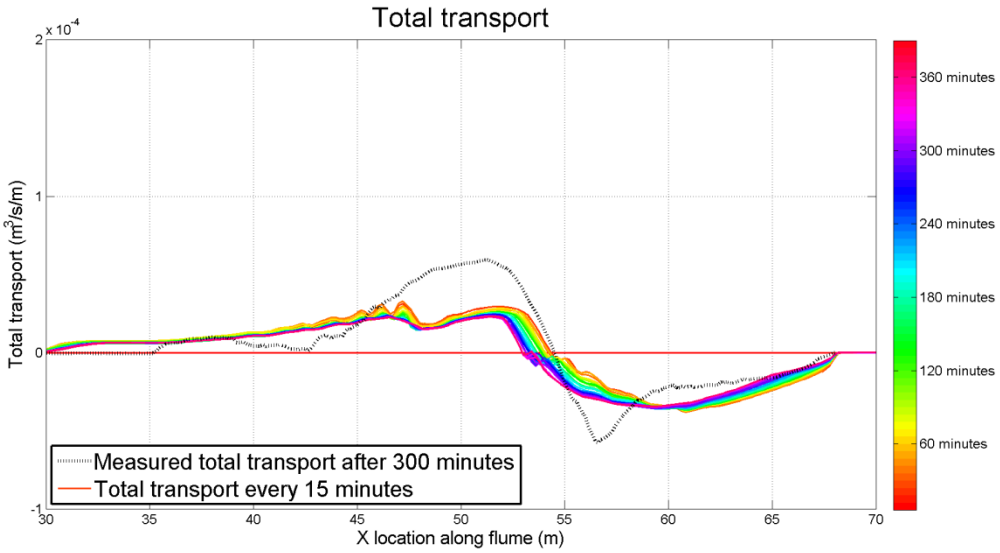

FIGURE 7-2: UPDATING OF THE TOTAL SEDIMENT TRANSPORT FOR 395 MINUTES WITHOUT WAVE BREAKING EFFECTS

7.1.2 *With wave breaking effect and γ_{tur} equals 2*

The result of the computation with wave breaking effect including the start and final bottom during the measurements is shown in Figure 7-3. The calibration factor for the turbulence has been set to 2. The location of the breaker is predicted more onshore compared to the measurements. This is probably due to an underestimation of the offshore directed suspended sediment transport as discussed in section 6.4.2. A deep trough is visible at location x = 68 m. This is due the sediment availability. For x > 68 m there is a fixed bottom without sediment. There is erosion for x < 68 m since there is no sediment transport towards x = 68 m.

Compared to the measurements the sediment transport is predicted poorly, this is mainly due to an underestimation of the offshore directed suspended sediment transport as indicated in 4.

It could be expected that after a certain amount of time the model would reach an equilibrium situation. The total sediment transport should become equal to zero after a certain time. The total transport has not decreased after 395 minutes (See Figure 7-4). Zero total transport can be

obtained by a balance between the offshore directed suspended sediment transport and the onshore directed near-bed sediment transport. Therefore either the near-bed sediment transport should decrease or the offshore directed suspended sediment should increase. Both, bed load-transport does not decrease (See Figure 7-5) and suspended transport does not increase (See Figure 7-6).

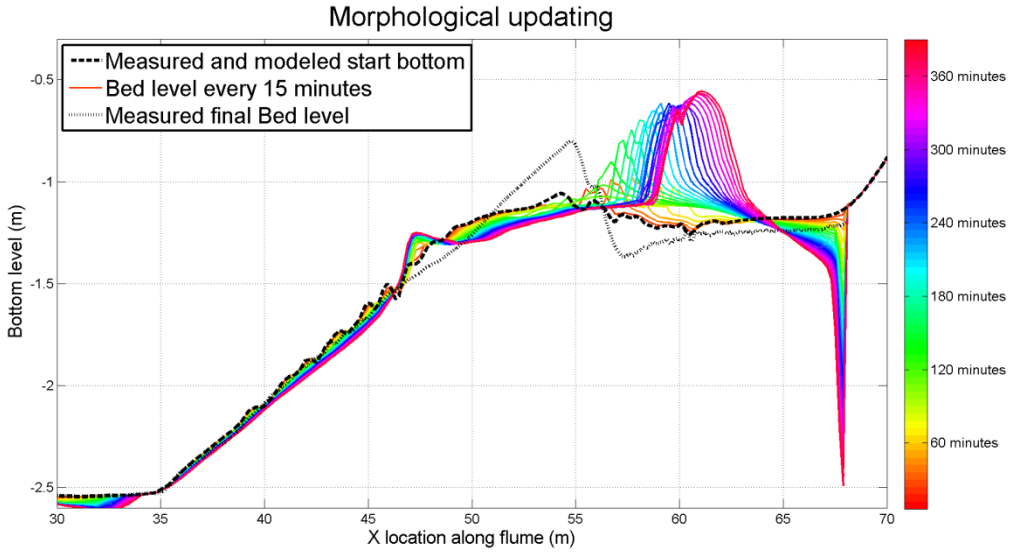

FIGURE 7-3: MORPHOLOGICAL DEVELOPMENT OF A BREAKER BAR FROM A NEARLY FLAT BOTTOM WITH WAVE BREAKING EFFECTS

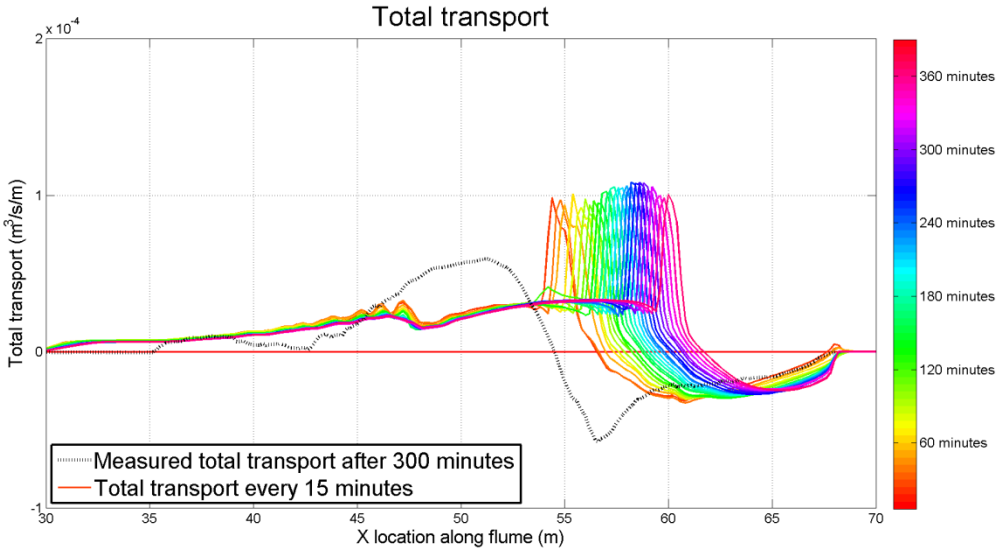

FIGURE 7-4: DEVELOPMENT OF SEDIMENT TRANSPORT DURING THE DEVELOPMENT OF A BREAKER BAR.

Since the suspended transport was underestimated during computations without morphological updating (See section 4.2.1), it is expected that during the morphological computation the suspended sediment transport is underestimated as well. The suspension transport is probably even more underestimated as the breaker bar develops. This could either be due to the net currents or it can be due to the sediment concentrations. The net currents at the top of the breaker bar do increase, but the total Mass flux stays approximately equal (See Figure 7-7). The concentrations also increase during the morphological updating; this is due to increasing sediment diffusivity (Reference concentrations stay approximately equal) (See Figure 7-8). The

depth integrated sediment concentration approximately stays equal. Since the depth integrated sediment concentration and the total mass flux at the top of the breaker both stay approximately equal the suspended sediment transport will stay equal as well. In both the net currents (See Figure 7-7) and the sediment concentrations (See Figure 7-8) at the top of the breaker and sudden decreases at approximately 0.2 meter below the water surface are visible. This is due to the roller mass flux which is only applied in the top part of the water column (See 3.1.4).

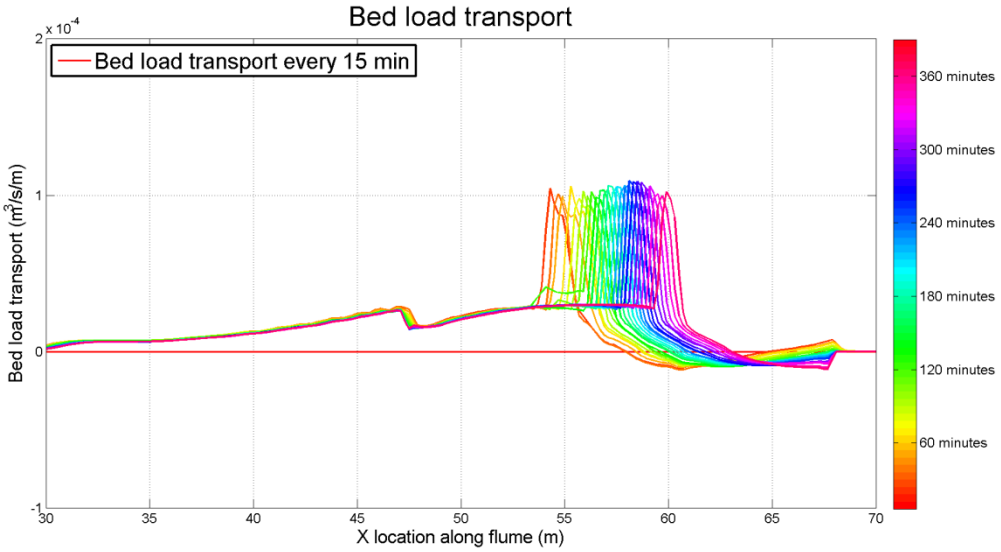

FIGURE 7-5: DEVELOPMENT OF BED-LOAD SEDIMENT TRANSPORT DURING THE DEVELOPMENT OF A BREAKER BAR

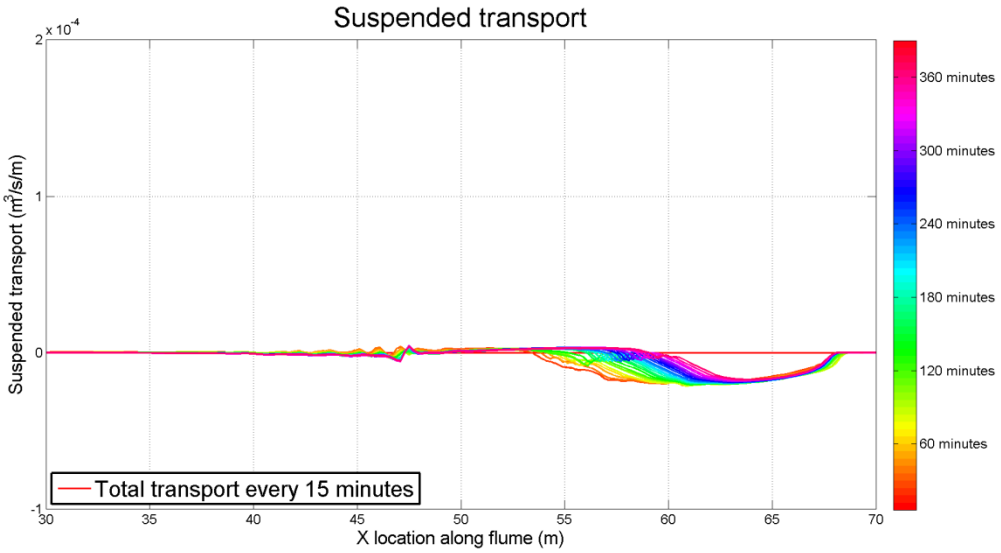

FIGURE 7-6: DEVELOPMENT OF SUSPENDED SEDIMENT TRANSPORT DURING THE DEVELOPMENT OF A BREAKER BAR.

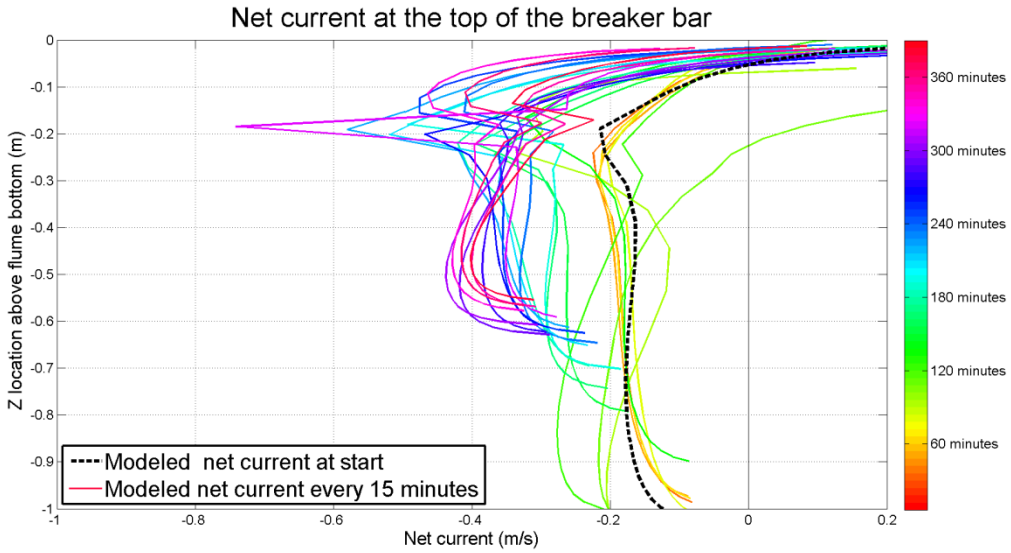

FIGURE 7-7: DEVELOPMENT OF THE NET CURRENT AT THE TOP OF THE BREAKER BAR DURING THE DEVELOPMENT OF A BREAKER BAR

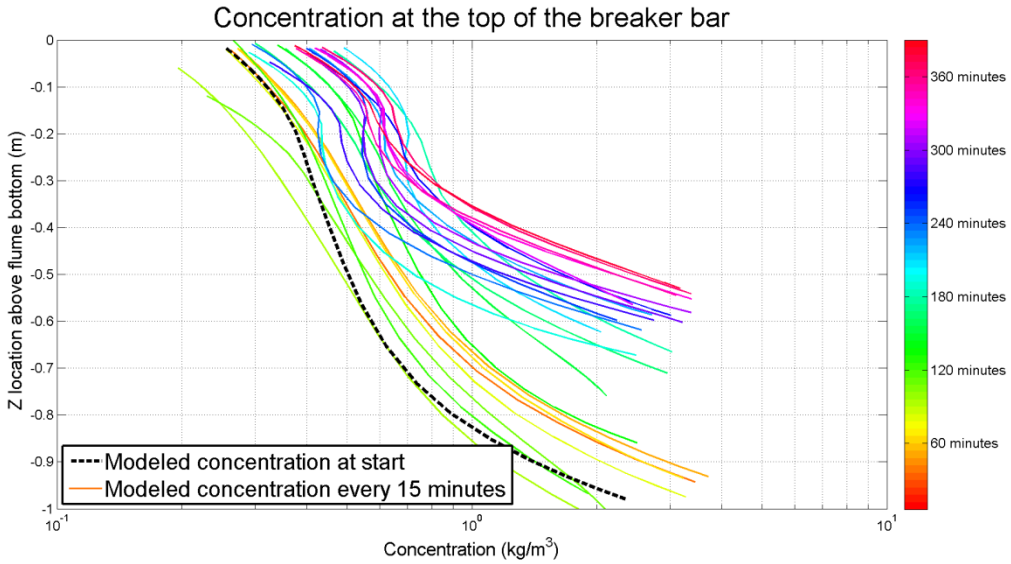

FIGURE 7-8: DEVELOPMENT OF THE SEDIMENT CONCENTRATION AT THE TOP OF THE BREAKER BAR DURING THE DEVELOPMENT OF A BREAKER BAR

7.2 LIP1B erosive case

The LIP1B case has been calibrated by Veen (2014). The wave heights and the bed elevation of the LIP1B cases are shown in Figure 7-9 (Reniers & Roelvink, 1995). The root mean squared wave height at the start of the flume is equal to approximately 0.85 meter with a wave period of 5 seconds. This causes an erosive case. Veen (2014) concluded that wave breaking effects were required to improve the prediction of sediment transport. Therefore the computations for the LIP1B erosive case have been performed again with and without wave breaking effects. The results for the computations with the bottom measured at the start of the experiment are shown in Figure 7-10 and the computations with the bottom measured at the end of the experiment are shown in Figure 7-11. The calibration factor γ_{tur} has been set to 0.5 for the LIP1B case.

At deeper water the sediment transport is predicted better without wave breaking effects. Wave breaking effects seems to overestimate the onshore directed sediment transport for this part of the wave flume. Since irregular waves are modeled, there is roller energy throughout the whole

flume. Since there is roller energy, there is near-bed turbulence and an increase of the onshore directed sediment transport.

This also increases the prediction of the onshore directed sediment transport x = 130 to x = 145 m. This is approximately the location of the breaker bar (Veen, 2014). This is also the location where most of the waves break and the locations with the highest roller energy. Therefore near bed turbulence is high near the location of the breaker bar (See EQ. 6-9) which increase the onshore directed sediment transport.

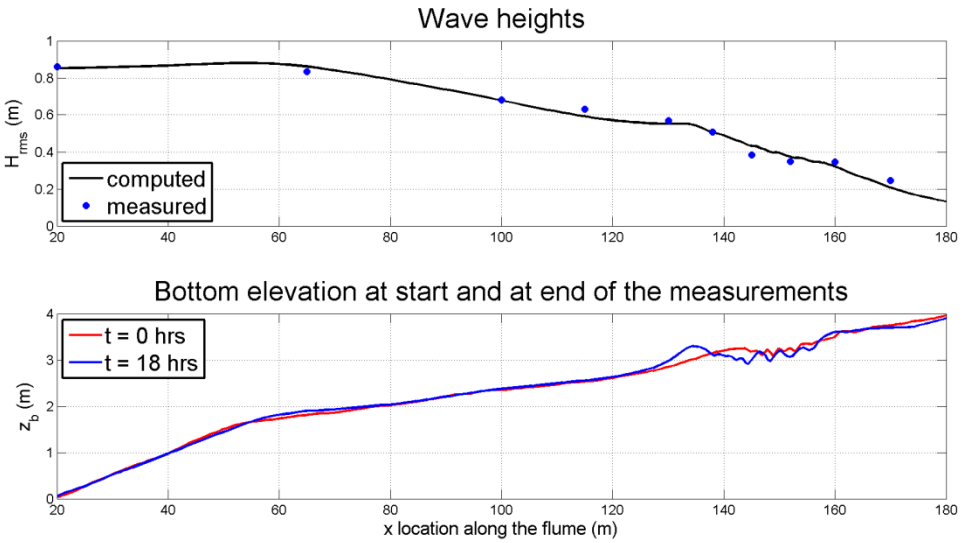

FIGURE 7-9: WAVE HEIGHTS AND BOTTOM ELEVATION AND THE START AND AT THE END OF THE MEASUREMENTS OF THE LIP1B CASE

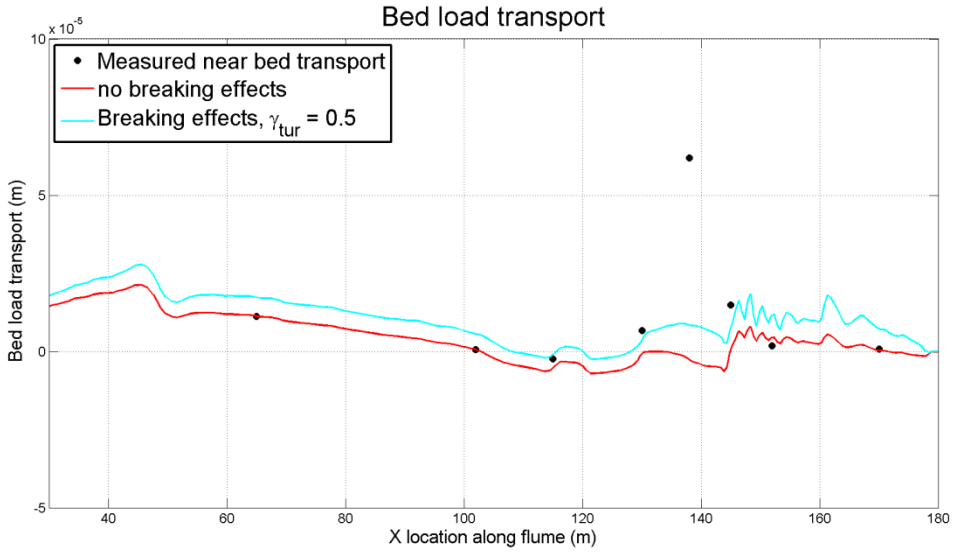

FIGURE 7-10: SEDIMENT TRANSPORT WITH AND WITHOUT WAVE BREAKING EFFECTS FOR THE LIP1B EROSIVE TEST CASE WITH THE BOTTOM AT THE START OF THE EXPERIMENT.

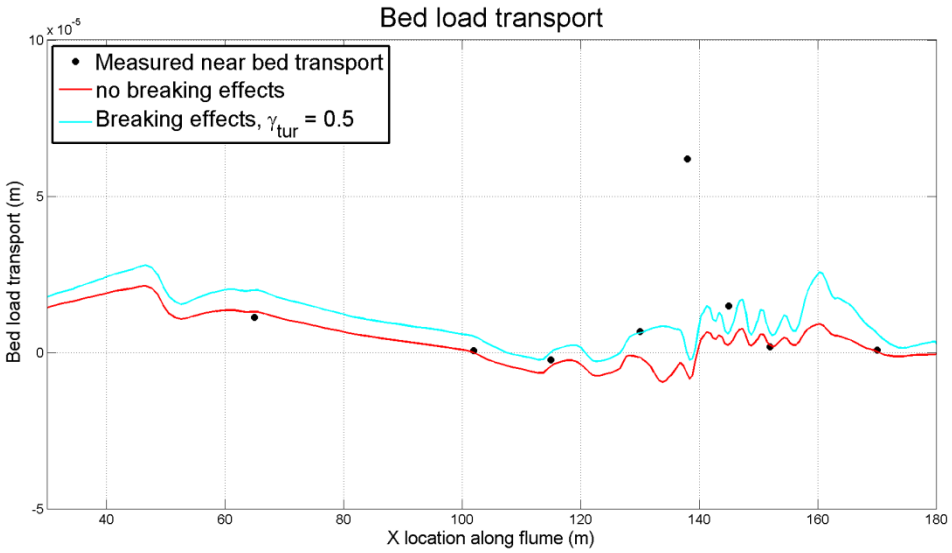

FIGURE 7-11: SEDIMENT TRANSPORT WITH AND WITHOUT WAVE BREAKING EFFECTS FOR THE LIP1B EROSIVE TEST CASE WITH THE BOTTOM AT THE END OF THE EXPERIMENT.

7.3 LIP1C accretive case

The LIP1C case has been calibrated in by Veen (2014) as well. The LIP1C case is shown with the wave heights and the bed elevation in Figure 7-12. The root mean squared wave height is 0.4 meter at the start of the flume with a wave period of 8 seconds, which causes an accretive case. The results of the models with and without implemented wave breaking effects are shown in Figure 7-13 with the use of the measured bottom at the start of the experiment and in Figure 7-14 with the use of the measured bottom at the end of the experiment. The calibration factor γ_{tur} has been set to 0.5 for the LIP1C case as well. At the location of wave breaking the onshore directed transport is better predicted using wave breaking effects. Without wave breaking effect the sediment transport was predicted poorly at the wave breaking location, this is clearly improved using 0.5 for the calibration factor, especially using the bottom measured at the end of the experiment.

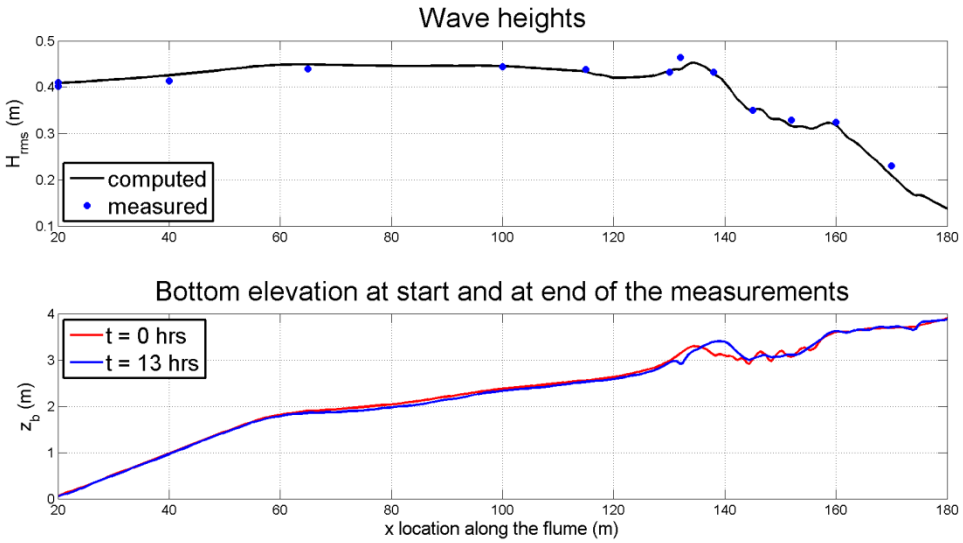

FIGURE 7-12: WAVE HEIGHTS AND BOTTOM ELEVATION AND THE START AND AT THE END OF THE MEASUREMENTS OF THE LIP1C CASE

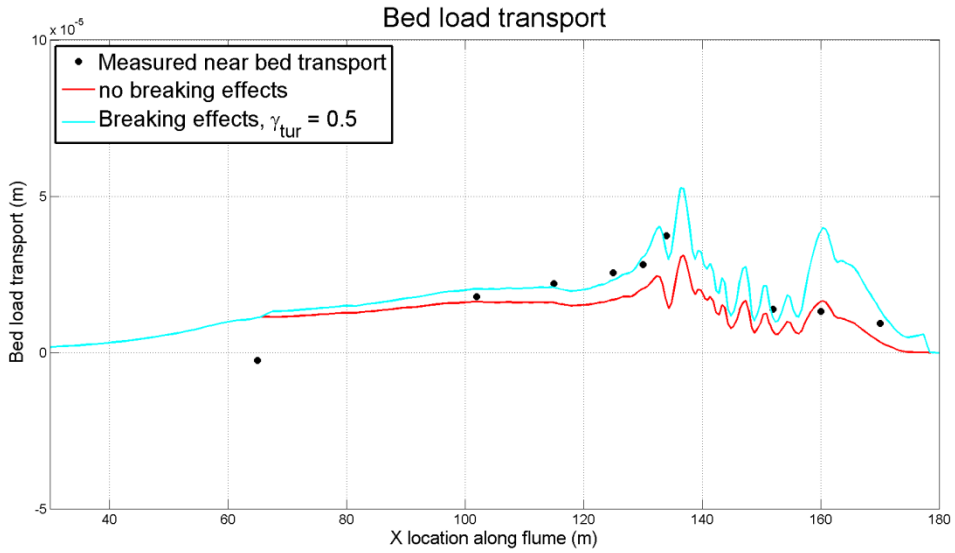

FIGURE 7-13: SEDIMENT TRANSPORT WITH AND WITHOUT WAVE BREAKING EFFECTS FOR THE LIP1C ACCRETIVE TEST CASE WITH THE BOTTOM AT THE START OF THE EXPERIMENT.

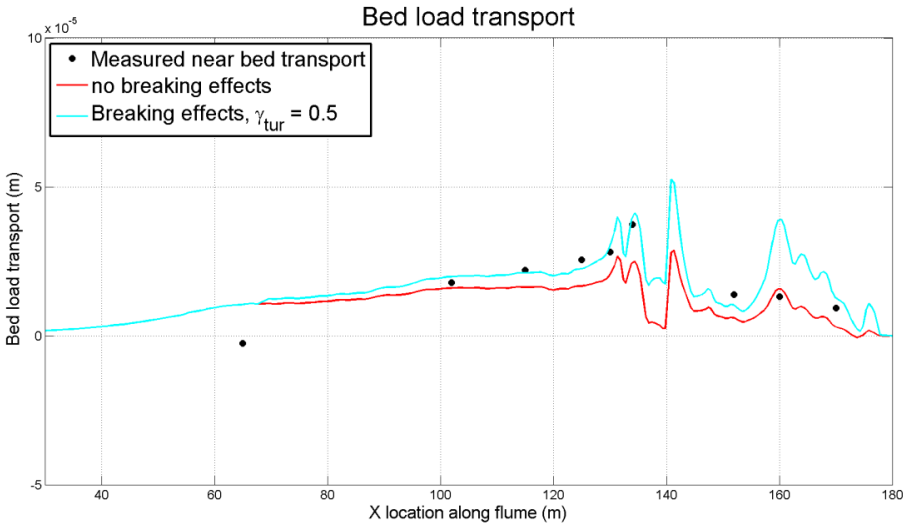

FIGURE 7-14: SEDIMENT TRANSPORT WITH AND WITHOUT WAVE BREAKING EFFECTS FOR THE LIP1C ACCRETIVE TEST CASE WITH THE BOTTOM AT THE END OF THE EXPERIMENT.

7.4 Conclusion

It depends a lot on the value of the calibration parameter for the importance of turbulence whether the sediment transport improves for the different test cases. For a morphological run starting with a nearly flat bottom a value of two for the calibration parameter predicts the location of the breaker bar more onshore compared to the measurements, this is probably due to an underestimation of the offshore directed suspended sediment transport. For both LIP cases a value for the calibration parameter of 0.5 is used. This causes an increase of onshore directed sediment transport for x = 130 to x = 145 m where there was under prediction at these locations. At the start of the flume for the erosive case and the middle of the flume for the accretive case the sediment transport is predicted a little bit worse using wave breaking effects. This is due to the use of roller energy dissipation with for irregular breaking waves are present at a large part of the wave flume. There is roller energy throughout the whole flume which causes near-bed turbulence and an increase of the onshore directed sediment transport throughout the whole flume.

8 DISCUSSION, CONCLUSIONS AND RECOMMENDATIONS

8.1 Discussion

During this study some choices were made and assumptions have been done. These choices and assumptions will be discussed in this section. This section particularly addresses (i) uncertainties/limitations of the used data; (ii) limitations of SANTOSS and Delft3D for this particular case; (iii) the implemented breaking-wave effects.

8.1.1 *Measurements*

During the measurements regular breaking waves were generated. This has been done to exclude to complexity of wave irregularity the measurements. However, it can be questioned how realistic regular waves are. Regular breaking waves will not occur under field conditions. Therefore it is doubtful whether wave breaking effects in the SANTOSS should be tested on regular breaking waves were the SANTOSS model is eventually meant to model sediment transport in field conditions with irregular breaking waves.

After the calibration of the Delft3D model it was found that the wave height at two of the measurements devices (PPTs) is probably overestimated due to measurements errors. This applies for the second and the fifth PPT (see x = 56 and x = 57.5 m in Figure 3-1). It would have been better to exclude these measurements. When it was found out that the wave height at those locations were probably overestimated the calibration of the hydrodynamics and the validation of the sediment transport was already finished. Redoing the calibration for the wave height would require a lot of work on doing new computation and making plots for a probably rather small effect on the results. Therefore this work has not been done.

It is hard to determine the accuracy of the measurements. There are definitely some uncertainties in the measurements that should be mentioned. There is especially uncertainty in the measured wave- and current related suspended transport and the bed load transport. The wave- and current related suspended transport are determined by integrating the multiplied net current and sediment concentration over the whole water column. These interpolations are not very certain since the interpolations of the net currents are based on 3 vertically aligned ADVs and the interpolations of the sediment concentrations are based on transverse suction measurements at six elevations.

8.1.2 *Modeling with SANTOSS within Delft3D*

The underestimation of undertow could either be due to the underestimation of the Stokes drift due to waves or rollers or it can be due to mismatches in the vertical distribution of the Stokes drift. Since the processes (velocities, turbulence, etc.) going on under a roller are currently not well understood (Deltares, 2014) it is more likely that the errors in the modeled undertow are due to mismatches in the modeled roller energy and the associated mismatch in the modeled mass flux of the roller. It has been tried, without success, to improve the undertow by changing the formulation for the Stokes drift due to rollers (See appendix C.2). Since it was not the objective of this research to improve the modeling of the hydrodynamics in Delft3D, not very much attention is paid to improving the modeling of the undertow. Further calculations have been done with errors in modeled undertow.

The parameterization for the orbital flow velocity used in Delft3D (Ruessink et al., 2012) seems to perform not very well for this test case. The parameterization method especially predicts underestimates the acceleration skewness. As Ruessink et al. (2012) indicates the

parameterization method is based on a calibration with field measurements and it may underestimate in particular the acceleration skewness for wave flume experiments. During field measurements waves mostly approach the beach oblique. The wave energy is then not completed directed towards the coast, which is different from a flume experiment where the wave propagation is mostly perpendicular towards the coast. This could cause the underestimation of the velocity and acceleration skewness. Another reason for the errors in the modeled velocity and acceleration skewness is that the Ursell number is not the only determining parameter for the velocity and acceleration skewness. For example, local bed slopes or the wave propagation speed could also have effect on the velocity and acceleration skewness. It has not been tried to improve the parameterization for this test case in the CIEM wave flume since this was not the objective of this research.

The errors in the sediment concentrations are due to errors in the modeled sediment diffusivity and errors in the modeled reference concentration. Since it would require a lot of time to improve the reference concentration and the sediment diffusivity this has not been done and the poor modeling of the sediment concentration had to be taken into account during further calculations. It is hard to say what the effect of the poorly modeled undertow is on the suspension transport.

The extraction of the suspended sediment transports due to waves from the measurements it looks suggests that the suspension transport higher in the water column cannot be neglected. SANTOSS only includes the suspended transport due to waves in wave boundary layer. Since this is only a fraction of the total suspended transport due to waves the modeled suspended transport due to waves is highly underestimated. This might be a cause for the underestimation of the onshore direction sediment transport modeled with SANTOSS. The wave-related suspended transport higher in the water column during the measurements might also be due to measurements errors. It might be possible that bubbles are measured instead of the sediment particles; this might overestimate the measured sediment concentration.

During the modeling with morphological updating the breaking criterion $\left(\frac{H}{h} > \gamma = 0.58\right)$ was kept constant. An initial breaker bar was required to let the wave break at the top of the breaker bar instead of close to shore at approximately x = 68 m. During the measurements waves broke at a fixed position approximately at x = 55 m. The breaker criterion seems to be not completely suitable for this situation, since wave breaking is not completely dependable on the relative water depth $\left(\frac{H}{h} > \gamma\right)$. The formulation that was used can possibly be improved by adopting the methods of Battjes & Stive (1985) and Ruessink, Wijnberg, Holman, Kuriyama, & van Enckevort (2003), who respectively make the wave breaking index γ dependable on the wave length and the wave number.

8.1.3 *Breaking waves effects*

In all possible improvements of the SANTOSS model for wave-breaking effects the roller energy dissipation is used as input. The roller energy dissipation depends on the roller energy (See EQ. 3-10). The roller energy is calculated with the roller balance model. This roller balance model is not available for a stand-alone computation. Therefore a parameterization for the roller energy is required. The parameterization of Uchiyama et al. (2010) was used. This parameterization is generated for irregular breaking waves. Since the roller energy is not measured both methods (Delft3D and parameterization method) cannot be validated with the measurements. Using the roller energy from Delf3D seems to work better on the sediment transport. But, using the roller energy from Delft3D also has a negative effect; other cases cannot be tested stand-alone without doing a Delft3D computation. A disadvantage of the parameterization is that the fraction of broken waves is required. For regular breaking waves this is either zero or one, for irregular waves this would also be very hard to determine stand-alone. Therefore the implemented wave breaking effects are not very suitable for stand-alone computations for other test-case. This is not

necessarily a problem since the SANTOSS formula is developed for computations within morphological models.

Within the SANTOSS formula, the wave Reynolds stress is used to quantify near-bed onshore progressive wave streaming (Nielsen, 2006; van der A et al., 2013). Consequently, the wave Reynolds stress has a positive effect on the bed shear stress during the crest period and a negative effect on the bed shear stress during the trough period. In section 6.1.1 it was assumed that the wave Reynolds stress only has a positive effect on the bed shear stress during the crest period. If the wave Reynolds stress would also have a negative effect on the bed shear stress during the trough period, the sand load entrained during the trough would have been decreased. This would probably improve the prediction of the sediment transport. The method would probably work better than currently is shown. Since the method is not very physically representative and since this wave breaking effect worked less than other wave breaking effects this has not been tested.

To increase the importance of the near-bed turbulence on the peak orbital crest velocity a calibration factor is required. During a stand-alone calibration a value of four for the calibration factor seems to give the optimal near-bed sediment transport. During a calibration in Delft3D it seems that a value of two was more optimal. This difference between Delft3D and stand-alone occurs from the fact that the hydrodynamics are poorly modeled in Delft3D and it illustrates the sensitivity of the parameterization for the hydrodynamic input. The factor for the importance of the turbulence was calibrated at 0.5 for the LIP test-cases. Difference with the CIEM wave flume experiments that causes the difference in the calibration factor is most likely the undertow. The measured/modeled undertow was much weaker for the LIP experiments compared to the CIEM wave flume experiments

The model used to calculate the near-bed turbulence which is added to the peak crest orbital velocity and to the Shields parameter is calculated with the assumption that turbulence is produced locally (Reniers et al., 2004) and that horizontal transport of turbulence can be neglected. It is not yet clear whether this assumption is valid for this test case since turbulence has not yet been extracted from the measurements. It is assumable that there is also some transport of turbulence. Therefore the method used to calculate the turbulence might be invalid.

Despite the implementation of the wave breaking effects the sediment transport is still underestimated in the shoaling/pre-breaking zone (from x = 48 to x = 52 meter). Suspended sediment concentrations are nearly zero in this section, so the observed onshore transport is predominantly attributed to bed-load. This underestimation is probably not due to missing breaking wave effects, since transport of turbulence under plunging breaking waves is directed onshore and the waves start breaking at approximately x = 52 meter. The underestimation of the onshore direction sediment transport therefore has another reason. This can for instance be due to an underestimation of near-bed (acceleration) skewness by the parameterization of Ruessink *et al.* (2012). Another explanation may be possible effects of intra-wave flow processes (e.g. momentum advection) that are not taken into account by Delft3D but which may be important for these highly non-uniform conditions with strong wave deformation.

Another reason for the errors in the modeled sediment transport with SANTOSS might be that the sediment transport is calculated locally. The direction and the order of magnitude of the sediment transports are determined by local hydrodynamics. The local bed load transport is probably also influenced by bed load transport or hydrodynamics like transport of turbulent kinetic energy at adjacent locations or transport of sediment at adjacent locations. This though is not taken into account in the SANTOSS model, which might be a reason for the poorly modeled sediment transport.

8.2 Conclusions

The objective of this research was to improve the prediction of sediment transport for breaking wave conditions using the SANTOSS formula. This objective has been achieved by answering the following research questions.

1. *How do the overall hydrodynamics below breaking waves look in the new Barcelona measurements and how well can Delft3D reproduce these hydrodynamics?*

Delft3D is able to, with an adapted wave energy dissipation model designed for regular waves, reproduce the measured wave heights and wave set up/down quite well. The net currents are reproduced quite well for some locations, but Delft3D had troubles to predict the strong (maximum value of 0.8 m/s) measured undertow at the onshore side of the breaker bar. The undertow is predicted quite well at locations with high wave energy, but at locations where there is a lot of roller energy the undertow is underestimated severely. This suggests a mismatch between data and model in terms of the magnitudes of roller energy and roller mass flux, and either affects the flow in the water column. The parameterization method used to determine the intra-wave velocities does not give satisfactory results for wave flume experiments. The results highlight the need of a parameterization that is better suitable for flume studies.

Combining these conclusions indicates that Delft3D is not very suitable for this test-case, especially due to an underestimation of the high undertow level.

2. *What are, according to measurements and Delft3D, the contributions of different transport components (bed-load, suspended load, current- and wave- related components) to the total sediment transport in the breaker zone and how well can Delft3D reproduce these transports with the SANTOSS and the van Rijn (2007ab)(Bed load and suspended load/concentration) model?*

According to the measurements both bed-load transport and suspended transport are important, while looking at Delft3d suspended transport is dominant. According to the measurements suspended transport is especially important onshore from the breaking point. Measured concentrations in front of the breaker bar are nearly zero, while concentrations behind the wave breaking locations are in the other of magnitude of 1 kg/m^3. The modeled sediment concentrations are underestimated for most locations due to errors in the modeled reference concentrations and sediment diffusivity. Including the underestimation of the undertow the suspended sediment transport due to currents is underestimated a lot onshore of the breaker bar. Though, this seems to be mainly due to errors in the modeled concentrations.

Although estimations of the wave-related transport rates are quite uncertain, the values agree quite well with predictions by the van Rijn (2007a) model within Delft3D. There is some over- and underestimation, probably due to errors in the modeled sediment concentration. The SANTOSS model only takes wave-related suspended transport in the wave boundary layer into account. Since there is, according to the measurements, also suspended sediment transport due to wave above the wave boundary layer, the SANTOSS model probably underestimates the wave-related suspended transport.

Since the SANTOSS model computes the near-bed sediment transport consisting of the bed-load transport including the wave related-suspended transport. Therefore a comparison between the model and the measurements is done on the bed-load transport including the wave related suspended transport. It seems that the magnitude of the bed-load transport is underestimated from offshore and at the breaker bar with a factor three. Onshore of the breaker SANTOSS reproduces the near-bed sediment transport well.

3. *How can the differences between Delft3D and the measured transport components be explained?*
    - 3.1. *Can wrong sediment transport predictions be explained by errors in the modeled overall hydrodynamics (wave height, set-up, undertow and orbital flow skewness/asymmetry)?*
    - 3.2. *Can sediment transport predictions be improved by changing the near-bed velocity reference height or by adding bed slope effects in the stand-alone model?*
    - 3.3. *Can wrong sediment transport predictions be explained by specific effects of wave breaking?*
    - 3.4. *Is it necessary to further improve the present Delft3D models for near-bed transport (SANTOSS) and /or suspended sediment transport?*

The measured and modeled hydrodynamics have been used as input in the stand-alone SANTOSS model to get insight in effect of the modeling errors in Delft3D on the modeled sediment transport. Differences especially occur due to errors in the modeled net current. The Shields parameter during the crest is underestimated a lot using Delft3D compared to the stand-alone SANTOSS model. This has effect on the sediment transport that is entrained during the crest, this is also underestimated. Using the modeled hydrodynamics there are also errors in the phase lag, friction factors and ripple dimensions. This causes under- and overestimation of the near-bed sediment transport at different locations. However, using the modeled hydrodynamics the sand transport seems to be better predicted compared to using the measured hydrodynamics. So, errors in the modeled (Delft3D) hydrodynamics cause a better prediction of the sediment transport using the stand-alone SANTOSS formula for this test case.

The prediction of the sediment transport depends on the near-bed velocity reference height. Choosing a very low near-bed velocity reference height, close to the bed level, improves and worsens the prediction of sediment transport for different locations. Using other heights like the average or the characteristic height obtained from Delft3D causes some differences, but those differences are not very remarkable. Bed slope effects have been added to the stand-alone SATOSS model, this increased the prediction of the sediment transport. The importance of the bed slope is hard to determine, since it is not known whether errors in the sediment transport occur from missing wave breaking effects or from an underestimation of the bed slope effects.

Using either the measured or the modeled hydrodynamics still causes an under prediction of the onshore directed bed-load transport offshore of the breaker bar. So it seems that there are missing wave breaking effects. Errors in the modeled sediment transport could also be due to restrictions of the model concept. But this is hard to determine with the current knowledge on the measured hydrodynamics and the measured sediment transport (bed load and suspended load).

The current models for suspended transport also require some improvements, but there are also errors in the net currents. This makes it impossible to check whether possible improvements on, for example the reference concentration or the sediment mixing, work well.

4. *How is it possible to account for wave-breaking effects in the SANTOSS transport model (stand-alone Matlab-model and/or Delft3D)?*
    - 4.1. *Which model concepts are available?*
    - 4.2. *How well do they compare with the data and with the current models?*
    - 4.3. *What is the best (calibrated) concept?*

Three different options to improve the sediment transport have been tested. The formulation of the wave Reynolds stress has been adapted and turbulence has been added to the formulation of the peak orbital crest velocity and the Shields parameter during the crest period. When the formulation for the wave Reynolds stress is adapted the onshore predicted sediment transport is predicted a little bit better. But the sediment transport is not increased enough and this model concept has not been used in literature before. Using turbulence in the formulation of either the

peak crest velocity (turbulence transport is directed onshore for plunging breaking waves) or on the Shields parameter during the crest period including a calibration factor for the importance of the turbulence works quite well. Advantage of the first concept, using the turbulent values on the peak crest velocity, is that it also increases the crest periods. Though, this concept has not been used, since it is not physically representative to increase the crest periods with turbulence. Therefore the concept which adds turbulence to the Shields parameter during the crest with a calibration factor has been used. Disadvantage of all model concepts is that the roller energy is required. The roller concept is not well understood and the roller energy cannot be calibrated.

The predicted sediment transport now depends a lot on the chosen value for the calibration factor. Doing computation in the stand-alone model a value of approximately four seems to perform best for the prediction of sediment transport under breaking waves. Doing a computation in Delft3D gives optimal results with a value of two for the calibration factor. The difference in this value is caused by the fact that Delft3D models the hydrodynamics quite poorly. A lower value in Dellft3D compensates for the poor modeling of the hydrodynamics.

The model concept seems to perform quite well, though there are still errors between the measured near-bed sediment transport and the modeled near-bed sediment transport with SANTOSS including wave breaking effects. Whether this is due to the wave breaking model is not clear, since (i) there are too many uncertainties in the modeled hydrodynamics (e.g. Roller Energy) (ii) there are other missing or uncertain processes within the SANTOSS formula (advection of sediment transport, slope effects, etc.)

5. *How does the SANTOSS model (in Delft3D or Matlab) with improvements for wave-breaking effects perform for other test cases?*

The SANTOSS formula including wave breaking effects has been tested on the CIEM wave flume experiments with a nearly flat bottom and on two LIP cases (1B and 1C). The sediment transport is improved for all test cases using the wave breaking effects in the SANTOSS model. Though, it depends a lot on the value used for the calibration parameter γ_{tur}. The breaker bar is predicted more onshore using a value of two for the calibration parameter. This is due to missing suspension transport. For both LIP cases a value of 0.5 is used. This improves the sediment transport near the breaker bar a little bit but it worsens the prediction of the bed load transport at the start of the wave flume due to the presence of roller energy due to irregular breaking waves.

8.3 Recommendations

Modeling test case in Delft3D did not work very well; therefore some recommendations with respect to modeling the CIEM wave flume experiments are given below.

- Delft3D uses a lot of parameterizations, these parameterizations are all suitable for irregular waves and they mostly are unsuitable for regular waves. Delft3D is also often used to reproduce measurements of wave flume experiments. In wave flume experiments it is quite well possible that regular waves are generated. To make a good comparison between Delft3D models and measurements of regular waves in wave flumes during other experiments an option to model regular waves in Delft3D instead of irregular waves would improve the modeling of hydrodynamics a lot.
- The modeled net current is not very well reproduced within Delft3D. This is possibly due to errors in the roller concept. The roller concept is currently quite poorly understood (Deltares, 2014). Additional research on the roller concept, the dissipation of wave energy to roller energy, the effect on turbulence and the effect on the undertow should give better insight in the modeling of rollers. A possible new model concept, developed with help of the research on rollers, can then be implemented in Delft3D to improve the modeling of breaking wave in Delf3D. A model that possibly improves the modeling of the undertow is given by Nam, Oumeraci, Larson, & Hanson (2014), they developed an reliable and robust undertow model. Disadvantage for the modeling of the CIEM wave flume experiments is that the undertow model is designed for irregular waves and it uses

the parameterization method of Ruessink et al. (2012) which seems to be not very useful for this case (See section 3.2).

- Sediment concentrations are underestimated at the top of the breaker bar and onshore of the breaker bar, which is due to errors in the reference concentration and the sediment diffusivity. Some more research into the model sediment concentrations could improve the modeling of the sediment concentrations. The sediment diffusivity can be improved, for example, by changing the empirical coefficient related to wave breaking (van Rijn, 2007b).
- Delft3D seems not suitable for this test case. The hydrodynamics are quite poorly modeled. Delft3D is a model using a lot of simplifications and assumptions so that the computation can be decreased. For this test case, a more advanced model hydrodynamic is required. Currently a member of the SINBAD project is working on the hydraulic model OpenFOAM, which is a much more advanced and detailed hydraulic model. Mai, Ohle, & Zimmermann (1999) also mention some other hydraulic wave models. One of these models which is also able to do morphological computations, this model is called Mike 3. Mike 3 solves the wave model based on the elliptic mild slope equation instead of the wave propagation theory used in Delft3D. In the elliptic mild slope equation surface elevation is calculated directly. This might work better modeling the CIEM wave flume experiments since the elliptic mild slope equation take more processes into account. One of these processes that might have considerable effect is reflection (DHI Software, 2007), which is not taken into account in the wave propagation theory in Delft3D.

In the SANTOSS model it can best be account for breaking wave effects using turbulence in the peak on the Shields parameter during the crest when modeling plunging waves. A calibration factor is required to determine the importance of the turbulence. Below some recommendations with respect to further improving the SANTOSS model for wave breaking effects are given.

- The implemented wave breaking effect is a physically representative effect that works quite well for the CIEM wave flume experiments. Though, it is still hard to assess how well the wave breaking effect works, since the SANTOSS formula is a simplifications of the reality and many processes are missing such as advection of sediment transport and slope effects. To quantitatively assess the performance of the wave-breaking effect such effect should be implemented in the SANTOSS model firstly.
- The turbulence is currently only added to the Shields parameter during the crest, because turbulence disappear almost completely during the trough period for plunging breaker waves according to Ting & Kirby (1995, 1996). It is therefore interesting to know how the current implemented model performs for spilling breaking waves. For spilling breaking waves turbulence is especially important during the trough period (Ting & Kirby, 1994, 1996). It would be interesting to know whether for spilling breaker the turbulence should be applied during the trough period.

To improve the modeling of this test case some more data from the measurements is required. Below some recommendations to extract data from the measurement is given.

- Very little information is currently known on Roller energy. The mass balance of the roller in Delft3D is based on the mass balance of the wave energy. Since the poorly modeled undertow probably originates from poorly modeled Roller energy investigation into the Rollers model would be quite interesting. It would be very interesting and useful to extract Roller energy from the measurements. Though, it has not been found in the literature how to extract the roller energy from the measurements. More research on this topic would be interesting to improve the modeling of CIEM wave flume experiment in a Delft3D model.
- The wave boundary layer thickness seems quite important for the amount of suspended sediment transport that had to be taken into account for a fair comparison between measured bed-load and the near-bed sediment transport modeled with the SANTOSS

model. SANTOSS models the near-bed sediment transport in the wave boundary layer. Therefore only suspended sediment above the wave boundary layer has to be taken into account to prevent for overlap between bed-load transport and suspended transport. The wave boundary layer thickness is therefore important and it would be interesting to get accurate measurements of the wave boundary layer thickness.

- The roller dissipation is used to calculated turbulence. Since the roller energy is required as input or a model suitable for irregular waves is required it might be better to use turbulence as input in the stand-alone model. When the turbulence is available some new computations with the stand-alone model will gives insight in the modeling errors of the turbulence when the measured turbulence is used. A comparison between the measured turbulence and the modeled turbulence is required to calibrate the modeled turbulence. It is also possible that transport of turbulent kinetic energy has effect on the sediment transport. Therefore it is interesting to have detailed information on turbulent and transport of turbulence. Currently, there are some turbulent values available, but these values are not very accurate.
- The effect of local bed slope is quite hard to estimate. Extracting very detailed near-bed sediment concentration and velocities from the ACVPs (van der Zanden et al., 2015) might gives some more information of the effect of the local bed slopes. It would be interesting to know whether near-bed sediment transport rolls over the bottom or if it is transported as near-bed suspension transport. If sediment especially rolls downward and is transport as suspension upwards slope effects are probably quite important.
- The SANTOSS model takes only wave-related sediment transport in the wave boundary layer into account, since it is assumed that most of the wave-related suspended transport for non-breaking waves takes place in the wave boundary layer (van der A et al., 2013). Non-accurate measurements indicate that this assumption is not valid for breaking waves. Therefore accurate measurements of the wave related suspended sediment transports for breaking waves are required.
- Sediment diffusivity has been extracted from the measured sediment concentrations. Though, vertical velocities have not been taken into account and it is assumed that the sediment diffusivity increases linearly from the bed to the surface level. Some more accurate information on the sediment diffusivity is required to make a good comparison between the measured and the modeled sediment diffusivity. Therefore it is recommended to do some more research on the measured sediment diffusivity.

9 BIBLIOGRAPHY

Abreu, T., Silva, P. a., Sancho, F., & Temperville, A. (2010). Analytical approximate wave form for asymmetric waves. *Coastal Engineering*, *57*(7), 656–667. doi:10.1016/j.coastaleng.2010.02.005

Apsley, D. D., & Stansby, P. K. (2008). Bed-Load Sediment Transport on Large Slopes: Model Formulation and Implementation within a RANS Solver. *Journal of Hydraulic Engineering*, *134*(10), 1440–1451. doi:10.1061/(ASCE)0733-9429(2008)134:10(1440)

Bagnold, R. A. (1966). An Approach to the Sediment Transport Problem from General Physics. *USGS Professional Paper*, 42.

Bakker, W. T., & Van Doorn, T. (1978). Near-bottom velocities in waves with a current. *Coastal Engineering Proceedings*, *1*(16), 1394–1413.

Baldock, T. E., Holmes, P., Bunker, S., & Van Weert, P. (1998). Cross-shore hydrodynamics within an unsaturated surf zone. *Coastal Engineering*, *34*, 173–196. doi:10.1016/S0378-3839(98)00017-9

Battjes, J. A. (1974). Surf Similarity. In *Proceedings of the 14th Coastal Engineering Conference, American Society of Civil Engineers* (pp. 466–780). doi:10.1007/978-1-61779-361-5

Battjes, J. A., & Stive, M. J. F. (1985). Calibration and verification of a dissipation model for random breaking waves. *Journal of Geophysical Research*, *90*(C5), 9159. doi:10.1029/JC090iC05p09159

Da Silva, P. A., Temperville, A., & Seabra Santos, F. (2006). Sand transport under combined current and wave conditions: A semi-unsteady, practical model. *Coastal Engineering*, *53*(11), 897–913. doi:10.1016/j.coastaleng.2006.06.010

Dean, R. G., & Dalrymple, R. A. (1991). *Water wave mechanics for engineers and scientists vol.2 of Advanced series on oncean engineering*. Singapore: World Scientific Publishing Company.

Deltares. (2014). Delft3D-Flow User Manual. Delft, The Netherlands: Deltares.

DHI Software. (2007). *MIKE 21 EMS Elliptic Mild-Slope Wave Module*. Hørsholm, Denmark.

Dibajnia, M., & Watanabe, A. (1992). Sheet flow under nonlinear waves and currents. In *Coastal Engineering Conference* (Vol. 2, pp. 2015 – 2028).

Dohmen-Janssen, M. (1999). Grain size influence on sediment transport in oscillatory sheet flow. Delft, The Netherlands: Delft University of Technology.

Dunn, S. L. (2003). *Wave setup in river entrances, PhD Thesis*.

Fredsoe, J., & Deigaard, R. (1992). Mechanics of Coastal Sediment Transport. In *Advanced series on Ocean Engineering, vol 3.* (p. 369). Singapore: World Scientific.

Giardino, A., Brière, C., & van der Werf, J. J. (2011). *Morphological modelling of bar dynamics with Delft3D*. Delft.

Grasmeijer, B. T. (2002). *Process-Based Cross-Shore Modelling of Barred Beaches*. *Ph.D. Thesis*. Utrecht, The Netherlands.

Isobe, M., & Horikawa, K. (1982). Study on water particle velocities opf shoaling and breaking waves. In *Coastal Engineering in Japan 25* (pp. 109–123).

Kranenburg, W. M., Ribberink, J. S., Schretlen, J. J. L. M., & Uittenbogaard, R. E. (2013). Sand transport beneath waves: The role of progressive wave streaming and other free surface effects. *Journal of Geophysical Research: Earth Surface*, *118*(1), 122–139. doi:10.1029/2012JF002427

Lesser, G. R., Roelvink, J. a., van Kester, J. a T. M., & Stelling, G. S. (2004). Development and validation of a three-dimensional morphological model. *Coastal Engineering*, *51*(8-9), 883–915. doi:10.1016/j.coastaleng.2004.07.014

Longuet-Higgins, M. S. (2005). On wave set-up in shoaling water with a rough sea bed. *Journal of Fluid Mechanics*, *527*, 217–234. doi:10.1017/S0022112004003222

Mai, S., Ohle, N., & Zimmermann, C. (1999). Applicability of Wave Models in Shallow Coastal Waters. In *Proc. of the 5 th Int. COPEDEC* (pp. 170–179).

Malarkey, J. (2008). *A review of freestream descriptions and velocity and acceleration skewness. Tech. Rep. SANTOSS UWV Internal Report Number 2*.

Malarkey, J., & Davies, a. G. (2012). Free-stream velocity descriptions under waves with skewness and asymmetry. *Coastal Engineering*, *68*, 78–95. doi:10.1016/j.coastaleng.2012.04.009

Nam, P. T., Oumeraci, H., Larson, M., & Hanson, H. (2014). Modeling undertow due to random waves. *Ocean Dynamics*, 1209–1219. doi:10.1007/s10236-014-0748-z

Nielsen, P. (2006). Sheet flow sediment transport under waves with acceleration skewness and boundary layer streaming. *Coastal Engineering*, *53*(9), 749–758. doi:10.1016/j.coastaleng.2006.03.006

Nomden, H. G. (2011). *SANTOSS sand transport model: Implementing and testing within the morphological model UNIBEST-TC*. Enschede, the Netherlands.

O'Donoghue, T., Doucette, J. S., van der Werf, J. J., & Ribberink, J. S. (2006). The dimensions of sand ripples in full-scale oscillatory flows. *Coastal Engineering*, *53*(12), 997–1012. doi:10.1016/j.coastaleng.2006.06.008

Reniers, a. J. H. M., Gallagher, E. L., MacMahan, J. H., Brown, J. a., Van Rooijen, a. a., Van Thiel De Vries, J. S. M., & Van Prooijen, B. C. (2013). Observations and modeling of steep-beach grain-size variability. *Journal of Geophysical Research: Oceans*, *118*(2), 577–591. doi:10.1029/2012JC008073

Reniers, a. J. H. M., Roelvink, J. a., & Thornton, E. B. (2004). Morphodynamic modeling of an embayed beach under wave group forcing. *Journal of Geophysical Research*. doi:10.1029/2002JC001586

Reniers, A. J. H. M., & Roelvink, J. a. (1995). *LIP 11D Delta Flume Experiment: a Dataset for Profile Model Validation*. WL|Delft Hydraulics.

Ribas, F., de Swart, H. E., Calvete, D., & Falqués, a. (2011). Modeling waves, currents and sandbars on natural beaches: The effect of surface rollers. *Journal of Marine Systems*, *88*(1), 90–101. doi:10.1016/j.jmarsys.2011.02.016

Ribberink, J. S. (1998). Bed-load transport for steady flows and unsteady oscillatory flows. *Coastal Engineering*, *34*(1-2), 59–82. doi:10.1016/S0378-3839(98)00013-1

Ribberink, J. S., & Al-Salem, A. A. (1994). Sediment transport in oscillatory boundary layers in cases of rippled beds and sheet flow. *Journal of Geophysical Research*. doi:10.1029/94JC00380

Ribberink, J., van der A, D. A., van der Zanden, J., O'Donoghue, T., Hurther, D., Cáceres, I., & Thorne, P. D. (2014). SandT-Pro: sediment transport measurements under irregular and breaking waves. In *Coastal Engineering* (Vol. 34). doi:10.9753/icce.v34.sediment.1

Roelvink, J. a. (1993). Dissipation in random wave groups incident on a beach. *Coastal Engineering*, *19*(1-2), 127–150. doi:10.1016/0378-3839(93)90021-Y

Roelvink, J. A., Meijer, T. J. G. P., Houwman, K., Bakker, R., & Spanhoff, R. (1995). Field Validation and Application of a Coastal Profile Model. In *Proceedings Coastal Dynamics Conderence* (pp. 818–828). Gdansk, Poland.

Roelvink, J. a., & Stive, M. J. F. (1989). Bar-Generating Cross-Shore Flow Mechanism on a Beach. *Journal of Geophysical Research*, *94*(C4), 4785–4800.

Rosman, J. H., Hench, J. L., Koseff, J. R., & Monismith, S. G. (2008). Extracting Reynolds stresses from acoustic Doppler current profiler measurements in wave-dominated environments. *Journal of Atmospheric and Oceanic Technology*, *25*(2), 286–306. doi:10.1175/2007JTECHO525.1

Ruessink, B. G., Ramaekers, G., & Van Rijn, L. C. (2012). On the parameterization of the free-stream non-linear wave orbital motion in nearshore morphodynamic models. *Coastal Engineering*, *65*, 56–63. doi:10.1016/j.coastaleng.2012.03.006

Ruessink, B. G., Wijnberg, K. M., Holman, R. A., Kuriyama, Y., & van Enckevort, I. M. J. (2003). Intersite comparison of interannual nearshore bar behavior. *Journal of Geophysical Research*. doi:10.1029/2002JC001505

Sleath, J. F. a. (1987). Turbulent oscillatory flow over rough beds. *Journal of Fluid Mechanics*, *182*, 369–409. doi:10.1017/S0022112087002374

Soulsby, R. (1997). *Dynamics of Marine Sands*. London: Thomas Telford Publications.

Stive, M., & Vriend, H. De. (1994). Shear stresses and mean flow in shoaling and breaking waves. *Coastal Engineering Proceedings*, *1*(24), 594–608. doi:10.9753/icce.v24.

Svendsen, I. a. (1984). Mass flux and undertow in a surf zone. *Coastal Engineering*, *8*(4), 347–365. doi:10.1016/0378-3839(84)90030-9

Swart, D. H. (1974). *Offshore sediment transport and equilibrium beach profile*. Delft.

Ting, F. C. K., & Kirby, J. T. (1994). Observation of undertow and turbulence in a laboratory surf zone. *Coastal Engineering*, *24*(1-2), 51–80. doi:10.1016/0378-3839(94)90026-4

Ting, F. C. K., & Kirby, J. T. (1995). Dynamics of surf-zone turbulence in a strong plunging breaker. *Coastal Engineering*, *24*(3-4), 177–204. doi:10.1016/0378-3839(94)00036-W

Ting, F. C. K., & Kirby, J. T. (1996). Dynamics of surf zone turbulence in a spilling breaker. *Coastal Engineering*, *27*, 131–160.

Toomas, L. (2001). Investigation of turbulence in a plunging breaking wave. *Proc. Estonian Acad. Sci. Eng*, *7*(1), 58–78.

Treffers, R. (2009). *Wave-Driven Longshore Currents in the Surf Zone*. Delft, The Netherlands.

Uchiyama, Y., McWilliams, J. C., & Shchepetkin, A. F. (2010). Wave-current interaction in an oceanic circulation model with a vortex-force formalism: Application to the surf zone. *Ocean Modelling*, *34*(1-2), 16–35. doi:10.1016/j.ocemod.2010.04.002

Ursell, F. (1953). The long-wave paradox in the theory of gravity waves. In *Proceedings of the Cambridge Philosophical Society 49 (4)* (pp. 685–694).

Van der A, D. a., Ribberink, J. S., van der Werf, J. J., O'Donoghue, T., Buijsrogge, R. H., & Kranenburg, W. M. (2013). Practical sand transport formula for non-breaking waves and currents. *Coastal Engineering*, *76*, 26–42. doi:10.1016/j.coastaleng.2013.01.007

Van der Werf, J. J. (2009). *Hydrodynamic validation of Delft3D using data from the SandyDuck97 experiments*. Delft, The Netherlands.

Van der Werf, J. J., Ribberink, J. S., O'Donoghue, T., & Doucette, J. S. (2006). Modelling and measurement of sand transport processes over full-scale ripples in oscillatory flow. *Coastal Engineering*, *53*(8), 657–673. doi:10.1016/j.coastaleng.2006.02.002

Van der Werf, J. J., Veen, R., Ribberink, J. S., & van der Zanden, J. (2015). TESTING OF THE NEW SANTOSS TRANSPORT FORMULA IN THE DELFT3D MORPHOLOGICAL MODELING SYSTEM. In *Coastal Sediments 2015, At San Diego* (pp. 1–14). San Diego, United States.

Van der Zanden, J., van der A, D. A., Ribberink, J. S., O'Donoghue, T., Hurther, D., Cáceres, I., & Thorne, P. D. (2015). SAND TRANSPORT PROCESS MEASUREMENTS UNDER LARGE-SCALE BREAKING WAVES. In *Proceedings of 8th Conference on Coastal Sediments*. San Diego, United States: World Scientific.

Van Rijn, L. C. (1984). Sediment transport, Part I: Bed Load Transport. *Journal of Engineering Mechanics*, *110*(10), 1431–1456. doi:10.1061/(ASCE)0733-9429(1984)110:10(1431)

Van Rijn, L. C. (1984). Sediment Transport, Part II: Suspended Load Transport. *Journal of Hydraulic Engineering*, *110*(11), 1613–1641. doi:10.1061/(ASCE)0733-9429(1984)110:11(1613)

Van Rijn, L. C. (1993). *Principles of Sediment Transport in Rivers Estuaries and Coastal Seas*. Blokzijl, the Netherlands: Aqua Publications.

Van Rijn, L. C. (2007a). Unified View of Sediment Transport by Currents and Waves. I: Initiation of Motion, Bed Roughness, and Bed-Load Transport. *Journal of Hydraulic Engineering*. doi:10.1061/(ASCE)0733-9429(2007)133:6(649)

Van Rijn, L. C. (2007b). Unified View of Sediment Transport by Currents and Waves. II: Suspended Transport. *Journal of Hydraulic Engineering*. doi:10.1061/(ASCE)0733-9429(2007)133:6(668)

Van Rijn, L. C., Ribberink, J. S., Van Der Werf, J., & Walstra, D. J. R. (2013). Coastal sediment dynamics: recent advances and future research needs. *Journal of Hydraulic Research*, *51*(5), 475–493. doi:10.1080/00221686.2013.849297

Van Rijn, L. C., & Wijnberg, K. M. (1996). One-dimensional modelling of individual waves and wave-induced longshore currents in the surf zone. *Coastal Engineering*, *28*, 121–145. doi:10.1016/0378-3839(96)00014-2

Van Rijn, L., Walstra, D., & Ormondt, M. Van. (2004). *Description of TRANSPOR2004 and Implementation in Delft3D-ONLINE*. *WL| Delft Hydraulics, Delft, The Netherlands*.

Van Thiel De Vries, J. S. M. (2009). *Dune erosion during storm surges*. Delft, The Netherlands.

Veen, R. (2014). *The implementation and testing of the SANTOSS sand transport model in Delft3D*. University of Twente, Enschede, the Netherlands.

APPENDIX A: DELFT3D

A.1. Grid Cells

The staggered grid, which is required to solve the numerical equations in Delft3D, is shown in Figure A-1.

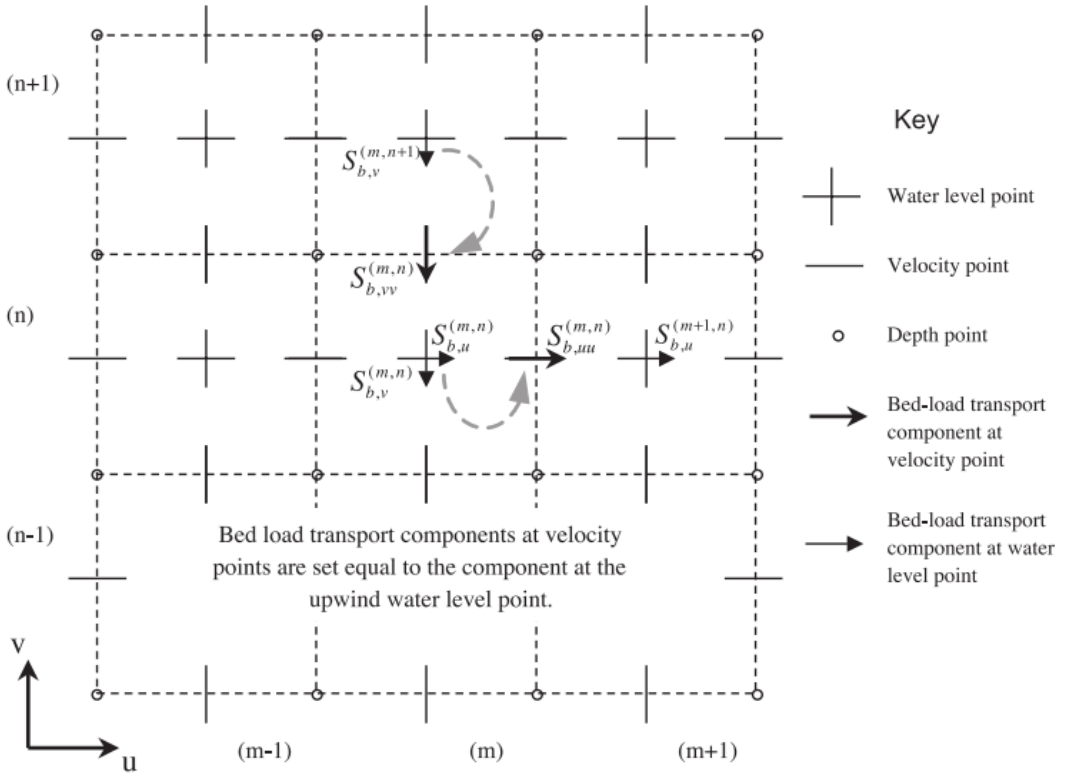

FIGURE A-1: STAGGERED GRID IN DELFT3D

Figure A-2 shows the different kind of layers which can be used in Delft3. On the left the σ-layers are shown and on the right the z-layers are shown.

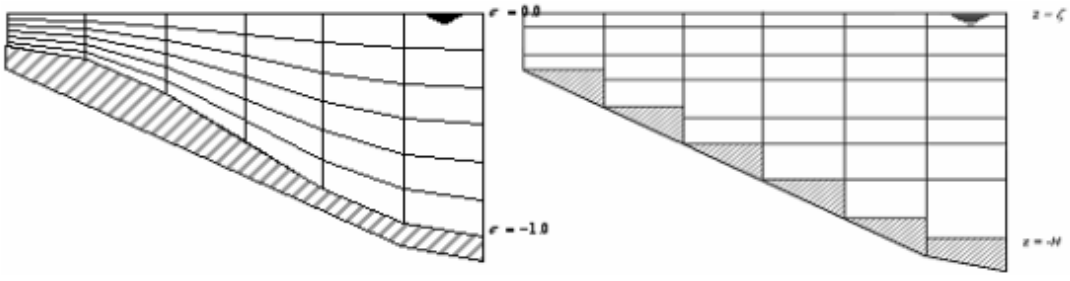

FIGURE A-2: σ-LAYERS AND Z-LAYERS (Deltares, 2014)

A.2. System of Equations

The continuity equation, the horizontal momentum equations, the transport equation and the turbulence closure model solved in Delft3D are shown below.

Continuity equation
For the derivation of the continuity equation the continuity equation for incompressible fluids is used. This continuity equation is integrated over the water depth. Therefore the kinematic boundary conditions at the bed and at the water surface are taken into account.

$$\frac{\partial \zeta}{\partial \mathrm{t}} + \frac{\partial [\mathrm{h}\bar{\mathrm{U}}]}{\partial x} + \frac{\partial [h\bar{V}]}{\partial y} = S \qquad \text{EQ. A-1}$$

Terms from left to right are:

- Transport of water in time, in the x direction and in the y direction
- Discharge or withdrawal of water

Horizontal momentum equations
The horizontal momentum equations are also based on the momentum equation for incompressible fluids. In these equations the density is neglected.

$$\frac{\partial U}{\partial t} + U\frac{\partial U}{\partial x} + v\frac{\partial U}{\partial y} + \frac{\omega}{h}\frac{\partial U}{\partial \sigma} - fV = -\frac{1}{\rho_0}P_x + F_x + M_x + \frac{1}{h^2}\frac{\partial}{\partial \sigma}\left(v_V \frac{\partial u}{\partial \sigma}\right) \qquad \text{EQ. A-2}$$

$$\frac{\partial U}{\partial t} + U\frac{\partial V}{\partial x} + V\frac{\partial V}{\partial y} + \frac{\omega}{h}\frac{\partial V}{\partial \sigma} - fU = -\frac{1}{\rho_0}P_y + F_y + M_y + \frac{1}{h^2}\frac{\partial}{\partial \sigma}\left(v_V \frac{\partial u}{\partial \sigma}\right) \qquad \text{EQ. A-3}$$

Terms from left to right for the horizontal momentum equation is the x and y direction

- Acceleration term
- Convective acceleration in x, y and σ direction
- Coriolis force
- Pressure term
- Horizontal Reynolds stresses
- External source or sink of momentum contribution
- Turbulence closure model

Transport Equation
The formula for the transport of dissolved matter is shown below (Deltares, 2014). The equation is an advection-diffusion equation in three directions. In this equation sink and source terms can be taken into account. Also decay terms can be taken into account through the transport equation.

$$\frac{\partial [hc]}{\partial t} + \frac{\partial [hUc]}{\partial x} + \frac{\partial [hVc]}{\partial y} + \frac{\partial [\omega c]}{\partial \sigma} = h\left[\frac{\partial}{\partial x}\left(D_H \frac{\partial c}{\partial x}\right) + \frac{\partial}{\partial y}\left(D_H \frac{\partial c}{\partial y}\right)\right] + \frac{1}{h}\frac{\partial}{\partial \sigma}\left[D_V \frac{\partial c}{\partial \sigma}\right] - \lambda_d h + S \qquad \text{EQ. A-4}$$

Terms from left to right are:

- Transport of dissolved matter in time, x direction, y direction and the σ direction
- Horizontal diffusivity in the x direction and in the y direction
- Vertical diffusivity in the σ direction
- First order decay process
- Source and sink

Turbulence closure model
The Turbulence closure model v_V from EQ. A-2 and EQ. A-3 can be implemented in Delft3D in four ways (Lesser et al., 2004):

- A constant coefficient

- Algebraic Eddy viscosity closure Model
- k-L turbulence closure model
- k-ϵ turbulence closure model

Difference between these models is how they calculate the turbulent kinetic energy k, the dissipation rate of the turbulent kinetic energy and/or the mixing length L.

APPENDIX B: VERTICAL LAYER DEPENDENCY

The amount of vertical layers is important for the distribution of the depth averaged velocity. According to Treffers (2009) the different results using different amount of vertical layers are small. The differences in the results converged with an increasing number of vertical layers. According to Treffers (2009) the differences in the results between models with 30 and 50 vertical layers are negligible. Four runs have been executed with a different amount of vertical layers. They have been executed respectively with 6, 12, 24, and 36 layers. Next to the effect on the vertical distribution on the depth average velocity it is also important to keep the computation time into account. The effect of the number of layers on the computational time is shown in de Table B-1

TABLE B-1: COMPUTATIONAL TIME FOR VARYING NUMBER OF VERTICAL LAYERS

Layers	**6**	**12**	**24**	**36**
Computation time (~min)	11	18	25	36

The sum of the distribution over the layer thickness must be equal to 100%. According to van der Werf (2009) it is important to have small layer thicknesses near the bottom and near the water surface. Small layer thicknesses near the bottom are required for a good computation of the bottom roughness. Small layer thicknesses near the water surface are important to deal with stresses due to wind and waves. Wind is not included in this model, but using small layer thicknesses near the water surface is still important for a good computation of the stresses due to waves and rollers. The layer thickness distribution is chosen when taken the following into account:

- Small layer thicknesses near the bottom and the water surface are required. The layer thickness can increase towards the middle of the water column.
- The layers below the middle of the water column are equally distribution as the layers above the middle of the water column.
- The variation factor between two successive layer should be around 0.7 to 1.4 (Deltares, 2014).

This results in the following layer thickness distribution. Only the bottom half of the layers are shown. The upper half of the layers are conversely located on top of the bottom half of the layers.

- 6 layers: 7%,14% and 29%
- 12 layers: 2%, 3.2%, 5%, 7.9%,12.4% and 19.6%
- 24 layers: 1%, 1.3%, 1.6%, 2%, 2.4%, 3.1%, 3.8%, 4.8%, 5.8%, 7%, 8.2 % and 9%
- 36 layers: 0.5%, 0.6%, 0.7%, 0.8%, 1%, 1.2%, 1.4%, 1.6%, 1.9%, 2.3%, 2.6%, 3%, 3.5%, 4.1%, 4.9%, 5.7%, 6.6% and 7.6%

The effect of the number of layers on the wave height and the set-up seemed negligible. There was some difference in the results near the shore due to drying and flooding, but this is outside the area of interest and it is not considered any further. The effect on the undertow is also small. Using 6 vertical layers the distribution of the undertow seems a little bit rough. 12 Vertical layers are enough to predict hydrodynamics well enough (See Figure B-1).

The effect of the number of vertical layers on the sediment concentration (See Figure B-2) seems more important. Using 6 vertical layers is clearly not enough to predict the sediment concentration well. The sediment concentrations near the bottom are predicted totally wrong using 6 vertical layers. Using 12 vertical layers the sediment concentrations near the bottom are

predicted a lot better. The sediment concentrations higher in the water column modeled with a different amount of vertical layers convergence with an increasing number of vertical layers. The differences in sediment concentrations using 24 and 36 vertical layers are minimal. Therefore 24 vertical layers is a desirable amount of vertical layers.

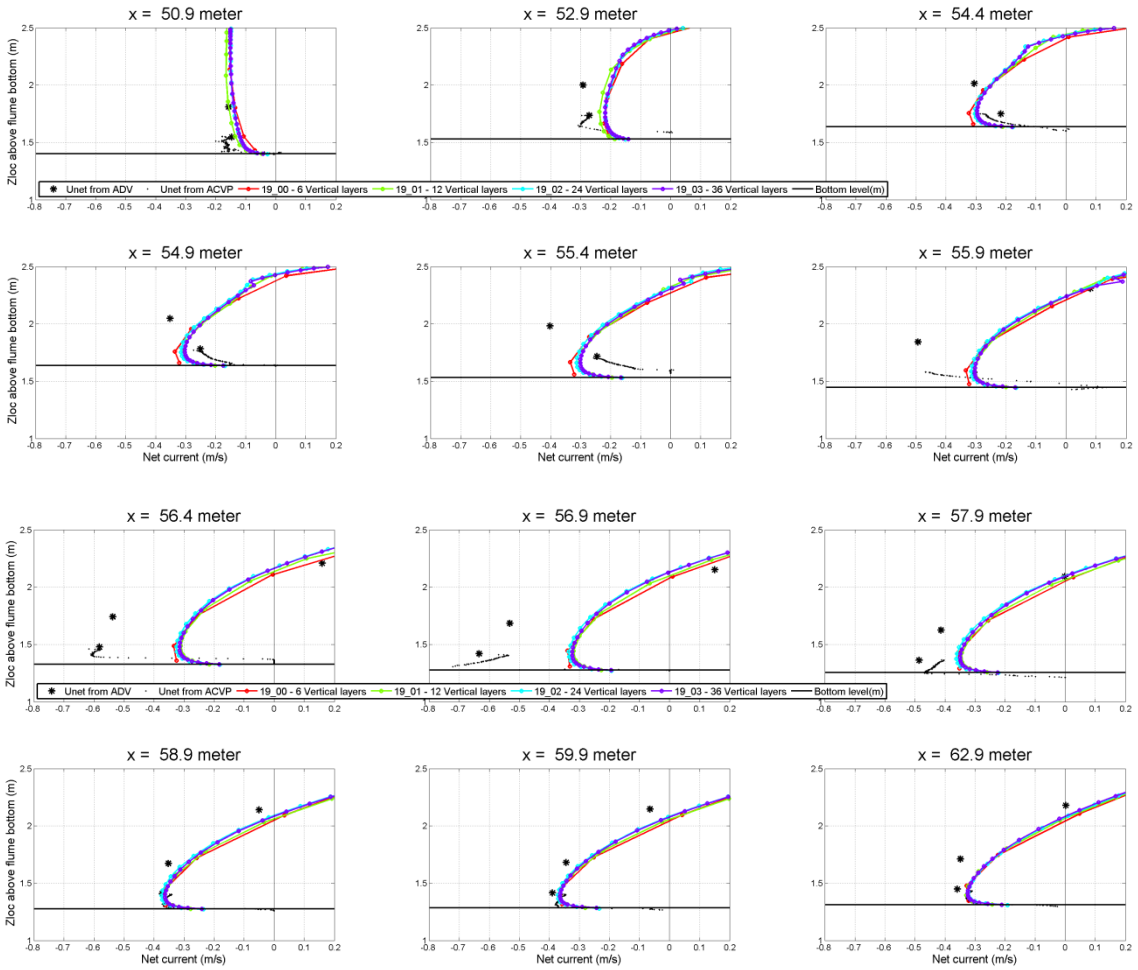

FIGURE B-1: UNDERTOW WITH VARYING NUMBER OF VERTICAL LAYERS

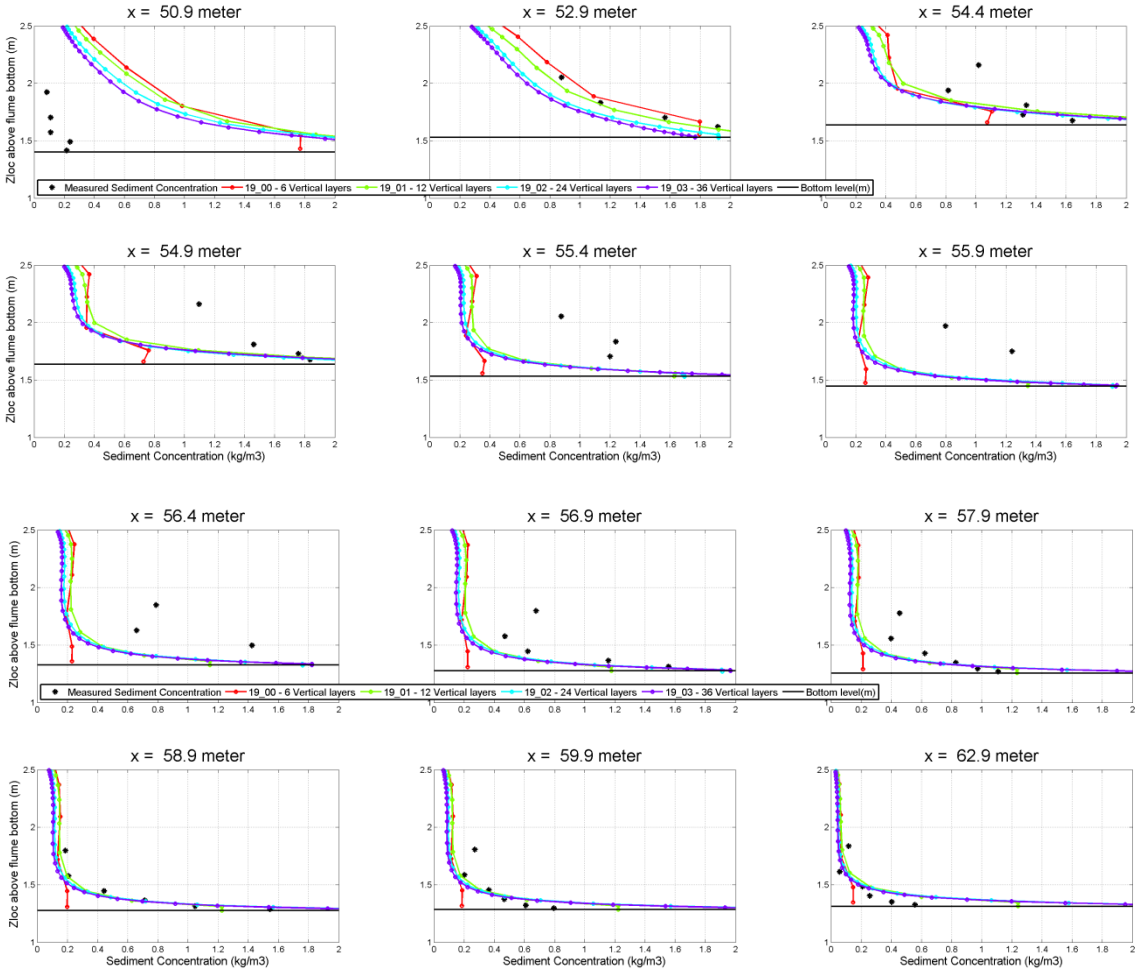

FIGURE B-2: SEDIMENT CONCENTRATIONS WITH VARYING NUMBER OF VERTICAL LAYERS

APPENDIX C: ADAPTATIONS TO THE HYDRODYNAMICS OF DELFT3D

Deltares has made the source code of Delft3D available and therefore users are able to adapt and compile the source code. During this study changes to the source code are made in the energy dissipation due to wave breaking model and the Stokes drift due to Rollers model. The changes in the source code, model concept and the reasoning behind the changes will be discussed below.

C.1. Roller energy dissipation due to wave breaking

The roller model in Delft3D is developed for irregular waves. During this study measurement from regular breaking waves are used. Where successive regular breaking waves break at the same locations, irregular waves do not. For the irregular breaking waves breaking a chance has been added. This breaking chance has been implemented according to Baldock et al. (1998) as shown in EQ. 3-4. This causes a gradually decreasing wave height near the peak wave height at the location of the breaker bar (see green line in Figure C-1). A high Alfaro (Alfaro = 20) is required to get the energy dissipation due to wave breaking close to the actual energy dissipation due to wave breaking (See the blue line in Figure C-1 with the highest Alfaro (Alfaro = 2) in the advised range (Alfaro = 0.5-2)).

The source code of the roller model has been changed to prevent the problem for wave irregularity. The source code for energy dissipation due to wave breaking was:

$$D_w = \frac{1}{4}\alpha_{rol}\rho_w g f_p \exp\left(-\frac{H_{max}^2}{H_{rms}^2}\right)(H_{max}^2 + H_{rms}^2) \qquad \text{EQ. C-1}$$

This changed into

$$\begin{aligned}
&if\ (wadire)\ then\\
&\quad if\ \left(\frac{H_{rms}}{h} \le \gamma\right) then\\
&\quad\quad Qb = 1\\
&\quad\quad dumQb = 1\\
&\quad elseif\ (dumQb = 1\ AND\ H_{rms} \ge reldep) then\\
&\quad\quad Qb = 1\\
&\quad else\\
&\quad\quad Qb = 0\\
&\quad endif\\
&\quad dumQb = Qb\\
&\quad D_w = \frac{1}{4}\alpha_{rol}\rho_w g f_p H_{rms}^2 * Qb\\
&else\\
&\quad D_w = \frac{1}{4}\alpha_{rol}\rho_w g f_p \exp\left(-\frac{H_{max}^2}{H_{rms}^2}\right)(H_{max}^2 + H_{rms}^2)\\
&endif
\end{aligned} \qquad \text{EQ. C-2}$$

This part of the source code assumes that when 'wadire = yes' (WAve DIssipation for Regular waves) a different kind of formula for energy dissipation due to wave breaking will be used. If the relative wave height $\frac{H_{rms}}{h}$ is higher than the breaking index there will be energy dissipation due to wave breaking. Another conditions has been added, waves continue breaking until the waves

decrease to a certain value (reldep). This value is a calibration factor and it is set at 0.35 meter for this case. If both conditions are not met, then waves do not break and there is no dissipation due to wave breaking. This results in the wave height shown with the red line in Figure C-1.

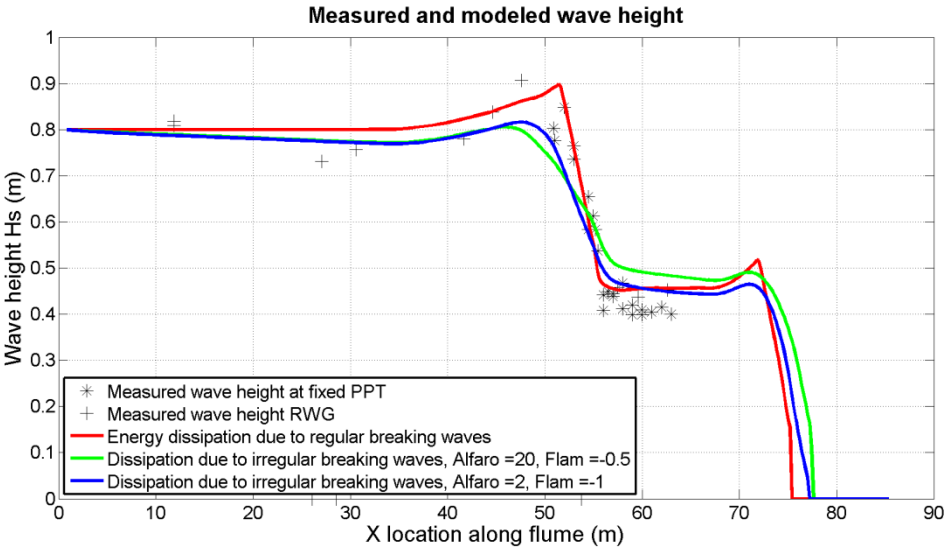

FIGURE C-1: WAVE HEIGHS ALONG THE FLUME SECTION. THE BLUE LINE SHOWS THE WAVE HEIGHT WITH THE ENERGY DISSIPATION DUE TO WAVE BREAKING MODEL OF BALDOCK ET AL. (1998). THE GREE LINE IS THE ENERGY DISSIPATION WITH AN UNREALISTIC HIGH WAVE BREAKING DISSIPATION COEFFICIENT. THE RED LINE SHOWS THE ENERGY DISSIPATION DUE TO REGULAR BREAKING.

C.2. Depth dependent second order Stokes drift due to roller mass flux

The depth dependent Stokes drift in Delft3D is the sum of the Stokes drift caused by waves and the Stokes drift caused by the Rollers. The depth dependent Stokes drift in the direction of the wave propagation is computed by the wave theory (Dean & Dalrymple, 1991):

$$u_{st,w}(z) = \frac{\omega k a^2 \cosh(2kz)}{2\sinh^2(kH)} \qquad \text{EQ. C-3}$$

With ω is the angular frequency, k is the wave number, a is the wave amplitude, z is the depth at which the Stokes velocity should be determined and H is the total water depth. The Stokes drift caused by the roller is applied in the top part of the water column from $z = \xi \; to \; z = a - \xi$ (see Figure C-2). In this part of the of the water column the net mass flux due to the second order stokes drift is equally divided. The Stokes drift due to rollers is given by:

$$z < a - \xi \rightarrow u_{st,r} = \frac{M^{s,ro}}{a} = \frac{2 * E_r * \rho_w * c_{ph}}{a} \qquad \text{EQ. C-4}$$
$$z > a - \xi \rightarrow u_{st,r} = 0$$

With $M^{s,ro}$ is the total Stokes mass flux caused by the roller, $E_r$is the roller energy, ρ_w is the water density and c_{ph} is the phase celerity of the roller. Because it seems that the undertow is mostly under predicted at the lee side of the breaker where there is roller energy (see Figure C-4), the formulation of the second order stokes drift due to rollers has been changed. Uchiyama, McWilliams, & Shchepetkin (2010) distribute the total roller mass flux equally to the distribution used for the distribution of the Stokes drift for waves used by Dean & Dalrymple (1991).

The total Stokes transport according to Uchiyama et al. (2010) is:

$$u_{st}(z) = \frac{\omega * k * \cosh(2kz)}{\rho_w * g * sinh^2(kD)} * (E + E_r) \quad \text{EQ. C-5}$$

In this formula the wave energy will be extracted from the linear wave theory. The energy of the roller will be distracted from the output of Delft3D since there is no suitable fundamental formulation available to calculate the Roller energy. To simplify the formulas the following formula are specified in Delft3D:

$$\begin{aligned} f_1 &= \omega k a^2 \\ f_2 &= \cosh(2kz) \\ f_3 &= 2\sinh(kD) \end{aligned} \quad \text{EQ. C-6}$$

Implementing f_2 and f_3 in EQ. C-5 and assuming sinusoidal waves to extract the wave height from the wave energy with $E = \frac{1}{8}\rho g H^2$ gives:

$$u_{st}(z) = \frac{2 * \omega * k * f_2}{\rho_w * g * f_3} * \frac{1}{8}\rho g H^2 + \frac{2 * \omega * k * f_2}{\rho_w * g * f_3} * E_r \quad \text{EQ. C-7}$$

Rewriting this formula using $H = 2a$ gives:

$$u_{st}(z) = \omega k * \frac{1}{4}(2a)^2 \frac{f_2}{f_3} + \frac{2\omega k}{\rho_w g} E_r * \frac{f_2}{f_3} \quad \text{EQ. C-8}$$

Simplifying this gives:

$$u_{st}(z) = \omega k a^2 \frac{f_2}{f_3} + \frac{2\omega k}{\rho_w g} E_r * \frac{f_2}{f_3} \quad \text{EQ. C-9}$$

Using f_1 and f_4:

$$u_{st}(z) = (f_1 + f_4) * \frac{f_2}{f_3} \quad \text{EQ. C-10}$$

With f_4 is equal to:

$$f_4 = \frac{2\omega k}{\rho_w g} E_r \quad \text{EQ. C-11}$$

Rewriting EQ. C-10 for f1 to f4 gives the Stokes drift due to waves and rollers:

$$u_{st}(z) = \left(\omega k a^2 + \frac{2\omega k}{\rho g} E_r\right) * \frac{\cosh(2kz)}{2\sinh^2(kH)} \quad \text{EQ. C-12}$$

The result of changing the calculation for the Stokes drift due to roller is shown in Figure C-2. The Stokes drift shown in this figure is distracted from the Generalized Lagrangian Mean velocity, this results in the Eulerian-velocity which is used for calculations of the sediment transports (Deltares, 2014).

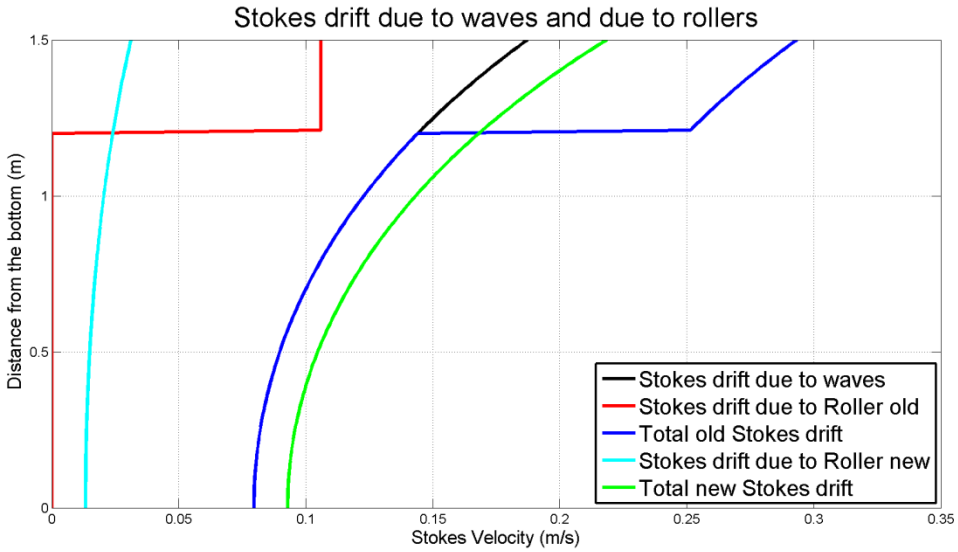

FIGURE C-2: NEW AND OLD STOKES DRIFTS TO WAVES AND ROLLERS WITH RANDOM REALISTIC WAVE PROPERTIES (WAVE NUMBER = 0.5, WAVE PERIOD = 4 S, WATER HEIGHT = 0.6 M, WAVE ENERGY = 300 J/M^2 AND ROLLER ENERGY = 50 J/M^2)

The result for the new model to distribute the Stokes drift due to rollers is shown with the green line in Figure C-3. From the red line is seems that the Stokes mass flux due to roller is underestimated. Therefore the Stokes drift has been multiplied by two to see the effect of a larger Stokes Mass flux. The effect is shown in the blue line in Figure C-3.

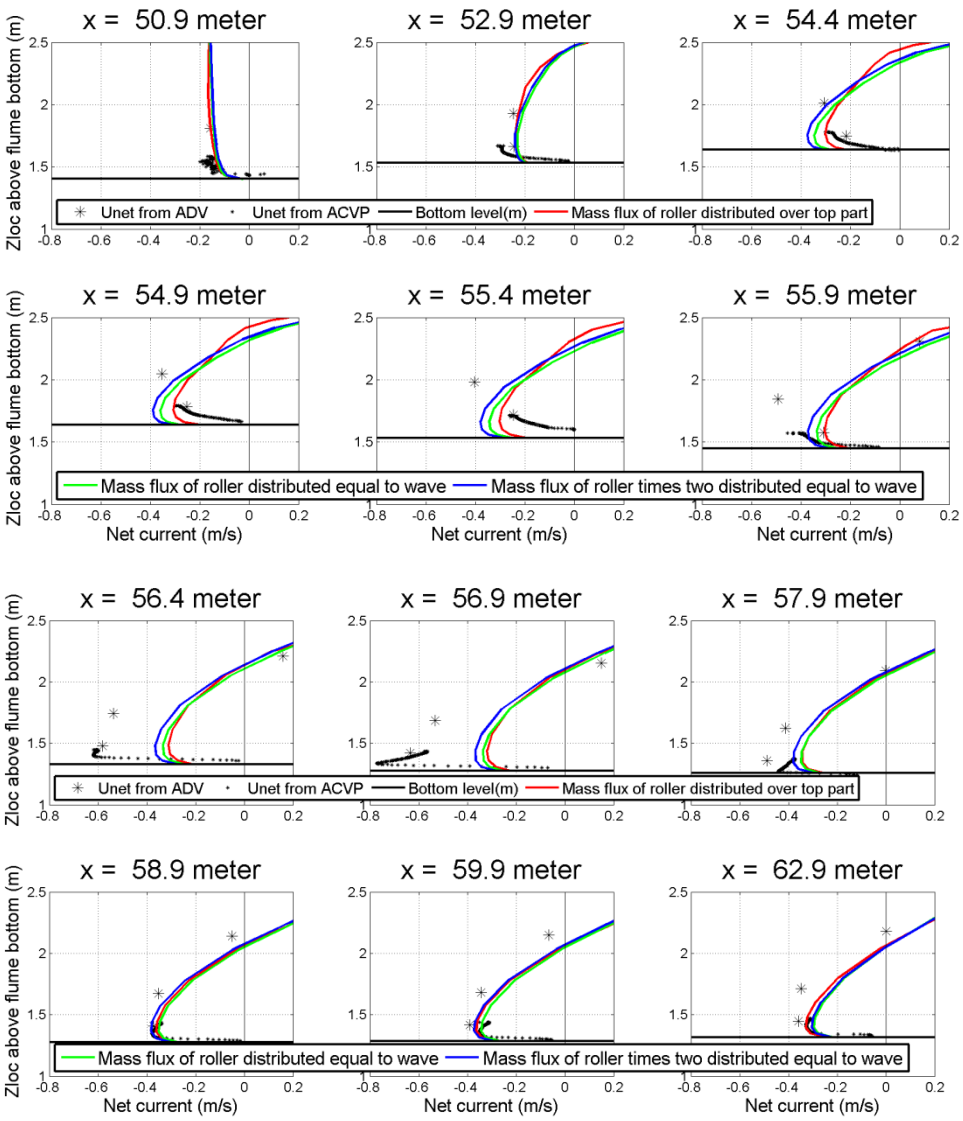

FIGURE C-3: UNDERTOW WITH DIFFERENT FORMULATION FOR THE STOKES DIRFT

Distributing the Stokes drift due to rollers equally to the distribution of the Stokes drift due to waves give better predicted results for the undertow for some locations and poorer results for other locations. The undertow get further overestimated for locations where it already was overestimated (From x = 54.4 to x= 55.9 m). For the locations at the lee-side of the breaker bar the undertow prediction is a little bit better. Since the Stokes drift is linearly dependable on the Energy of the roller, the undertow gets larger where there is roller energy. Figure C-4 shows the wave and roller energy. The roller energy is large at locations where the undertow is already overestimated. This explains why the undertow is even more overestimated with distribution of the Stokes drift mentioned above.

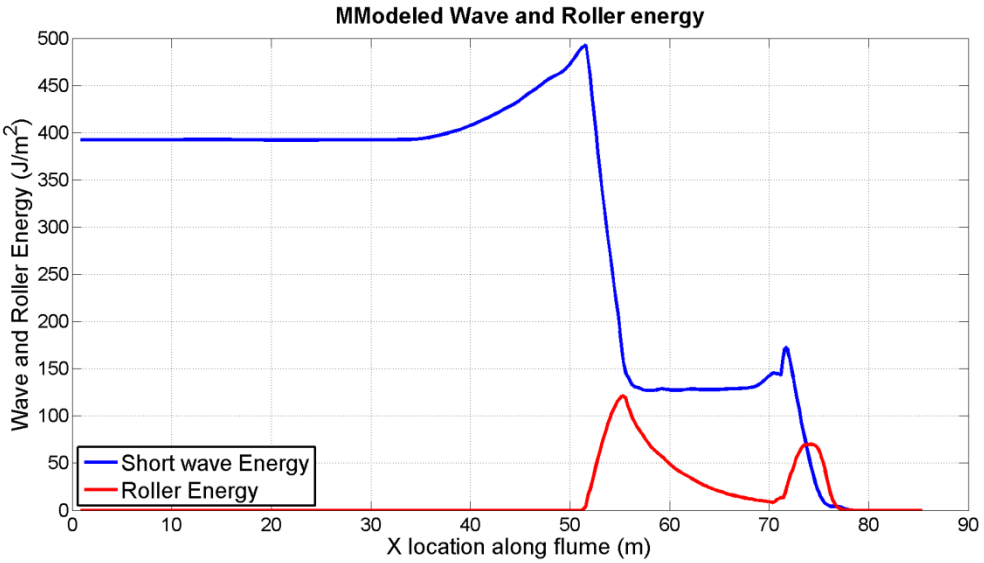

FIGURE C-4: WAVE AND ROLLER ENERGY

APPENDIX D: VARIATION OF CALIBRATION PARAMETERS

In this appendix some variations of important calibration parameters are shown. The parameter Alfaro, Gamdis and Betaro seemed extremely important to predict the hydrodynamics well. Other parameters on which calibrated is done in section 3.1 are not shown here. The bottom friction factor, breaker delay parameter, Vertical Eddy Viscosity, Horizontal Eddy Viscosity and the Reflection parameter are all set to zero. This was done to respectively exclude effects from dissipation due to bottom friction, breaker delay, background vertical and horizontal eddy viscosity and damping of reflection of waves. The vertical eddy background diffusivity seems important for the distribution of the suspended sediment concentration. Results of varying the vertical eddy diffusivity has been shown in this section as well.

D.1. Alfaro

By default the Alfaro parameter (Roller energy dissipation parameter) is equal to 1, and the advised parameter range is 0.5-2. Alfaro has been varied in a large range. Figure D-1 shows the model results with an Alfaro equal to 5, 6 and 7. When using Alfaro with a value lower than 6 the wave energy dissipation caused by wave breaking is underestimated. With a value higher than 6 the wave energy dissipation due to wave breaking is overestimated.

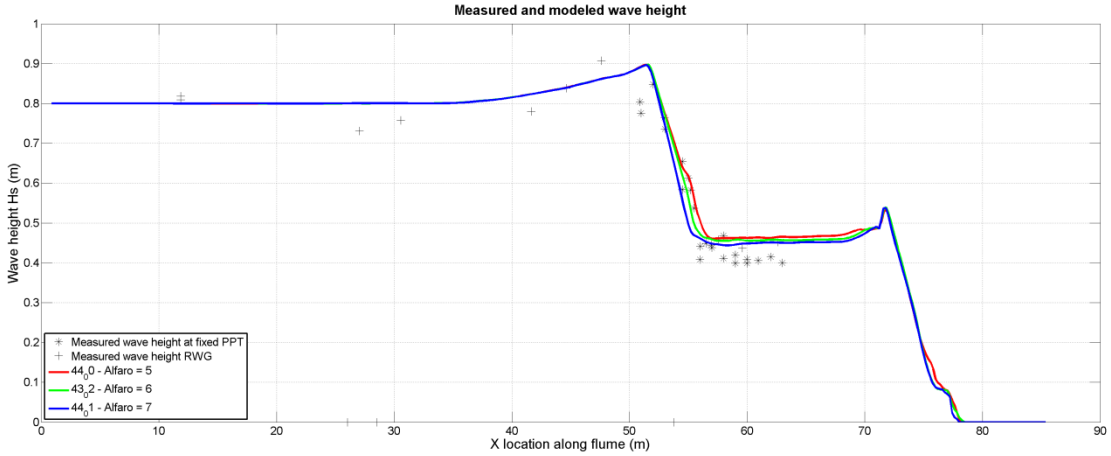

FIGURE D-1: WAVE HEIGHTS WITH VARYING THE ROLLER ENERGY DISSIPATION

D.2. Gamdis

By default Gamdis (wave breaking index) is equal to 0.55. This is derived from Roelvink (1993). With a wave breaking index of 0.55 (see red line in Figure D-2) the wave seems to break a little too early compared with the measurements. The optimal wave breaking index is 0.58 (green line in Figure D-2). Using a higher wave breaking index (0.6 for example, see the blue line in Figure D-2) starts the waves breaking too late for this test case.

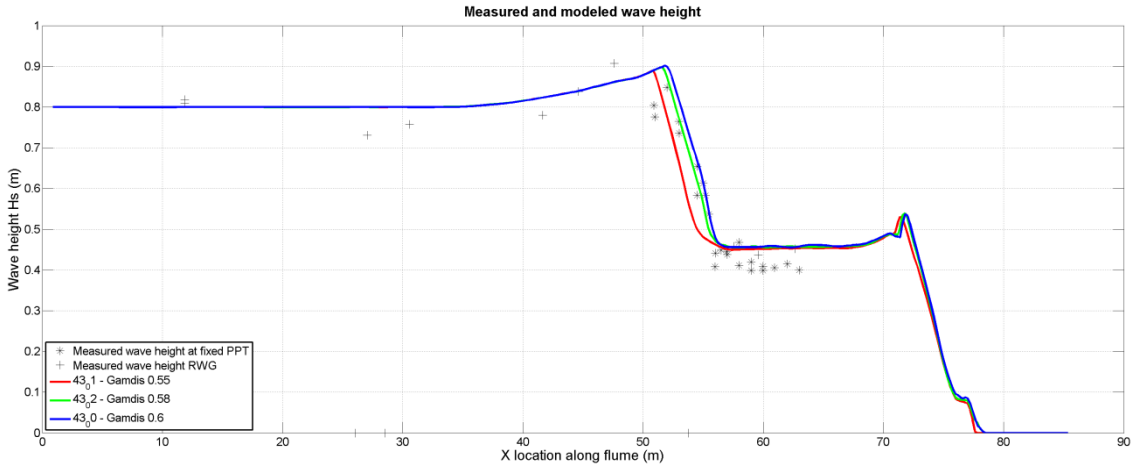

FIGURE D-2: WAVE HEIGHT WITH VARYING WAVE BREAKING INDICES

D.3. Betaro

Betaro (roller dissipation coefficient) is used to estimate the Roller energy dissipation from the roller to the underlying water. Betaro is an important parameter to estimate the undertow. The undertow is shown in Figure D-3 with Betaro varied with 0.15 (red line), 0.2 (green line) and 0.25 (blue line). Choosing the optimal value for Betaro is hard since for some locations (x = 56.4 to x = 57.9 m a high value (0.25) for Betaro is better and for other locations (x = 54.4 to x = 55.4 m) a low value (0.15) for Betaro predicts the undertow better. To get optimal predictions on average a value for Betaro of 0.2 has been used for further calculations.

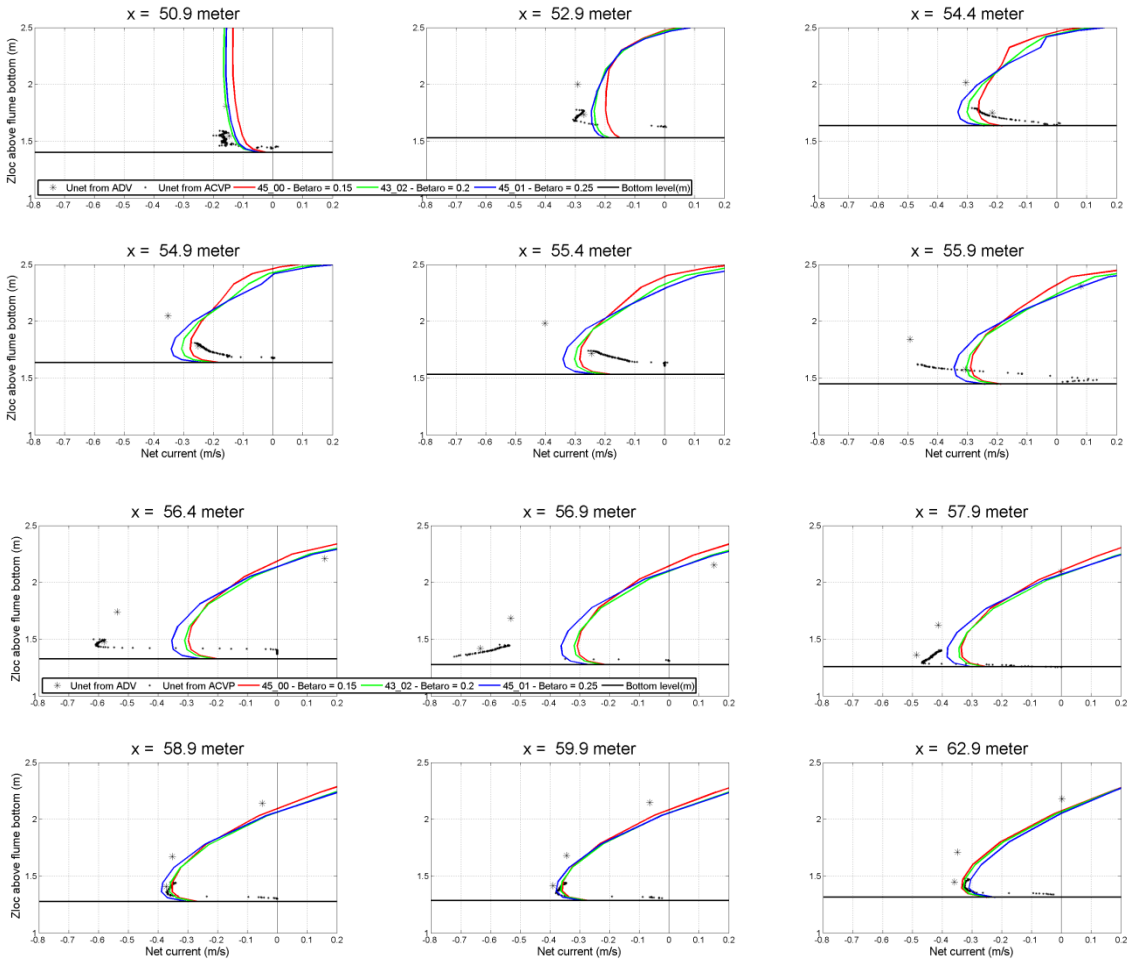

FIGURE D-3: UNDERTOW WITH VARYING ROLLER DISSIPATION COEFFICIENTS

D.4. Dicouv

Dicouv, the background horizontal eddy diffusivity, is the background horizontal diffusion rate. The background diffusion rate is added to the diffusion due to sub-grid scale and the vertical diffusion rate (Deltares, 2014). It determines to which extent sediment is mixed due to eddy motion. Dicouv has been varied from the possible upper and lower limit (0 - 1000 m^2/s). A large background eddy diffusivity 1000 m^2/s resulted in no suspension concentration. From Figure D-4 it becomes clear that different values for the background eddy diffusivity at different locations show the best suspended sediment concentrations. In front of the breaker bar (x = 50.9 m) a large background eddy diffusivity seems best. At the breaker bar (x = 52.9 to x = 55.4 m) no background eddy diffusivity seems to predict the suspended sediment concentrations best. Behind the breaker bar a background eddy diffusivity of approximately 1 m^2/s seems to predict the suspended sediment concentrations best. Since the optimal prediction of the sediment concentration is dependable on different values of Dicouv for different locations the default value of 0.01 m^2/s will be used.

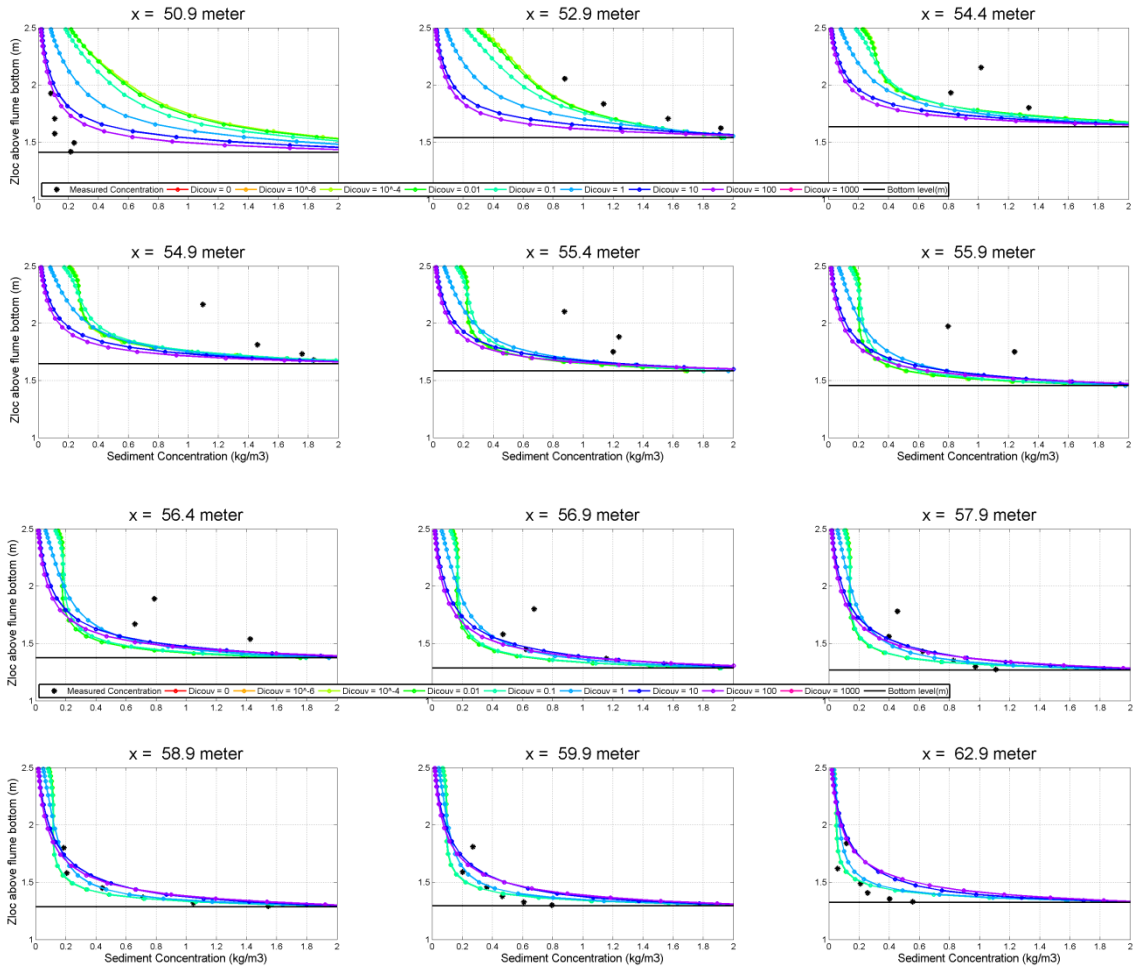

FIGURE D-4: SUSPENDED SEDIMENT CONCENTRATION WITH VARYING HORIZONTAL EDDY DIFFUSIVITY

APPENDIX E: EFFECT OF FINAL BOTTOM ON SEDIMENT TRANSPORT

The effect of using the final bottom on the modeled sediment transport will be shown in this appendix. The measured sediment transport is based on the difference between the bottom profile after 30 minutes of measurements and the bottom profile at the start of the measurements.

The hydrodynamics used in this study are measured between the start of the measurements and after 15 minutes of measurements. Therefore the bottom profile after 30 minutes of measurements and the bottom profile at the start of the measurements have been averaged to determine the bottom profile after 15 minutes of measurements. The bottom profile at the start of the measurements and the bottom profile after 15 minutes of measurements are shown in Figure E-1.

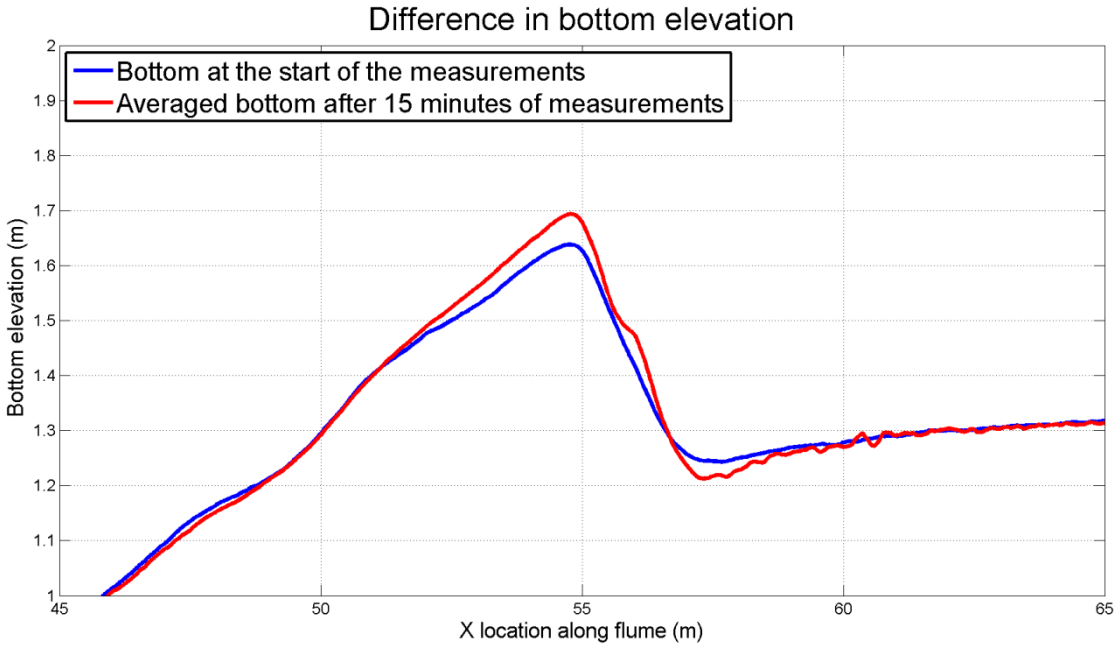

FIGURE E-1: BOTTOM PROFILE AT THE START OF THE MEASUREMENTS AND AFTER 15 MINUTES OF MEASUREMENTS

The effect on the bottom profile on the net current is shown in Figure E-1. At the breaker bar (x= 52.9 to x = 55.9 m) there is some increase of net current due to a decreasing water depth. Further onshore there is almost no change of the net current due to the bottom profile updating. The effect off the bottom updating on the sediment transport is shown in Figure E-3. There are some minor difference between the model results with the bottom at the start of the measurements and the bottom after 15 minutes of measurements. These differences especially occur at the top of the breaker bar where the water level decrease due to bottom updating is at its maximum. The effect off the changes of the net current and the sediment concentration is shown in Figure E-4. The differences are very small, and therefore bottom updating will not be taken into account any further.

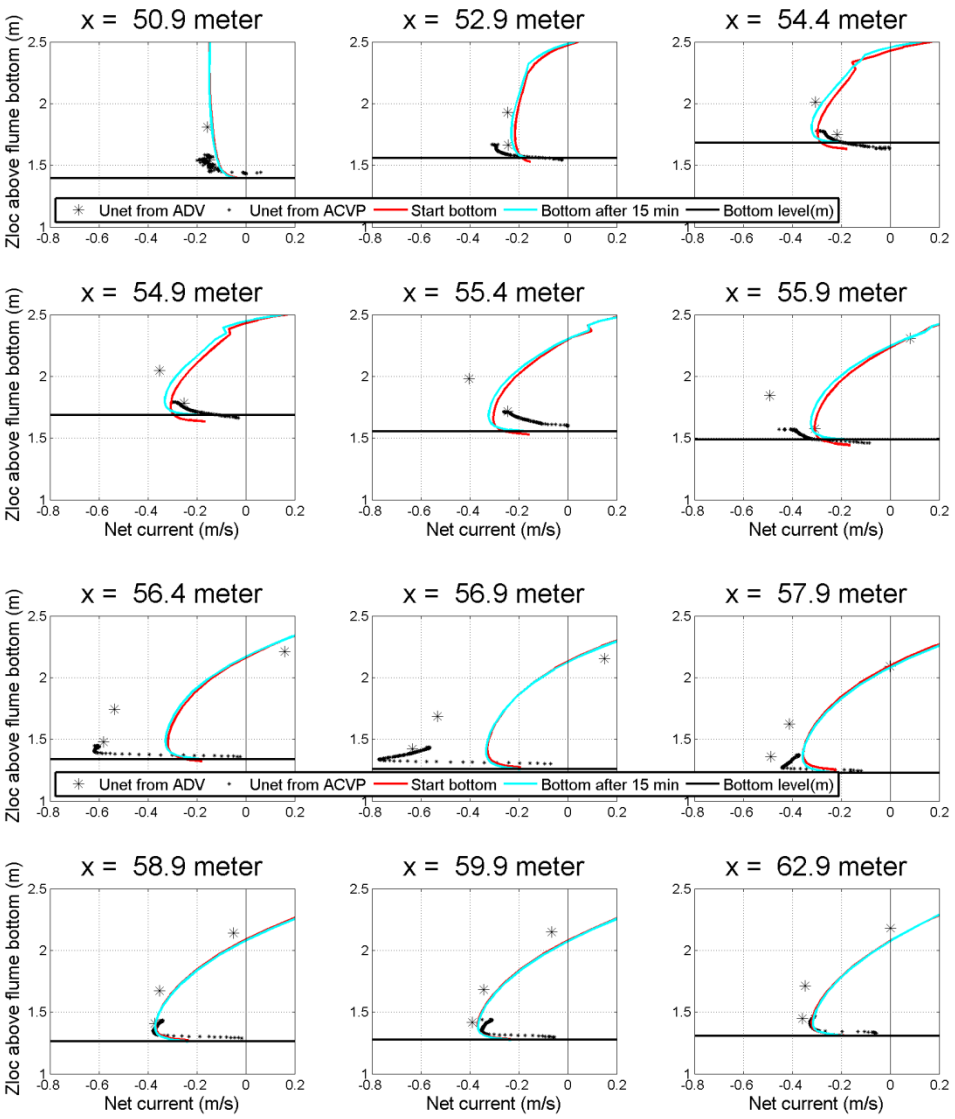

FIGURE E-2: NET CURRENTS WITH DIFFERENT BOTTOM PROFILES

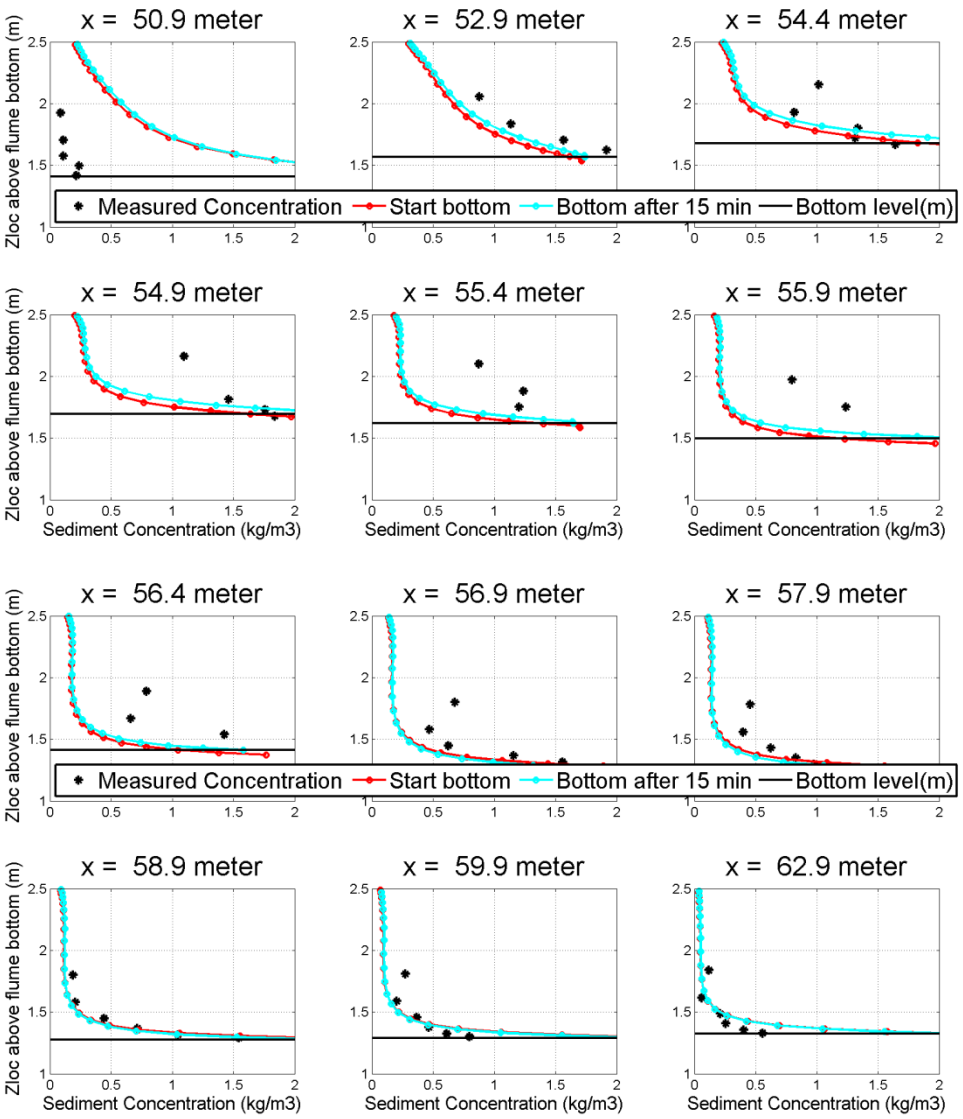

FIGURE E-3: SEDIMENT CONCENTRATION WITH DIFFERENT BOTTOM PROFILES

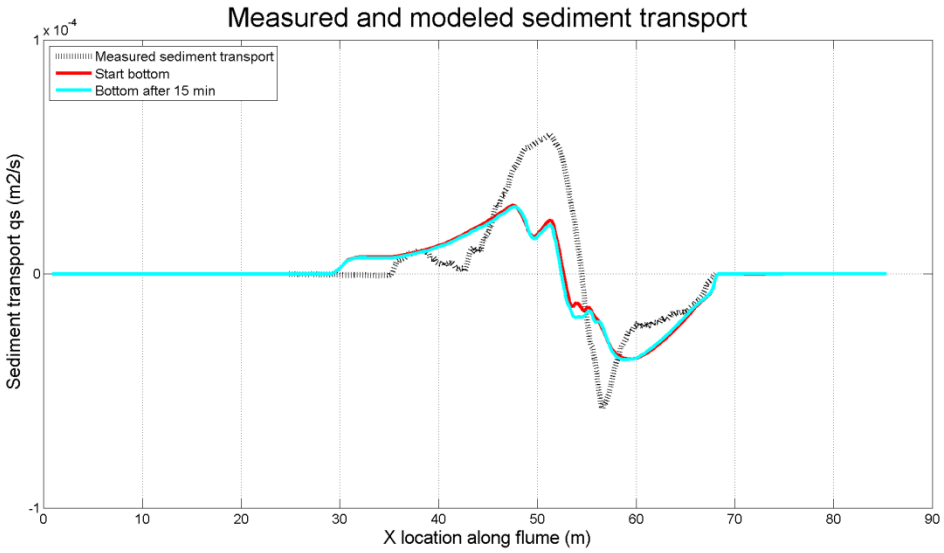

FIGURE E-4: TOTAL SEDIMENT TRANSPORT WITH DIFFERENT BOTTOM PROFILES

APPENDIX F: INTEGRATED MEASURED AND MODELED VELOCITIES AND CONCENTRATIONS

To appoint errors in the modeled suspended sediment transport due to currents the measured net currents can multiplied with the modeled concentrations and the measured concentrations can be multiplied with modeled net currents. These resulting fluxes are shown in Figure F-1. The legend of the figure is visible in Figure F-2.

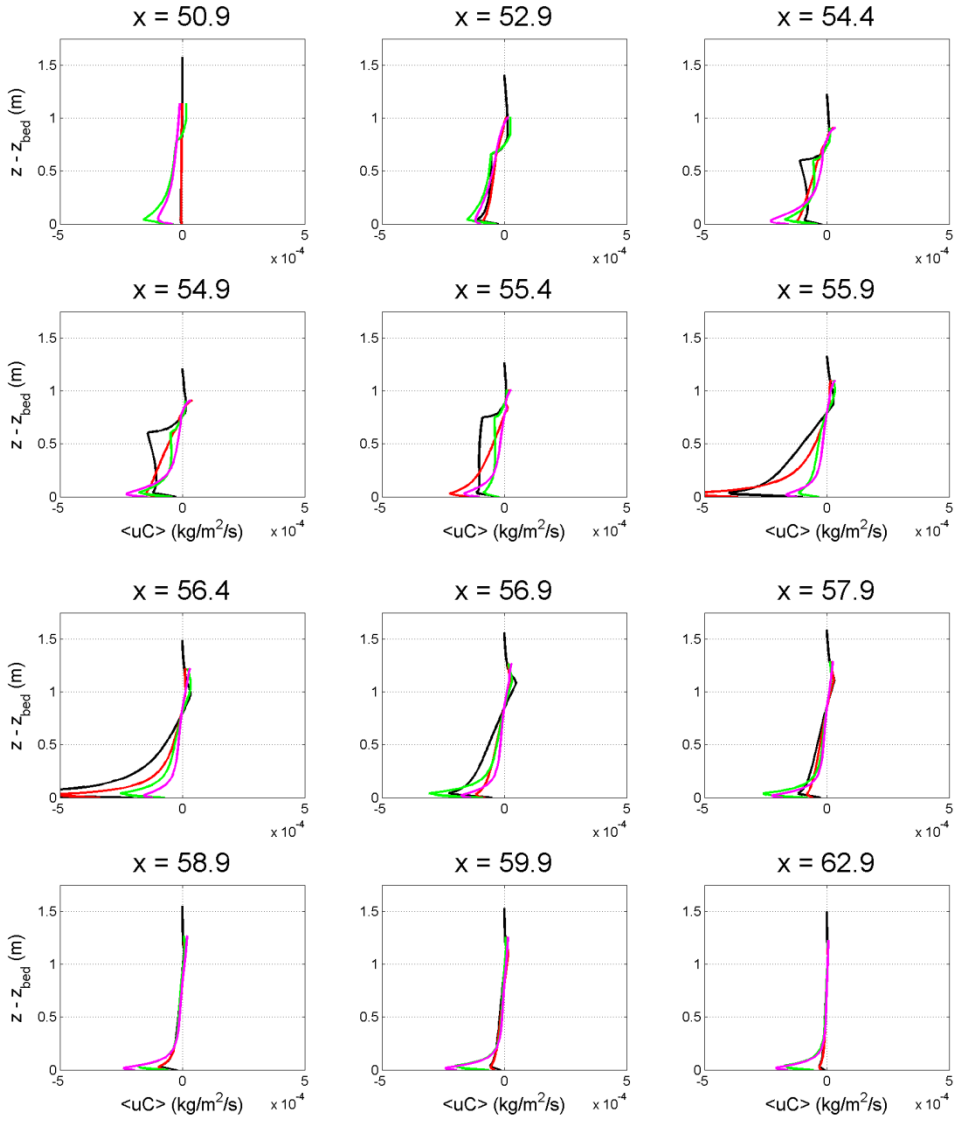

FIGURE F-1: FLUXES CALCULATED WITH THE MEASURED AND MODELED VELOCITIES AND CONCENTRATIONS. THE LEGEND IS VISIBLE IN FIGURE F-2.

The eventual transports can be calculated by using the measured and modeled velocities and currents. This results in four different suspended transports (EQ. F-1). When the fluxes from Figure F-1 are integrated over the water depth the suspended sediment transport can be calculated. The results are visible in Figure F-2. Using the modeled net current including the measured concentrations causes a smaller error in the suspended sediment transport due to

currents compared to the modeled concentrations multiplied with the measured net currents. This applies especially offshore of the breaker bar and at the breaker bar. As indicated before, the modeled net currents are underestimated; this underestimation also causes an underestimation of the suspended transport due to currents. The modeled concentrations were overestimated in front of the breaker bar and underestimated at the rest of the flume. This results in an overestimation of the suspended transport due to currents in front of the breaker and an underestimation at the breaker bar and at the onshore side of the breaker bar. Onshore of the breaker bar (x > 59 m) the suspended transport are overestimation using the modeled concentrations. This is due to the fact that the concentrations low in the water column is overestimated. Higher in the water column they are underestimated. The underestimation low in the water column causes an overestimation over the suspended sediment transport due to currents.

Critical note to this comparison is that the integration between the modeled net current and the modeled concentrations does not match up with the modeled depth average suspended transport (See Figure 4-5 and Figure F-2). This is probably due to the interpolation method used, it might be due to the fact that diffusive terms in the suspension transports are not taken into account or sometimes might be done wrong during the calculation.

$$q_{s,cur} = \int_{z=-h}^{z=0} < u_{meas} * C_{meas} >$$
$$q_{s,cur} = \int_{z=-h}^{z=0} < u_{mod} * C_{meas} >$$
$$q_{s,cur} = \int_{z=-h}^{z=0} < u_{meas} * C_{mod} >$$
$$q_{s,cur} = \int_{z=-h}^{z=0} < u_{mod} * C_{mod} >$$

EQ. F-1

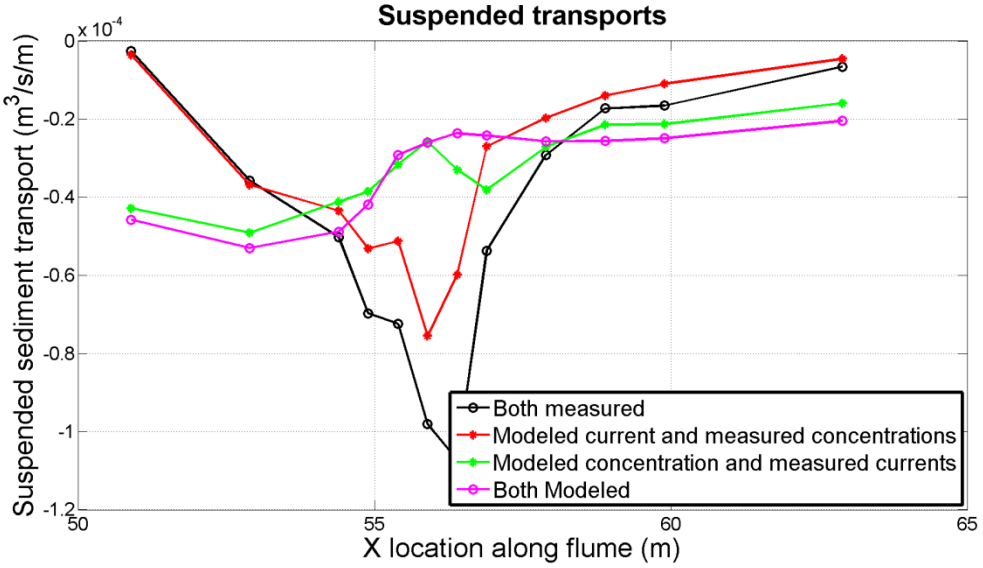

FIGURE F-2: SUSPENDED SEDIMENT TRANSPORT DUE TO MEASURED AND MODELED SEDIMENT VELOCITIES AND CONCENTRATIONS.

APPENDIX G: INTERPOLATION OF VELOCITIES AND CONCENTRATIONS

G.1. Net currents

The interpolations of the net currents are shown in Figure G-1. The steep angle at approximately 70 centimeter above the bed shown for some locations is due to the absence of measurement during the trough level of the wave. During the trough of the wave the ADVs (measurement device) were sometimes not below the water level. The ADVs could not measure velocities in this case. The onshore directed net current is due to the fact that there were no intra wave offshore directed velocities (See Appendix G.2). Due to the onshore directed net current onshore directed suspended sediment transport in the top of the wave column occurs. This cause some underestimation of the offshore directed suspended sediment transport. This effect tough is expected to be rather smaller, while the currents are relatively small in the top of the water column and the sediment concentrations high in the water column are also lower compared to lower in the water column (See Appendix G.3).

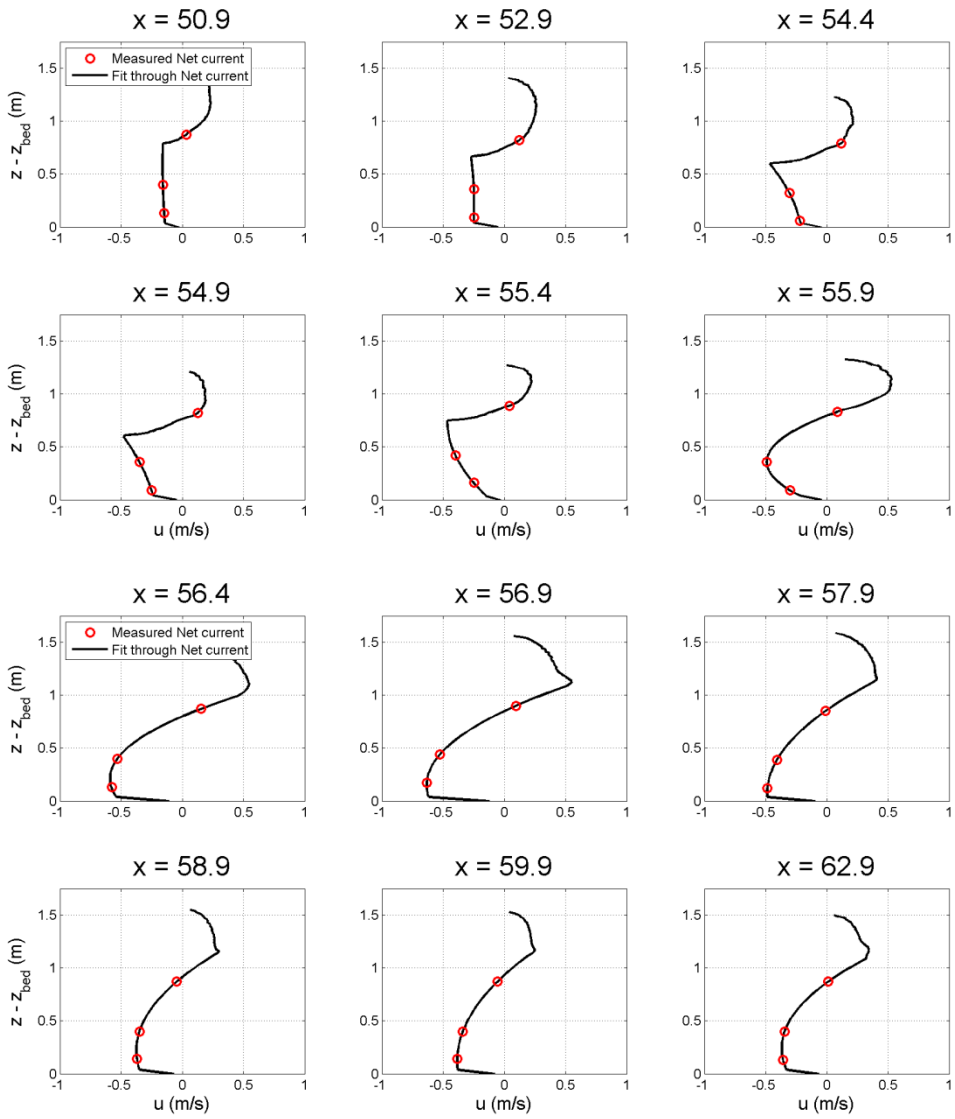

FIGURE G-1: MEASURED NET CURRENT AND FIT THROUGH THE MEASURED NET CURRENT

G.2. Intra-wave orbital velocities

The intra wave orbital velocities during ten stages of the wave are shown in Figure G-2. Since the net current is distracted from the orbital velocities the orbital velocities also show a steep angle at the water level during the trough of the wave. This could cause some underestimation of the onshore directed suspended sediment transport due to waves. For the suspended sediment transport due to wave it is expected that this effect is larger compared to the suspended sediment due to currents. Distracting the net current from the orbital velocities only has effect during the crest of the wave. The onshore directed suspended sediment due to waves is probably underestimated.

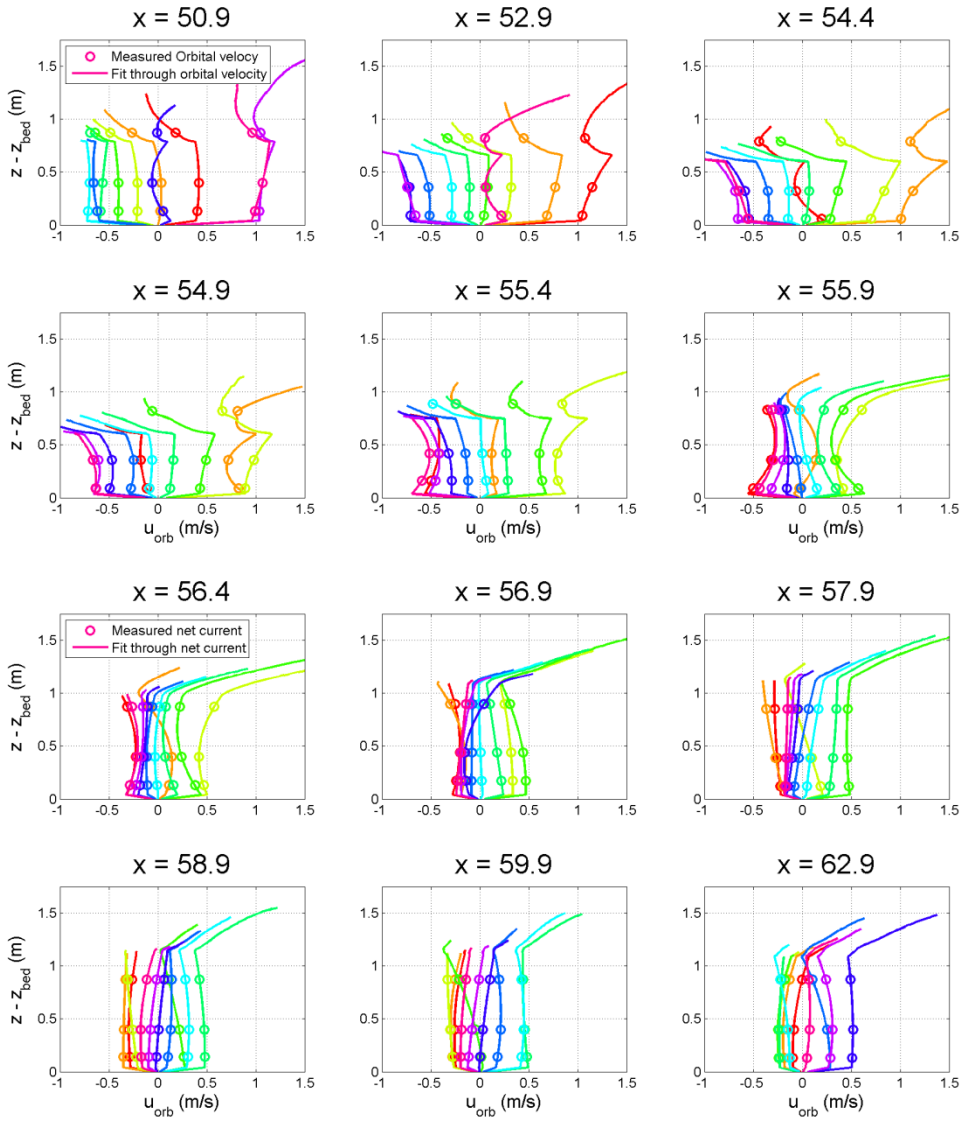

FIGURE G-2: MEASURED ORBITAL VELOCITY AND FITS TROUGH THE MEASURED ORBITAL VELOCITIES DURING DIFFERENT STAGES OF THE WAVE.

G.3. Intra-wave sediment concentrations

The intra wave sediment concentrations are shown in Figure G-3. High in the water column there are some differences during several wave stages, but lower in the water column almost no difference in sediment concentrations occur. The differences during several stages of the wave probably occur due to the presence of bubbles during the measurements. The sediment concentrations in the top part of the water column are measured with OBVs (van der Zanden et al., 2015). This OBVs are influenced by bubbles, therefore the measured intra-wave sediment concentration are not very accurate.

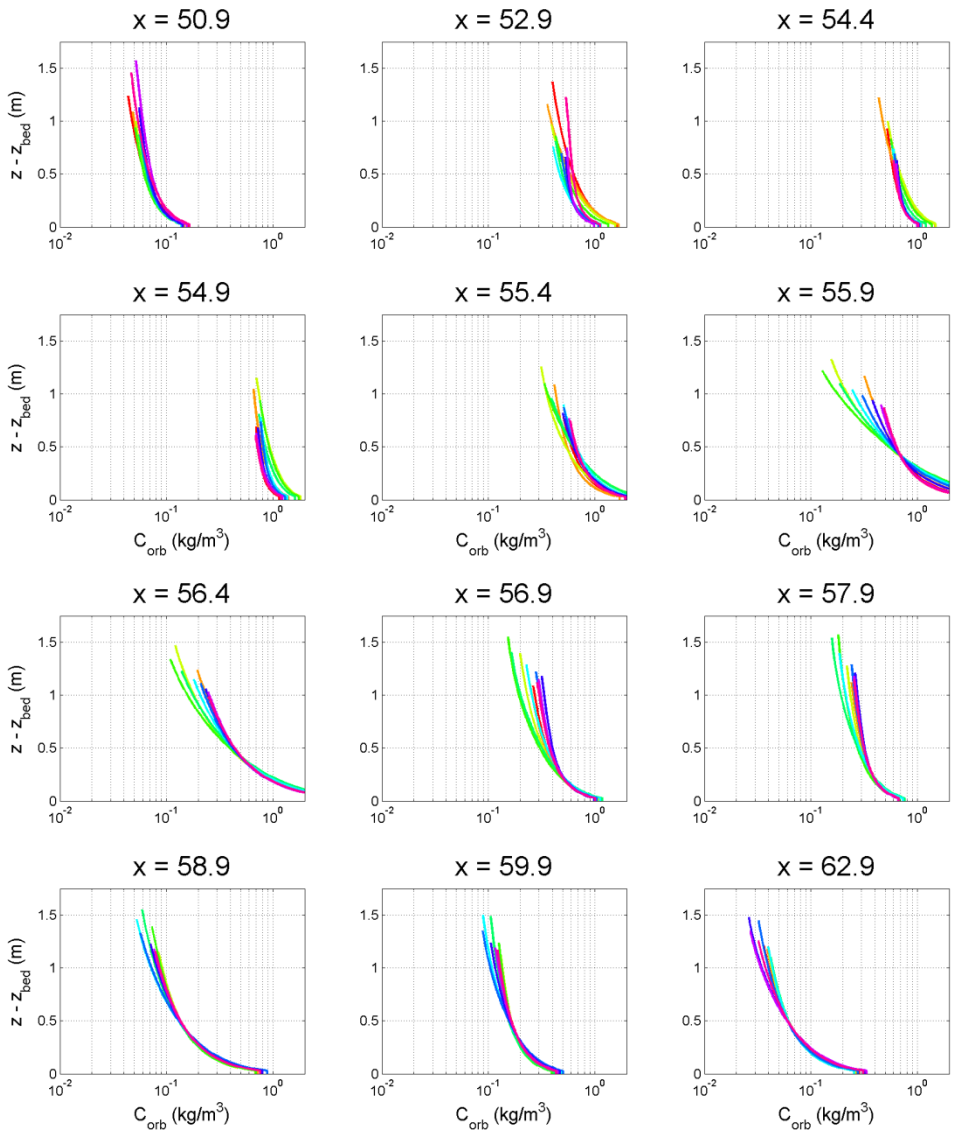

FIGURE G-3: MEASURED SEDIMENT CONCENTRATION DURING SEVERAL WAVE STAGES.

APPENDIX H: ADJUSTMENTS STAND-ALONE SANTOSS MODEL

To get an optimal comparison between the results of the stand-alone SANTOSS model and the results of the SANTOSS model in Delf3D some adaptations to the stand-alone SANTOSS code have been done.

- The velocities due to currents and waves where input for the phase lag calculations. Equation 27 and 28 in van der A et al. (2013) indicates that the peak orbital velocities should be used. While using the orbital velocities instead of the velocities due to currents and waves results in a lower phase lag during the trough period and a higher phase during the crest period.

- Effects of vertical orbital velocities were excluded from phase lag calculations in the stand-alone SANTOSS model. The phase lag depended only on the still water settling velocity. Equation 29 and 30 in van der A et al. (2013) show that the peak vertical water particle velocity should be taken into account. Including effect of vertical orbital velocities increases the phase lag effects.

- In the stand alone model the wave boundary layer thickness was constant at 0.2 meter. In the SANTOSS model in Delft3D the wave boundary layer thickness is calculated according to EQ. 4-14. In the discussion in van der A et al. (2013) it is mentioned that 0.2 meter is well above the actual wave boundary layer. It seemed that for this case the wave boundary layer thickness was quite important for the bed-load transport. Therefore computation of the wave boundary layer thickness in the stand-alone SANTOSS model has been changed equally to the computation in SANTOSS in Delft3D.

- An option has been added to the stand-alone SANTOSS model to use measured periods instead of modeled periods. This excludes effects of poorly modeled periods on the sediment transport. From the measured periods it seems that the crest periods were generally shorter compared to the modeled crest periods. This is due to an underestimation of the strong measured net current.

APPENDIX I: ERRORS IN THE HYDRODYNAMICS

I.1. Periods

The wave periods (See Figure 2-2) in the stand-alone SANTOSS model are calculated with the net currents, the peak orbital velocities and the acceleration skewness. Firstly it should be determined if the peak orbital crest velocity is smaller than the net current. If this is the case, the period of the crest is equal to zero and the trough period is equal to the total period. If the crest period is not equal to zero the crest orbital period T_{cw} will be calculated. This period does not take the net current into account.

$$T_{cw} = \frac{T}{\pi}\cos^{-1}\left(\frac{-0.5 * (u_{wc} + u_{wt}) + 0.5 * (9 * u_{wc}^2 + 9 * u_{wt}^2 - 14 * u_{wc} * u_{wt})^{0.5}}{2 * (u_{wc} - u_{wt})}\right) \quad \text{EQ. I-1}$$

With T is the total wave period equal to four seconds and u_{wc} and u_{wt} are respectively the peak orbital crest and trough velocity. The crest period T_c is calculated as follows:

$$T_c = T_{cw} * \left(1 - \frac{2}{\pi} * \sin^{-1}\left(\frac{u_{net}}{u_{wc}}\right)\right) \quad \text{EQ. I-2}$$

With u_{net} is the net current and u_{wc} is the peak orbital crest velocity. The trough period is then the total period minus the crest period. If there is a crest period, the acceleration period of the crest and the deceleration period of the trough will be calculated with the following formula based on Malarkey (2008):

$$T_{cu} = T_c \frac{\cos^{-1}(2 * \beta - 1)}{\pi}$$
$$T_{td} = T_t \frac{\cos^{-1}(2 * \beta - 1)}{\pi} \quad \text{EQ. I-3}$$

The deceleration period of the crest and the acceleration period of the trough are respectively calculated by the period of the crest minus the acceleration period of the crest and the period of the trough minus the deceleration period of the trough.

The periods in Delft3D are calculated differently, in Delft3D they are determined with the orbital velocity times series obtained from Abreu et al. (2010) (See EQ. 3-17). The net current is added to the orbital velocity time series. Positive orbital velocities are then part of the crest period and negative orbital velocities are part of the trough period. The result is shown in Figure I-1.

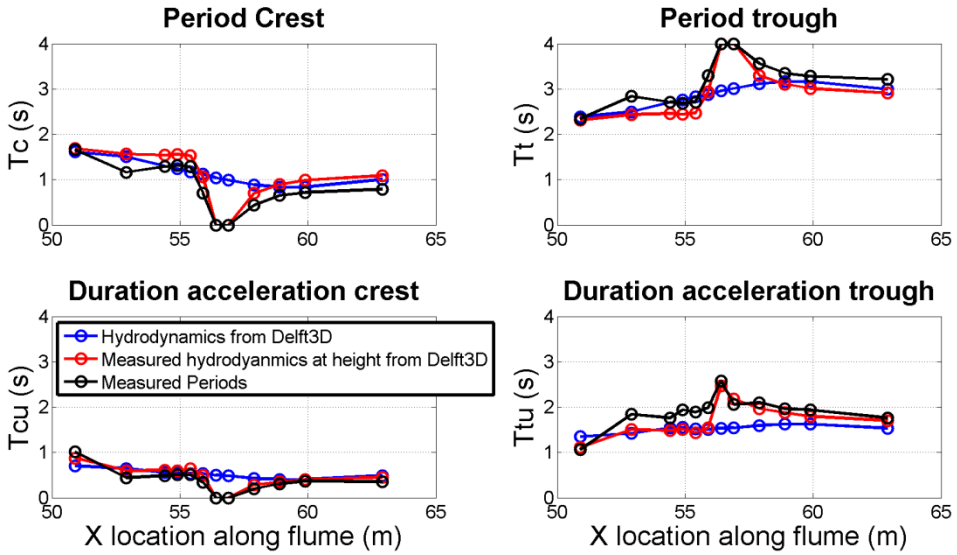

FIGURE I-1: CREST AND TROUGH PERIODS AND DURATION ACCELERATION CREST AND TROUGH MODELED WITH THE MEASURED HYDRODYNAMICS AND THE MODELED (DELFT3D) AND THE MEASURED PERIODS

The most noticeable difference between the results of the computation with the modeled and the measured hydrodynamics is that for the measured hydrodynamics crest periods of zero are predicted. Using the modeled hydrodynamics a zero crest period is not predicted, this is an immediate consequence of the under prediction of the net current. Using the modeled hydrodynamics the orbital crest velocity will not be lower than the net current; therefore a zero crest period will not be predicted.

Using the measured hydrodynamics, the periods are predicted quite well. Only the duration of the acceleration of the trough is under predicted. The modeled periods with the hydrodynamics from Delft3D change much more gradually. This is due to the modeled hydrodynamics, the modeled hydrodynamics with Delft3D also change much more gradually compared to the measurements.

I.2. Current and wave related friction factors

The combined current and wave related friction factor $f_{w\delta i}$ Is the linear combination of the wave friction factor and the current friction factor proposed by Ribberink (1998):

$$f_{w\delta i} = \alpha f_\delta + (1-\alpha) f_{wi} \qquad \text{EQ. I-4}$$

Where α is ratio between the current velocity and the sum of the current velocity and the orbital velocity amplitude. f_δ Is the current friction factor given by:

$$f_\delta = 2\left[\frac{0.4}{\ln\left(\frac{30\delta}{k_{s\delta}}\right)}\right]^2 \qquad \text{EQ. I-5}$$

In which δ is the wave boundary layer thickness calculated in EQ. 4-14. $k_{s\delta}$ Is the current related roughness according to Ribberink (1998):

$$k_{s\delta} = \max\{3d_{90}, d_{50}[\mu + 6(\langle|\theta|\rangle - 1)]\} + \frac{0.4\eta^2}{\lambda} \qquad \text{EQ. I-6}$$

f_{wi} Is the wave related friction factor for the crest and the trough based on Swart (1974), modified by da Silva et al. (2006):

$$f_{wi} = 0.00251 \exp\left[5.21\left(\frac{\left(\frac{2T_{iu}}{T_i}\right)^{2.6}\hat{a}}{k_{sw}}\right)^{-0.19}\right] \quad \text{EQ. I-7}$$

k_{sw} Is the wave related roughness calculated in EQ. 4-15. T_{iu} and T_i are respectively the acceleration duration of the period of the crest and the trough and the period of the crest and the trough. $\hat{a}$ Is the orbital excursion amplitude. The current related factor is under estimated with the modeled hydrodynamics for x < 55 meter. This is due to the prediction of the presence of ripples with the modeled hydrodynamics (see section I.4). This increases the roughness height, which decreases the current-related friction factor. The wave related friction factor is overestimated by the modeled hydrodynamics. The presence of ripples increases the wave related roughness, therefore the wave related friction factor decreases for the case with the modeled hydrodynamics. The difference in the period does not have much effect on the wave related friction factor.

The wave related friction factor seems dominant by determining the combined wave and current related friction factor (See Figure I-2). The combined wave and current related friction factor is for the case with the modeled hydrodynamics more dependable on the current for x < 55.5 meter while in this part the net current is overestimated. Further onshore the net current is underestimated, in this case the measured hydrodynamics depend more on the wave-related friction factor compared to the modeled hydrodynamics.

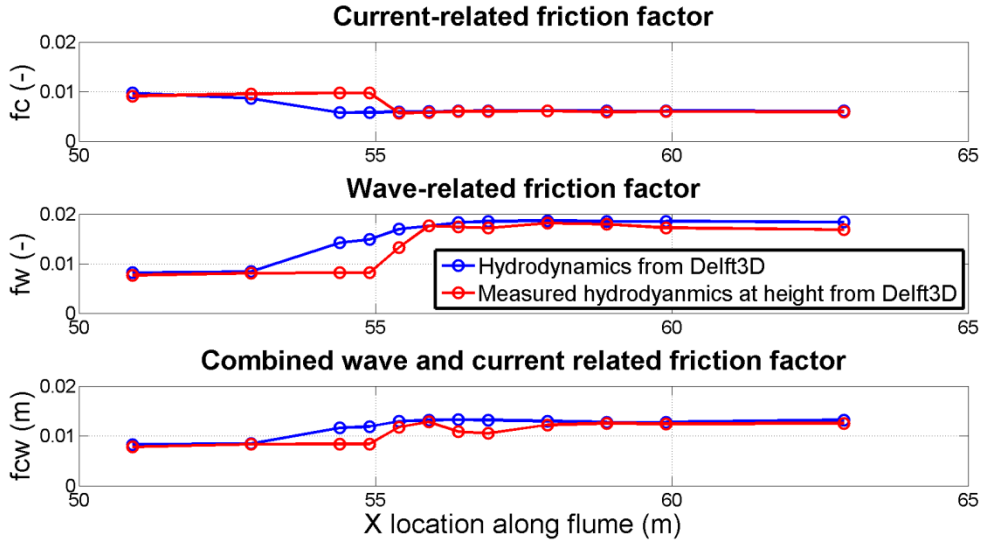

FIGURE I-2: CURRENT-RELATED, WAVE-RELATED AND COMBINED WAVE AND CURRENT-RELATED FRICTION FACTOR MODELED WITH THE MEASURED HYDRODYNAMICS AND WITH THE MODELED (DELFT3D) HYDRODYNAMICS

I.3. Dimensionless bed shear stress Shields Parameter

The dimensionless bed shear stress or the Shields parameter for the crest and the trough θ_i in the direction of the wave propagation without alongshore current can be distracted from EQ. 2-15 and is:

$$\theta_i = \frac{\frac{1}{2} f_{w\delta i} |u_{i,r}|^2}{(s-1) g d_{50}} + \frac{\tau_{wRe}}{(s-1) g d_{50}} \quad \text{EQ. I-8}$$

The subscript i stands for either the crest or the trough. $u_{i,r}$ Is the representative orbital velocity given by the root mean square of the orbital crest and trough velocity amplitude u_{ic}:

$$u_{i,r} = \frac{1}{2}\sqrt{2}u_{wi} \qquad \text{EQ. I-9}$$

The wave Reynolds stress τ_{wRe} is calculated as follows (Fredsoe & Deigaard, 1992; Nielsen, 2006):

$$\tau_{wRe} = \rho \frac{f_{w\delta}}{2c_w} \alpha_w \hat{u}^3 \qquad \text{EQ. I-10}$$

With c_w equal to the wave speed, α_w parameter equal to 0.424 and $\hat{u}$ is the representative orbital velocity amplitude. The Shields parameter of the crest period is underestimated with the modeled hydrodynamics.

Difference for the crest Shields parameter occur due to an over estimation of the net current by the modeled hydrodynamics (See Figure I-3). The representative crest parameter decreases due to an overestimation of the net current this also decreases the Shields parameter for the crest. Shields parameter is over- and underestimated for different locations. Most important is the under- and over prediction of the net current. Where the net current is overestimated the Shields parameter of the trough is also overestimated by the modeled hydrodynamics and vice versa.

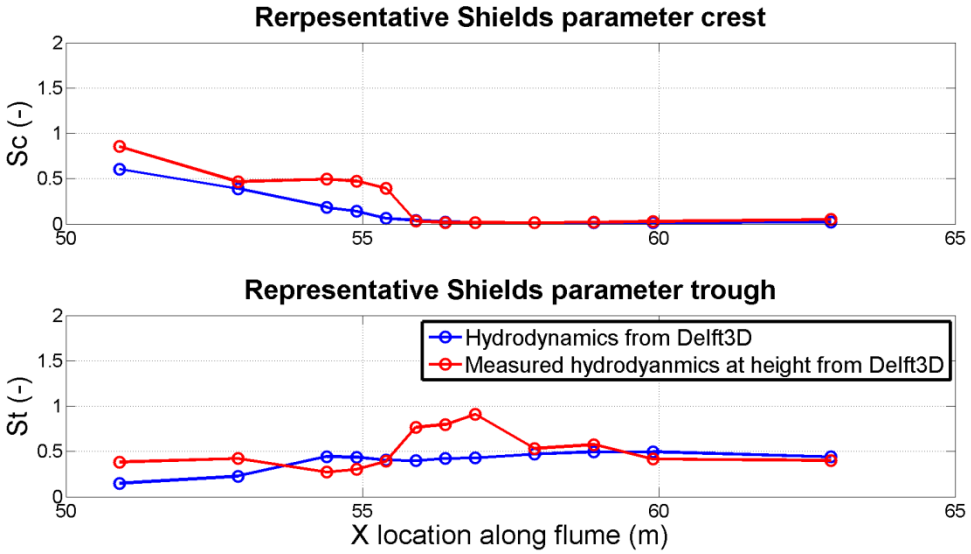

FIGURE I-3: SHIELDS PARAMETER DURING THE CREST AND THE TROUGH MODELED WITH THE MEASURED AND THE MODELED (DELFT3D) HYDRODYNAMICS

I.4. Ripples, Sheet flow layer thickness and phase lag

The ripples are calculated according to EQ. 2-18 (O'Donoghue et al., 2006). The prediction of ripples depends on the mobility number (See equation EQ. 2-19), which depends on the maximum peak orbital velocity quadratic. If the mobility number exceeds 240, then there are no ripples. Using the modeled hydrodynamics the maximum peak orbital velocity is lower than measured. Ripples are not predicted at x < 55 meter using the measured hydrodynamics. Once ripples are predicted the mobility number is off less importance. The ripples are then, using the measured and the modeled hydrodynamics, of almost equal dimensions.

If ripples are not present then a sheet flow layer thickness will be used to calculate the phase lag effects. The calculation for the sheet flow layer thickness is based on Dohmen-Janssen (1999). Using a median grain size diameter d_{50} of 0.246 mm the sheet flow layer thickness δ_{si} is calculated as follows:

$$\delta_{si} = 13\hat{\theta}_i d_{50} \qquad \text{EQ. I-11}$$

With $\hat{\theta}_i$ is the Shields parameter based on the crest/trough velocity amplitude $\hat{u}_i$:

$$\hat{\theta}_i = \frac{\frac{1}{2} f_{w\delta i} \hat{u}_i^{\,2}}{(s-1) g d_{50}} \qquad \text{EQ. I-12}$$

$f_{w\delta i}$ Is in this formula the wave-current friction factor (J. S. Ribberink, 1998). The sheet flow regime only occurs for locations without ripples. If ripples are present, the sheet flow layer thickness is set to zero. Using the hydrodynamics modeled with Delft3D, a sheet flow regime is only present at x = 50.9 m (See Figure I-4). The sheet flow layer with the modeled hydrodynamics is a little bit thinner then with the measured hydrodynamics. This is due to the under predicted velocity amplitude.

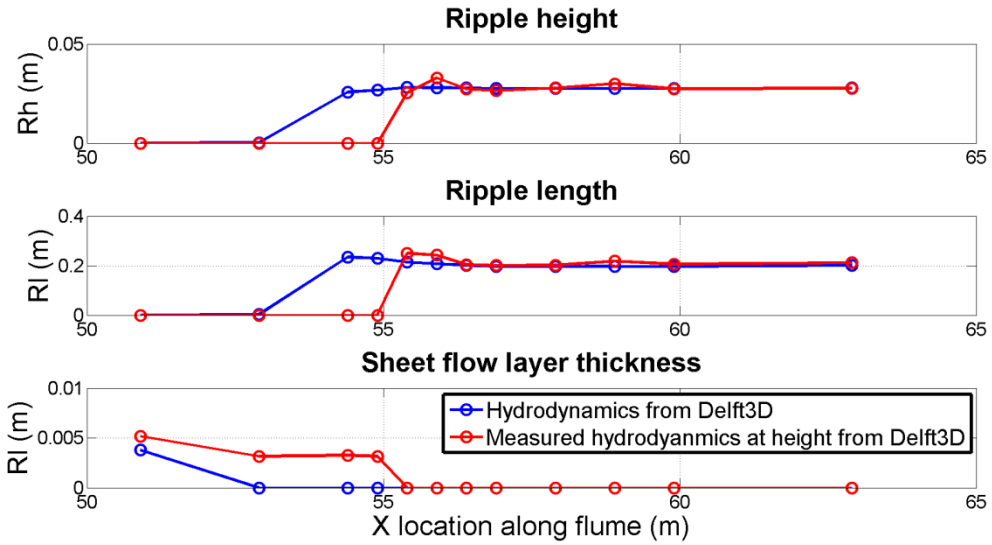

FIGURE I-4: RIPPLE HEIGHT AND LENGTH AND SHEET FLOW LAYER THICKNESS MODELED WITH THE MEASURED AND MODELED (DELFT3D) HYDRODYNAMICS. WHEN THERE ARE RIPPLES (RIPPLE HEIGHT IS LARGER THEN ZERO) THEN THE SHEET FLOW LAYER THICKNESS IS EQUAL TO ZERO.

The phase lag for the crest P_c and trough P_t are calculated with the following formulas:

$$P_c = \begin{cases} \alpha\left(\dfrac{1-\xi\hat{u}_c}{c_w}\right)\dfrac{\eta}{2(T_c - T_{cu})w_{sc}} & if\ \eta > 0\ (Ripple\ regime) \\ \alpha\left(\dfrac{1-\xi\hat{u}_c}{c_w}\right)\dfrac{\delta_{sc}}{2(T_c - T_{cu})w_{sc}} & if\ \eta = 0\ (Sheet\ flow\ regime\ regime) \end{cases}$$

$$P_t = \begin{cases} \alpha\left(\dfrac{1+\xi\hat{u}_t}{c_w}\right)\dfrac{\eta}{2(T_t - T_{tu})w_{st}} & if\ \eta > 0\ (Ripple\ regime) \\ \alpha\left(\dfrac{1+\xi\hat{u}_t}{c_w}\right)\dfrac{\delta_{sc}}{2(T_t - T_{tu})w_{st}} & if\ \eta = 0\ (Sheet\ flow\ regime\ regime) \end{cases} \qquad \text{EQ. I-13}$$

In which α and ξ are a calibration factor equal to 8.2 and 1.7, $\hat{u}_c$ and $\hat{u}_t$ are the peak crest and peak trough velocities, c_w is the wave speed, η and δ_{sc} are the ripple height and the sheet flow layer thickness , T_c and T_t are the crest and trough period, T_{cu} and T_{tu} are the acceleration periods of the crest and the through and w_{sc} and w_{st} are the settling velocities during the crest and the trough half cycle given by:

$$w_{sc} = w_s - w_{min}(r_c)$$

$$w_{st} = \max(w_s + w_{max}(r_t), 0)$$

EQ. I-14

With w_s is the still water settling velocity according to Soulsby (1997), $w_{min}(r_c)$ and $w_{max}(r_t)$ are the peak negative and peak positive water particle velocity and height r_i.

Phase lag during the crest periods barely occur due to the low peak crest velocity (See Figure I-5). Negative phase lag during crest occur due to a negative peak crest velocity. The phase lag during the trough is overestimation for x < 55, since ripples where predicted with the modeled hydrodynamics and they were not predicted with the measured hydrodynamics. Further onshore underestimation of the modeled hydrodynamics occurs due to an underestimation of the net current.

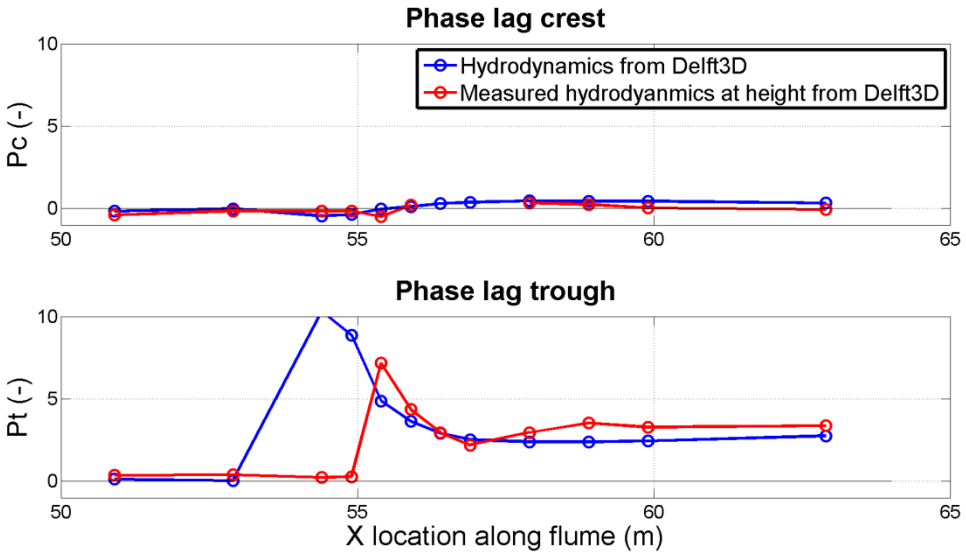

FIGURE I-5: PHASE LAG DURING THE CREST AND TROUGH MODLED WITH THE MEASURED AND THE MODELED (DELFT3D) HYDRODYNAMICS.

I.5. Sand loads entrained

The sand load entrained for the crest and trough is calculated with the EQ. 2-14 with values for the calibration factors m and n of 11.0 and 1.2. The sand load entrained is only dependable on the Shields parameter; locations with differences are equal to the differences in the predicted Shields parameter (See Figure I-6). For x > 56 meter no sand load is entrained during the crest period, because the Shields parameter did not exceed the critical Shields number.

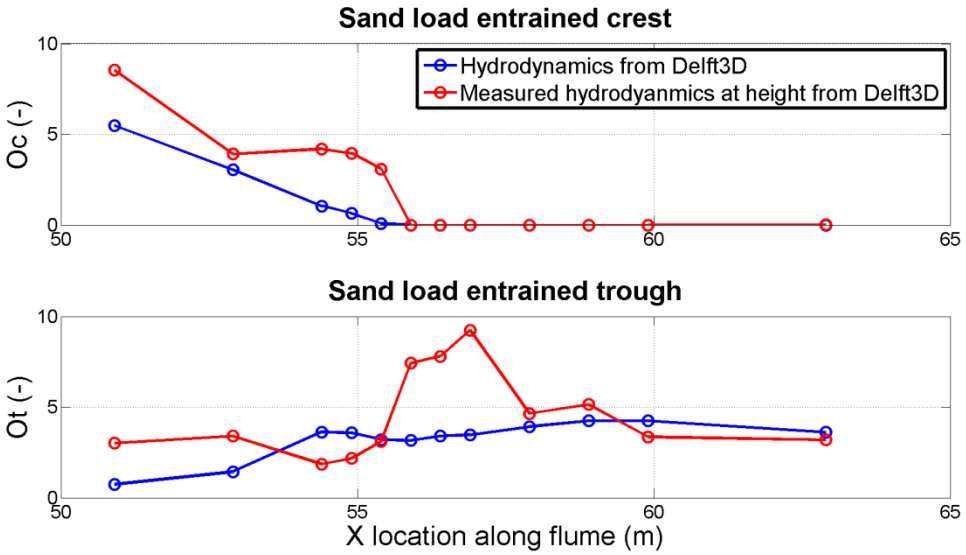

FIGURE I-6: SAND LOAD ENTRAINED DURING THE CREST AND THE TROUGH MODELED WITH THE MEASURED AND THE MODELED (DELFT3D) HYDRODYNAMICS

Whether the entrained sand is transport in the same period depends on the phase lag. If the phase lag exceeds one then there is exchange of sand between the crest and the trough period and vice versa.

$$\Omega_{cc} = \begin{cases} 0 & if\ P_c \leq 1 \\ \frac{1}{P_c}\Omega_c & if\ P_c > 1 \end{cases}$$

$$\Omega_{ct} = \begin{cases} 0 & if\ P_c \leq 1 \\ \left(1 - \frac{1}{P_c}\right)\Omega_c & if\ P_c > 1 \end{cases}$$

EQ. I-15

$$\Omega_{\mathrm{tt}} = \begin{cases} 0 & if\ P_t \leq 1 \\ \frac{1}{P_t}\Omega_t & if\ P_t > 1 \end{cases}$$

$$\Omega_{\mathrm{tc}} = \begin{cases} 0 & if\ P_t \leq 1 \\ \left(1 - \frac{1}{P_t}\right)\Omega_t & if\ P_t > 1 \end{cases}$$

APPENDIX J: MEASURED AND MODELED WAVE REYNOLDS STRESS

The wave Reynolds stress has been extracted from the measurements with the following formula (Rosman, Hench, Koseff, & Monismith, 2008):

$$\rho\overline{\tau_{br}} = -\rho\left(\overline{u'w'}\right) \qquad \text{EQ. J-1}$$

In which u' and w' are the turbulent components of the horizontal and the vertical velocity given by:

$$u' = u - \bar{u} - \tilde{u}$$
$$w' = w - \bar{w} - \tilde{w} \qquad \text{EQ. J-2}$$

In these formula u and w are the horizontal and vertical velocity components, $\bar{u}$ and $\bar{w}$ are the horizontal and vertical component of the net current and $\tilde{u}$ and $\tilde{w}$ are the horizontal and vertical component of the orbital velocities. The horizontal and vertical components of the net current are determined by averaging the velocity over a wave cycle. The horizontal and vertical components of the orbital velocities are determined by smoothing the residual of $u - \bar{u}$ and $w - \bar{w}$.

Due to slope effects the vertical components are overestimated and the horizontal components are underestimated. Therefore a coordinate transformation has been done, the vertical and horizontal components has been transformed to a components parallel to the bed and a component perpendicular to the bed. An example of a raw and smoothed time series of the component parallel to the bed is shown in Figure J-1.

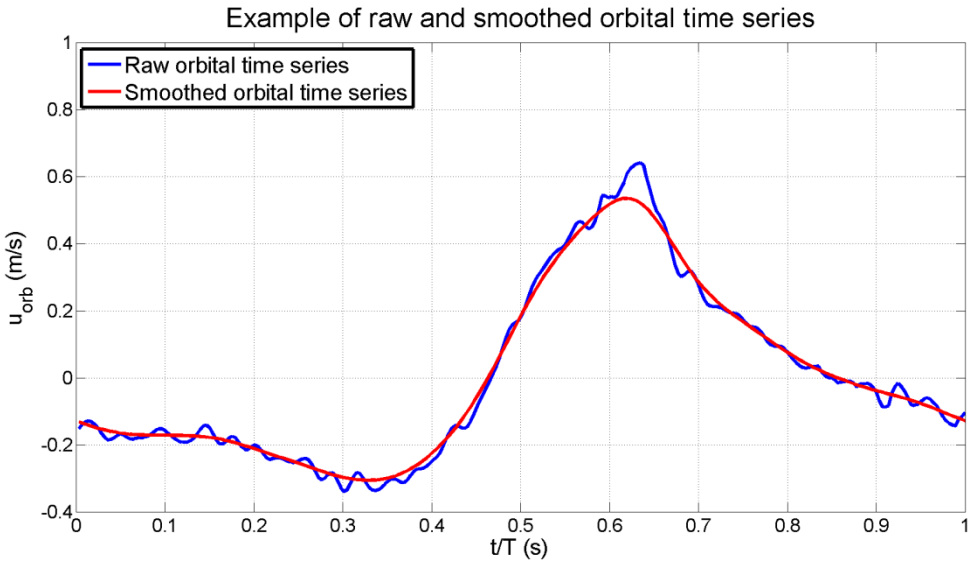

FIGURE J-1: EXAMPLE OF A RAW AND SMOOTHED TIME SERIES OF THE COMPONENT PARALLEL TO THE BED

The resulting measured wave Reynolds stresses are shown in Figure J-2. The modeled wave Reynolds stresses are overestimated from x = 52.9 to x = 55.4 m for all models. From x = 55.9 to x = 57.9 m the wave Reynolds stresses are not overestimated using (Nielsen, 2006). From x =

58.9 to x = 62.9 m. The wave Reynolds stress model of Nielsen (2006) (See EQ. I-10) predicts the wave Reynolds stress best.

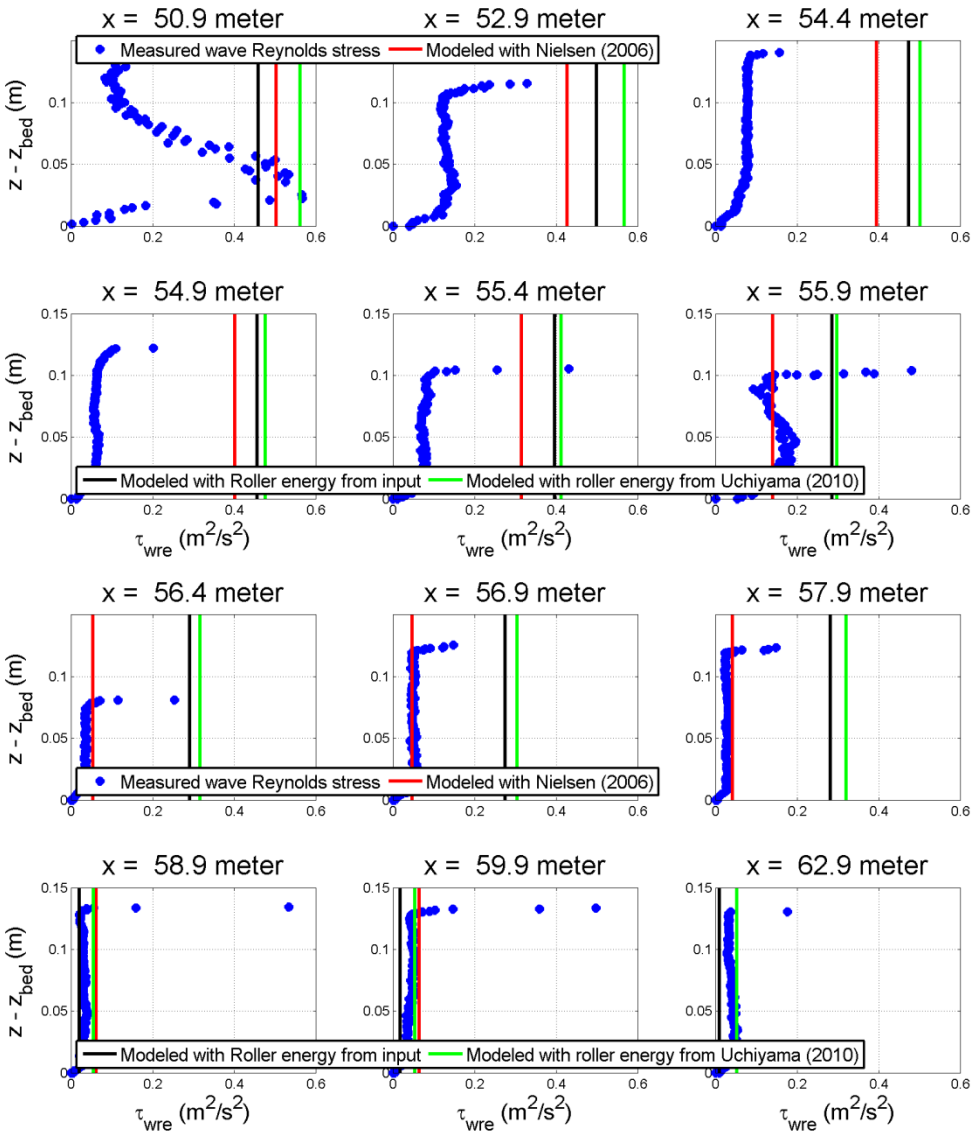

FIGURE J-2: MEASURED AND MODELED WAVE REYNOLDS STRESSES

APPENDIX K: MEASURED AND MODELED TURBULENCE

Preliminary turbulent values have been extracted from the measurements. Errors in the measured turbulence are quite well possible, since the measured turbulent values are not very accurate yet. Though, a comparison of the modeled turbulence with the measured turbulence is required and therefore the preliminary turbulent values are shown in Figure K-1. The modeled average turbulence $\bar{k}$ is calculated with Reniers et al. (2004):

$$\bar{k} = (D_r/\rho)^{2/3} \qquad \text{EQ. K-1}$$

This model assumes that turbulence in produced locally and turbulent transport is not taken into account. The near-bed turbulence is modeled with EQ. 6-9. Using γ_{tur} equal to seven increases the near-bed turbulence with a factor seven. The modeled turbulence is overestimated a lot. This can be due to poorly processed measurements, but it is more likely that the overestimation is due to the model concept.

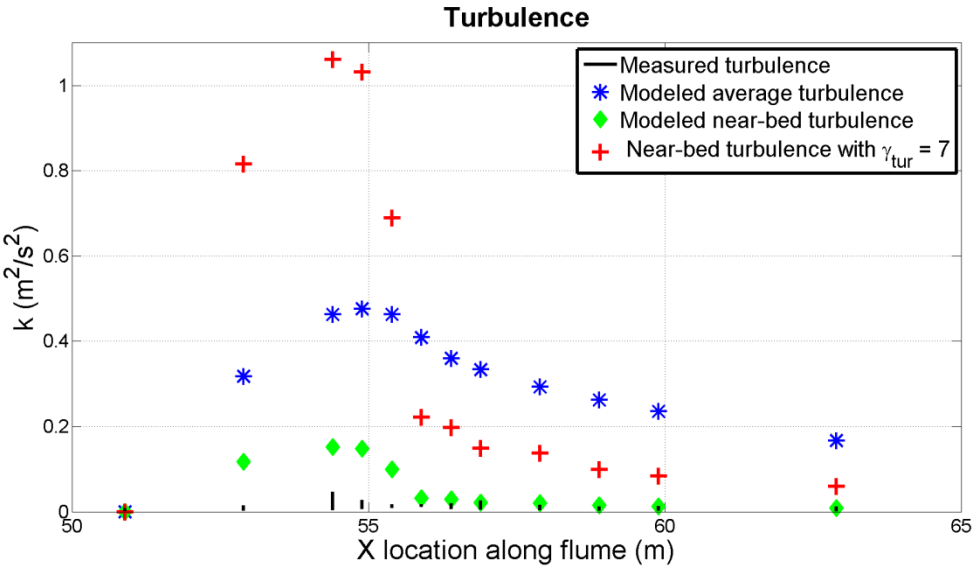

FIGURE K-1: MEASURED AND MODELED TURBULENCE